NASA CONTRACTOR REPORT

NASA CR-2561

2.11/2

4.

APPLICATION OF ACTIVE CONTROLS TECHNOLOGY TO THE NASA JETSTAR AIRPLANE

R. H. Lange, J. F. Cahill,
M. C. Campion, E. S. Bradley,
D. G. MacWilkinson, and J. W. Phillips

3.

Prepared by
LOCKHEED-GEORGIA COMPANY
Marietta, Ga. 30060
for Flight Research Center

5.

NATIONAL AERONAUTICS AND SPACE ADMINISTRATION • WASHINGTON, D. C. • JUNE 1975

1. Report No.	2. Government Accession No.	3. Recipient's Catalog No.
NASA CR-2561		

4. Title and Subtitle	5. Report Date
APPLICATION OF ACTIVE CONTROLS TECHNOLOGY TO THE NASA JETSTAR AIRPLANE	June 1975
	6. Performing Organization Code: H-868

7. Author(s)	8. Performing Organization Report No.
R. H. Lange, J. F. Cahill, M. C. Campion, E. S. Bradley, D. G. MacWilkinson and J. W. Phillips	
	10. Work Unit No.

9. Performing Organization Name and Address	11. Contract or Grant No.
Lockheed-Georgia Company Marietta, Georgia	NAS4-2121
	13. Type of Report and Period Covered: Contractor Report - Final

12. Sponsoring Agency Name and Address	14. Sponsoring Agency Code
National Aeronautics and Space Administration Washington, D. C. 20546	

15. Supplementary Notes

NASA Technical Monitor: Dwain A. Deets, NASA Flight Research Center

16. Abstract

A study has been made of the feasibility of modifying a JetStar airplane into a demonstrator of benefits to be achieved from incorporating active control concepts in the preliminary design of transport type aircraft. Substantial benefits are shown in terms of fuel economy and community noise by virtue of reduction in induced drag through use of a high aspect ratio wing which is made possible by a gust alleviation system. An intermediate configuration was defined which helps to isolate the benefits produced by active controls technology from those due to other configuration variables. Also, an alternate configuration which incorporated composite structures, but not active controls technology, was defined in order to compare the benefits of composite structures with those of active controls technology.

17. Key Words (Suggested by Author(s))	18. Distribution Statement
Active controls technology Control-configured vehicle Supercritical wing Design techniques	Unclassified - Unlimited STAR Category 05

19. Security Classif. (of this report)	20. Security Classif. (of this page)	21. No. of Pages	22. Price*
Unclassified	Unclassified	206	$7.25

For sale by the National Technical Information Service, Springfield, Virginia 22151

TABLE OF CONTENTS

TABLE OF CONTENTS (Cont'd)

FIGURES

FIGURES (CONT'D)

FIGURES (CONT'D)

FIGURES (CONT'D)

FIGURES (CONT'D)

FIGURES (CONT'D)

TABLES

APPLICATION OF ACTIVE CONTROLS TECHNOLOGY TO THE NASA JETSTAR AIRPLANE

By R. H. Lange, J. F. Cahill, M. C. Campion, E. S. Bradley, D. G. MacWilkinson and J. W. Phillips

SUMMARY

The requirements and feasibility study of flight demonstration of Active Controls Technology (ACT) on the NASA 814 airplane program was conducted by the Lockheed-Georgia Company for the NASA under Contract NAS4-2121. The primary objective of the study was the determination of the benefits accruing from the use of active controls concepts in terms of reduced fuel consumption and reduced community noise levels without compromising the ride quality of the airplane. These improvements were to be obtained at the current design cruise Mach number, long range cruise speed, range, handling qualities, and at or below the current take-off gross weight of the NASA Model-1329-6A JetStar. Configurational changes to enhance active controls technology benefits included the use of supercritical wing technology in order to make the results applicable to future transports. An assessment is made of the applicability of the study results to transport class aircraft in general.

The approach used in the Model 1329-6A JetStar redesign is to increase the lift-to-drag ratios in all flight regimes by exploiting the characteristics of active controls technology. Increased L/D in take-off, climb, cruise, approach and landing produces a direct reduction in fuel required. Beginning with the Model 1329-6A JetStar as the reference aircraft, the first step is the application of supercritical wing technology in the redesign of the wing. The wing redesign is directed toward the achievement of adequate mission fuel volume inside the wing and thus the elimination of the need for external fuel tanks as was the case with the reference aircraft. The redesign then follows two separate paths leading to an Intermediate Configuration and a final ACT Configuration. The Intermediate Configuration does not utilize Active Controls Technology. The ACT Configuration derived from this process is then compared to the Intermediate Configuration in order to isolate the contribution to improved performance provided by ACT alone. An Alternate Configuration was also designed utilizing filamentary composite materials in the wing and with no ACT.

Structural analyses indicated that the dominant loading condition for the wing is that due to gust conditions; therefore, the major function of the Active Controls System for the wing is gust load alleviation. The trailing edge active controls required for gust load alleviation consist of five (5) segments occupying the full semi-span of each wing. Of these, the inboard segments immediately beneath the nacelles of the engines are high lift devices. The four (4) segments remaining on each side operate as active controls and high lift devices.

The ACT Configuration developed from parametric analysis resulted in an aspect ratio of 9.0, a wing sweep of 0.096 rads (5.5 degs), and a wing area of 52.02 square meters (560 square feet). At the same time, the empennage configuration was changed to a tee-tail arrangement, and with the relaxation of static stability, a 40 percent reduction in surface areas is achieved.

The results of the study indicate a reduction in fuel consumption of 20 percent attributable to the application of ACT. Additional benefits from the use of ACT include a reduction in approach noise by 6 EPNdB and take-off flyover noise by 8 EPNdB, and an improvement in ride quality characteristics.

The applicability of the results from a feasibility study of this type to transport class aircraft in general is difficult to assess; however, in general, it is felt that benefits can be expected to transport aircraft performance due to ACT application.

INTRODUCTION

Active Controls Technology is a developing technology which has the potential to provide substantial benefits for the air transport industry. Three aspects must be developed before active controls is ready for application. These are: 1) the development of highly reliable fly-by-wire systems; 2) the implementation of active control functions; and 3) the integration of the active control system into the airplane preliminary design process. The first of these, fly-by-wire, is being addressed by NASA in the F-8 Digital Fly-By-Wire (DFBW) program (References 1 & 2) and by the military. The second aspect, implementation of active control functions, is progressing rapidly in programs such as the B-52 CCV flight tests (Reference 3) in which procedures and modeling techniques used in the design are being validated by flight tests for single design points. Active control functions have also been introduced into operational aircraft as a means of expanding aircraft capability. One example, the C-5A lift distribution control systems (Reference 4), reduces wing fatigue. Limited uses of active controls are also entering into initial design activities, and this is exemplified by the relaxed static stability system of the YF-16 which is part of the stability augmentation system (Reference 5). The third aspect, integration of active control systems into preliminary design, has not progressed as rapidly, although it is only through the process of airplane resizing that the maximum benefits using active controls technology can be realized.

The ATT System Studies (Reference 6) integrate active controls into the preliminary designs, but the designs were never implemented so that benefit verification was never possible. Active Controls, therefore, emerge as having great potential for certain airplane applications although the position regarding realizable benefits for civil transport is not clear, as discussed in Reference 7. Thus, there is a serious lack of flight verification that the predicted performance benefits due to ACT are actually achievable for transport aircraft. The NASA has recognized this situation and is considering various approaches for demonstrating the benefit potential due to ACT in ways calculated to develop confidence within the air transport community. One approach, the subject of the study presented, is to modify an existing jet transport using Active Controls Technology and thus verify, in flight, the performance benefits.

This report presents the results of the requirements and feasibility study of flight demonstration of active controls technology (ACT) on the NASA 814 airplane program. The study was performed at the Lockheed-Georgia Company under the direction of Roy H. Lange, Transport Design Department Manager. J. F. Cahill was designated Study Manager. Responsibility for Aerodynamics, Structures, and Design Integration was assigned to D. G. MacWilkinson, M. C. Campion, and E. S. Bradley, respectively. Other contributors to the study included S. D. Higham, J. G. Hewell, R. E. Stephens, C. M. Jenness, K. P. Burton, J. W. Phillips, J. F. Honrath, C. A. Mason, and R. T. Blair.

SYMBOLS

α	Angle of attack
α_{FRL}	Angle of fuselage reference lines
AR	Aspect ratio
A. C.	Aerodynamic center
α_{OL}	Zero lift angle
b	Wing span
$\bar{c}$	Mean aerodynamic chord
C_{AVG}	Average chord
C	Local chord
CC_{IO}	Basic lift distribution

C_D	Drag coefficient
C_{D_P}	Profile drag coefficient
$C_{D_{TRIM}}$	Total trimmed drag
C_f	Flat plate skin friction coefficient
c_f	Flap chord
c_f/c	Rudder chord ratio
C.G.	Center of gravity
C_H	Hinge moment coefficient
C_{h_α}	Hinge moment per unit angle of attack
C_{h_o}	Hinge moment at zero lift angle of attack
C_{h_δ}	Hinge moment per unit deflection of control surface
C_L	Lift coefficient
$C_{L_{A-h}}$	Tail-off lift coefficient
C_{l_α}	Two-dimensional lift curve slope
C_{L_α}	Wing or aircraft lift curve slope
$C_{L_{\alpha M_D}}$	Value of C_{L_α} at drag rise Mach number
$C_{L_{CR}}$	Cruise lift coefficient

$C_{L_{DES}}$	Wing design lift coefficient
$C_{L_{MAX}}$	Maximum lift coefficient
$C_{l_{MAX}}$	Two-dimensional maximum lift coefficient
$C_{L_{STALL_{FAR}}}$	Value of $C_{L_{MAX}}$ occurring in flight at an FAR defined STALL entry rate of -1 knot/sec
C_{L_T}	Horizontal tail lift coefficient
C_M	Pitching moment coefficient
$C_{M_{CL}}$	Longitudinal stability parameter
C_{M_δ}	Pitching moment per unit deflection of control surface
C_{M_O}	Wing or aircraft zero-lift pitching moment
C_{m_o}	Two-dimensional zero-lift pitching moment
C_{N_β}	Yawing moment coefficient per unit side slip
$(C_N)_{\delta_R}$	Yawing moment coefficient due to rudder deflection
CR	At cruise condition
$(C_Y)_{\delta_R}$	Side force coefficient due to rudder deflection
$\Delta C_{D_{i_T}}$	Horizontal tail induced drag
$\Delta C_{D_{TRIM}}$	Incremental trim drag

$\Delta C_{D_{TANK}}$	External tank drag coefficient
$\Delta C_{L_{MAX}}$	Incremental maximum lift coefficient
$\Delta \phi$	Incremental bank angle
δ	Control surface deflection
$\dot{\delta}$	Control surface rate
δ_f	Flap angle
$\dot{\delta}/\dot{\delta}_o$	Ratio of flap rate to no load flap rate
$\delta_{F_{IB}}$	Deflection of inboard flap
$\delta_{F_{OB}}$	Deflection of outboard flap
δ_{ST}	Incremental stick deflection
EAS	Equivalent airspeed
EI	Bending stiffness
EPNdB	Equivalent perceived noise level
e	Wing span efficiency factor
ϵ	Downwash at horizontal tail
G_F	Gain
G	Damping coefficient
g	Acceleration due to gravity
G_E	Elevator gain
GJ	Torsional stiffness

H	Altitude
HM	Hinge moment
H.Q.	Handling qualities
Hz	Hertz
η	Non-dimensional spanwise location
$\dot{\theta}$	Pitch rate
K_{α}	Angle of attack feedback gain
$K_{\dot{\delta}_t}$	Horizontal tail gain
$K_{\dot{\theta}}$	Pitch rate gain
kts	Knots
L/D	Lift to drag ratio
LRC	Long range cruise
Λ	Sweep angle
$\Lambda_{\bar{c}/4}$	Sweep angle at quarter chord
M	Mach number
M_C	Cruise Mach number
M_D	Drag rise Mach number
$M_{x'}$	Root bending moment
n_z	Normal acceleration factor
$(N)_{\delta_R}$	Yaw acceleration due to rudder

q	Dynamic pressure
P_1	Hydraulic pressure input
P_2	Hydraulic pressure output
p	Roll rate
R_n	Reynolds number
r	Yaw rate
ρ	Damping ratio
R.S.	Rear spar
S	Basic wing area
SF	Shape factor
S_f	Flap area
Σ	Summation
T	Time
T.E.	Trailing edge
T_w	Washout time constant
t/c	Thickness to chord ratio
τ	Time constant
V_B	Design speed for maximum gust intensity
V_C	Design cruise speed
V_D	Design dive speed

V_E	Equivalent airspeed
$\bar{V}_H$	Horizontal tail volume coefficient
ω_D	Dutch-roll frequency
X/C	Non-dimensional chord location
Z/C	Non-dimensional height location
$\frac{\partial C_M}{\partial \delta}$	Rate of change of pitching moment with flap angle
$\frac{\partial C_L}{\partial \delta}$	Rate of change of lift coefficient with flap angle

ABBREVIATIONS

ACT	Active Controls Technology
ATT	Advanced Technology Transport
DFBW	Digital Fly-By-Wire
DLC	Direct Lift Control
FAR	Federal Aviation Regulations
GW	Gross Weight
MAC	Mean Aerodynamic Chord
MLG	Main Landing Gear
NBAA	National Business Aircraft Association
OWE	Operating Weight Empty
RDI	Ride Discomfort Index
STOL	Short Take-off and Landing
VFR	Visual Flight Rules
WT	Wind Tunnel

STUDY OBJECTIVES, TECHNICAL APPROACH, AND DESIGN REQUIREMENTS

Study Objectives

The requirements and feasibility study described in this report has as the primary objectives the determination as to whether substantial performance benefits can be shown by a synergistic redesign of the NASA 814 airplane (JetStar) utilizing Active Controls Technology (ACT) concepts, to establish the magnitude of these benefits where they exist, and to direct the configuration development toward that configuration showing the greatest potential in terms of the reduction of fuel consumption. The utilization of other advanced technologies is encouraged where the interaction of these technologies can be shown to enhance the benefits arising from the use of Active Controls Technology.

The latter objective was directed toward the use of supercritical aerodynamics and filamentary composite materials for application to the wing design. These were considered to be important aspects of the study in order to make the study results applicable to future transports.

Technical Approach

The methodology for the conduct of the study consists of a program plan which divides the study into nine (9) related elements. The study plan, Figure 1 , consists of the following elements: 1) establish initial baseline ACT configuration, 2) engineering analyses and redesign, 3) establish baseline composite wing configuration, 4) parametric variations, 5) selection of ACT airplane configuration, 6) selection of the intermediate airplane configuration, 7) selection of composite wing airplane configuration, 8) flight ACT demonstrator configuration refinement and evaluation, and 9) program development plan.

The application of Active Controls Technology to the NASA 814 airplane is to be accomplished using as much of the original airframe as possible. The technical approach calls for drag reduction, primarily induced drag, as the principal means of demonstrating ACT benefits in a highly visible manner. Thus, the major configurational changes are executed on the wing by optimizing the airplane configuration to an aspect ratio higher than the unmodified NASA 814 airplane. The reduction in drag thus achieved will result in improved fuel usage and a decrease in community noise levels due to a reduction in the thrust level required during take-off and approach.

Since the Active Controls Technology is combined with the application of supercritical aerodynamics to the wing, in order to clearly identify the contribution to improved performance through ACT alone, an intermediate configuration is established in which supercritical aerodynamics is applied to the wing design and ACT is omitted.

Similarly, in the case of the application of filamentary composite materials to the wing, an Alternate Configuration is defined in which Active Controls Technology is excluded from the design.

The effects of ACT can, therefore, be isolated by comparing the ACT Configurations with the Intermediate and Alternate Configurations.

The study results consist of an assessment of the application of ACT, a prediction of the applicability of the benefits to transport aircraft in general, and a projected program plan for the design and modification of Model 1329-6A JetStar to flight validate the Active Controls design approach.

Design Requirements

The design requirements for the ACT airplane were established from the corresponding requirements of the Model 1329-6A JetStar configuration. The basic definition of airworthiness requirements for the modified airplane in the FAR Part 25 (Reference 8) augmented by the new criteria necessary for the active control systems definition was used as the airworthiness guideline for this study.

Performance requirements. - The significant items of airplane performance for the modified airplane are listed in Table I.

TABLE I
PERFORMANCE REQUIREMENTS

a) Range - At least 3371 km (1820 nm) using the NBAA jet aircraft VFR range format, cruising at a Mach number of 0.76 at maximum take-off weight and with full fuel.

b) FAA take-off field length - No greater than 1981 m (6500 ft) at a weight of 18561 kilograms (40,920 pounds).

c) FAA landing field length - No greater than 1676 m (5500 ft) at a weight of 13607.7 kilograms (30,000 pounds).

d) Maximum cruise speed - M = 0.82 at altitudes above 9144 m (30,000 ft).

Structural design requirements. - The analyses to determine structural design loads will be confined to symmetrical loading conditions using the design parameters listed in Table II.

TABLE II
STRUCTURAL DESIGN REQUIREMENTS

a) Design weights.

i)	Maximum zero fuel weight	10886.2 kilograms (24,000 pounds)
ii)	Maximum landing weight	13607.7 kilograms (30,000 pounds)
iii)	Maximum take-off weight	18561.0 kilograms (40,920 pounds)

b) Center of gravity envelope. The limits of the center of gravity envelope are those defined by Figure 2.

c) Design air speeds. The design air speeds are those defined by Figure 3.

d) Design load factor.

Pitch maneuver cruise configuration +2.5 g max, -1.0 g min

e) Gust load factor capability. (Reference 8)

Gust load factor capability will be based on encounters of gusts of:

i) 22.12 m/s (66 fps) at speeds up to V_B

ii) 15.24 m/s (50 fps) at speeds up to V_C

iii) 7.62 m/s (25 fps) at speeds up to V_D

The initial study will be conducted using the 15.24 m/s (50 fps) gust up to V_C.

f) Landing and ground handling.

i)	Sink speed at maximum landing weight	3.05 m/s (10 fps)
ii)	Sink speed at maximum take-off weight	1.83 m/s (6 fps)

Taxi load factors due to discrete bump -1.7 g

Flutter deformation and fail safe criteria. The aircraft will be designed to be free from flutter, divergence, and control reversal at all speeds up to 1.2 V_D in accordance with Paragraph 4b.308 of Reference 9. These requirements will be met with the active control systems either operative or inoperative.

Fail safe considerations will be satisfied by designing the airplane to be free from flutter at all speeds up to V_D after any reasonably probable single failure, malfunction, or adverse condition of a principal structural element, or element in the main control system including the automatic flight control system or tab control system.

Control system. - The criteria to be applied to the design of the flight control system are divided into two parts; the first, shown in Table III, defines the applicable specifications, and the second covers other criteria including system performance shown in Table IV.

TABLE III
ACT FLIGHT CONTROL SYSTEMS SPECIFICATIONS

i) MIL-F-8785B - Flying qualities of piloted aircraft.

ii) MIL-F9490D (Proposed) - General specification for flight control system, design, installation, and test of piloted aircraft.

iii) MIL-H-5540F - Hydraulic systems, Aircraft Type I and II design installation and data requirements. A deviation from this specification for the ACT airplane requires the use of MIL-H-5606 hydraulic fluid instead of the specified MIL-H-83282.

TABLE IV
DESIGN CRITERIA FOR ACTIVE CONTROL FUNCTIONS

i) Handling qualities. - The existing handling qualities of the Model 1329-6A JetStar airplane will, as a minimum requirement, not be degraded but will be improved where possible. The commonly accepted measures of handling qualities of Reference 10 will be used to define existing value.

ii) Ride quality. - The data of Reference 11 will be used to evaluate the existing and projected ride quality. It should be noted that the parameters defining ride quality are not established to the degree that the parameters of other characteristics are defined and that Reference 11 is undergoing revision to establish ride quality criteria.

iii) Relaxed static stability. - The criteria necessary to define the requirement for relaxed static stability lack adequate definition at the present time. The principal parameters involved are horizontal and vertical tail volume, center of gravity range, and the weathercock characteristics, C_{N_β}.

iv) Empennage Sizing

Horizontal tail. - The following criteria will be used to size the horizontal tail:

- Stabilizer effectiveness for nose wheel lift-off
- Stabilizer effectiveness for landing approach trim
- Stabilizer effectiveness for pitch acceleration from landing approach trim point
- Minimum static margin requirements for adequate spread in stick force/g
- Active controls for longitudinal damping requirements.

Vertical tail. - The following criteria, obtained from Reference 10 and Reference 12, will be used to size the vertical stabilizer:

- Sufficient rudder to balance a 0.262 rads (15 degs) side-slip on approach with a 55.56 kms/hr (30 kts) wind.
- Sufficient rudder to trim engine-out, 1 and 2 engines.
- Sufficient rudder to trim engine-out in a crosswind from the dead engine side.
- Sufficient directional stability to balance an engine-out with zero rudder and 50% wheel throw.
- Sufficient rudder to achieve a yaw acceleration of 0.24 rads/sec^2 (13.75 degs/sec^2).
- Active controls to meet Dutch-roll damping requirements.

Control system configuration. - The flight control system will be configured from quadruple electrical command terminals through the control surfaces, such that the mission, reliability, and maintainability requirements of the ACT airplane are satisfied.

METHODOLOGY AND BASIC DATA

Aerodynamic Data

Developments in the aerodynamics of advanced technology airfoil sections in recent years have included extensive wind tunnel and flight test verification of theoretical principles. The F-8 program, for example, demonstrated the improvements in drag-rise Mach number at speeds in the region of M = 0.95, and the U. S. Navy-Rockwell program on the T-2C aircraft showed that the drag-rise Mach number in the region of 0.70 for an unswept wing of aspect ratio 5.07 could be matched using a supercritical wing having a thickness/chord ratio of 5% greater.

Studies at the Lockheed-Georgia Company in association with the Study of Application of Advanced Technologies to Long Range Aircraft (Reference 13) led to a simplified empirical method for estimating the drag-rise Mach number for transport type aircraft having varying degrees of wing technology. The method applies correction factors to Mach number to account for wing thickness/chord ratio, aspect ratio, wing quarter chord sweep, and to the technology level which is representative of airfoil sections having reduced shock strength, through a correlation parameter defining the airfoil curvature at the crest. Correlation of the method with test data indicates good agreement of M_D and post-drag-rise characteristics for a wide range of aircraft at cruise conditions. This method is applicable to wing-fuselage combinations in which the junctions are designed to minimize interference effects.

A review of the wind tunnel and flight test data of the T-2C aircraft fitted with a supercritical wing indicated that the apparent technology factor resulting from use of the advanced airfoil was conservatively estimated to be an increment of 0.075 in M_D. This study assumes a similar approach in that the gain in M_D is traded against an increase in wing thickness/chord ratio. To obtain a basis for selecting the optimum aerodynamic parameters, several candidate supercritical wings were studied having variations in thickness/chord ratio, aspect ratio, and sweep angle capable of producing the same drag-rise Mach number as the Model 1329-6A JetStar wing-body combination. A matrix of point designs is presented on Figure 4 showing t/c at the wing MAC varying typically from 16% at 0.524 rads (30 degs) sweep to 12% at low sweep. These values compare with 11.2% for the Model 1329-6A JetStar which has 0.524 rads (30 degs) sweep at the wing quarter chord. These data are used in conjunction with desi n al structural load considerations in the determination of the selected wing configuration.

The rationale and aerodynamic data used in the design of the ACT wing are contained in Appendix A .

Structural Loads Data

The primary objective of the loads analysis was the establishment of the relationship between aspect ratio and wing weight with active controls for wings with supercritical airfoil technology applied, so that appropriate solutions to the airplane performance optimization could be obtained. A secondary objective was the study of various active control system parameters so that candidate systems could be compared and a feasible system selected. Because of the short duration of the study, and with the probability that several wing planforms would require analysis, it was considered more useful to perform a preliminary analysis of a broad range of parameters rather than to conduct a refined analysis involving a reduced number of parameters.

The basic intent of the structural load studies was the investigation of the performance benefits possible through the use of active controls technology, rather than to establish design loads for a specific airplane configuration. It was therefore decided that time history solutions for suitable discrete gust (or maneuver) conditions would offer greater visibility of the influence of the active controls technology than would result from spectral density analyses. The load levels obtained from these analyses should therefore be interpreted as describing the effects of typical active controls systems in a representative flight condition and should not be regarded as definitive loads for the structural design.

The detailed structural loads analysis of the Active Controls Technology Configuration, including the influence of the active control system, is contained in Appendix B .

Design Integration

The modification of the Model 1329-6A JetStar airplane to incorporate active controls technology requires redesign of the wing and empennage and modification of the fuselage center section structure. In the interests of minimizing program costs, the design changes were considered in relation to the constraints imposed by the existing wing attachment frames in the fuselage, the landing gear support structure, and the empennage support structure, and design exercises were conducted within these constraints to establish the feasibility of the overall design of the Active Controls Technology Airplane and for the Intermediate and Alternate Airplanes developed for comparative purposes.

The results of the design integration considerations and constraints for all three configurations are given in Appendix C .

Active Control System Development

The basic philosophy used in the development of the active flight controls is to provide a safe, reliable, integrated flight control system of the fly-by-wire type decoupled in the pitch, roll, and yaw axes as far as possible. This philosophy required early consideration of all flight control functions to avoid interface problems at later stages in the design process.

The specific functions considered in the study were:

- Gust load alleviation
- Maneuver load control
- Ride quality control
- Relaxed static stability (pitch)
- Relaxed dynamic stability (roll and yaw)
- Handling qualities
- Direct lift control

These functions are to be compatible with the basic digital flight control computer as far as redundancy, data rate, switching logic, and fault logic are concerned. During the study, it was found that most of the functions overlapped and commonality of elements could be achieved without loss of effectiveness or reliability. Gust load alleviation in the pitch axis, for example, provided maneuver load control and ride quality control capability with minor additional compensation.

ACT CONFIGURATION DEFINITION

Parametric Analysis

The final parametric studies to define the ACT Configuration initially considered a matrix of aspect ratios from 5 to 10. These were later reduced to values of 7, 8, and 9, when it became apparent that the optimum wing from the structural loads and aerodynamic performance trade studies was within this range.

The relationship of mission fuel requirement and operating weight empty for a matrix of configurations having cruise lift coefficients varying from 0.30 to 0.40 is shown in Figure 5. The data are for a mission cruise segment range of 3429.84 kilometers (1850 nautical miles) and a start cruise altitude of 12,192 meters (40,000 feet). Corresponding fuel flow in kilograms/kilometers (pounds/nautical miles) is presented in Figure 6. Selection of the final configuration was obtained from the intercept of a line representing adequate fuel volume and a value of minimum fuel consumption which is achieved with an aspect ratio of 9 and a cruise lift coefficient of 0.38. This gives a fuel flow rate of 1.35 kgm/km (5.5 lb/nm). All candidate configurations were shown to satisfy the Ride Discomfort Index criteria. The value of RDI for the selected ACT Configuration was calculated to be 0.206.

Wing Definition

The selected ACT Configuration has an aspect ratio 9 wing, quarter chord sweep of 0.096 rads (5.5 degs), basic wing area of 52.025 square meters (560 square feet), basic wing taper ratio 0.30, and streamwise thickness/chord ratio at the MAC of 12.7%. The Lockheed-Georgia STOL airfoil section, discussed in Appendix A, was applied to this wing design. The mean camber line for a design lift coefficient of 0.35 is shown on Figure 7.

An analysis of the wing spanwise load distributions obtained by the use of a lifting surface computer program indicated that a relatively small spanwise twist would be required in order to develop span load distributions at the cruise condition, close to the optimum elliptic shape. The required wing-fuselage angle setting was estimated to be 0.0175 rads (1 deg) at the root in order to meet the necessary rotation requirements at lift-off and to ensure a cabin floor angle of zero degrees in the cruise condition. The combined wing twist and root setting angle are also shown in Figure 7. At the design twist distribution, given in Figure 7, the calculated wing span efficiency factor at a cruise condition of $M = 0.76$, $C_L = 0.38$, was 0.961.

All wing planforms considered in this study included an inboard leading edge extension which was defined on a basis of root chord/basic chord = 1.35, where the root chord location is taken at BL 41.5. Apart from the improved fuel volume capability resulting from this additional volume, the rationale was based principally on aerodynamic improvements resulting from improved wing isobar distributions and hence lower wing-fuselage interference effects in the cruise condition. This concept was developed in detail during the NASA-ATT program (Reference 13) for the $M = 0.95$ transport. The design principles apply equally, however, to aircraft of this study.

Empennage Sizing and Definition

Horizontal tail sizing. - It was determined that the Model 1329-6A JetStar tail volume provided more than adequate static stability but that the short period damping was deficient at the critical flight condition of maximum gross weight and an aft center of gravity location at a Mach number of 0.8. This deficiency was corrected by adding a low gain pitch rate feedback to the horizontal tail. A reduction in tail size was then achieved by providing positive angle-of-attack feedback summed with pitch rate feedback to a movable tail. Preliminary estimates indicate that a 52% reduction in horizontal tail area can be achieved in this way. Figure 8 shows the effect of trim and static stability requirements on horizontal tail volume, and Figure 9 shows the migration of the short period roots as a result of tail volume reduction and angle-of-attack feedback to a movable tail.

Vertical tail sizing. - The major change to the empennage affecting sizing of the vertical tail is the relocation of the horizontal tail from a mid-span for the Model 1329-6A JetStar to a tee-tail configuration for the ACT airplane. This change increases the lift-curve slope of the vertical tail, permits the use of a full span rudder, and leads to a reduction in vertical tail volume coefficient for the same design criteria as the Model 1329-6A JetStar. At a given rudder chord, the engine-out sideslip requirement provides an upper limit on fin size. At a rudder chord ratio of 0.3, the vertical stabilizer maximum volume coefficient allowable is 0.042, as shown in Figure 10. However, with no augmentation the minimum volume coefficient would be 0.047 due to Dutch-roll time constant requirements. Assuming that ACT will satisfy the damping requirement, as shown in Figure 11, then the vertical stabilizer volume coefficient can be reduced to either the limit line for yaw acceleration, 0.027, or to the rudder-free engine-out requirement, 0.025. A reasonable choice for vertical stabilizer volume coefficient with ACT would be of the order of 0.037 which would provide the same $(C_N)_{\delta_R}$ as the Model 1329-6A JetStar. This level of volume coefficient would lead to a reduction in the size of the Model 1329-6A vertical stabilizer by 37.3%.

Empennage definition. - A tee-tail configuration consisting of a fixed vertical stabilizer having an all-flying horizontal stabilizer attached at the top was chosen for the ACT airplane configuration. The empennage geometry, shown in Figure 12, has a horizontal stabilizer 6.577 square meters (70.8 square feet) in area, an aspect ratio of 4.0, and a taper ratio of 0.30. The sweep angle at the wing quarter chord is 0 rad (0 deg). The airfoil section thickness/chord ratio is 13% and the airfoil section was derived by transposing the upper ordinates of a Lockheed-Georgia Company developed supercritical section about the section chord line to achieve a symmetrical section. The horizontal stabilizer is pivoted at the 25% chord and angular motion is achieved by means of dual tandem actuators. The horizontal stabilizer sizing was based upon the tail-arm of the Model 1329-6A JetStar and a tail volume coefficient of 0.29.

The vertical stabilizer sizing was also based upon the Model 1329-6A JetStar tail-arm and a volume coefficient of 0.037. The selected stabilizer has an area

of 6.875 square meters (74 square feet), an aspect ratio of 1.4, and a taper ratio of 0.37. The sweep angle of the stabilizer quarter chord is 0.524 rads (30 degs) and the stabilizer basic root chord is located on fuselage water line 100.0. The section thickness/chord ratio is 14% and the section was derived in a manner similar to that for the horizontal stabilizer. A 30% chord rudder, hinged at the 70% chord line, is operated by dual tandem actuators located in the fuselage at the lower end of the rudder.

Control Surface Definition

The ACT Configuration control system consists of an arrangement of wing trailing edge surfaces, an all-flying horizontal stabilizer, and a 30% chord rudder. All surfaces are operated by dual tandem electro-hydraulic actuators controlled by a fly-by-wire computer system.

The wing trailing edge surfaces consist of five segments hinged at the 75% generator of the wing. The inboard surfaces, extending from the wing roots to the wing breaks, are used for high-lift generation only. The remaining four segments of each wing are of equal span and function as active controls for gust load alleviation and as high-lift devices. Each segment is mounted on three hinges and is operated by dual tandem actuators. Control surface movement is 0.349 rads (20 degs) each side of a neutral position for ACT operation with an additional 0.349 rads (20 degs) of movement for high-lift generation.

A single piece rudder, hinged along the 70% chord of the vertical stabilizer, has a movement of $\pm$ 0.524 rads (30 degs). The horizontal stabilizer is hinged at the 25% chord and operates over a maximum angular movement of 0.349 rads (20 degs) nose down and 0.174 rads (10 degs) nose up. This angular movement is obtained by means of dual tandem actuators located at the lower portion of the rudder.

Loads

The selected wing configuration for the active control airplane was essentially similar to that used for the baseline configuration in Appendix B and the conclusions outlined in that and subsequent sections are therefore expected to be valid as far as demonstrating the feasibility of achieving adequate reduction of dynamic gust loads. The conditions examined in Appendix B, however, should not be interpreted as representing the full envelope necessary for a definitive structural design. A comprehensive study of the dynamic response to continuous turbulence will be required to ensure the absence of adverse coupling between the structure and the active controls system throughout the expected frequency range.

Flutter

The ACT Configuration wing, because of the close geometric similarity of the baseline configuration wing, analyzed in Appendix B, is expected to exhibit essentially identical flutter characteristics. The small reduction in planform area will cause an insignificant increase in the vibration and flutter mode frequencies and a small reduction in the torsional stiffness required for flutter prevention. The empennage configuration of the ACT airplane was not analyzed for flutter, since empennage weight was estimated

on the basis of statistical data which include torsional stiffness weight increments for flutter prevention. Additional flutter prevention weight increments, if required, would not significantly affect the predicted benefits due to ACT, and no attempt has been made to quantify them.

Configuration Description

The general arrangement for the Active Controls Aircraft Configuration is illustrated in Figure 13. The aircraft is a modified Model 1329-6A JetStar featuring a high aspect ratio, low sweep angle wing having a supercritical airfoil, active controls, and a tee-tail. The existing fuselage is utilized for the design and is modified only in the area of wing and empennage attachment.

The new wing, as illustrated on Figure 14, features a supercritical airfoil, an extended leading edge, and active control trailing edge surfaces. Dimensions of the basic wing are: basic root chord, 3.699 meters (145.63 inches) at centerline; tip chord, 1.109 meters (43.69 inches); and span, 21,638 meters (851.92 inches). The wing root is located at BL 41.5 where it is attached to the fuselage frames previously described. The extended inboard portion of the wing which has a constant t/c ratio of 13.17% extends outwards to the wing break at BL 102.79 and coincides with the geometrical intersection of the existing auxiliary spar and inboard rear spar locations. The outboard portion of the wing extends from this break to the tip, at which point the t/c ratio is reduced linearly to 11.3%. Wing incidence varies from 0.0175 rads (1 deg) at the root to 0.0141 rads (0.81 degs) at the break to 0.00698 rads (0.4 degs) at the tip. The dihedral angle is 0.035 rads (2 degs) originating at the root.

The horizontal stabilizer basic dimensions are: span, 5.17 meters (203.5 inches); root chord, 1.97 meters (77.7 inches); and tip chord, 0.59 meters (23.3 inches). The stabilizer is hinged at the 25% chord line which is also the location of the front spar. The rear spar is located at 65% chord. The center section box structure extends forward from the front spar to provide sufficient moment arm for the active controls actuation system. The fixed vertical stabilizer basic dimensions are: span, 3.11 meters (122.24 inches); root chord, 3.24 meters (127.5 inches); and tip chord, 1.20 meters (47.17 inches). The stabilizer basic root chord is located on fuselage water line 100.0, and the front spar is located at 15% and the rear spar at 62% of the chord.

Weight Summary

The weight summary for the ACT airplane configuration is shown on Table V.

Airplane Performance

The ACT airplane configuration high-lift system consists of five 25% chord trailing edge surface segments covering the full span from wing root to tip. The four outer segments are activated individually for gust load alleviation. For airfield take-off and approach conditions, all segments are deflected at a constant angle.

TABLE V

ACT AIRPLANE WEIGHT SUMMARY

	Kilograms	Pounds
Wing	1659.2	3658
Horizontal	109.3	241
Vertical	169.2	373
Fuselage	1808.0	3986
Nose Landing Gear	99.8	220
Main Landing Gear	390.5	861
Nacelle - Pylon	485.8	1071
Propulsion	1735.4	3826
Surface Controls	468.1	1032
Instruments	54.0	119
Hydraulics	168.7	372
Electrical	898.1	1980
Avionics	492.6	1086
Furnishings	992.5	2188
Air Conditioning	275.8	608
Auxiliary Gear	4.1	9
Weight Empty	9811.2	21630
Operating Equipment	501.2	1105
OWE	10312.4	22735
Fuel	5776.5	12735
Gross Weight	16088.8	35470

Maximum lift requirements in order to match take-off and landing distances are estimated on the assumption of equal wing loadings between the ACT configuration and the Model 1329-6A JetStar. However, as indicated elsewhere in this report, wing loadings of the ACT configuration are slightly lower than the Model 1329-6A JetStar, so that some improvement in field length is expected for the ACT configuration. The full scale values of $C_{L_{MAX}}$ were estimated using equation (A7) of Appendix A for the AR = 9 wing and are shown in Table VI. In this case, no aspect ratio correction was applied; thus, $\Delta C_{L_{MAX_{AR}}} = 0$.

TABLE VI

FULL SCALE MAXIMUM LIFT COEFFICIENTS - $C_{L_{MAX}}$

Flap Angle	ACT Configuration	Model 1329-6A JetStar
δ_f = 0 rad (0 deg)	1.64	1.53 (Take-off 40% flap)
δ_f = 0.087 rads (5 degs)	1.80	1.71 (Landing 100% flap)
δ_f = 0.175 rads (10 degs)	1.94	

Table VI indicates that the take-off requirement can be easily met without flaps. A flap angle of 0.087 rads (5 degs) is required to achieve comparable landing field performance.

The drag polars for the high lift conditions are shown on Figure 15 and are based on the methods described in Appendix A. The combination of high aspect ratio and low flap setting produces substantial improvements in lift/drag ratios at lift-off and approach conditions. Comparable figures for the ACT configuration and Model 1329-6A JetStar are shown in Table IX.

TABLE VII

L/D RATIO COMPARISON

	Model 1329-6A JetStar	ACT Configuration
Lift-Off (1.2 V_{Stall})	8.95	14.10
Approach (1.3 V_{Stall} +18.52 kms/hr (10 kts), gear down)	5.2	11.50

Definitive cruise performance data were calculated for the ACT configuration in addition to the preliminary analysis conducted during earlier parametric studies. From procedures outlined in Appendix A cruise drag polars were developed for the selected configuration for an aspect ratio 9 wing of 52.025 square meters (560 square feet) basic area. These are presented in Figure 16. A series of specific range data for various cruise altitudes is shown on Figures 17 through 22. These data were used to calculate range for a typical mission based on NBAA rules under VFR conditions. A step-climb technique is employed. Comparative range values for the Model 1329-6A JetStar and the ACT configuration are 3667 kilometers (1980 nautical miles) and 3704 kilometers (2000 nautical miles), respectively.

Active Controls System Implementation

Pitch axis. - The active control functions which were considered for implementation in the pitch axis were the following:

- o gust load alleviation
- o maneuver load control
- o stability and control augmentation
- o direct lift control

These functions are discussed separately below:

Gust load alleviation. - The purpose of the gust load alleviation subsystem is to reduce the structural loads imposed on the airframe by atmospheric turbulence to an acceptable level. As indicated, the flexible airframe characteristics were dominant in determining the type of signal shaping required for the actuation of the wing trailing edge and horizontal tail surfaces to effectively reduce the wing root bending moment peak values.

The normal accelerometer and pitch rate gyro sensors will be quad redundant to comply with the "two fail op" requirements and will also serve as feedback signal sources for the pitch stability and control augmentation subsystems. Although there appears to be a benefit from differential deflection and phasing of the inboard to outboard trailing edge surfaces, definitive numerical data were not developed for these functions during the study.

Maneuver load control. - The requirement for limiting maneuver loads to 2.5g normal load factor proved to be much less demanding than the gust load alleviation requirement. Thus, the control surface effectiveness, deflection, and rate limits satisfying gust load alleviation requirements are more than adequate to provide the necessary load reduction and trim compensation. The steady state character of maneuver loads as compared to gust loads requires additional signal shaping. Since the two phenomena are well separated in the frequency domain, no significant problems are expected in providing suitable additive shaping networks using normal acceleration feedback blended with pitch rate compensation for stability.

Stability and control augmentation. - The control augmentation system is identical to the basic fly-by-wire flight control system where no direct mechanical link exists from column to actuator. A model following implementation of the C-star type is proposed, conforming to the requirements of Reference 10 short period characteristics. A first order lag or fixed gain model in many cases provides better response characteristics over the entire flight regime. Further analysis is necessary to determine the precise model for the ACT airplane.

The stability augmentation function in pitch has been approached in two ways. First, a compromise feedback gain was used for both disturbance and control response feedback signals (blended normal acceleration at the pilot's station and pitch rates). This results in less than optimum response to both inputs but may be acceptable with added shaping. The other approach was to split the feedback gains as shown in Figure 23. This scheme presupposes that either the control or disturbance input is dominant, while the other one is relatively small. In the case where one of the inputs is zero, this scheme provides optimum gains, contingent on the accuracy of the response model.

Direct lift control. - Although not strictly an active control function, direct lift control is provided as an inherent function of the ACT airplane flight control system. As shown in Figure 24, this function is selectable, primarily for flight path control, and provides symmetrical actuation of the eight outboard trailing edge surfaces through a shaping network, consisting of a gain and a short term washout. Pitching moment produced by direct lift control will be compensated by a shaped deflection command to the horizontal stabilizer.

Roll and yaw axes. - The following active control functions in roll and yaw were analyzed for application to the ACT JetStar:

- o stability and control augmentation
- o relaxed dynamic stability

Stability and control augmentation. - The basic manual flight control system in the roll and yaw axes will provide the following functions conforming to the requirements of Reference 10:

- o roll performance
- o spiral stability
- o Dutch-roll damping
- o turn coordination
- o smooth turn entry and exit

The basic system configuration is as shown in Figure 25. As a result of further flight simulation throughout the flight envelope, system gains may require scheduling with airspeed or dynamic pressure. A Lockheed-Georgia developed computer program is used to compute the optimum gain values for a given flight condition to accommodate the five functions listed above. The gains are a function of the lateral-directional stability derivatives, airspeed, dynamic pressure, and airplane physical constants.

Stability derivatives were estimated at cruise conditions for various vertical stabilizer configurations and are compared with the Model 1329-6A JetStar data in Figure 26. The basic lateral-directional stability augmentation gains required for smooth turn coordination, neutral spiral stability, Dutch-roll damping, and adequate roll response for compliance with the requirements of MIL-F-8785B (Reference 10) have been computed for each configuration. Achievement of Case 2 of Reference 10 involves configuring the empennage to a tee-tail configuration which increases the lift-curve-slope of the vertical stabilizer and allows an additional reduction in area. A set of nominal gains was obtained which provides good Dutch-roll performance for all cases except Case 4 (Reference 11). In order to stabilize this configuration adequately, an additional feedback signal may be required from a lateral accelerometer. This is due to the marginal "weathercock" stability which results from the reduced vertical stabilizer size. Figure 11 shows the benefit to Dutch-roll performance produced by the fixed augmentation gains on the Model 1329-6A JetStar and Cases 1, 2, and 3 as defined above. The gain values used, implicit in these data, are:

	Rudder	Aileron
Roll rate	$\frac{K_{R_p}}{0.01}$ deg/deg/sec	$\frac{K_{A_p}}{0.6}$ deg/deg/sec
Yaw rate	$\frac{K_{R_r}}{1.0}$ deg/deg/sec	———

	Rudder	Aileron
Bank angle	K_{R_ϕ} -0.075 degs/deg	K_{A_ϕ} 0.005 degs/deg

Integration of functions. - A concerted effort has been initiated to "unitize" the entire flight control system so that duplication of components and functions is eliminated or minimized. In this way, redundancy may be achieved at minimum penalty in weight and cost. The following system groups occur by similarity of functions and can theoretically be mechanized as single systems with multiple functions:

Group 1

Gust load alleviation
Maneuver load control
Ride quality control

Group 2

Flight augmentation
Manual flight controls (FBW)
Relaxed static stability (pitch)
Direct lift control
Relaxed dynamic stability (yaw)

The total electrical command signal to any given surface servo will be provided by four identical channels consistent with the redundant mechanization described for the servos in the following section.

Active Controls System Redundancy

Digital fly-by-wire input system. - The conceptual development of the control surface power servos was based on the assumption that a full-time digital fly-by-wire input control system would be available, having a reliability equivalent to that of the Model 1329-6A JetStar aircraft structure. In addition, consideration of the digital flight control computer redundancy and interface characteristics was excluded from the study, although these are recognized to play an important role in the overall system performance. It was assumed, for the purposes of the study, that four (4) independent outputs would be available from the computer as command signals to the actuator servos. Digital system design constraints may dictate some variation in this assumption but will not significantly affect the downstream control system mechanization.

Control system design philosophy. - The design philosophy adopted was the provision of a two (2) fail-operative control system which would permit continued safe

flight and landing (excluding jamming of an actuator output) after any of the following failures:

a) Any single failure such as jamming of an input to a control surface power servo, disconnection or failure of a mechanical element, structural failure of a hydraulic component such as an actuator, control spool housing,or valve.

b) Any combination of failures not shown to be extremely improbable, such as an electrical failure in combination with any single hydraulic failure, any combination of two electrical failures, any combination of two hydraulic failures,or any single mechanical failure in combination with any probable single hydraulic or single electrical failure. With respect to the digital fly-by-wire input control system and that portion of the power servos concerned with the transformation of the electrical input to a mechanical output, a two-fail operate capability with no degradation in the system performance will be provided.

The definition of a continued safe flight and landing is such that the aircraft should possess flying qualities sufficient to permit safe control, although pilot workload may exceed specification limits or mission effectiveness may be degraded, or both. This may be Level 3 as defined in Reference 10 and Reference 12 or Level 4 as defined in the proposed revision (D) of MIL-F-9490.

Control surface servo trade study. - In order to conduct an in-depth trade study involving a detailed comparison of the various servo mechanisms possible, reliability requirements for the ACT airplane such as the Mean Time Between Non-Critical Failures and the Mean Time Between Catastrophic Failures must be known. It has, however, been possible to evaluate the merits of various proposed or existing servo designs without knowledge of these values.

Based on considerations relating to the two fail operate criterion of the ACT airplane as well as the objective of minimizing weight and hydraulic power, 16 different combinations of redundant design that appear logical and practical were identified in the trade study. The merits of these various combinations of redundancy were evaluated primarily on the basis of the following considerations:

a) Use or non-use of an electric command input actuator.

b) Command summing technique.

c) Mechanical output variable summed.

d) Predicted actuator synchronization.

e) Susceptibility to failure induced transients.

f) Estimated reliability.

g) Estimated feasibility.

h) Failure monitoring provisions internal to servo.

Applying a weighted value scale to each of these considerations, the concept receiving the greatest number of points and shown schematically in Figure 27 involves the use of an electrical command actuator consisting of four separate active command channels operating in parallel through individual detents to drive a dual tandem power control valve by means of a common output. The power control valve in turn controls two separate single hydraulic system power actuators which drive the control surface. A salient feature of this concept is that each channel within the electric command actuator and the final power output stage of the servo uses mechanical feedback. It is anticipated that the rudder and horizontal stabilizer servos will be identical in concept to the trailing edge surface servos.

Impact on aircraft systems. - The initial estimate of the wing trailing edge surface servo hydraulic demand indicated a level significantly higher than that available with existing hydraulic system of the Model 1329-6A JetStar. Consequently, efforts have been made throughout the study to reduce the flow demand. These efforts have been successful in producing significant reductions in the flow demand because of:

a) Revision of trailing edge surface geometry.

b) Refinement of the computer program input data; e.g., the use of a loaded actuation rate at the design point of 0.698 rads/sec (40 degs/sec) (trailing edge) instead of the 1.05 rads/sec (60 degs/sec) rate originally used.

c) Improved accuracy of the hinge moment data used to size the actuators.

Based on the requirements for an actuation rate of 0.698 rads/sec (40 degs/sec) trailing edge down, a no-load rate of approximately 1.05 rads/sec (60 degs/sec) is produced. Using this rate for the trailing edge surface servos and estimating the flow rate for the horizontal stabilizer and rudder servos, requires a total demand from each hydraulic system of approximately 71.92 liters/minute (19 gallons/minute).

The adaptation of a digital fly-by-wire input control system to the ACT airplane will have a minimal impact on the electrical power generation system of the airplane, but a major impact on the hydraulic power generation system since each inboard engine of the Model 1329-6A JetStar powers separate hydraulic systems through the use of single hydraulic pumps. As the ACT airplane will require four separate hydraulic systems, each of the four engines will power individual hydraulic systems. In addition to the pump

mountings on the inboard engines, pump pads already exist on each of the outboard engines and no problem in modifying the engine installation for the additonal pumps is envisioned. The existing pump pads are also capable of accommodating larger pumps.

INTERMEDIATE CONFIGURATION DEFINITION

Parametric Analysis

The Intermediate Configuration is defined as an aircraft with a supercritical wing, optimized for minimum fuel flow and satisfactory ride qualities but with no active control system. The feasible range of wing aspect ratios is thus somewhat lower than for that of the ACT airplane configuration.

A parametric study was performed to determine the sensitivity of the primary variables of aspect ratio, wing sweep, and cruise lift coefficient on airplane size and performance. The candidate configurations assumed supercritical wing aerodynamics, Model 1329-6A JetStar fuselages and nacelles, and were matched to give the Model 1329-6A JetStar cruise segment range of 3426.2 kilometers (1850 nautical miles). Examples of typical variations in the mission fuel requirement and operating weight empty are shown in Figure 28. The initial cruise altitude for the AR = 6 configuration is 11,290 meters (37,000 feet). For lower aspect ratio cases, the increase in induced drag forces the initial cruise altitude down to 10,980 meters (36,000 feet) and 10,360 meters (34,000 feet) for aspect ratios of 5 and 4, respectively. Mission fuel is seen to decrease substantially with aspect ratio and cruise lift coefficient due to improvements in lift/drag ratio. Sizing of the wing, as a function of aspect ratio and cruise lift to achieve the range requirement, is reflected in the total operating weight data in the lower carpet.

Selection Procedure

The selection of this configuration is heavily dependent on matching the ride quality of the basic Model 1329-6A JetStar. The criterion used in this study is the Ride Discomfort Index, or RDI, proposed in MIL-F-9490D. This index is shown to be approximately proportional to wing lift-curve slope divided by wing loading. In order to satisfy ride quality requirements, it will be seen that the Intermediate Configuration must have a relatively low aspect ratio wing with a moderate sweep angle in order to reduce the lift-curve slope and gust sensitivity. Analysis of the Model 1329-6A JetStar ride qualities indicated that the highest value of RDI occurs in the high speed descent condition at M = 0.394. This gives an index of 0.320. Corresponding values of RDI for the candidate configurations were obtained from the following relationships:

$$(RDI)_{Int} = \frac{0.32 \times (C_{L_\alpha} \,/\, W/S)_{Int}}{(C_{L_\alpha} \,/\, W/S)_{J/S}} \qquad (1)$$

Carpet plots of RDI for a series of aircraft are shown in Figure 29 for wing sweep angles at the quarter chord of 0.122 rads (7 degs) and 0.524 rads (30 degs), respectively. For the 0.524 rads (30 degs) swept case, it is seen that a range of configurations from AR = 4, $C_{L_{CR}}$ = 0.337 to AR = 6, $C_{L_{CR}}$ = 0.392 could provide ride qualities equal to or better than the Model 1329-6A JetStar.

The selection of the final configuration was determined from the data of Figure 30, which shows fuel flow in kilograms per kilometer (pounds per nautical mile) for the candidate configurations together with three boundary constraints superimposed. Because of moderate wing area requirements for this aircraft, a fuel volume capability limitation is included and the practical design constraints imposed by the wing structure are shown. These boundaries result in a fairly narrow band of possible configurations.

The selected aircraft has an aspect ratio of 5.0, quarter chord wing sweep of 0.524 rads (30 degs), and cruises at a lift coefficient of approximately 0.38. The wing thickness/chord ratio is 16% at the MAC. The fuel consumption for the selected airplane is seen to be 12% lower than that for the Model 1329-6A JetStar.

High Lift Data

As noted in preceding sections, maximum lift capability was based on the use of a plain, full-span trailing edge surface and no wing leading edge devices. For the Intermediate Configuration, a three-segment flap system was chosen. The two outboard segments occupy 25% of the chord and extend spanwise 35% and 30% semispan, respectively. The inboard segment of 20% semispan was reduced to a constant, normal chord of 0.609 meters (24 inches) to comply with clearance requirements of the landing gear stowage area in the wing. This resulted in an average chord for the inboard flap segment of 16.5%.

Using equation (A7) of Appendix A, the following values of full scale $C_{L_{MAX}}$ were calculated for a wing sweep angle of 0.524 rads (30 degs), assuming $\Delta C_{L_{MAX}}{}_{AR} = -0.1$ for AR = 5

Flap Angle	$C_{L_{MAX}}$
δ_f = 0 rad (0 deg)	1.33
δ_f = 0.0874 rads (5 degs) (all segments)	1.50
δ_f = 0.1748 rads (10 degs) (all segments)	1.73

These data indicate that a take-off flap setting of 0.0874 rads (5 degs) and a landing value of 0.175 rads (10 degs) are sufficient to match the airfield performance of the Model 1329-6A JetStar.

The drag polars for the low speed, high lift condition were developed using the methods outlined under Appendix A. Figure 31 presents drag polars for the clean airplane and for flap angles of $\delta_f = 0.0874$ rads (5 degs) (take-off) and $\delta_f = 0.175$ rads (10 degs) (approach-landing, gear down). The principal benefit resulting from use of low flap angles is in the climb gradient improvement leading to lower noise levels. Details of noise profiles are given in the ACT Benefit Analysis. For the purposes of calculating noise comparisons with the Model 1329-6A JetStar, lift/drag ratios are required at the specified FAR Part 36 conditions. For climb-out, at $1.2\ V_{Stall}$, L/D = 8.70 and approach at $1.3\ V_{Stall}$ + 18.54 kilometers/hour (10 knots), L/D = 7.88.

Design Integration

The general arrangement for the Intermediate Configuration is illustrated in Figure 32. The aircraft is a modified Model 1329-6A JetStar featuring a reduced area, 0.524 rads (30 degs) swept wing, with a supercritical airfoil. The aircraft retains the Model 1329-6A JetStar empennage and control system.

The Model 1329-6A JetStar fuselage is utilized for the design and is modified only in the area of the wing attachment. The primary modification of the fuselage structure is the replacement of the lower segments of the five mainframes in a manner similar to that previously described for the Active Control Configuration.

The wing selected for the Intermediate Configuration is 45.52 square meters (490 square feet) in area, has an aspect ratio 5, a quarter chord sweep of 0.524 rads (30 degs), and a taper ratio of 0.30. This wing, as illustrated in Figure 33, features a supercritical airfoil and an extended leading edge. Trailing edge flaps are of the simple hinged type with a conventional method of operation.

Weight Summary

The weight summary for the Intermediate Configuration is shown on Table VIII.

TABLE VIII
INTERMEDIATE CONFIGURATION WEIGHT SUMMARY

Component	Weight Kilograms	Weight Pounds
Wing	1659.7	3659
Horizontal	230.0	507
Vertical	169.2	373
Fuselage	1694.6	3736
Nose Ldg Gear	99.8	220
Main Ldg Gear	390.5	861
Nacelle - Pylon	485.8	1071
Propulsion	1701.0	3750
Surface Controls	425.9	939
Instruments	49.0	108
Hydraulics	153.3	338
Electrical	816.5	1800
Avionics	447.7	987
Furnishings	992.5	2188
Air Conditioning	275.8	608
Aux Gear	4.1	9
Weight Empty	9595.2	21154
Operating Equip.	501.2	1105
OWE	10096.5	22259
Fuel	7058.8	15562
Gross Weight	17155.2	37821

ALTERNATE CONFIGURATION DEFINITION

The Alternate Configuration was evaluated on a basis similar to that of the Intermediate Configuration to provide a direct comparison of the benefits derived by the use of a composite filamentary material for the wing structure. The basis of the composite wing structural design is taken from the data of the NASA-ATT study (Reference 13). In this study candidate materials were compared on the basis of weight and cost for specific applications to the airframe structure. Selections were made for three levels of advanced material application on the basis of cost per pound of weight saved compared to conventional aluminum structure. These were:

i) Maximum level - utilizing the maximum amount of composite materials to obtain the minimum weight.

ii) Intermediate level - utilizing approximately 60% by weight of composite materials.

iii) Minimum level - utilizing approximately 40% by weight of composite materials.

Technology factors were computed for the three levels of application for wing, fuselage, and empennage by substituting different materials and structural concepts and computing the weight of structural elements for identical structural requirements.

The component weights used in the analysis included non-optimum factors for joints, splices, and seals, and the calculated base weights for the composite structures were increased approximately 25% to allow for lightning protection and additional weight in joints. Composite material component costs were estimated using statistical production data for large aircraft and experience on the C-5A composite slats, together with material projected costs.

The weight technology factors were then used in the weight equations to parametrically size the airplanes of that study. The direct operating costs were computed and an economic analysis of each airplane conducted to determine the Return-On-Investment. The results of the study showed that a 60% utilization rate was the most economical. The weight technology factor for a wing structure for 60% utilization of composite materials was found to be 0.635.

Parametric Analysis

The Alternate Configuration was evaluated on a basis similar to that of the Intermediate Configuration to provide a direct comparison of the benefits derived by the use of a composite materials wing structure. Parametric studies for a range of aspect ratios and cruise lift coefficients were conducted, and the results are shown in Figure 34. Reductions in OWE, relative to the Intermediate Configuration, and due to the use of composite materials, are indicated in the data. As shown by Figure 34, the OWE values for this configuration are approximately 5% less than the corresponding data for the Intermediate Configuration. The selection of the optimum Alternate Configuration is made from the fuel flow data of Figure 35. A reduction in wing loading due to the lighter wing structure produces slightly higher values of the Ride Discomfort Index and results in a smaller range of acceptable configurations as shown on Figure 35. The intercept of the maximum fuel volume capability line and the spar intercept boundary produces a selected configuration having an aspect ratio of 5.5 and a cruise lift coefficient of 0.409.

Design Integration

The general arrangement for the Alternate Configuration is illustrated in Figure 36. The aircraft is a modified Model 1329-6A JetStar featuring a reduced area, 0.524 rads (30 degs) swept wing with a supercritical airfoil and a wing constructed from composite filamentary materials. The aircraft retains the Model 1329-6A empennage and system of control.

The Model 1329-6A JetStar fuselage is utilized for the design and is modified only in the area of the wing attachment. The primary modification of the fuselage structure is the replacement of the lower segments of the five mainframes in a manner similar to that previously described for the ACT Configuration.

The wing selected for the Alternate Configuration is 44.22 square meters (476 square feet) in area, has an aspect ratio of 5.5, a quarter chord sweep of 0.524 rads (30 degs), and a taper ratio of 0.30. This wing, illustrated in Figure 37, features a supercritical airfoil and an extended leading edge. Trailing edge flaps are of the simple hinge type with conventional methods of operation. The primary box structure consists of upper and lower surface panels, spars, ribs, and fittings. A typical surface panel is a bonded assembly of graphite-epoxy composite skins, graphite-epoxy composite moulded stringers, shear clips, and composite reinforced titanium spar caps. The inboard portion of each panel terminates in a titanium doubler embedded into the composite structure. Spars are of a bonded stiffened web type construction comprised of graphite-epoxy composite webs with moulded graphite-epoxy composite stiffeners and composite reinforced titanium spar caps. Ribs are of moulded graphite-epoxy composite truss type construction. Bulkheads are of graphite-epoxy composite stiffened web type construction. The inboard end of each box is provided with five adapter fittings which serve to transfer the load from the skins to the fuselage frames. The landing gear support structure is comprised of an auxiliary spar and bracing riblets. The auxiliary spar is a bonded assembly of composite webs and moulded composite stiffeners. Titanium fittings

are bonded to the structure for the support of the landing gear trunnion and retracting mechanism. Bracing riblets are of moulded composite construction. Fixed trailing edges and wing tips are of conventional aluminum construction.

Weight Summary

The weight summary for the Alternate Configuration is shown on Table IX.

TABLE IX
ALTERNATE CONFIGURATION WEIGHT SUMMARY

Component	Weight Kilograms	Pounds
Wing	1002.0	2209
Horizontal	230.0	507
Vertical	169.2	373
Fuselage	1694.6	3736
Nose Ldg Gear	99.8	220
Main Ldg Gear	390.5	861
Nacelle - Pylon	485.8	1071
Propulsion	1686.0	3717
Surface Controls	425.9	939
Instruments	49.0	108
Hydraulics	153.3	338
Electrical	816.5	1800
Avionics	447.7	987
Furnishings	992.5	2188
Air Conditioning	275.8	608
Aux Gear	4.1	9
Weight Empty	8786.5	19371
Operating Equip.	501.2	1105
OWE	9451.0	20836
Fuel	6461.8	14246
Gross Weight	15912.8	35082

Performance

Since the selected Alternate Configuration wing was very similar to the Intermediate Configuration wing geometry, no significant differences in $C_{L_{MAX}}$ of the clean wing were recognized. Structural design considerations did, however, limit the chord of the inboard flap segment to 0.381 meters (15 inches) compared with 0.610 meters (24 inches) for the Intermediate Configuration. The estimated maximum lift values for this configuration are shown in Table X.

TABLE X

ALTERNATE CONFIGURATION MAXIMUM LIFT COEFFICIENT - $C_{L_{MAX}}$

Flap Angle	$C_{L_{MAX}}$
δ_f = 0 rad (0 deg)	1.28
δ_f = 0.087 rads (5 degs)	1.45
δ_f = 0.175 rads (10 degs)	1.68

No further performance data were evaluated for this configuration.

ACTIVE CONTROL TECHNOLOGY BENEFIT ANALYSIS

Ride Qualities

The definitions for ride quality for the study configuration have been discussed in preceding sections, especially with regard to the selection of the Intermediate Configuration with no ACT system. In summation, the criterion of matching or improving the Ride Discomfort Index of the Model 1329-6A JetStar has been satisfied for the study configuration and a comparison of the following values of RDI for a high speed descent case are shown in Table XI.

TABLE XI

COMPARISON OF RDI

	RDI
Model 1329-6A JetStar	0.32
ACT Configuration	0.206
Intermediate Configuration	0.32
Alternate Configuration	0.32

It is concluded that the application of active controls leads to a direct improvement in the Ride Discomfort Index from a value of 0.32 for the Intermediate Configuration to 0.206 for the ACT Configuration.

Community Noise Reduction

The basic performance parameters which influence the noise profile evaluation under FAR Part 36 rules are summarized on Figure 38. Substantial improvement in L/D is obtained for the ACT Configuration through use of active controls as a result of the high aspect ratio wing. This leads to an improved climb-out gradient for the ACT Configuration and a higher altitude for cutback power to a 4% climb gradient. In the approach phase, improved L/D allows a decreased thrust level on a 0.052 rads (3 degs) glideslope. Incremental noise levels relative to the Model 1329-6A JetStar with P&W JT 12D-6 engines were calculated from flyover noise test data reported in Reference 14. Figure 39 shows a noise profile comparison for the JetStar and study configurations. For the climb profile the ACT Configuration achieves a cutback altitude of 866.24 meters (2,842 feet) compared with 463.3 meters (1,520 feet) for both the Model 1329-6A JetStar and Intermediate Configurations. The direct benefits of the ACT system on noise levels are seen to be reduction of 8 EPNdB for climb and 6 EPNdB for approach, respectively. The ACT Configuration noise levels of 93 EPNdB and 91 EPNdB for climb and approach comply with FAR Part 36 rules.

Performance Improvement

This section summarizes the performance improvements. The fuel consumption in kgs/km (lb/nm) for each configuration studied is compared to the Model 1329-6A JetStar in Table XII.

TABLE XII

STUDY CONFIGURATIONS FUEL CONSUMPTION COMPARISON

	Kgm/Km	Lb/NM
Model 1329-6A JetStar	1.92	(7.84)
ACT Configuration	1.35	(5.50)
Intermediate Configuration	1.70	(6.93)
Alternate Configuration	1.57	(6.39)

Thus, the relative improvements in fuel economy are:

(1) ACT over Intermediate 21%

(2) Alternate over Intermediate 8%

The data of Table XII differ from the data of Reference 7, inasmuch as fuel consumption rates shown in Table XII relate to the cruise segment of the airplane mission, whereas the data of Reference 7 are based upon the fuel consumption rate for the total mission.

Weight Comparison

A comparison of the weights of the Model 1329-6A JetStar and the Intermediate airplane and of the percentage change in weight for the ACT and Alternate Configurations is shown on Table XIII. A comparison of individual components indicates that the Alternate Configuration experiences a considerable reduction in wing weight relative to the ACT and Intermediate Configurations, and that the ACT Configuration horizontal tail is significantly reduced in weight relative to the Intermediate and Alternate Configurations. Those weight groups of the ACT Configuration which experience considerable weight increase, are all associated with the Active Control System. From the standpoint of take-off gross weight, the Alternate Configuration has a slight weight advantage over the ACT Configuration. The important weight item, the fuel weight, shows a considerable reduction for the ACT Configuration relative to the Alternate and Intermediate Configurations. This improvement is evident when the data of Table XII, Fuel Consumption Comparison, are compared.

TABLE XIII
COMPARISON OF WEIGHTS

COMPONENT	MODEL 1329-6A JetStar		INTERMEDIATE CONFIGURATION		PERCENT WEIGHT CHANGE FROM INTERMEDIATE CONFIGURATION	
	Kg	Lb	Kg	Lb	ACT CONFIGURATION	ALTERNATE CONFIGURATION
Wing	1339.9	2954	1659.7	3659	0	-39.6
Horizontal	230.0	507	230.0	507	-52.5	0
Vertical	169.2	373	169.2	373	0	0
Fuselage	1694.6	3736	1694.6	3736	6.7	0
Nose Landing Gear	99.8	220	99.8	220	0	0
Main Landing Gear	390.5	861	390.5	861	0	0
Nacelle - Pylon	485.8	1071	485.8	1071	0	0
Propulsion	1725.5	3804	1701.0	3750	2.0	-0.88
Surface Controls	425.9	939	425.9	939	9.9	0
Instruments	49.0	108	49.0	108	10.2	0
Hydraulics	153.3	338	153.3	338	10.1	0
Electrical	816.5	1800	816.5	1800	10.0	0
Avionics	447.7	987	447.7	987	10.0	0
Furnishings	992.5	2188	992.5	2188	0	0
Air Conditioning	275.8	608	275.8	608	0	0
Aux Gear	4.1	9	4.1	9	0	0
Wt Empty	9300.0	20503	9595.2	21154	2.3	-8.4
Operating Wt	501.2	1105	501.2	1105	0	0
OWE	9801.2	21608	10096.5	22259	2.1	-6.4
Fuel	7606.7	16770	7058.8	15562	-18.2	-8.5
TOGW	17407.9	38378	17155.2	37821	-6.2	-7.2

BENEFIT PROJECTIONS FOR NEW DESIGNS

The applicability of the results of this study to transport aircraft in general is difficult to assess, but some generalizations are possible.

The results of this study are consistent with other similar studies such as those of Reference 13 which demonstrate that the same benefit from Active Controls Technology can be expected when applied to transport aircraft. These studies show, however, active control usage to be highly configuration sensitive so that it would be erroneous to assume that the magnitude of the benefits obtained in this study is applicable to new transport aircraft design.

In general, the design strategy employed for a new ACT transport would be essentially the same as that employed in this study. This includes wing optimization to satisfy system requirements of fuel volume, ride quality, and stability and control.

Since ride quality criterion is an important design parameter for ACT aircraft, it is clear from this study that a more realistic definition of ride quality criterion is required.

STUDY CONCLUSIONS

It is concluded from this study that the application of Active Controls Technology to the NASA JetStar airplane:

- Significantly reduces fuel consumption without penalizing aircraft performance.
- Reduces community noise levels.
- Improves ride quality.
- Can be achieved by structural modification of the Model 1329-6A JetStar wing/fuselage and empennage/fuselage attachment structures.

No assessment has been made of the total burden attributable to the active controls system for the airplane or of the changes required to the flight station and to the aircraft systems other than that necessary to determine the hydraulic system flow requirement.

The indications from this study are that the active controls system burden will not significantly affect aircraft performance and that the modifications to the airplane in other than the primary structural areas discussed are feasible.

The use of filamentary composite materials for the non-ACT airplane although improving fuel consumption does not show the significant benefits obtained through the use of ACT. The addition of composite filamentary materials to the ACT Configuration, however, will enhance the benefits obtained through the use of Active Controls Technology.

REFERENCES

1. Szalai, Kenneth J.: Flight Test Experience with the F-8 Digital Fly-By-Wire System: A Forecast for ACT. Preprint for Symposium Advanced Control Technology and Its Potential for Future Transport Aircraft (Los Angeles, Calif.), July 9-11, 1974.

2. Jarvis, Calvin R.: An Overview of the F-8 Digital Fly-By-Wire Technology Development Program. Preprint for Symposium Advanced Control Technology and Its Potential for Future Transport Aircraft (Los Angeles, Calif.), July 9-11, 1974.

3. Arnold, James I., and Murphy, Frank B.: B-52 Control Configured Vehicle Flight Test Results. Preprint for Symposium Advanced Control Technology and Its Potential for Future Transport Aircraft (Los Angeles, Calif.), July 9-11, 1974.

4. Hargrove, W. J.: The C-5A Active Lift Distribution Control System. Preprint for Symposium Advanced Control Technology and Its Potential for Future Transport Aircraft (Los Angeles, Calif.), July 9-11, 1974.

5. Anderson, Charles A.: Development of An Active Fly-By-Wire Control System. Preprint for Symposium Advanced Control Technology and Its Potential for Future Transport Aircraft (Los Angeles, Calif.), July 9-11, 1974.

6. Hood, Ray V.: A Summary of the Application of ACT in the Advanced Transport Technology System Studies. Preprint for Symposium Advanced Control Technology and Its Potential for Future Transport Aircraft (Los Angeles, Calif.), July 9-11, 1974.

7. Lange, Roy H. and Deets, Dwain A.: Study of an ACT Demonstrator with Substantial Performance Improvements Using a Redesigned JetStar. Preprint for Symposium Advanced Control Technology and Its Potential for Future Transport Aircraft (Los Angeles), July 9 - 11, 1974.

8. Federal Air Regulations, Part 25.

9. Civil Air Regulations.

10. MIL-F-8785B, "Flying Qualities of Piloted Airplanes".

REFERENCES (Cont'd)

11. MIL-F-9490, General Specification for Flight Control System, Design, Installation, and Test of Piloted Aircraft.

12. MIL-F-83300, "Flying Qualities of Piloted V/STOL Aircraft".

13. Lange, R. H., et al, "Study of the Application of Advanced Technologies to Long Range Transport Aircraft," Lockheed-Georgia, NASA CR 112088.

14. Bolt, Beranek & Newman, Inc., "Exterior Noise from Flight and Ground Operations of the Four Engined Lockheed JetStar," Report 810. 1961.

APPENDIX A

AERODYNAMIC DATA AND DESIGN RATIONALE

Basic Aerodynamic Data

During the early phases of the program, aerodynamic data were evaluated to provide a basis for predicting total aircraft performance, loads, and handling characteristics. Particular attention was paid to the magnitude of wing lift-curve slope, C_{L_α}, and zero-lift pitching moment, C_{M_O}, resulting from the use of high aspect ratio supercritical wings. These parameters were of primary importance in determining wing loads and ride qualities for the ACT configuration.

The wing aerodynamic preliminary design considerations were based on the use of an airfoil section similar to that employed on the U. S. Navy Rockwell T-2C aircraft. Excessive values of negative pitching moment coefficient ($-C_{m_o}$) indicated by these data, due to the high degree of aft camber on the section, led to the use of an alternative supercritical airfoil designed at Lockheed-Georgia. This section had less aft loading capability and consequently lower values of $-C_{m_o}$. The principal characteristics of the airfoil design are:

- Thickness/chord ratio = 0.16
- $M_D = 0.74$ for $0.1 \leq C_L \leq 0.4$
- Minimum drag creep
- Large trailing edge volume

Tests on this airfoil have been completed in the Lockheed-Georgia Company Compressible Flow Facility and some of the principal test data are shown in Figure A1. These test results indicate that the basic force data are sensitive to scale effects. The values of $-C_{m_o}$ with transition fixed, for example, although indicating a favorable trend at high Mach numbers, are unreliable due to an over-fixing of boundary layer transition for the test Reynolds number. This has the effect of reducing the aft loading to levels well below those predicted and subsequently obtained in a high Reynolds number transition free test case. At high Mach number conditions, the values of $-C_{m_o}$ for free transition are considered to be a good indication of the full scale levels, and at low Mach number, the values of $-C_{m_o}$ in the region of -0.04 are approximately 50% of those measured on the T-2C supercritical airfoil. The two-dimensional lift-curve-slope

data for the 16% thickness/chord ratio airfoil are also shown in Figure A1. These indicate that the characteristically large peak values of lift slope are of the order of 50% greater than predicted for conventional airfoil sections by a Prandtl-Glauert type of compressibility rule. The increase results from the development of high lift in the mixed-flow case at cruise Mach numbers, due to aft shock movement and lower surface loading, as seen in Figure A2.

When applied to the ACT Configuration, the airfoil basic thickness distribution was modified to give a thickness/chord ratio of t/c = 12.70% at the wing MAC and the mean camber line was modified to give $C_{L_{DES}} = 0.35$. The reduction in thickness/chord ratio allows the drag-rise Mach number, M_D, to increase to approximately 0.77, which is compatible with the cruise requirements of the ACT configuration.

Wing Lift-Curve-Slope Prediction

The lift-curve slope for the complete aircraft was estimated by a combination of the following methods:

(a) Two-dimensional airfoil data, corrected for planform effects using Reference A1 applied to the subcritical range of Mach numbers.

(b) Transonic peak effects due to compressibility and shock-induced separation from flight test data for the T-2C supercritical wing aircraft.

An analysis of the T-2C data indicated that the peak value of C_{L_α} occurred at a Mach number 0.03 higher than the drag-rise Mach number of the configuration. This same margin was applied to the ACT study configuration. The increment in C_{L_α} above that value at M_D was based on the ratio $C_{L_\alpha}{}_{PEAK} / C_{L_\alpha}{}_{M_D}$ for the T-2C aircraft, and the resulting values of C_{L_α} for the ACT configuration are presented in Figure A2 with the basic Model 1329-6A JetStar curve shown for comparison.

Parallel studies to determine aerodynamic static loads were made using a discrete element vortex-lattice lifting surface program. The preliminary lift-curve slopes from this analysis were derived from a potential flow method and did not include the large compressibility effect due to mixed flows. These data were corrected to give the same levels of C_{L_α} as presented in Figure A2.

Drag Prediction

This section describes the basic methods and procedures adopted to estimate cruise drag levels for the study configurations. The procedure adopted was to develop drag polars for the airplane in the clean configuration by incremental modifications to the Model 1329-6A JetStar data (Reference A2).

Analytical methods. - The profile drag of the Model 1329-6A JetStar in a trimmed condition is defined as

$$C_{D_{P_{J/S}}} = C_{D_{TRIM_{J/S}}} - \left\{ \frac{C_{L_{A-h}}^2}{\pi ARe} \right\}_{J/S} - \Delta C_{D_{i_{T_{J/S}}}} - C_{L_T} \tan \epsilon_{J/S} - \Delta C_{D_{TANKS}} \quad \text{(A1)}$$

where $C_{D_{P_{J/S}}}$ represents the total configuration profile drag, $\left\{ \frac{C_{L_{A-h}}^2}{\pi ARe} \right\}_{J/S}$ is the wing induced drag at the trimmed condition, $\Delta C_{D_{i_{T_{J/S}}}}$ is the induced drag of the horizontal tail, $C_{L_T} \tan \epsilon_{J/S}$ is the tail lift vector, and $\Delta C_{D_{TANKS}}$ is the drag of the external wing tanks.

The total profile drag of the Model 1329-6A JetStar configuration is expressed as

$$C_{D_{P_{J/S}}} = C_{D_{P_{FUS + NAC}}} + C_{D_{P_{WING_{J/S}}}} + C_{D_{P_{EMP_{J/S}}}} \quad \text{(A2)}$$

The drag build-up of the ACT configuration will include the same fuselage and nacelle components as the Model 1329-6A JetStar. Thus

$$C_{D_{P_{FUS + NAC}}} = \frac{S_{J/S}}{S} \left\{ C_{D_{P_{J/S}}} - C_{D_{P_{WING_{J/S}}}} - C_{D_{P_{EMP_{J/S}}}} \right\} \quad \text{(A3)}$$

where $\frac{S_{J/S}}{S}$ is the ratio of wing areas of the reference airplane and the ACT airplane. Inherent in the value of $C_{D_{P_{FUS + NAC}}}$ are interference and/or separation effects due to wing-fuselage root design, pylon-nacelle installation, and addition of the empennage, which are lift and Mach number dependent, and it is assumed that these factors apply to the ACT configuration. It is recognized that a new wing and wing-fuselage junction design will affect these interference levels. For the purposes of this feasibility study, no attempt has been made to recognize these complex effects.

The total drag of the study configuration is, therefore,

$$C_{D_{ACT}} = C_{D_{P_{FUS+NAC}}} + C_{D_{P_{WING}}} + \frac{C^2_{L_{A-h}}}{\pi ARe} + \Delta C_{D_{TRIM}} + C_{D_{P_{EMP}}} \quad (A4)$$

Model 1329-6A JetStar data. - A set of drag polars for the Model 1329-6A JetStar in the clean configuration trimmed at 25% MAC is shown in Figure A3. These data represent the $C_{D_{TRIM_{J/S}}}$ term in equation (A1). The magnitudes of the tail induced drag $\Delta C_{D_{i_{T_{J/S}}}}$ and tail vector $C_{L_T} \tan \epsilon_{J/S}$ terms were estimated to be small and compensating over the cruise Mach number range or were ignored in the prediction of the $C_{D_{P_{J/S}}}$ term in equation (A1). For wing induced drag, a value of 0.90 was assumed for the span efficiency factor. Figure A4 presents incremental external wing tank drag as a function of Mach number and lift coefficient. These data were obtained from wind tunnel tests reported in Reference A3.

The drag-rise characteristics of the Model 1329-6A JetStar, complete aircraft configuration and the wing-fuselage combination only, are shown on Figure A5. Performance data from Reference A4 indicate that the optimum long-range cruise speed of the airplane is M = 0.76. The value of M_D for the wing-body combination estimated by means of the empirical method and correlated with the data of Reference A4 is M = 0.784. The external tanks on the Model 1329-6A JetStar contribute large compressibility effects to the drag-rise characteristics of the complete configuration and since the external tanks are deleted from the ACT airplane configuration, matching of the cruise Mach number is accomplished by using the wing-body value of M = 0.784. The residual effects due to pylons and nacelles are assumed to be the same as those for the Model 1329-6A JetStar.

Drag estimation of study configurations. - The wing profile drag, $C_{D_{P_{WING}}}$, was calculated from

$$C_{D_{P_{WING}}} = C_f \times (SF) \times \frac{S_{WET}}{S} \quad (A5)$$

where the values of flat plate skin friction coefficient, C_f, for fully turbulent flow at cruise Reynolds number were obtained from Reference A5. The shape factor (SF), calculated from a modified form of the Hoerner equation, based on Lockheed-Georgia Company studies, is expressed as follows:

$$SF = 1 + 2.7\,(t/c) + 100\,(t/c)^4 \qquad (A6)$$

For induced drag a value of span efficiency factor of 0.95 was used.

Trim drag. - The tail-off pitching moment characteristics for a center of gravity location of 25% of the MAC from the Model 1329-6A JetStar (Reference A6) indicate a slightly favorable trend with respect to trim drag, due to a small positive residual pitching moment at cruise lift coefficient. By comparison, the supercritical wings of the study configurations exhibit negative pitching moment characteristics ($-C_{m_o}$) as discussed in this Appendix under "Basic aerodynamic data."

The trim drag levels for the study configurations were assessed by correcting the supercritical wing data for the effects of finite wing span and reduced by camber to achieve the design lift coefficient. The value of negative pitching moment ($-C_{m_o}$) due to the wing so obtained was then applied to the fuselage and nacelle estimates generated by the vortex-lattice program and used to develop the complete tail-off pitching moment characteristics for various candidate configurations. A typical example of the level of pitching moment resulting, over a Mach number range from 0.20 to 0.78, is given in Figure A6 for a configuration with a wing aspect ratio of 8.0. These data indicate that for a cruise lift coefficient of about 0.40 at cruise Mach number, the trim drag penalty is of the order $C_D = 0.0007$.

The expected reduction in the size of the horizontal and vertical stabilizers for the ACT configuration is estimated to result in a profile drag reduction of the order of $C_D = 0.0008$. The cruise drag of the ACT configuration is estimated to be slightly conservative when both the trim and reduced empennage drag size components are excluded from the total.

High Lift Data

In accordance with the criteria for matching or improving airfield performance of the Model 1329-6A JetStar, it was estimated that the requirement on maximum lift coefficient of the study configuration would be small, as use of the supercritical airfoil section provides values of $C_{L_{MAX}}$ considerably higher than those of the clean wing values for the Model 1329-6A JetStar. The high $C_{L_{MAX}}$ capability of a supercritical wing has been demonstrated in the U. S. Navy-Rockwell program on the T-2C aircraft. Emphasis, in the study, was given to achieving similar takeoff and landing field lengths as the Model 1329-6A JetStar, and the maximizing of lift/drag ratios in climb-out and approach as an aid to demonstrating noise profile reductions. Because of the available $C_{L_{MAX}}$ of the clean wing, the field performance requirements can be met by the use of a simple hinged, plain trailing edge flap at little or no deflection and without the use of leading edge devices. To obtain compatibility with the active control gust

alleviation requirements, full span segmented flaps were considered desirable. This feature is beneficial to the high lift system performance, since full span uniform deflections can be utilized without penalizing wing span efficiency through distortion of the span load distributions.

Test Data And Methods

Figure A7 presents basic two-dimensional section data for the Lockheed-Georgia supercritical airfoil section design obtained from tests in the Compressible Flow Facility. The full scale value of $C_{L_{MAX}}$ was calculated by using the equation:

$$C_{L_{MAX}} = 1.15 \left[0.95\, C_{l_{MAX}} \cos \Lambda_{\bar{c}/4} + \Delta C_{L_{MAX_{AR}}} + \Delta C_{L_{MAX_{FLAP}}} \right] \quad (A7)$$

Equation (A7) represents an empirical estimation procedure for full scale $C_{L_{MAX}}$. There is, however, a substantial amount of analytical and test data available to validate this approach. The estimate of the finite wing $C_{L_{MAX}}$ is obtained through application of three corrections: a factor of 0.95, a sweep correction of $\cos \Lambda_{\bar{c}/4}$, and an aspect ratio correction, $\Delta C_{L_{MAX_{AR}}}$. The value 0.95 represents the reduction in infinite wing maximum lift capability due to finite wing effects for high aspect ratio planforms ($AR \geq 8$). This is based on studies of optimum wing configuration designs through a spanwise strip analysis technique, comparing maximum section lift available and section load capability at high angles of attack near stall. In addition to this, the aspect ratio correction $\Delta C_{L_{MAX_{AR}}}$ is included for low aspect ratio cases, based on information given in Reference A7. The sweep factor, $\cos \Lambda_{\bar{c}/4}$, is based on test data for large leading edge radii sections with trailing edge separation characteristics (Reference A8). Flap incremental data, $\Delta C_{L_{MAX_{FLAP}}}$, are estimated using the charts given in References A1 and A7.

The factor 1.15 given in equation (A7) represents a combined scale effect, due to differences in the data base Reynolds number and full scale values, and a correction for overshoot in an FAR stall, defined as the minimum speed attained in a -1.852 kms/sec^2 (-1 kt/sec) entry rate. Analysis of flight test data for several transport aircraft indicates that the overshoot effect is of the order of an 8% correction to the 1 'g' condition. The Reynolds number effect is a conservative estimate for wings with no leading edge devices. Total values of $C_{L_{STALL_{FAR}}}/C_{L_{MAX_{WT}}}$ are shown in Figure A8 for a number of transport aircraft.

The drag estimation procedure for the low speed, high lift condition was based on the following:

(i) Clean wing low speed drag polar using the method described under "Drag prediction."

(ii) Drag at $C_L > 0.9$ based on the factor

$$(C_D/C_L^2)_{C_L > 0.9} \Big/ (C_D/C_L^2)_{C_L < 0.9}$$

for the Model 1329-6A JetStar.

(iii) Plain flap minimum profile drag and part-span factors from Reference A7.

(iv) Lift-dependent profile drag from Reference A9 modified for a selection of low flap angles.

No part-span induced drag effects due to flaps were included, since all take-off and landing conditions are assumed to be met with all flap segments set at a constant angle.

For the approach and landing condition, gear drag increments were taken from the Model 1329-6A JetStar data presented in Reference A4.

Basic Data For Structural Loads

The data for structural loads were developed through the use of a discrete element, vortex-lattice computer program. The airplane is modelled using 108 panels per side, 90 of which define the wing. Corrections to the program results have been made to account for the effects of viscosity and Mach number on supercritical airfoils.

The tail-off lift and pitching moment characteristics for a configuration having a wing of aspect ratio 8.0 are presented on Figure A9. The wing alone lift and pitching moment characteristics are shown in Figures A10 and A11, respectively. Spanwise load distributions were developed for this wing at Mach 0.78, the Mach number of specific interest for structural loads. The basic and additional lift distributions are shown in Figures A12 and A13, respectively. Wing spanwise aerodynamic centers are given in Figure A14, and Figure 15 presents the basic pitching moment distribution.

Flap effectiveness factors were generated for the aspect ratio 8.0 wing assuming that all the flap panels outboard of the wing break have identical movement. Flap geometry is defined in Figure A16. No data are presented for the inboard flap since that flap is not considered a part of the primary control system. The effect of flap deflection on lift and pitching moment is shown in Figure A17 and the incremental spanwise load distributions due to flap deflection are shown on Figure A18.

Estimated flap hinge moment coefficients, which are approximate for all flaps when proper volume parameters are used, are given in Figure A19. In addition, wing spanwise load distributions have been generated for a wing of aspect ratio 9.0 having the T-2C supercritical airfoil. These data, with corrections applied to account for the differences in camber line, and for viscosity and Mach number effects of the supercritical airfoil, are used in the structural analyses. The spanwise load distributions at angles of attack of 0 rad (0 deg) and 0.105 rads (6 degs) and a Mach number of 0.8 are presented in Figures A20 and A21. Incremental load distributions due to flap deflections are shown in Figures A22 through A29. Flap effectiveness is shown in Figure A30. The flap data contained in Figures A22 through A30 must be corrected for viscosity effects by multiplying by 0.85, a correlation factor developed from previous programs.

Longitudinal Characteristics

Lift and pitching moment data for a complete airplane are presented in Figure A31 for a configuration using the Model 1329-6A JetStar horizontal tail. Comparisons of lift and pitching moment characteristics between this ACT airplane and the Model 1329-6A JetStar are shown in Figures A32 and A33. Application of the ACT wing will enable the aircraft to cruise in a level attitude rather than at the nose-up angle of attack of the Model 1329-6A JetStar.

APPENDIX B

STRUCTURAL LOADS ANALYSIS FOR THE ACT CONFIGURATION

Selection Of Flight Condition

The selection of the flight condition required an initial estimation of the discrete upgust loads along the V_c - altitude line. This estimation showed that the 6100 meters (20,000 feet) corner occurred close to the Mach number at which the C_{L_α} curve for the supercritical wing was predicted to reach its peak, and also close to the peak gust acceleration given by the approximate method of FAR Part 25. This condition, shown on Figure B1, was therefore selected as the basic flight condition for the gust loads survey. A rigid, steady 2.5g pull-up condition was also examined and found to confirm the fact that, with the increased C_{L_α} of the supercritical wing, the maneuver loads were not significant when compared to the gust loads.

One outcome of this selection was the realization that the increased C_{m_o} of the supercritical wing was causing such a large increase in the tail down load in the level flight, with a correspondingly increased up-load on the wing, that the resulting 1g root bending moment for the supercritical wing was greater than the 2.5g bending moment of the Model 1329-6A JetStar wing. A modification to the wing section was therefore incorporated to reduce the value of C_{m_o} to half the original value, and this value was used during the execution of the remainder of the study.

Wing Weight Analysis

Wing loads survey. - Wing lift distribution data were obtained for several Mach numbers, for two angles of attack with flaps neutral, and with flaps deflected. All other data were obtained from the Model 1329-6A JetStar data (Reference A4) by superimposing the ACT wings on the original body, nacelles, and tail.

A reduction of computation time was achieved by the use of the rigid response program (MCRES) which employs normalized bending, shear, and torsion coefficients expressed in terms of the total lift or pitching moment due to each variable. Values of these coefficients were calculated for four key stations on the wing, with the elastic axis assumed to coincide with the 38.5 percent generator of the outer wing.

Wing weight derivation. - A two phase structural study of a baseline airplane configuration was conducted to provide data from which wing weight for a wing structure having active controls incorporated could be derived. The definition of the wing of the baseline configuration obtained from preliminary performance analyses was:

Area	54.997 square meters (592 square feet)
Aspect ratio	9.0
Thickness chord ratio at MAC - 12.75%	
Sweep at wing quarter chord - 0.113 rads (6.5 degs)	
Taper ratio	0.3

The active controls of this wing comprising the trailing edge consisted of five (5) spanwise segments hinged along the 75% chord generator of the wing.

The first phase of this study used a Lockheed-Georgia Company developed computer program (MCRES) to derive the rigid gust response with a variety of control system parameters. The results of this study were used to assess the relative sensitivity of the peak loads to variations in the input parameters and, hence, to limit the range of the second phase.

The second phase of this study also used a Lockheed-Georgia Company computer program, identified as PADS, to derive the response of the flexible aircraft with control system parameters initially chosen from the first phase results, and then adjusted to determine whether changes would improve the loads.

Wing weight estimation. - Wing weight data were first estimated, using a Lockheed-Georgia Company weight prediction program, with the initial assumption that the root bending moment was approximately equal to that of the Model 1329-6A JetStar, 0.51×10^6 N•m (4.5×10^6 lb in).

When analyzed, the low weight of the baseline configuration wing from this approach was found to be incompatible with the values of bending moment. By iterating root bending moment, wing weight, and stiffness, a matching condition was determined at a nominal value of root bending moment of 1.0×10^6 N•m (9.0×10^6 lb in).

The zero usable fuel condition, with a payload of 930 kg (2050 lb) at a forward center of gravity location, was selected for this part of the loads study.

The gust condition assumed for the parametric study was the "standard" FAR Part 25 discrete gust of 15.24 m/s (50 fps) EAS amplitude, of 25 chords length, and with a (1-cosine) profile. At the chosen flight condition, the true airspeed was 247 m/s (810 fps), and the gust duration was 0.274 secs with a mean chord of 2.71 m (8.9 ft).

Rigid Loads Study

Rigid gust loads study. - The conditions examined to determine rigid gust loads are summarized on Table B1.

In order to provide a datum for the assessment of the active controls technology, the first cases investigated were without the active controls. Both up and down gusts were evaluated, and typical time history data of normal acceleration (load factor), angle

TABLE BI SUMMARY OF RIGID GUST CONDITIONS

RIGID

CASE		2400 2500	2505	2410	2355	2412	2356	2357	2415	2510	2511	2509	2514	
GUST VELOCITY		15.2	-15.2	15.2	15.2	15.2	15.2	15.2	-15.2	15.2	-15.2	15.2	-15.2	m/s
		50	-50	50	50	50	50	50	-50	50	-50	50	-50	fps
CONTROL RATE (NO-LOAD)		-	-	1.05	1.05	1.05	1.05	1.05	1.05	0.52	1.57	1.57	1.57	rads/sec
		-	-	60	60	60	60	60	60	30	30	90	90	degs/sec
FLAPS	SENSOR LOC.	-	-	RS	RS	RS	RS	RS	RS	RS	RS	RS	RS	
	TIME CONST.	-	-	1000	5	1	0.5	0.2	1	1	1	1	1	sec
	GAIN	-	-	-.087	-.087	-.087	-.087	-.087	-.087	-.087	-.087	-.087	-.087	rads/g
		-	-	-5	-5	-5	-5	-5	-5	-5	-5	-5	-5	degs/g
ELEVS.	SENSOR LOC.	-	-	NOSE	NOSE	NOSE	NOSE	NOSE	NOSE	NOSE	NOSE	NOSE	NOSE	
	TIME CONST.	-	-	1000	1	1	1	1	1	1	1	1	1	sec
	GAIN	-	-	.056	.087	.087	.087	.087	.087	.087	.087	.087	.087	rads/g
		-	-	3.2	5	5	5	5	5	5	5	5	5	degs/g
N_z AT C.G.		5.13	-3.13	3.06	3.04	3.05	3.05	3.21	-1.98	3.90	-2.48	2.88	-1.57	g
WING ROOT B.M. X 10^{-6}		1.02	-0.36	0.49	0.48	0.48	0.48	0.48	-0.03	0.68	-0.17	0.42	0.08	N•m
		9.04	-3.19	4.32	4.24	4.25	4.26	4.29	-0.23	6.05	-1.47	3.70	0.71	lb in
NOTES		No ACT	No ACT	St Gain		Datum ACT			Datum ACT					

TABLE BI SUMMARY OF RIGID GUST CONDITIONS (CONTINUED)

RIGID

CASE		2442	2443	2436	2437	2438	2439	2800	2801	2820	2821			
GUST VELOCITY		15.2	-15.2	15.2	15.2	15.2	15.2	9.9	9.9	15.2	15.2			m/s
		50	-50	50	50	50	50	32.5	32.5	50	50			fps
CONTROL RATE (NO-LOAD)		1.05	1.05	1.05	1.05	1.05	1.05	-	1.05	-	1.05			rads/sec
		60	60	60	60	60	60	-	60	-	60			degs/sec
FLAPS	SENSOR LOC.	RS	RS	RS	RS	RS	RS	-	RS	-	RS			
	TIME CONST.	0.1	0.1	1	1	1	1	-	1	-	1			sec
	GAIN	-.087	-.087	-.175	-.175	-.175	-.175	-	-.087	-	-.087			rads/g
		-5	-5	-10	-10	-10	-10	-	-5	-	-5			degs/g
ELEVS.	SENSOR LOC.	NOSE	NOSE	NOSE	NOSE	NOSE	NOSE		NOSE		NOSE			
	TIME CONST.	1	1	1	1	1	1	-	1	-	1			sec
	GAIN	.087	.087	.087	.140	.175	.087	-	.087	-	.087			rads/g
		5	5	5	8	10	5	-	5	-	5			degs/g
N_z AT C.G.		3.46	-1.98	2.95	2.92	2.90	2.95	2.95	2.24	2.68	2.16			g
WING ROOT B.M.X10^{-6}		0.52	-0.03	0.45	0.44	0.44	0.45	0.58	0.39	0.49	0.34			N•m
		4.58	-0.23	4.02	3.93	3.88	4.02	5.11	3.41	4.33	2.97			lb in
							Reduced C_{h_o}	No ACT Datum (Max. Alt.)		No ACT Datum (Descent)				

TABLE BI SUMMARY OF RIGID GUST CONDITIONS (CONCLUDED)

RIGID

CASE		2602	2607	2451	2452	2414	2413	2418	2411	3411	2416 2501	2502		
GUST VELOCITY		7.6	-7.6	15.2	-15.2	15.2	15.2	15.2	15.2	15.2	15.2	-15.2		m/s
		25	-25	50	-50	50	50	50	50	50	50	-50		fps
CONTROL RATE (NO-LOAD)		1.05	1.05	1.05	1.05	1.05	1.05	1.05	1.05	1.05	1.05	1.05		rads/sec
		60	60	60	60	60	60	60	60	60	60	60		degs/sec
FLAPS	SENSOR LOC.	RS	RS	RS	RS	RS	RS	RS	RS	RS	RS	RS		
	TIME CONST.	1	1	1	1	1	1	1	1	1	1	1		
	GAIN	-.087	-.087	-.087	-.087	-.052	-.052	-.052	-.087	-.087	-.087	-.087		rads/g
		-5	-5	-5	-5	-3	-3	-3	-5	-5	-5	-5		degs/g
ELEVS.	SENSOR LOC.	NOSE	NOSE	NOSE	NOSE	NOSE	NOSE	NOSE	NOSE	NOSE	NOSE	NOSE		
	TIME CONST.	1	1	1	1	1	1	1	1	1	1	1		sec
	GAIN	.087	.087	.087	.087	.056	.087	.087	.035	.056	.140	.140		rads/g
		5	5	5	5	3.2	5	5	2	3.2	8	8		degs/g
N_z AT C.G.		1.94	-0.10	3.05	-1.29	3.42	3.41	3.38	3.04	3.06	3.02	-1.96		g
WING ROOT B.M.X 10^{-6}		0.37	0.24	0.48	0.13	0.54	0.54	0.52	0.50	0.49	0.47	-0.02		N·m
		3.31	2.14	4.25	1.16	4.80	4.74	4.65	4.43	4.34	4.25	-0.17		lb in
NOTES				Reduced C_{h_o}										

of attack and root bending moment are shown on Figure B2. It is apparent from these data that the peak loads occur close to the peak gust velocity vector inclination (0.137 secs), and long before any significant response due to pitching motion of the aircraft occurs. This confirmed that the fundamental purpose of the gust load alleviation system should be to destroy the gust-induced lift and not to reduce the induced angle of attack by anticipating the gust and pitching the aircraft.

An initial trial was then performed using simple flap gains of -0.087 rads/g (-5 degs/g), with the signals for each flap taken from accelerometers located on the wing rear spar at the flap mid-spans. A corresponding elevator gain of 0.056 rads/g (3.2 degs/g) was superimposed from signals provided by an accelerometer located in the aircraft nose in order to counteract the pitching moment due to this flap movement. No signal shaping, washout, or lag were used for this trial.

Because of the particular characteristics of the baseline airplane configuration, i.e., a flexible wing and a relatively rigid fuselage, it appeared logical to utilize the ILAF (Identical Location of Accelerometer and Force) concept for the wing. However, it also appeared probable that the acceleration variations at the nose would be less violent than at the tail, and that less coupling between elevator and aircraft would exist with the former, which was later confirmed.

The control surface rate was initially based on a no-load rate of 1.05 rads/sec (60 degs/sec), modified to give an achieved rate 15 percent greater when the required motion was aided by the existing hinge moment, and reduced to a lower value when opposed by the existing hinge moment. The assumed law is shown on Figure B3.

The resulting time histories for the chosen upgust showed that although the angle of attack was essentially unchanged during the passage of the gust (up to T = 0.274 sec), the flap movement was sufficient to reduce the lift substantially thereby reducing the incremental load factor by 50 percent and the wing root bending moment by 77 percent. The greater reduction in bending moment was due to the shift of the lift due to the active flaps (segments 2 through 5) farther outboard.

A washout form of signal shaping was next introduced, to ensure signal decay. Time constants of 5 sec, 1 sec, 0.5 sec, and 0.2 sec were used and indicated that the 1 sec value in conjunction with an elevator gain of 0.087 rads/g (5 degs/g) appeared to be most promising.

A baseline active control system was defined by the following parameters:

Trailing edge surface segments 2-5:

Gain = G_F = -0.087 rads/g (-5 degs/g)

Time constant = T_w = 1 sec (washout)

Sensor location: wing rear spar at mid flap span
Control surface rate = 1.05 rads/sec (60 degs/sec) at no load

Elevators:

Gain = G_E = 0.087 rads/g (5 degs/g)

Time constant = T_w = 1 sec (washout)

Sensor location: nose (3 MACs ahead of 0.25 MAC location)
Control surface rate = 1.05 rads/sec (60 degs/sec) at no load

The effects of this baseline system are shown in Figure B4 for the upgust and downgust.

Variations of the parameters from the datum values were then explored. Changes in the control surface no-load rate gave the biggest changes in loads. The non-linearity of the system, due to the different control surface rates in the up and down directions, was apparent from the time histories for upgusts and downgusts, and led to non-linearity with gust velocity.

The achieved control surface rates were found to be very different in different parts of the response. With the high standing hinge moment on the trailing edge segments in level flight, a rapid upward movement of 1.2 rads/sec (69 degs/sec) could be attained, which permitted substantial alleviation of the peak upgust. However, reversal of this motion occurred at much lower rates, approximately 0.6 rads/sec (35 degs/sec), which resulted in an unduly large negative swing in both load factor and bending moment.

In the downgust case, the required downward control movement was at the lower rate, preventing the development of the full alleviation benefits in the initial peak; the reversed movement, being aided by the standing hinge moment, then gave an unduly large positive swing in bending moment.

It appeared that the incorporation of aerodynamic balance would improve the situation, by permitting the attainment of control surface rates closer to the no-load rate. The load response was therefore calculated with the hinge moment coefficient at zero angle of attack arbitrarily reduced from -0.205 to -0.050, with the hinge moment derivatives due to angle of attack and trailing edge surface deflection left unchanged.

The marked improvement in upgust response, Figure B5, shows that the second positive peak load factor is almost eliminated. In the downgust, the initial alleviation was significantly improved, as was the tendency to over-swing to high positive values of load factor and bending moment.

Overall, the effect was to restore much of the symmetry which was lost due to the different control surface rates in the two directions, and comparison with the corresponding data of Figure B4 reveals the improvement in gust response, particularly with regard to bending moment.

The results of the parametric variations are summarized in Figures B6 through B16. Where not otherwise stated, control system parameters have the datum values as defined

previously. The most notable feature is the relative insensitivity of the load factor and wing root bending moment peak values to all but a few parameters. Control surface rate is the apparent key to the success of the active control system in alleviating gust loads, whether this is expressed as a no-load rate or as an achieved rate in the presence of a standing hinge moment.

The effect of the baseline active controls system on the gust loads was examined also at two other flight conditions. One condition was at $M_C = 0.82$ at 12500 m (41000 ft), and the other at $V_C = 129$ m/s (250 kts) at 1525 m (5000 ft). These conditions corresponded to maximum operating altitude, and to the critical ride quality condition, respectively. Satisfactory gust alleviation, with small control surface angles, was maintained.

Rigid maneuver loads study. - The large number of possible definitions of a pilot-induced checked maneuver implied difficulty in conducting a meaningful comparison. Thus, the response to a step input was chosen as the basis for comparison of the aircraft with and without active controls. The elevator angle was adjusted so that the initial peak load factor was 2.5g. The datum active controls system was used, but variations in the elevator gain were studied. Since this study was for comparative purposes only, the same weight condition was used as for the gust study. The resulting time histories of load factor, angle of attack, flap angle, elevator angle, pitch attitude, and bending moment are shown in Figure B17.

Without the active controls system (as defined for gust alleviation), the response was quickly damped to a "steady" 2.37 g, with -0.0123 rads (-0.707 degs) of elevator deflection, and the peak bending moment of 0.590×10^6 N·m (5.22×10^6 lb in) was almost identical to the steady 2.5g bending moment, and settled down to a "steady" value of 0.566×10^6 N·m (5.01×10^6 lb in). The peak n_z of 2.5g occurred 1.05 secs after initiation of the elevator movement and corresponded to a change in pitch attitude of 0.046 rads (2.64 degs).

With the baseline active controls system, the peak (2.5g) n_z occurred slightly later (at 1.31 secs after initiation), but the pitch response was actually faster, the change in attitude being 0.056 rads (3.21 degs) in 1.05 secs. The bending moment at peak (2.5g) n_z was reduced to 0.42×10^6 N·m (3.72×10^6 lb in), but as the response was slowly divergent, higher values occurred later.

Increasing the elevator gain from 0.087 rads/g (5 degs/g) to 0.139 rads/g (8 degs/g) worsened the divergence, although the initial n_z time history was almost identical to that without the active controls system. The pitch attitude response was more rapid than without the active controls. Reducing the elevator gain to 0.056 rads/g (3.2 degs/g) effectively removed the divergence in load factor, but at the expense of pitch damping, so that an oscillatory angle of attack response occurred. The pitch attitude response was

slower than without the gust alleviation control system. The variations of the first three peak values with elevator gain are shown in Figure B18.

The study showed that leaving the gust alleviation active controls system free to operate during pilot-induced maneuvers would probably cause some impairment of the handling qualities, but that relatively minor adjustments in the control system parameters would probably result in an acceptable compromise.

Summary of rigid loads study. - The high lift-curve slope of the supercritical wing caused gust loads greatly in excess of those of the Model 1329-6A JetStar, and also greatly in excess of the 2.5g maneuver loads, and the incorporation of an active gust alleviation system, comprised of the wing trailing edge surfaces and the horizontal stabilizer elevators, was shown to be a feasible solution, capable of achieving a dramatic reduction in the wing lift due to the discrete design gust.

The peak gust loads were clearly due to the rapid change in direction of the airstream in the gust, and it was shown that the trailing edge surface rates should be high enough for their effect to coincide with the lift build-up due to the gust, so that the gust-induced lift was destroyed. Changes in aircraft response were insignificant during this phase.

The presence of a high standing hinge moment due to the camber shape of the wing tended to limit the achievable trailing edge surface rate on penetration of a downgust, and to limit the rate at which the initial movement of the surfaces could be removed following the upgust penetration. The resultant non-linearity was found to be largely removed by reducing the hinge moment at zero angle of attack through the incorporation of aerodynamic balance.

Selection of the control system gains and time constants was not critically sensitive in terms of the resultant wing root bending moment. A baseline active controls system was selected as a starting point for the flexible loads study, as having:

Trailing edge surface segments 2-5:

Gain = -0.087 rads/g (-5 degs/g)

Time constant = T_w = 1 sec (washout)

Sensor location at wing rear spar, at surface segment mid-span

Elevators:

Gain = 0.087 rads/g (5 degs/g)

Time constant = T_w = 1 sec (washout)

Sensor location at nose (3 MACs ahead of .25 MAC location)

If the gust alleviating system operated full time and reacted to pilot input, some changes to the active controls system constants would be required to prevent divergence in pitch, but these changes would have little effect on the peak gust loads.

Dynamic Loads Study

The conditions analyzed using a Lockheed-Georgia Company flexible wing discrete gust program (PADS) are summarized on Table B11.

A datum for comparison of the benefits of the active controls technology was established by first analyzing both up and down gust conditions without active controls. Time history values for accelerations at three spanwise wing stations, and center-of-gravity vertical and pitch accelerations, together with wing root vertical bending moment are shown in Figures B19 and B20. These data are for a 15.2 m/s (50 fps), 25 chord length discrete gust. At a forward speed of 247 m/s (810 fps) and mean aerodynamic chord of 2.7 m (8.9 ft), the peak gust force on the airplane occurs in 0.137 seconds. It can be seen from Figure B19, that the wing root maximum bending moment of 1.48×10^6 N·m (13.8×10^6 lb in) occurs at 0.18 seconds. The phase lag between the net bending moment and the peak gust loading is primarily due to the dynamic response of the flexible system in which the inertial component of the bending moment contributes to the net bending moment. Comparisons between the rigid and flexible bending moment and center-of-gravity load factor are presented in Figures B21 and B22, and show a dynamic magnification of 1.67 in the peak incremental wing root bending moment.

The datum control system from the rigid analysis was analyzed to determine the interaction of this control system with the flexible aircraft. Compared with the non-active control flexible aircraft values, this system resulted in an initial peak wing root bending moment reduction of 33.5 percent and a center-of-gravity load factor reduction of 26.1 percent. The greater reduction in bending moment was due to the change in the spanwise lift distribution caused by the outboard trailing edge segments. The large over-swing of the bending moment in the downward direction was due to the different control surface rates in the up and down direction. A rapid upward control movement was attained which substantially reduced the peak upgust load. Reversal of the control motion occurred at lower rates, resulting in large negative swings in both wing bending moment and load factor.

The control surface rates were changed to a constant 1.05 rads/sec (60 degs/sec) to obtain more rapid reversal in the control surface motion after passage of the peak, and produced an improvement in the upgust response giving a 33.9 percent reduction in the downward swing in wing root bending moment. The up-bending moment was increased 7.9 percent.

The effect on wing root bending moment of the use of a lag filter only in the trailing edge control system was next investigated. The gains and constant rate limits were the same as those with the washout filter system. The time constants on the control surface lag filters were changed from 1.0 seconds to 0.2 seconds. This system resulted in a wing root bending moment reduction of 28.4 percent and a center-of-gravity load

TABLE BII FLEXIBLE GUST STUDY CONDITIONS

CASE			4000	4007	4012	4009	4008	4001	4004	4005	4006	4010			
CONTROL RATE					1.05	1.05	1.05	1.05	1.05	1.05	1.05	1.05			rads/sec
					60.	60.*	60.*	60.*	60.*	60.	60.	60.			degs/sec
FLAPS		SENSOR LOC.			R.S.	R.S.	R.S.	R.S.	R.S.	R.S.	R.S.	R.S.			
	#2	TIME CONST.			1.0	1.0	.20	.20	.20	.20	.20	.20			sec
		GAIN			.087	.087	.087	.087	.087	.087	.087	.087			rads/g
					5.0	5.0	5.0	5.0	5.0	5.0	5.0	5.0			degs/g
	#3	TIME CONST.			1.0	1.0	.20	.20	.20	.20	.20	.20			sec
		GAIN			.087	.087	.087	.087	.087	.087	.087	.087			rads/g
					5.0	5.0	5.0	5.0	5.0	5.0	5.0	5.0			degs/g
	#4 #5	TIME CONST.			1.0	1.0	.20	.20	.20	.20	.20	.20			sec
		GAIN			.087	.087	.087	.087	.087	.087	.087	.087			rads/g
					5.0	5.0	5.0	5.0	5.0	5.0	5.0	5.0			degs/g
ELEVATORS		SENSOR LOC.			NOSE	NOSE	NOSE	NOSE	NOSE	NOSE	NOSE	NOSE			
		TIME CONST.			1.0	1.0	1.0	1.0	1.0	1.0	1.0	1.0			sec
		GAIN			.087	.056	.056	.056	.056	.056	.056	.056			rads/g
					5.	3.2	3.2	3.2	3.2	3.2	3.2	3.2			sec/g
N_z AT C.G.			6.3	-4.3	4.6	4.9	5.0	4.8	-2.8	4.6	-3.5	3.9			g
WING ROOT B.M.X 10^{-6}			1.5	-.83	.99	1.1	1.1	1.1	-.40	1.0	-.55	.83			N·m
			13.2	-7.3	8.8	9.5	9.4	9.4	-3.5	8.8	-4.8	7.4			lb in
NOTES			No ACT Up Gust	No ACT Down Gust	Rigid Datum	Rigid Datum	Lag Filter	Lag + Wash.	Down Gust	Up Gust	Down Gust	Up Gust			

* Rate Constant with Hinge Moment

factor reduction of 20.5 percent. The system with either a washout filter or a lag filter in the trailing edge surface control system resulted in approximately the same load reduction. The washout filter configuration did require up to 0.52 rads (3 degs) more control surface deflection.

The trailing edge control surface lag and washout filters were then combined into a single control system with gains of 0.087 rads/g (5 degs/g) and constant rate limits of 1.05 rads/sec (60 degs/sec). The time constant used was 0.20 seconds. The elevator gain remained at 0.056 rads/g (3.2 degs/g) with a time constant of 1.0 seconds. Results for this configuration are presented in Figures B23 and B24. This system which resulted in the best overall response for the flexible system, having a wing root bending moment reduction of 28.7 percent, was selected as the datum control system for the flexible aircraft. The comparison of wing root bending moment with the data for no active controls is presented in Figure B25.

The effect of available control surface rate with hinge moment was investigated with the datum system using an allowable rate of 1.22 rads/sec (70 degs/sec) when the required motion is aided by hinge moment and 0.61 rads/sec (35 degs/sec) when opposed by hinge moment. Using this system for the upgust case, the net result was to reduce the initial peak wing root bending moment due to the increased control surface rate. The reduced allowable rate in the downward direction resulted in an increase in the down bending moment for the up and down gust cases. The rates were then increased to 1.83 rads/sec (105 degs/sec) and 0.916 rads/sec (52.5 degs/sec) and the effects investigated.

The results of the variations of the system parameters are summarized in Figures B26 through B31. It is apparent from these data that the bending moment and load factor reduction are relatively insensitive to variations of all the system parameters except trailing edge surface control rate.

Summary of dynamic loads study. - The incorporation of an active control system consisting of trailing edge surface controls and horizontal stabilizer elevators is a feasible system for dynamic gust load alleviation. The control surface rates must be of sufficient magnitude to achieve full benefit as the gust reaches its peak.

The stiffness distribution for the baseline configuration wing provided compatible values of root bending strength and achieved bending moment, so that this wing structure represented one solution for the baseline configuration at aspect ratio 9.0. The resulting wing structure weight, therefore, provided a datum for the relationship between aspect ratio and wing weight with active controls.

The differences between rigid and flexible response were sufficient to suggest that the effects of flexibility must be included in any realistic active controls system analysis.

Flutter Studies

The supercritical airfoil, increased aspect ratio, reduced sweep, and alleviated design loads of the ACT wing combine to increase flutter and divergence criticality relative to that of the Model 1329-6A JetStar wing. Flutter studies were therefore conducted to establish wing preliminary torsional stiffness requirements for flutter and divergence prevention and, thereby, to enhance the validity of the structural analysis and weight predictions.

Flutter and divergence analyses were conducted by means of computer programs developed by the Lockheed-Georgia Company. The flutter program is man-machine interactive and facilitates rapid changes in stiffness, mass, and other important input parameters. The flutter analyses included wing vertical bending and torsion, and fuselage rigid body degrees of freedom. Oscillatory aerodynamic forces and moments were represented by Theodorsen strip theory coefficients, modified to yield the same steady lift-curve-slope and aerodynamic center distributions as were used in the dynamic gust load analyses. These distributions were calculated by compressible lifting surface theory (vortex-lattice) and were adjusted in level to agree with T-2C flight test data. The effects of the active gust load alleviation and stability augmentation systems were not included in these preliminary analyses, but they are not expected to significantly alter the torsional stiffness levels required for flutter prevention.

The flutter and divergence design criteria used during this study are the same as the Model 1329-6A JetStar and are consistent with FAR Part 25 requirements. These criteria state that the airplane should be designed to be free from flutter and divergence at speeds up to 1.2 times the design dive speed. The Model 1329-6A JetStar structural design airspeed envelopes are shown on Figure B32. The required 20 percent flutter safety margin was applied to V_D to yield a required flutter speed of 263 m/sec (510 kts). The constant density wing flutter speed boundary shown in Figure B32 was estimated on the basis of the T-2C wing lift-curve-slope variation with Mach number. The maximum lift-curve slope, and, therefore, the minimum flutter speed, occur at M = 0.8. The flutter design point was selected as the intersection of the 1.2 V_D boundary with M = 0.8, which occurred at a density altitude of 610 meters (2000 feet). All flutter analyses were, therefore, conducted for the Mach number and density conditions associated with the flutter design point, and the wing torsional stiffnesses were adjusted to yield minimum flutter speeds of approximately 1.2 V_D.

Flutter analysis results. - Flutter analyses were conducted for the three wing iterations - the iterations corresponding to wing root bending moments of approximately 0.5×10^6 N·m (4.5×10^6 lb in), 0.7×10^6 N·m (6×10^6 lb in), 1.0×10^6 N·m (9.0×10^6 lb in). The major differences in the iterations occurred only in the levels of mass and stiffness distributions so that the flutter characteristics of each iterated wing were similar. An initial divergence analysis of the wing corresponding to the 0.5×10^6 N·m (4.5×10^6 lb in) root bending moment indicated that the torsional stiffness required for flutter prevention exceeded that required for divergence prevention by

a considerable margin. Thus, no further divergence analyses were conducted. Representative flutter analysis results for the final iteration that correspond to a wing root bending moment of 1.0×10^6 N·m (9×10^6 lb in) are shown in Figures B33 and B34. Variations of frequency and damping with airspeed are shown in Figure B33 for the important symmetric modes at zero fuel. The modes are identified in order of ascending frequency at zero airspeed. Mode 1 consists primarily of wing fundamental symmetric bending and is not shown because of its minor participation in the critical flutter instability. Modes 2 and 3 consist primarily of wing second bending and wing first torsion, respectively. The frequencies of these two modes are seen to coalesce at a frequency of approximately 17 Hz and a speed near the critical flutter speed (the lowest speed at which the damping required for neutral stability g exceeds a value of +0.03). Thus, the critical flutter instability appears to consist principally of wing second bending coupled with wing first torsion.

The effect of fuel mass on the wing flutter speed is shown in Figure B34. The figure depicts a preliminary fuel tank arrangement and a usage sequence in which fuel is maintained in the outboard tanks until all other tanks are exhausted. The symmetric and antisymmetric flutter speeds remain essentially constant until fuel is used from the outboard tanks, at which point they begin to reduce, reaching a minimum at the zero fuel condition. The zero fuel condition is, therefore, established as the most critical condition, and very little difference is shown to exist between the symmetric and antisymmetric flutter characteristics. The flutter frequencies vary from approximately 8.5 Hz at full fuel to 15 Hz at zero fuel. Considerable frequency separation exists between the critical flutter frequency (15 Hz) and the predominant gust response frequency (approximately 5 Hz). Relatively simple filtration of the gust load alleviation feedback signals is, therefore, expected to adequately limit the effect of this system on the critical flutter speeds.

The spanwise distribution of torsional stiffness required for flutter and divergence prevention is shown in Figure B35, together with the available vertical bending stiffness, EI. The torsional stiffness distribution, together with approximate design loads, was used in establishing the preliminary structural design and weight estimate for the baseline airplane configuration wing.

APPENDIX C

DESIGN INTEGRATION

Model 1329-6A JetStar Description

Airplane configuration description. - The Model 1329-6A JetStar, Figure C1, is a four engine, medium range, high speed, pressurized commercial transport with provision for a crew of two, pilot and co-pilot, and a maximum payload equivalent to ten (10) passengers. The airplane is a low wing configuration having a wing area of 50.53 square meters (542 square feet), a sweep angle of 0.523 rads (30 degs) at the wing quarter chord, and an aspect ratio of 5.27. Mission fuel is contained in integral tanks in the wings and in external tanks mounted at approximately the mid-semi-span of each wing.

The airplane is powered by four (4) P&W JT12A-6 engines, each producing 13,344 N (3000 pounds) of static thrust at sea level standard day conditions, and is designed to cruise at an altitude of 12,496.8 meters (41,000 feet) at Mach numbers of 0.78 for long range cruise and 0.82 for maximum cruise speed.

Structural configuration description. - The wing attachment structure in the fuselage consists of five circular frames located as shown in Figure C2. Each circular frame is configured as indicated on Figure C2 and carries fittings for tension type wing attachment bolts. Each circular frame is made up of four segments which are upper and side circular segments and the lower structural carry-through segment. Attachment of the lower segments to the side segments is by means of a fixed location splice as shown in Figure C2.

The main landing gear attachment structure consists of a fixed location pivot point mounted in a triangulated structure formed by the rear spar of the inboard panel of the wing and an auxiliary beam. This arrangement is also illustrated on Figure C2. The geometry of this structure is preserved in order to obviate the need for costly modification to the main landing gears, and the effect of this constraint on wing geometry will be shown in later discussion.

The empennage consists of a single unit conventional type horizontal and vertical stabilizer. The vertical stabilizer is attached to the fuselage structure by means of a pivot joint located at the lower end of the rear spar and by means of twin actuators and a scissors linkage pinned to the lower end of the front spar.

Design Philosophy

The initial objectives and assumptions made for the design study were:

- The conversion to the ACT configuration was to be accomplished with minimum modification to fuselage structure.
- A supercritical airfoil section was to be used.

- The existing main landing gears would be utilized and the present location maintained. No portion of the stowed gear would be permitted to protrude through the wing contour.

- The ACT wing would be located longitudinally so that the quarter chord MAC point would coincide with the Model 1329-6A JetStar quarter chord MAC point; i.e., at fuselage station 477.90.

- The wing would be located vertically so that its lower surface at the root would not project below the existing wing/fuselage fairing contour line.

- A root incidence angle of +0.0175 rads (+1.0 deg) and a dihedral angle of 0.0349 rads (2 degs) were assumed.

- The front spar was assumed to be at 12% and the rear spar at 65% of the basic wing chord.

- Full span trailing edge surfaces, hinged at the 75% chord, were assumed.

- The existing wing/fuselage bolt pattern would be utilized and the fuselage main frames at fuselage stations 410, 430, 450, 470, and 490 would not be changed.

- The inboard portion of the wing would feature an extended leading edge. This extended root chord at buttock line 41.5 would be 1.35 times the basic wing chord.

- The location of the wing break would be determined by the intersection of the inboard rear spar/gear attachment structure and the basic wing 65% chord generator, or by the apex of the gear triangulated structure where the spar intercept occurs at a chordwise location aft of the 65% generator.

- The empennage attachment structure of the Model 1329-6A JetStar in the aft fuselage would be unchanged.

During the course of the design study, it became apparent that the bolt pattern of the wing/fuselage attachment could not be utilized due to the considerable increase in the root bending moment generated by the higher aspect ratio wing and that it would be necessary to redesign the lower segment of each main frame. In order to achieve a deeper frame segment, the restriction on wing lower contour was relaxed to permit the lower surface of the wing root to project beyond the fairing contour line.

Wing geometry matrix and design study. - A design study was conducted using the following matrix in order to ascertain the relationship with the Model 1329-6A JetStar wing/fuselage attachments and main landing gear and to obtain wing fuel capacity. The wing planform matrix consisted of aspect ratios of 8, 9, and 10 and sweep angles of 0 rad (0 deg), 0.175 rads (10 degs), 0.262 rads (15 degs), 0.349 rads (20 degs) for a wing area of 53.88 square meters (580 square feet). Each wing featured a supercritical airfoil section, and the inboard portion of the wing leading edge was extended for aerodynamic reasons and to provide a transitional structure for attachment to the center fuselage main frames. Layouts were generated for each wing from which the structural geometry, space, and fuel volume characteristics were established.

The design study showed that in order to avoid compromising the main landing gear trunnion hinge points, the auxiliary spar and the inboard portion of the rear spar must retain the geometric locations of the Model 1329-6A JetStar.

The effect of sweeping the wing in relation to the fixed geometry of the landing gear and wing location was found to be adverse. At small angles of sweep, the wing/fuselage attachment bolt pattern is located within the contour of the extended chord root section, and sufficient section depth exists at the landing gear pivot to permit stowage of the gear within the wing contour. Adequate space is available behind the rear spar for the installation of the systems and surfaces necessary for active controls. The geometric effects of wing sweep are shown on Figure C3.

Wing final configuration. - A baseline wing of aspect ratio 9.0 was subjected to further study to determine the most practical sweep angle for the wing and to identify geometric or structural problems. As in the initial studies, the auxiliary spar and inboard rear spar locations were retained so that the landing gear trunnion pivot points were not compromised. The intersection of these spars occurs at fuselage station 519.17 and buttock line 102.79, and this point also determines the wing break location. The basic wing quarter chord MAC point is located at fuselage station 477.9. The wing was rotated about this fixed point until the rear spar at 65% chord was aligned with the intersection. The sweep angle, at the quarter chord, thus obtained, was 0.113 rads (6.5 degs). The wing was located vertically so that its lower surface at the root coincided with the wing/fuselage fairing contour of the Model 1329-6A JetStar. It was found necessary to move the origin of the wing dihedral angle from the wing root to the wing break station to prevent the main landing gear trunnion from protruding through the lower surface of the wing. The wing geometry, Figure C4, shows the relationship of the Model 1329-6A JetStar wing/fuselage attachment bolts within the ACT wing root contour. The main landing gear, when retracted, is contained within the wing lower contour; however, the lug provided on the shock absorber strut for the retraction jack does protrude slightly but can be covered by a local fairing on the landing gear door. A space of approximately 0.152 meters (6.0 inches) is available between the auxiliary spar and trailing edge surface leading edge.

The wing box structure which also serves as a fuel tank is bounded by the root and tip ribs and the front and rear spars. A root rib, located 0.127 meters (5 inches) outboard of the wing root, serves as the inboard boundary of the fuel tank and permits a dry bay area for access to the root joint. The front spar is located at 12% of the basic chord for the outer wing and extends inboard from the break to a point 0.093 meters (3.68 inches) forward of fuselage station 410 of the existing Model 1329-6A JetStar. The rear spar follows the existing JetStar location from root to break. The outer wing panel rear spar is located at 65% chord at the break and radiates outward to a point 0.604 meters (23.80 inches) aft of the wing tip leading edge thus departing from the 65% chord generator. This was necessary to allow sufficient space for the active controls actuators in the outer portion of the wing. The existing landing gear retains its location, and the wing has sufficient thickness at this point to enclose the main landing gear struts. The relationship of the wing trailing edge with the existing engine nacelles is shown on Figure 14. The wing is of conventional type structure, manufactured in aluminum and other metallic material.

Fuselage modification. - The primary modification to the fuselage consists of removing the lower segment of the five main frames at fuselage stations 410, 430, 450, 470, and 490 and replacing these with new deeper frame segments. This modification is illustrated in Figure C5. The existing splice, as shown in the figure, between lower and side frame segments is retained. New skins and new longerons are required between fuselage stations 410 and 490. The existing floor between these stations is removed and replaced by a new floor in a slightly higher location. New wing-to-fuselage fillet fairings are required. The new empennage is designed to suit the existing empennage fuselage attachment points, and the fuselage modifications are limited only to the installation of new dorsal fairings and the addition of mounting structure for the rudder actuation system.

Empennage modification. - The modification to the empennage of the ACT Configuration involves a change in the configuration from a mid-span horizontal stabilizer location to a tee-tail configuration together with area reductions for both vertical and horizontal tail surfaces due to the application of ACT. In order to minimize changes to the fuselage attachment structure, the vertical stabilizer theoretical root chord is located on fuselage waterline 100.0, and the front and rear spars are located at 15% and 62% of the vertical stabilizer chord to permit compatibility of the primary box structural attachment to the fuselage. The upper portion of the vertical stabilizer front spar terminates in an actuator attachment fitting, and the lower portion carries fittings which are attached to a fixed bracing structure which replaces the trim actuators and scissors linkage of the Model 1329-6A JetStar. The rear spar of the vertical stabilizer terminates at the upper end in a hinge fitting to which the horizontal stabilizer is attached and at the lower end in a pivot fitting bolted to the existing fuselage structure. A bullet fairing mounted at the junction of the vertical and horizontal stabilizers serves to reduce interference drag and provides space to permit a wide base for the horizontal stabilizer hinge.

The horizontal stabilizer geometry is arranged so that the sweep of the stabilizer 25% chord generator is 0.0 rad (0 deg). Positioning the stabilizer front spar at this location permits the use of a continuous front spar structure across the full span of the

stabilizer. The rear spar is placed at the 65% chord generator and carries the surface hinge at the center box structure.

Intermediate And Alternate Configurations Analysis

A basis of comparison for assessing the benefits of ACT was provided by the development of an Intermediate and an Alternate configuration.

Intermediate configuration definition. - The Intermediate configuration featured a supercritical wing and maintained the performance and ride characteristics of the ACT configuration.

Alternate configuration definition. - The Alternate configuration featured the maximum utilization of filamentary graphite composite materials in the wing structure only in addition to the supercritical wing consideration.

Wing geometric matrix. - A matrix of wing geometry consisting of wing areas of 44.59, 50.17, and 53.88 square meters (480, 540, and 580 square feet); aspect ratios of 4, 6, and 8; and wing sweep angles of 0, 0.262, and 0.524 rads (0, 15 and 30 degs) was investigated to determine wing geometric characteristics and fuel volumes to be applied to the airplane performance matrix to aid in the selection process of each configuration.

Investigation of the geometric characteristics of each wing in the matrix revealed that:

- For all planforms, the fuselage/wing attachments could be enclosed within boundaries of the root contour.
- At aspect ratio 8 and 0.524 rads (30 degs) of sweep, the landing gear location is too close to the wing trailing edge and cannot be contained within the wing contour. At all other aspect ratios and sweeps considered, the gear containment within the wing contour is possible.
- At aspect ratio 8 and 0.524 rads (30 degs) sweep, a 25% chord trailing edge control surface is not attainable due to the location of the rear spar. Reduction of aspect ratio to 6 permits a 25% chord flap outboard of the wing break, but a reduced chord flap is required inboard of the break. Reduction of aspect ratio to 4 permits a 25% chord flap for the full span.
- For wings of 0.262 rads (15 degs) sweep and aspect ratio 8, a 25% chord flap can be attained outboard of the wing break, but a reduced chord flap is required inboard of the break. Reduction of the aspect ratio to 6 and below permits 25% chord flaps to be attained over the full span.

- For wings of 0 rad (0 deg) sweep and for all aspect ratios, a 25% chord flap can be attained over the full span.

- At the low aspect ratios, distributing the thickness/chord ratio in the same way as the ACT airplane resulted in excessively thick root sections so that the lower surface of the wing root projected an unreasonable distance below the existing wing/fuselage fairing contour line. As an example, the wing root lower surface for the 53.88 square meter (580 square feet) wing at aspect ratio 4 and 0.524 rads (30 degs) would be located approximately 0.635 meters (25 inches) below the existing fairing contour, leaving a ground clearance of only 0.254 meters (10 inches). This is considered unacceptable, as ground clearance and ground clearance angle at rotation are reduced below acceptable values. In addition, substantial increases in fuselage center section weight and drag would occur due to the increased size of the wing/fuselage fairing. To ensure a practical configuration arrangement, it was necessary to depart from the method of determining the thickness/chord ratio of the inboard portion of the wing so that instead of maintaining a constant thickness/chord ratio from the break station to the root, the break station thickness was projected into the root section. The effect of this change was to decrease the wing thickness/chord ratio from the break station to the wing root, linearly, and reduce the root thickness to practical dimensions. To offset the loss of fuel volume due to the reduction in root thickness/chord ratio, additional fuel space was provided in the extended leading edge. A typical matrix of wing planforms and the effects of sweep and thickness is shown in Figure C6.

  Further aerodynamic investigation of ride qualities resulted in a decision to consider wings of 0.524 rads (30 degs) of sweep only for the Intermediate and Alternate wing configurations. To aid in the selection of wing planforms for these aircraft, a series of charts was produced depicting the geometric restraints and fuel volume for the range of aspect ratios and wing areas at a fixed 0.524 rads (30 degs) sweep angle. These are shown in Figure C7 through Figure C11.

- The constraint imposed by the landing gear is illustrated in Figure C7. The depth of the wing at the main landing gear is plotted against aspect ratio for the three wing areas considered. The minimum depth permitted is based on the Model 1329-6A JetStar depth of 0.284 meters (11.2 inches). Inspection of the chart shows that this constraint eliminates aspect ratios above 6.3 from further consideration.

- The constraint imposed by the trailing edge flaps is illustrated in Figure C8. In order to allow space at the root for systems installation, this constraint was based on a datum line parallel to the wing trailing edge and intersecting the wing break at the 70% chord line. The distance between this datum line and the auxiliary spar at the root is plotted against aspect ratio for the considered wing areas. When this

dimension equals zero, approximately 5% of the chord will remain between auxiliary spar and flap hinge for the installation of the above system.

Inspection of the chart shows that this constraint eliminates all aspect ratios above 4.30 from further consideration.

- The constraint imposed by the intercept of the outer rear spar with the landing gear structure is shown on Figure C9. The distance between the 65% chord line and the intersect of the landing gear support structure is plotted against aspect ratio for the considered wing areas. When the dimension is positive (+), the outer rear spar is at some chord location less than 65% with a resulting loss of available box fuel volume. When the dimension is negative (-), the outer rear spar is located at some percentage chord greater than 65% with a resulting loss of space between spar and flap hinge line. The optimum is attained when the dimension equals zero.

  The effect of the previous geometric constraints on available fuel weight, relative to the aspect ratio, for the three wing areas considered is shown on Figure C10. The data show that the inboard flap clearance constraint limits the aspect ratio to 4.25. Relaxing this constraint and permitting a reduced chord for the inboard flap will allow the aspect ratio to increase slightly in excess of 5.

  The available fuel weight versus wing area for the range of aspect ratios considered is given on Figure C11. It should be noted that the fuel weights are based on the volume capacity of the thinned root section and the addition of fuel in the extended leading edge. The geometric constraints, obtained from Figures C7, C8, and C9, are also included. A set of curves for mission fuel required for aspect ratios 4 to 6, both for the Intermediate and Alternate configurations, is superimposed on the chart.

Intermediate configuration description. - The Intermediate configuration, Figure 32, has a wing designed to take advantage of supercritical airfoil characteristics, and was optimized for minimum fuel consumption. The Ride Discomfort Index of the Model 1329-6A JetStar, RDI = 0.32, occurs at an aspect ratio of 5.0 with a sweep angle at the wing quarter chord of 0.524 rads (30 degs).

The wing, which is also designed to contain all the mission fuel so that external tanks are not required, has the following dimensions for the basic planform: span, 15.08 meters (594.0 inches); basic root chord (at center line), 4.642 meters (182.76 inches); and tip chord, 1.392 meters (54.83 inches). As illustrated on Figure 33, the wing root is located at buttock line 41.5, where it is attached to the fuselage main frames, and the extended root chord is 1.35 times the basic chord at this point. The extended inboard portion of the wing extends outward to the wing break at buttock line 102.79 and coincides with the apex of the structural triangle formed by the auxiliary spar and

inboard rear spar, which retain their existing locations. In order to minimize the root depth, a constant thickness is utilized for this portion of the wing, rather than a constant thickness/chord ratio. The thickness dimensions are those generated by the t/c ratio of 16.68% at the wing break. The outer portion of the wing extends from this break to the tip at which point the t/c ratio is reduced linearly to 15.10%. Wing incidence varies from 0.0175 rads (1 deg) at the root to 0.013 rads (0.74 degs) at the break to 0.00698 rads (0.4 degs) at the tip. The dihedral angle is 0.349 rads (2 degs) originating at the root. The box structure which also serves as a fuel tank is bounded by the root and tip ribs and by the front and rear spars. A rib located 0.127 meters (5.0 inches) outboard of the root serves as the inboard boundary of the tank and permits a dry bay area at the root joint. The front spar is located at 12% of the basic wing chord and extends inboard of the break to a point located 0.093 meters (3.68 inches) forward at fuselage station 410. The rear spar follows the existing Model 1329-6A JetStar location from root to break and then radiates out to the 65% chord generator at the tip. The existing landing gear retains its present location, and the new airfoil provides ample room for stowage as illustrated in Figure 33. The trailing edge is divided into three spanwise segments. The inboard flap segment is of the simple hinge type extending from wing root to wing break. It is hinged along a line located 0.609 meters (24.0 inches) forward of the trailing edge. The outer flap segment and aileron are both hinged along the 75% chord generator line. The outer flap extends from the wing break to a point 5.283 meters (208 inches) from the center line, the aileron extending from this point out to the tip. Additional fuel tankage space is provided in the batted portion of the wing leading edge between the front spar and tank closure beam located at 8.4% of the batted chord. The wing is of conventional type structure, manufactured in aluminum and other metallic materials.

As in the case of the ACT Configuration, the landing gear and landing gear location are maintained for the Intermediate configuration. It was assumed that no changes from the Model 1329-6A JetStar configuration would occur other than those related to change in wing configuration. Thus, the power plant and assembly and empennage design and the fuselage design except in the region of the wing/fuselage attachment are considered to be those of the Model 1329-6A JetStar.

Alternate configuration description. - The Alternate configuration was developed to investigate the effect of the use of filamentary composite materials in the design of the wing structure applied from buttock line 41.5 to the wing tip for an airplane optimized for minimum fuel consumption and for a wing designed to provide the same Ride Discomfort Index, RDI = 0.32. The wing, which utilizes supercritical airfoil sections, contains all the mission fuel and has an aspect ratio of 5.5 and a sweep angle at the wing quarter chord of 0.524 rads (30 degs).

The dimensions of the basic wing are: span, 15.6 meters (614 inches); basic root chord (at center line), 4.36 meters (171.75 inches); and tip chord, 1.30 meters (51.24 inches). As illustrated on Figure 37, the wing root is located at buttock line 41.5, where it is attached to the fuselage main frames, discussed previously.

The extended root chord is 1.35 times the basic chord at this location, and the extended inboard portion of the wing continues outboard to the wing break at buttock line 102.79 which coincides with the apex of the triangle formed by the auxiliary spar and inboard rear spars, both of which retain their existing locations. In order to minimize the root depth, a constant thickness wing section is utilized for this portion of the wing, rather than a constant thickness/chord ratio, and the thickness dimensions are those corresponding to the t/c ratio of 16.55 at the wing break. The outer panel of the wing extends from the break station to the tip, where the t/c ratio is reduced to 14.94% by a linear variation from the break station t/c. Wing incidence varies from 0.0175 rads (1 deg) at the root to 0.013 rads (0.75 degs) at the break to 0.00698 rads (0.40 degs) at the tip. Dihedral angle is 0.035 rads (2 degs), originating at the root.

The box structure which also serves as a fuel tank is bounded by the root and tip ribs and by the front and rear spars. A rib located 0.127 meters (5.0 inches) outboard at the root serves as the inboard boundary of the tank and permits a dry bay area at the root joint. The front spar is located at 12% of the basic chord and extends inboard at the break to a point located 0.0935 meters (3.68 inches) forward of fuselage station 410. The rear spar follows the Model 1329-6A JetStar location from root to break and then radiates to the 65% chord generator at the tip. The Model 1329-6A JetStar landing gear retains its present location, and as shown on Figure 37, the supercritical airfoil section provides ample space for stowing the gear. The trailing edge is divided into three spanwise segments. The inboard flap segment is of a simple hinge type and extends from wing root to wing break with the hinge located along a line 0.38 meters (15.0 inches) forward of the trailing edge. The outer flap segment and aileron are both hinged along the 75% wing generator. The outboard flap extends from the wing break to a point 5.47 meters (215.5 inches) from the center line, and the aileron extends from this point to the wing tip. Additional fuel tankage space is provided in the extended leading edge between the front spar and a tank closure beam located at 8.4% of the extended chord.

(This page intentionally left blank.)

APPENDIX REFERENCES

A1. R.Ae.S Sheets, Wings 70011, Royal Aeronautical Society.

A2. "Results of Flight Tests to Show Compliance with Civil Airworthiness Requirements, Airplane Performances." Lockheed-Georgia Company, ER 4730, Part IV, Volume IV A. October 15, 1961.

A3. "Wind Tunnel Tests on JetStar Model 1329," CWT Report 764. February 1960.

A4. "C-140 Aerodynamics Substantiating Data Report", Lockheed-Georgia ER 5862. October 1968.

A5. "Fluid Dynamics Methods." Lockheed-Georgia Company, ER 6223.

A6. Searls, C. W., Jr.: "Additional Subsonic Wind Tunnel Tests of a 0.1 Scale, Sting Mounted Model of the Lockheed Modified GL-329 Airplane," Southern California Cooperative Wind Tunnel Report 747-11, December 1959.

A7. USAF. Datcom 4.1.3.4.

A8. Furlong, G. C., and McHugh, J. G.: "A Summary and Analysis of the Low Speed Longitudinal Characteristics of Swept Wings at High Reynolds Numbers." NACA Report 1339, 1957.

A9. Monk, J. R., et al: "STOL Tactical Aircraft Investigation", Volume IV, AFFDL TR-73-19, May, 1973.

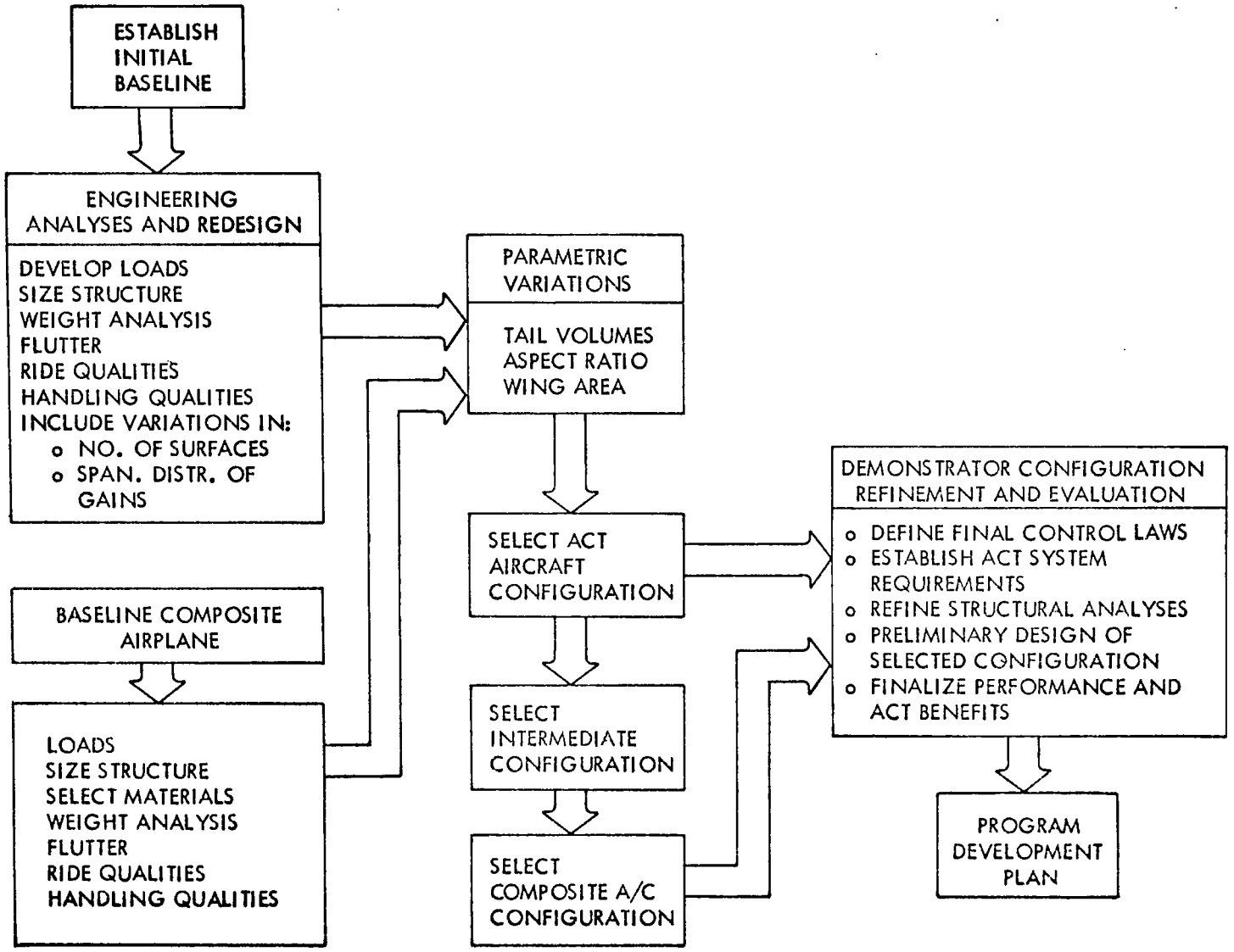

FIGURE 1 STUDY PLAN

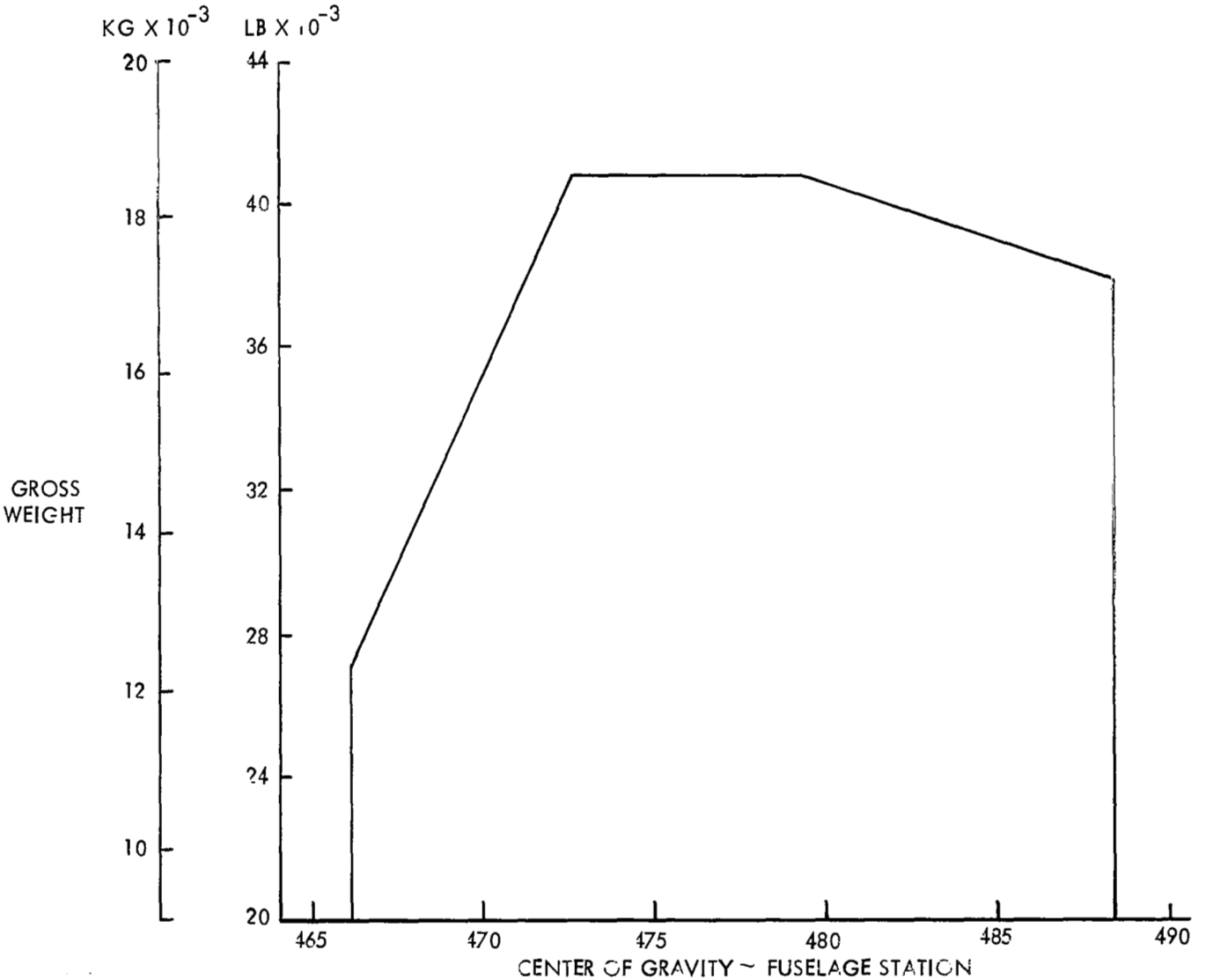

FIGURE 2 CENTER OF GRAVITY ENVELOPE

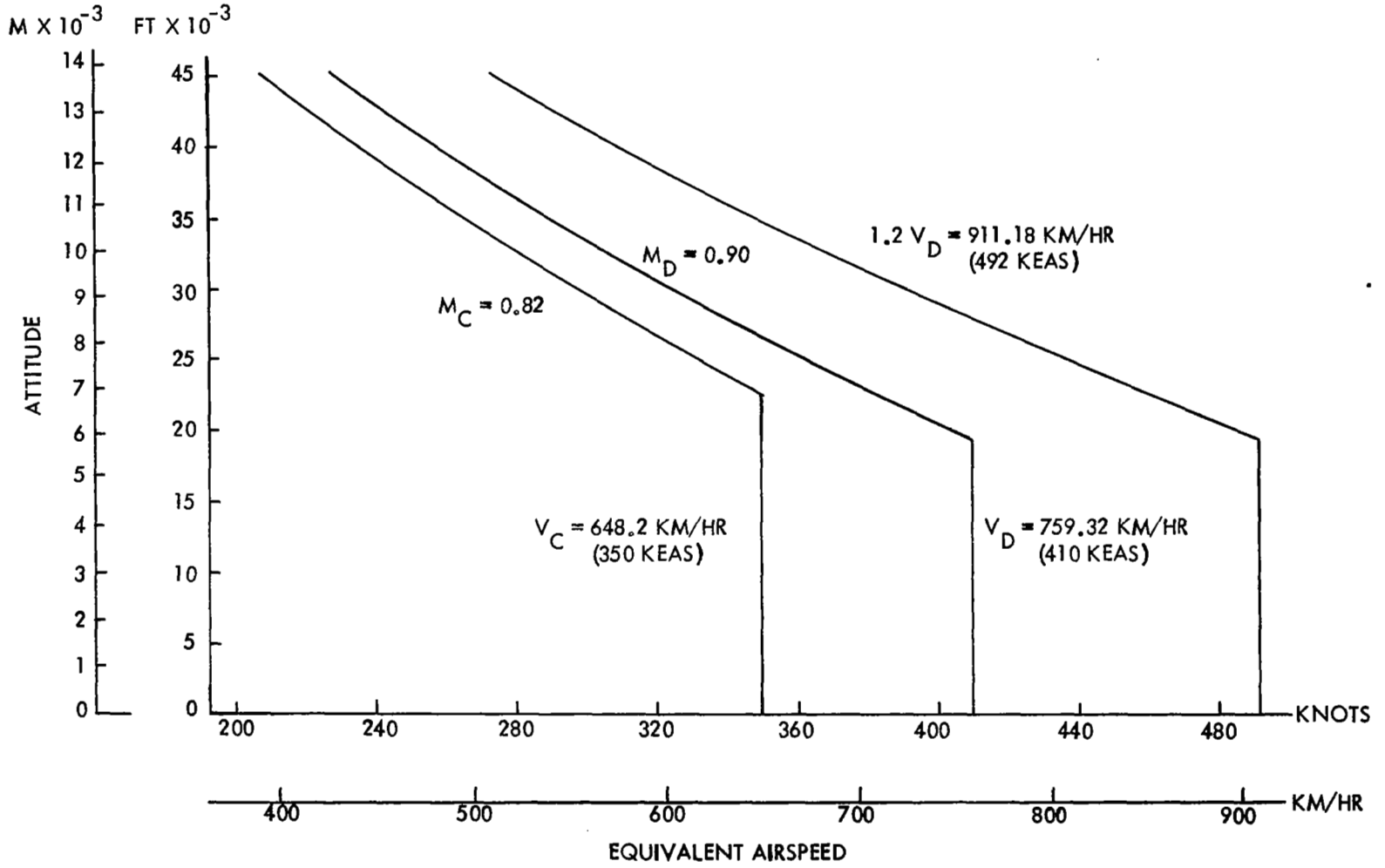

FIGURE 3 STRUCTURAL DESIGN AIRSPEEDS

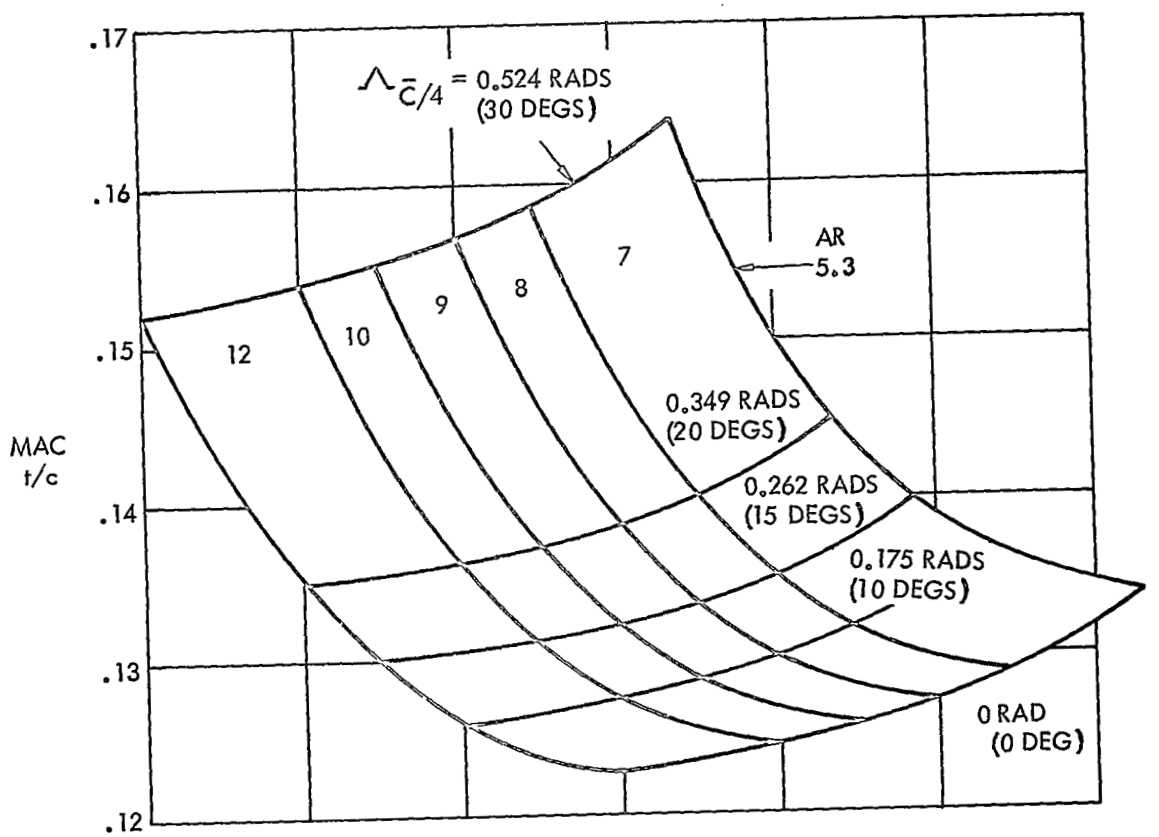

FIGURE 4 WING THICKNESS RATIO

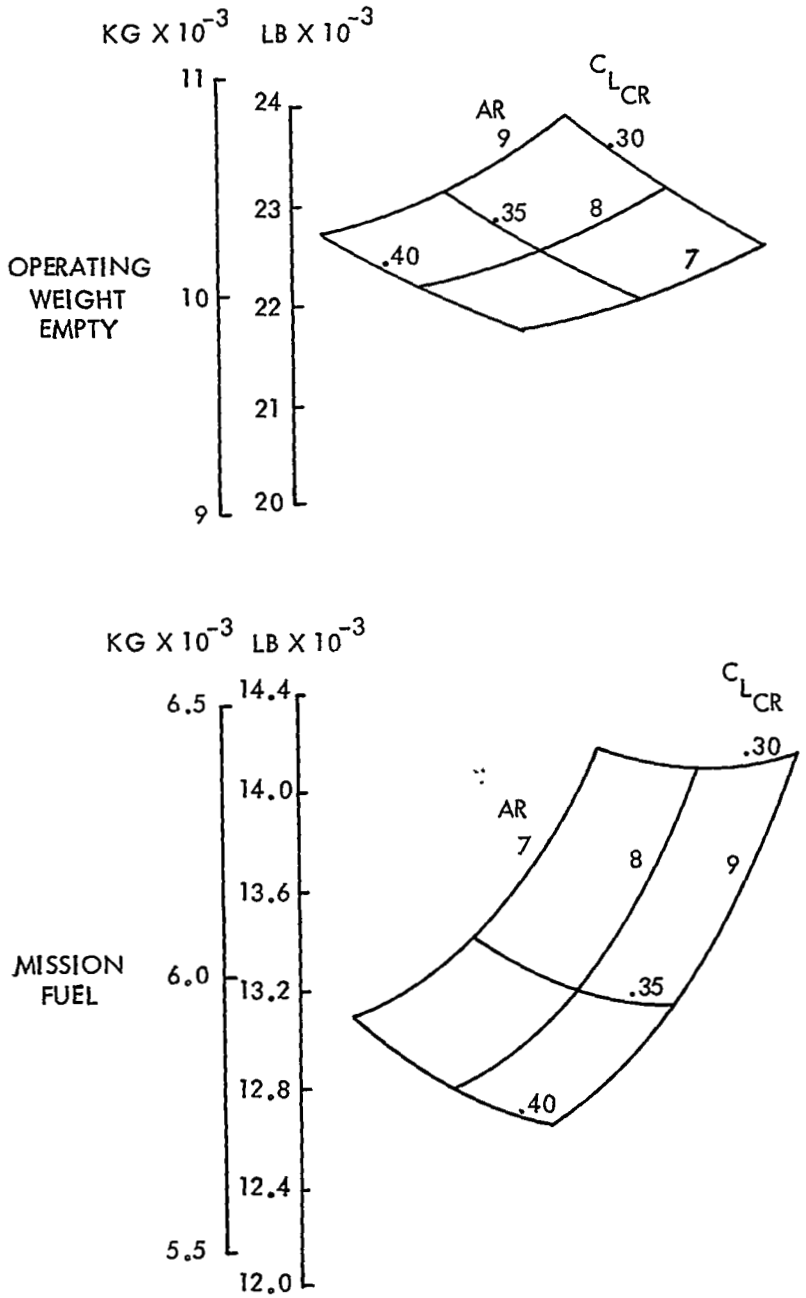

FIGURE 5 ACT CONFIGURATION OPERATING WEIGHT AND MISSION FUEL REQUIREMENT MATRIX

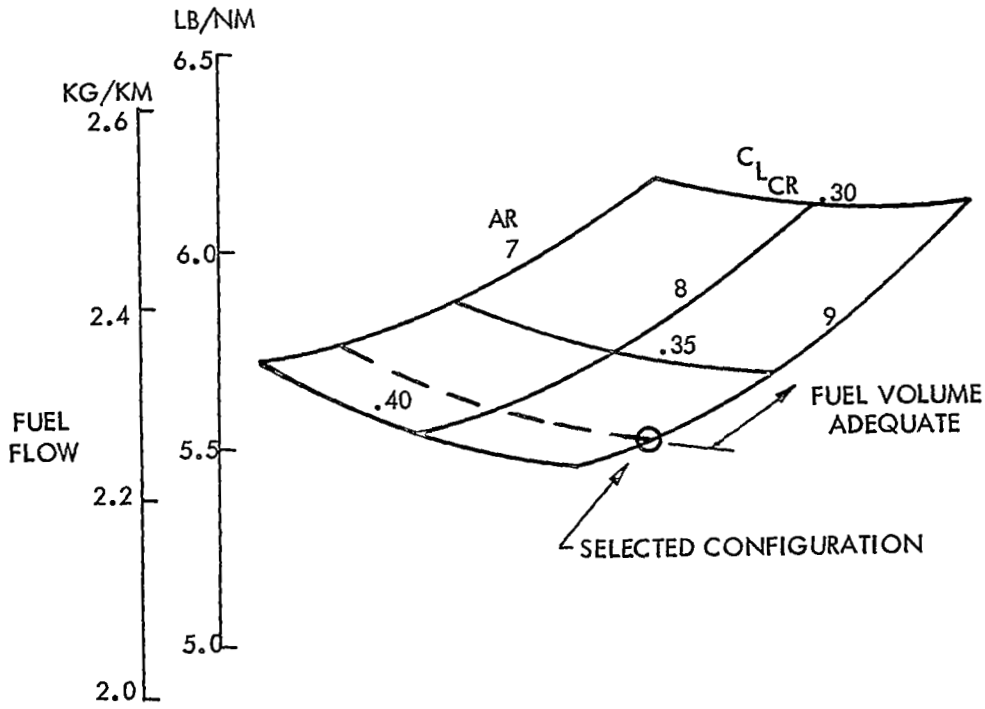

FIGURE 6 SELECTION OF ACT CONFIGURATION

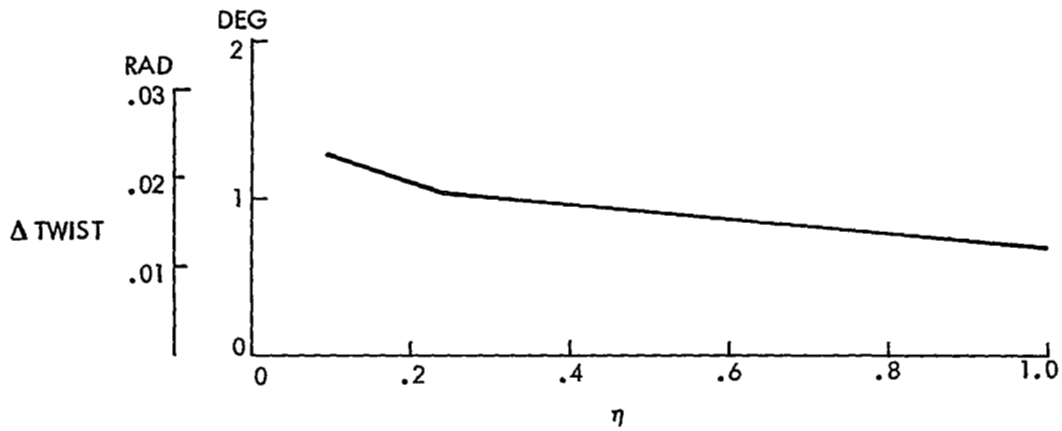

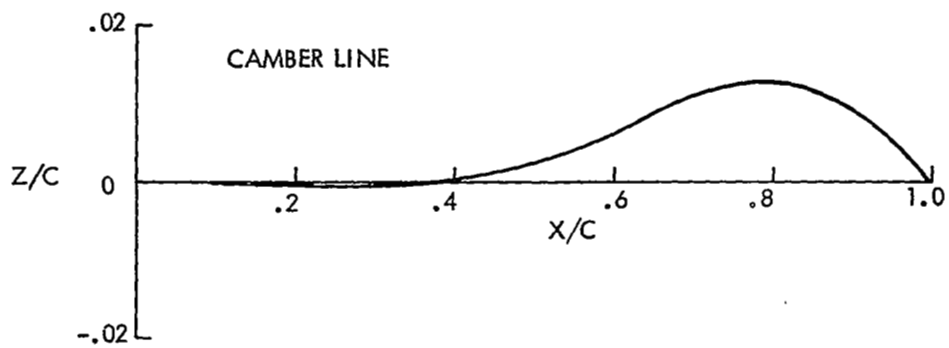

FIGURE 7 WING TWIST AND CAMBER

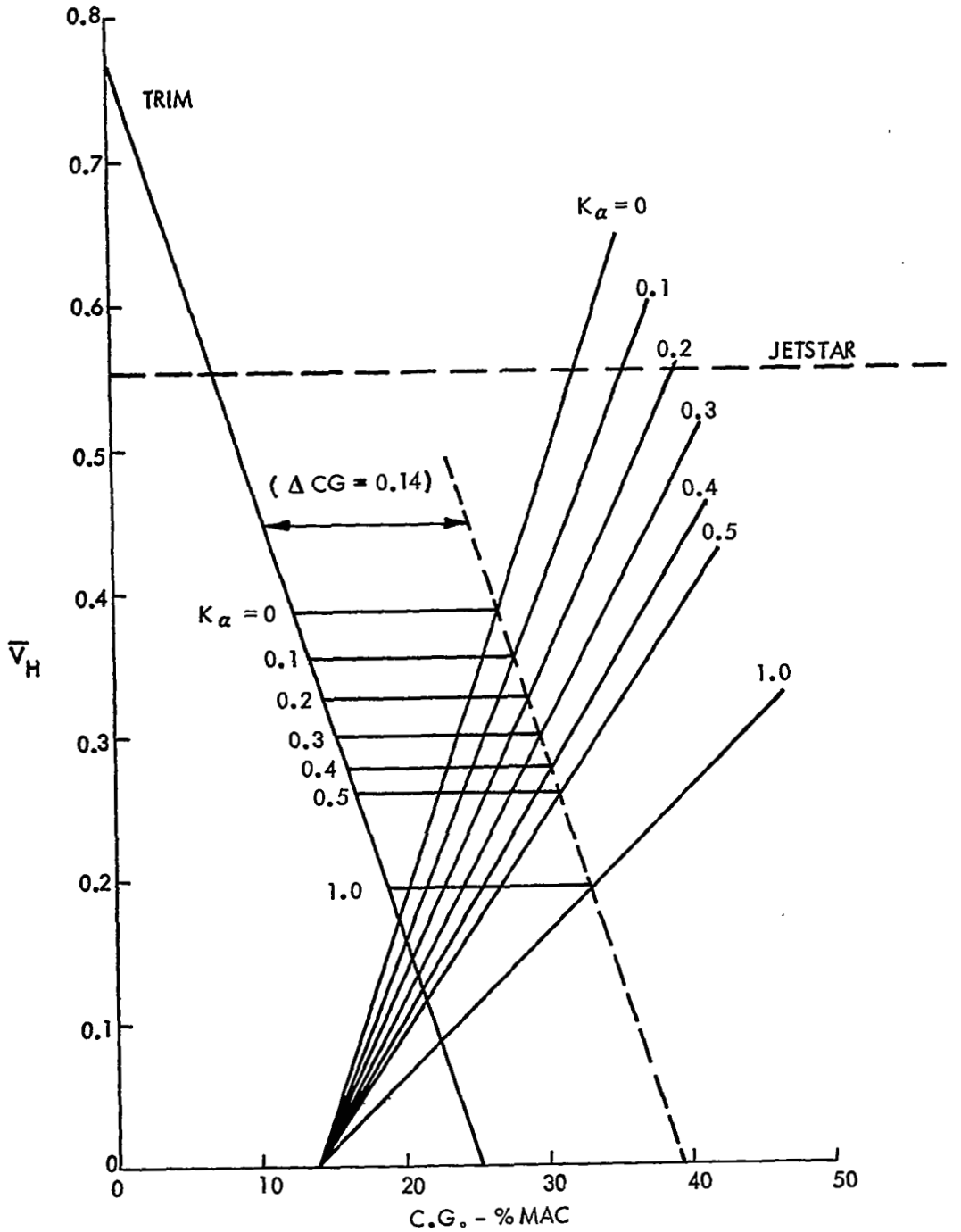

FIGURE 8 EFFECT OF TRIM AND STABILITY ON HORIZONTAL TAIL VOLUME

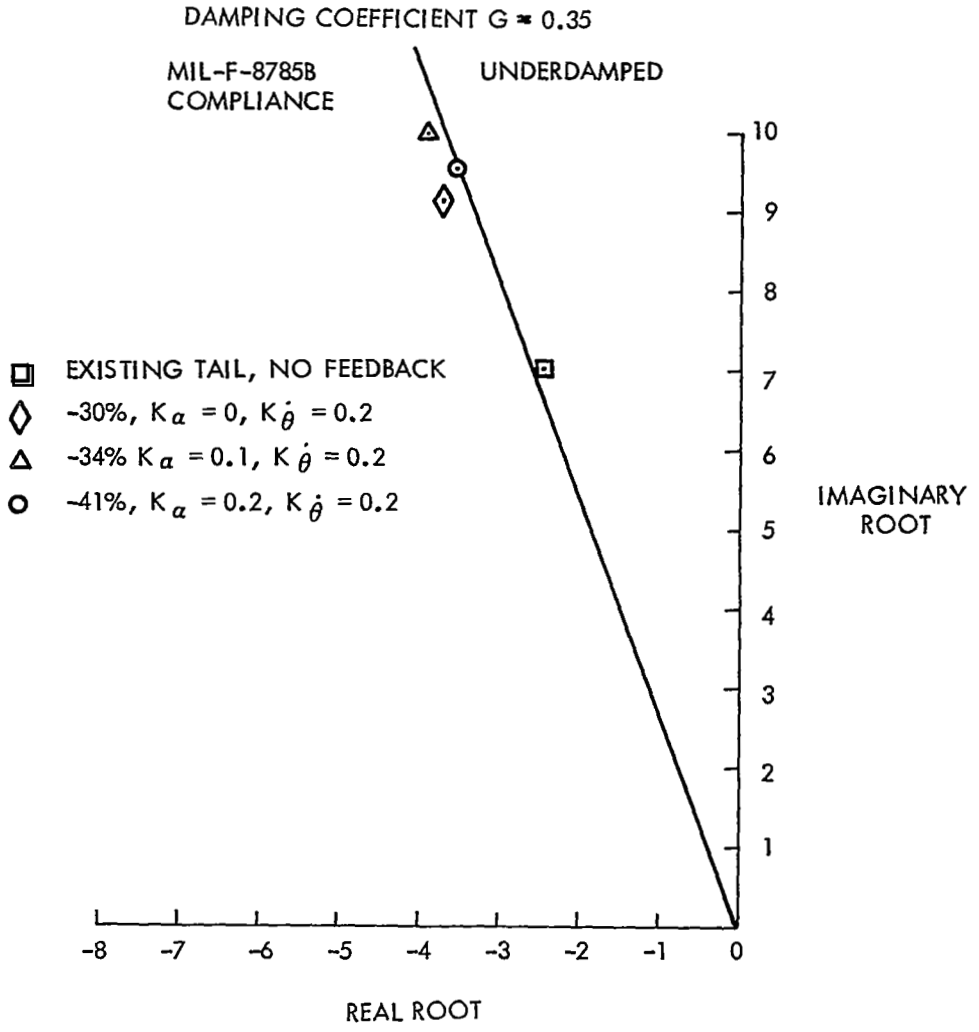

FIGURE 9 EFFECT OF HORIZONTAL TAIL VOLUME ON SHORT PERIOD DAMPING

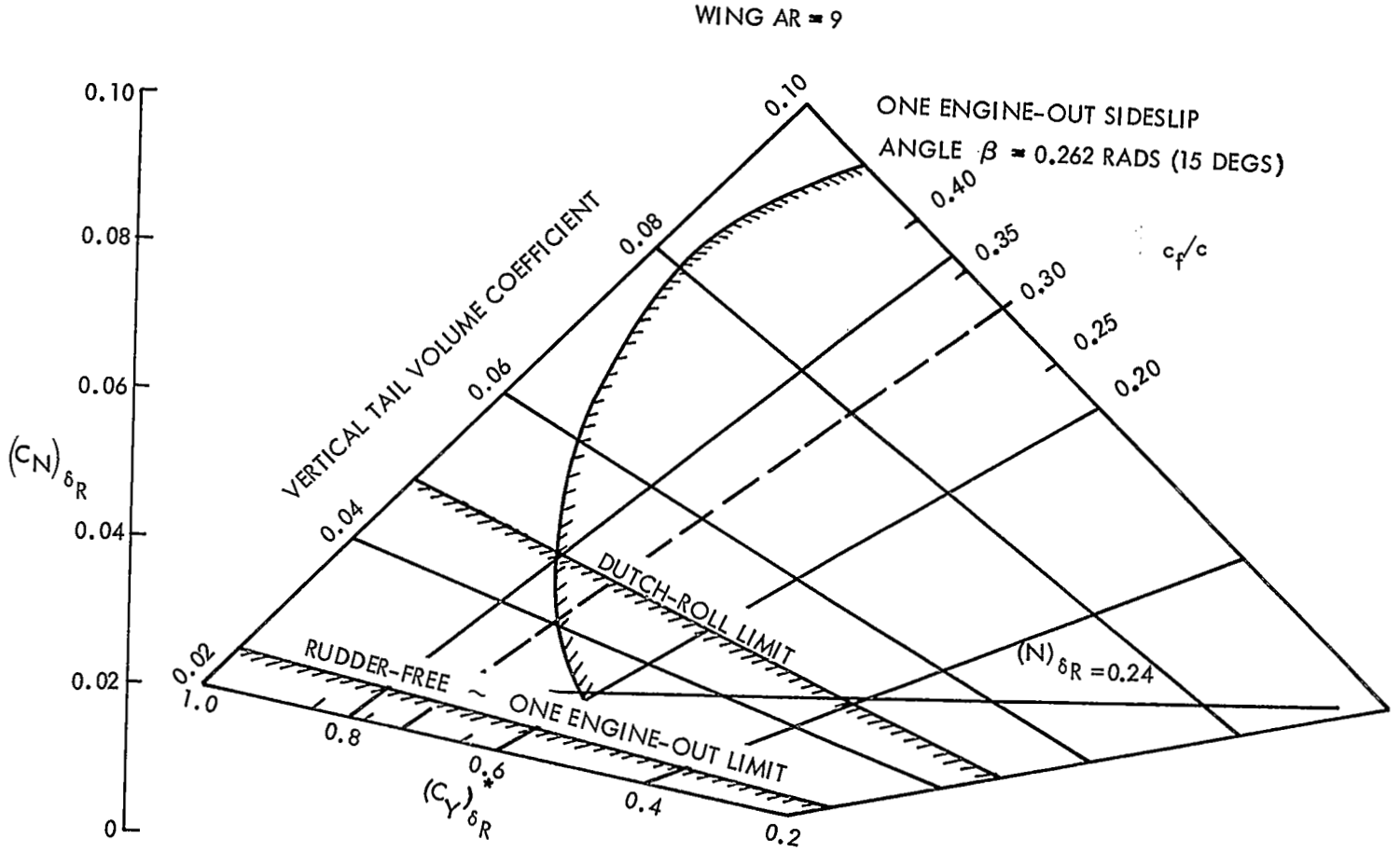

* DENOTES VERTICAL TAIL REFERENCE MOMENT AREA

FIGURE 10 VERTICAL TAIL SIZING

CRUISE CONFIGURATION

MACH = 0.76 ALT = 12,801.6 M (42,000 FT)

SYM	CONFIGURATION
○	J - MODEL 1329-6A JETSTAR
◇	1 - JETSTAR + NEW WING
⊡	2 - 1 + TEE TAIL
△	3 - 2 + 65% VERTICAL TAIL AREA
▽	4 - 2 + 37.5% VERTICAL TAIL AREA

FLAGGED SYMBOLS ARE WITH AUGMENTATION

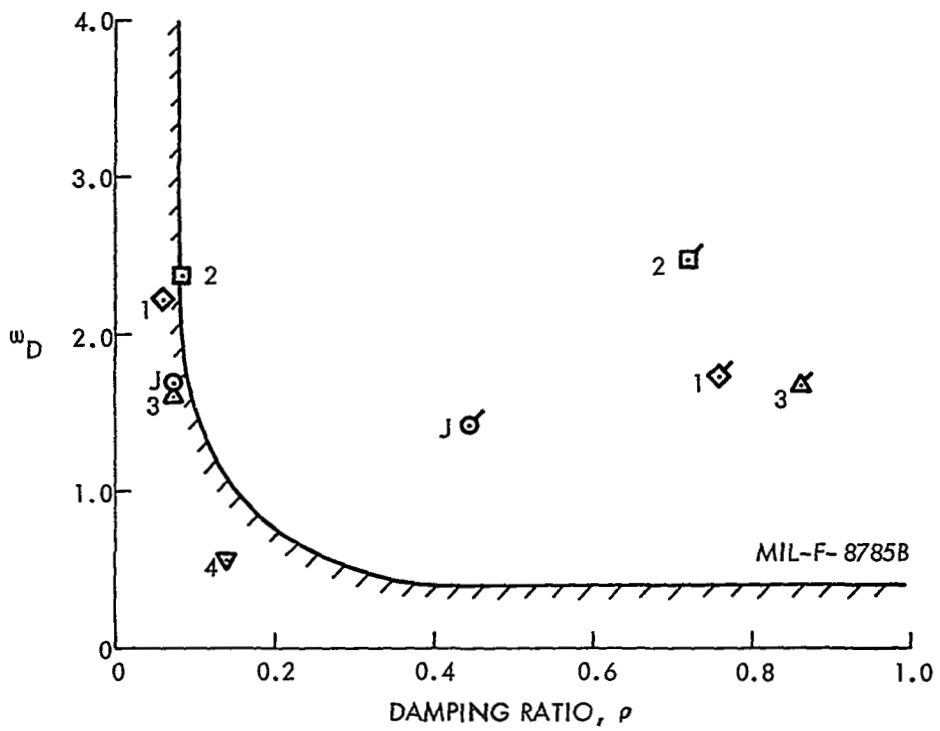

FIGURE 11 DUTCH-ROLL REQUIREMENTS

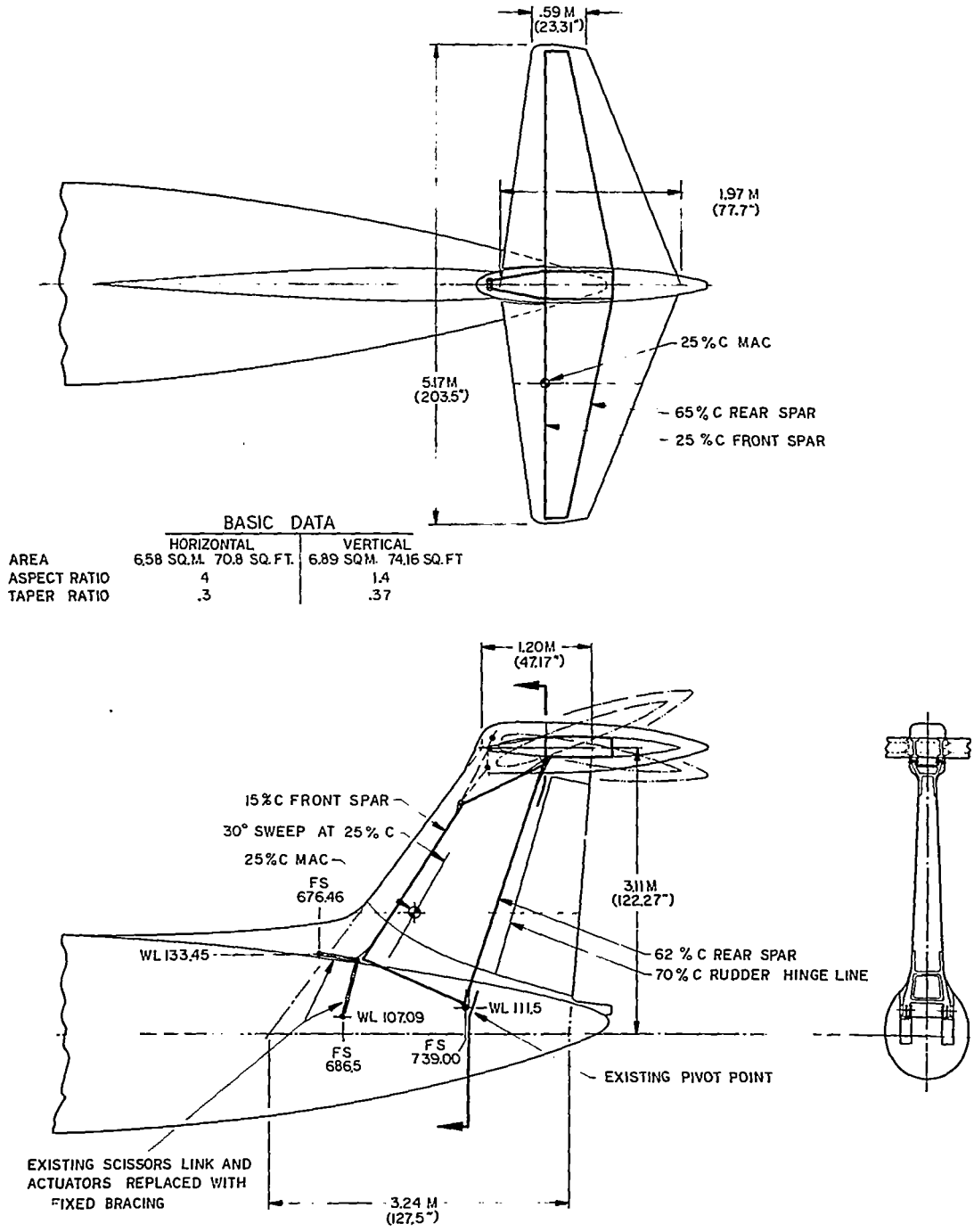

FIGURE 12 ACT CONFIGURATION EMPENNAGE GEOMETRY

SPAN 21.72M (71.28 FT)
LENGTH 24.91M (62.28 FT)
HEIGHT 5.32M (17.45 FT)

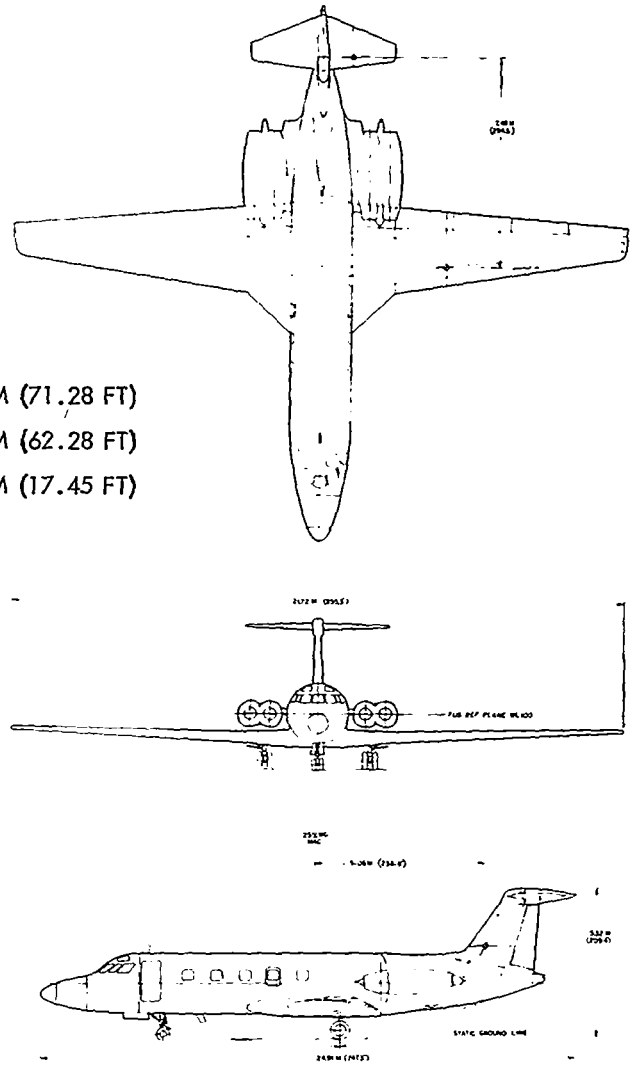

FIGURE 13 ACT AIRPLANE CONFIGURATION

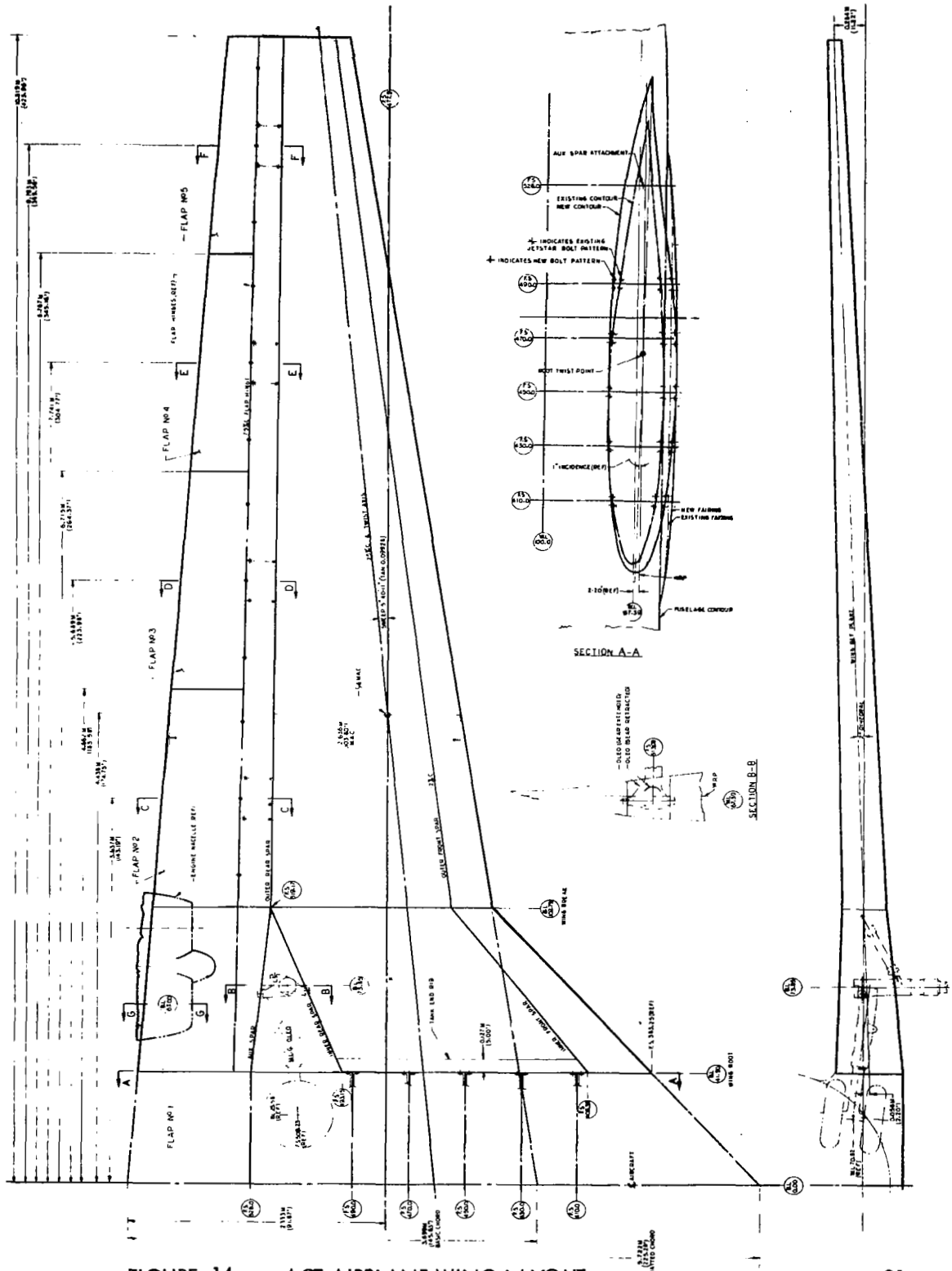

FIGURE 14 ACT AIRPLANE WING LAYOUT

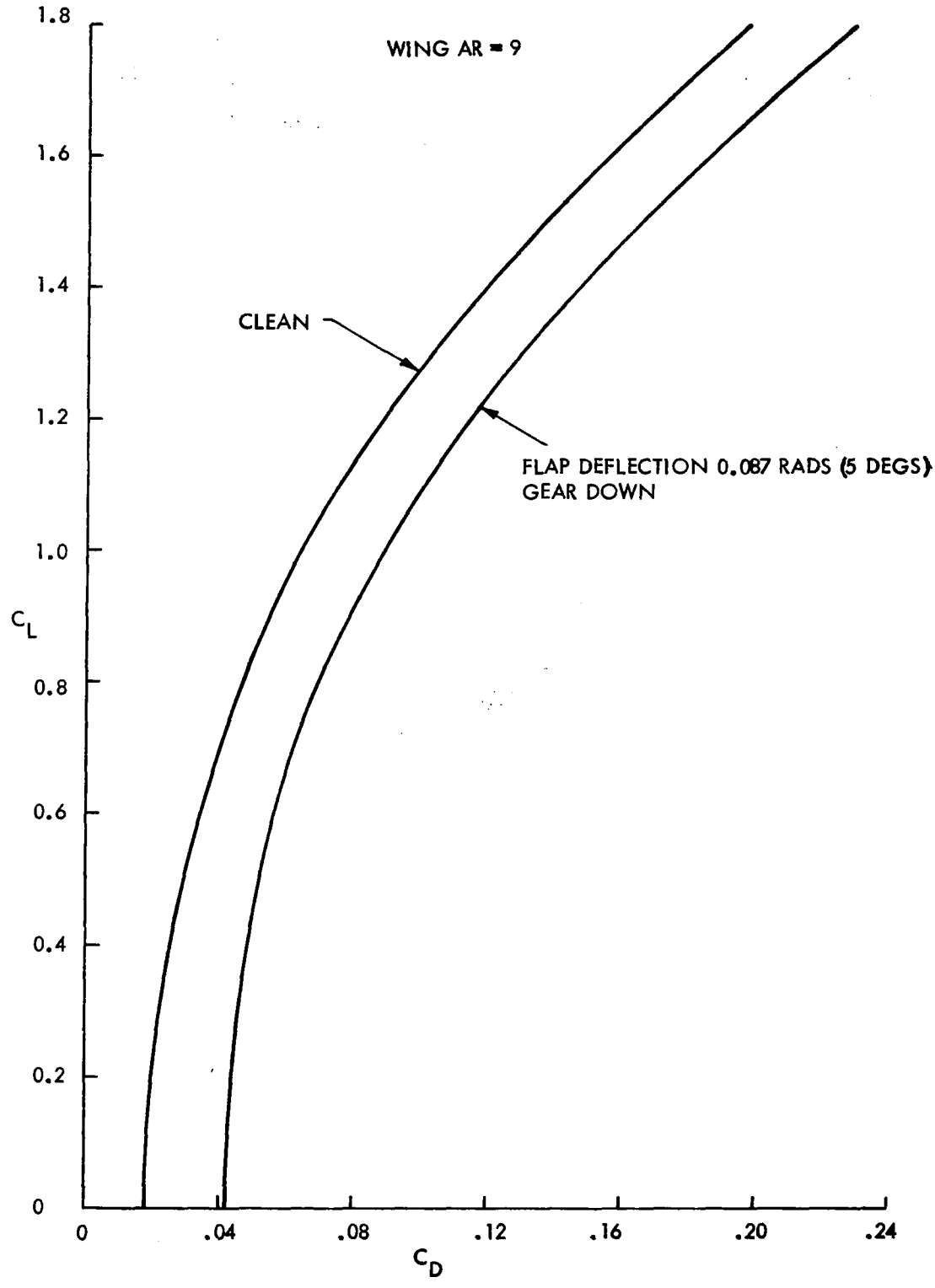

FIGURE 15 ACT CONFIGURATION LOW SPEED DRAG POLARS

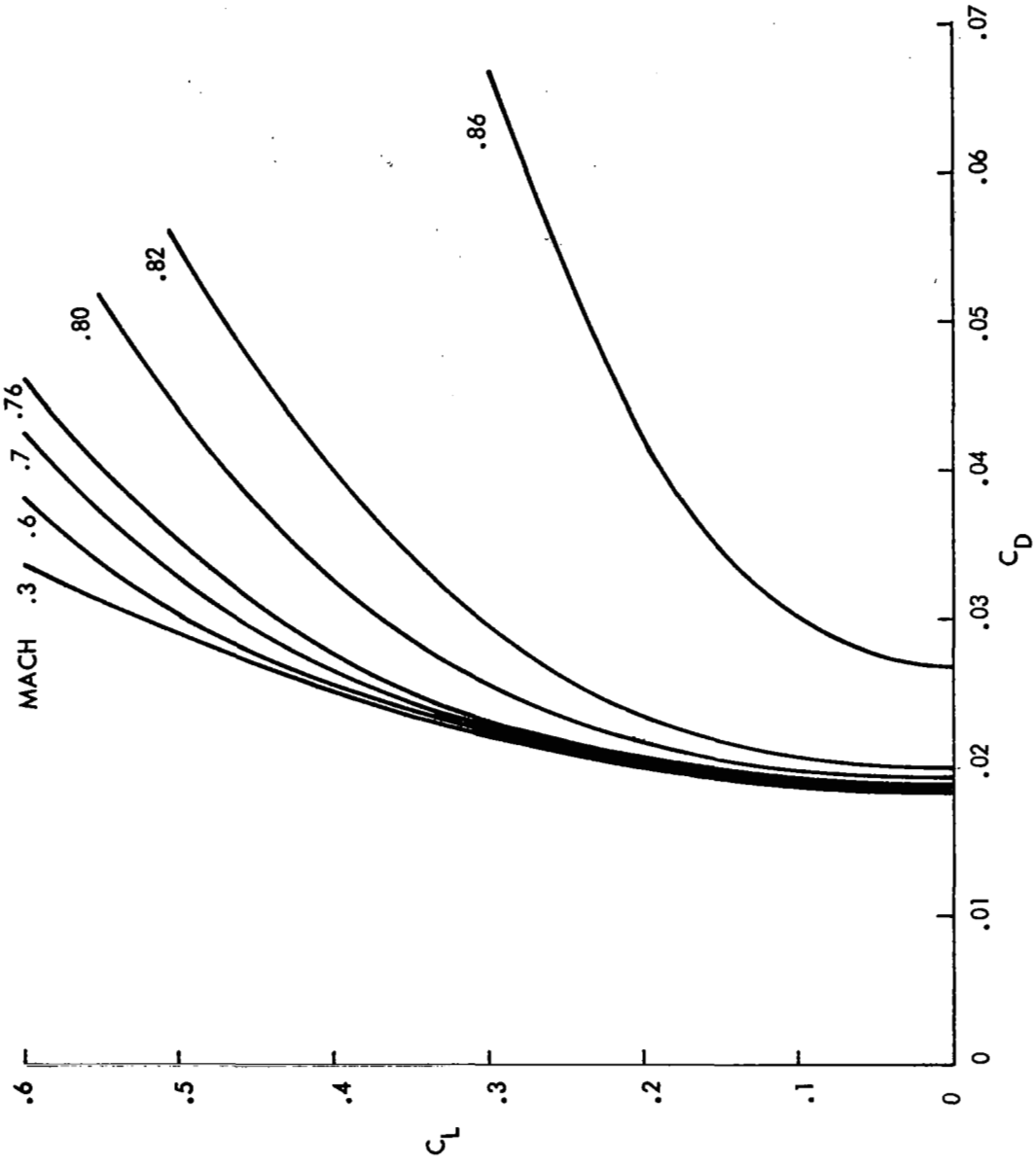

FIGURE 16 ACT CLEAN CONFIGURATION DRAG POLARS

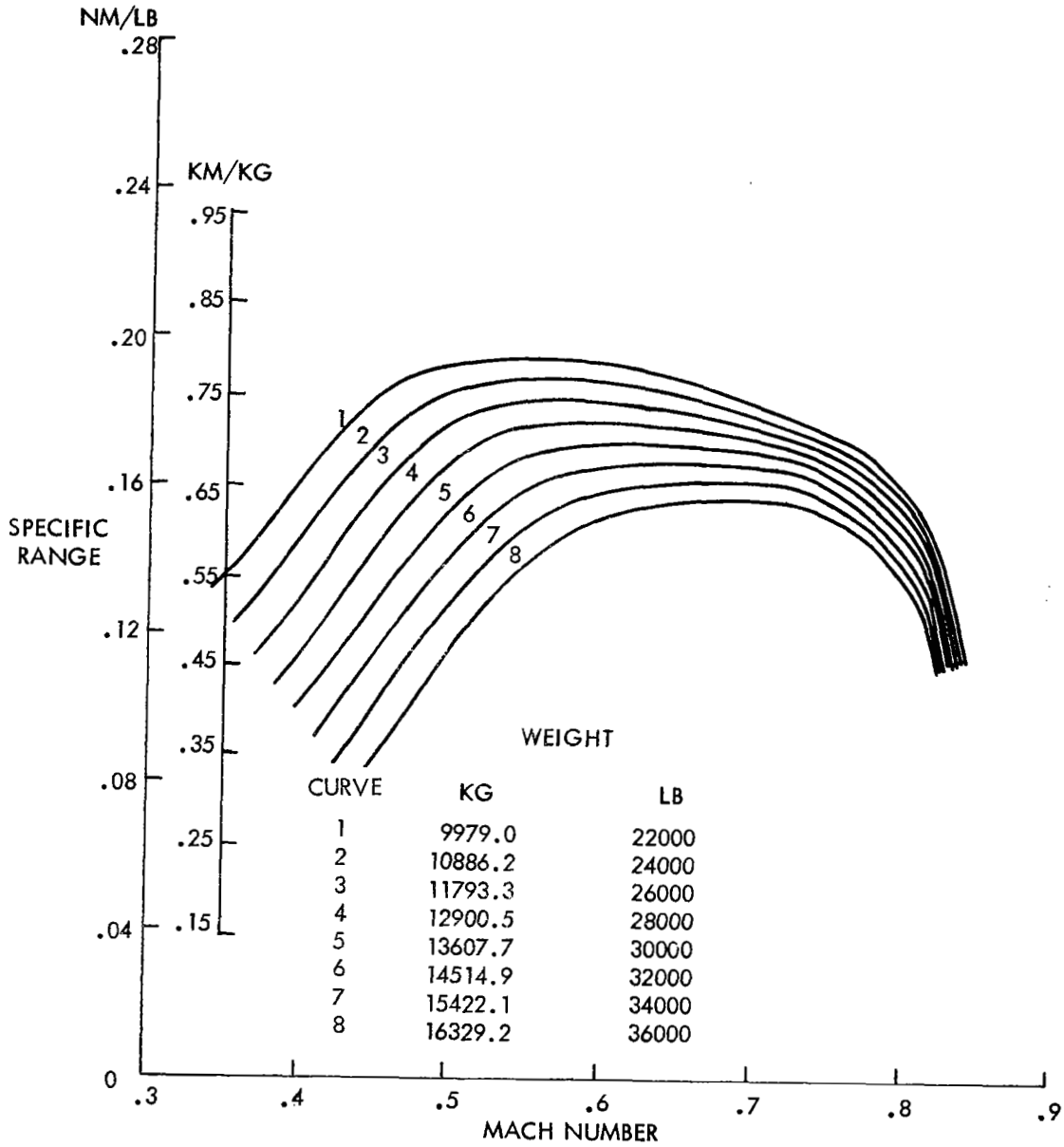

FIGURE 17 ACT CONFIGURATION SPECIFIC RANGE DATA, 10668 M (35000 FT)

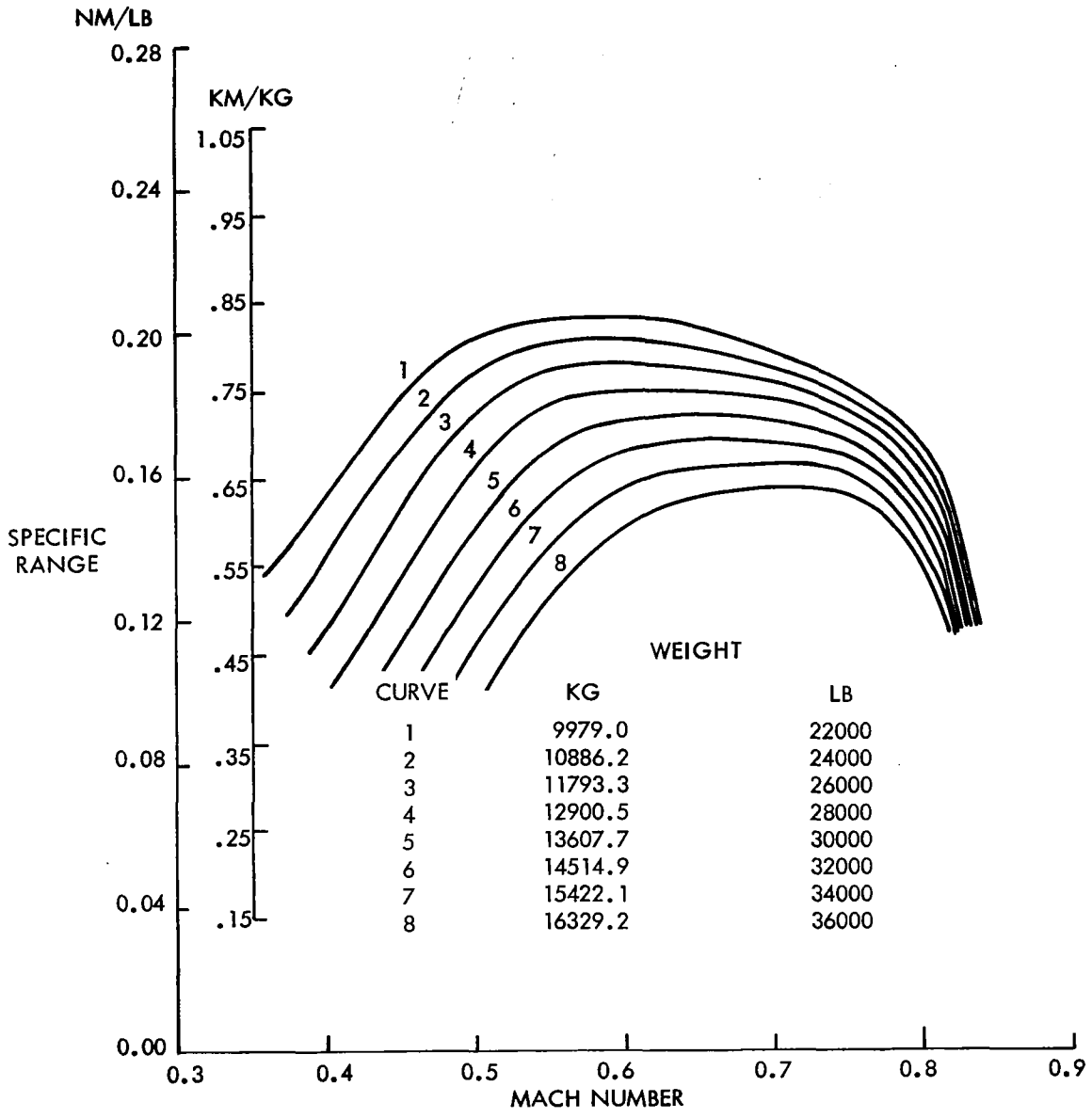

FIGURE 18 ACT CONFIGURATION SPECIFIC RANGE DATA, 11277.6 M (37000 FT)

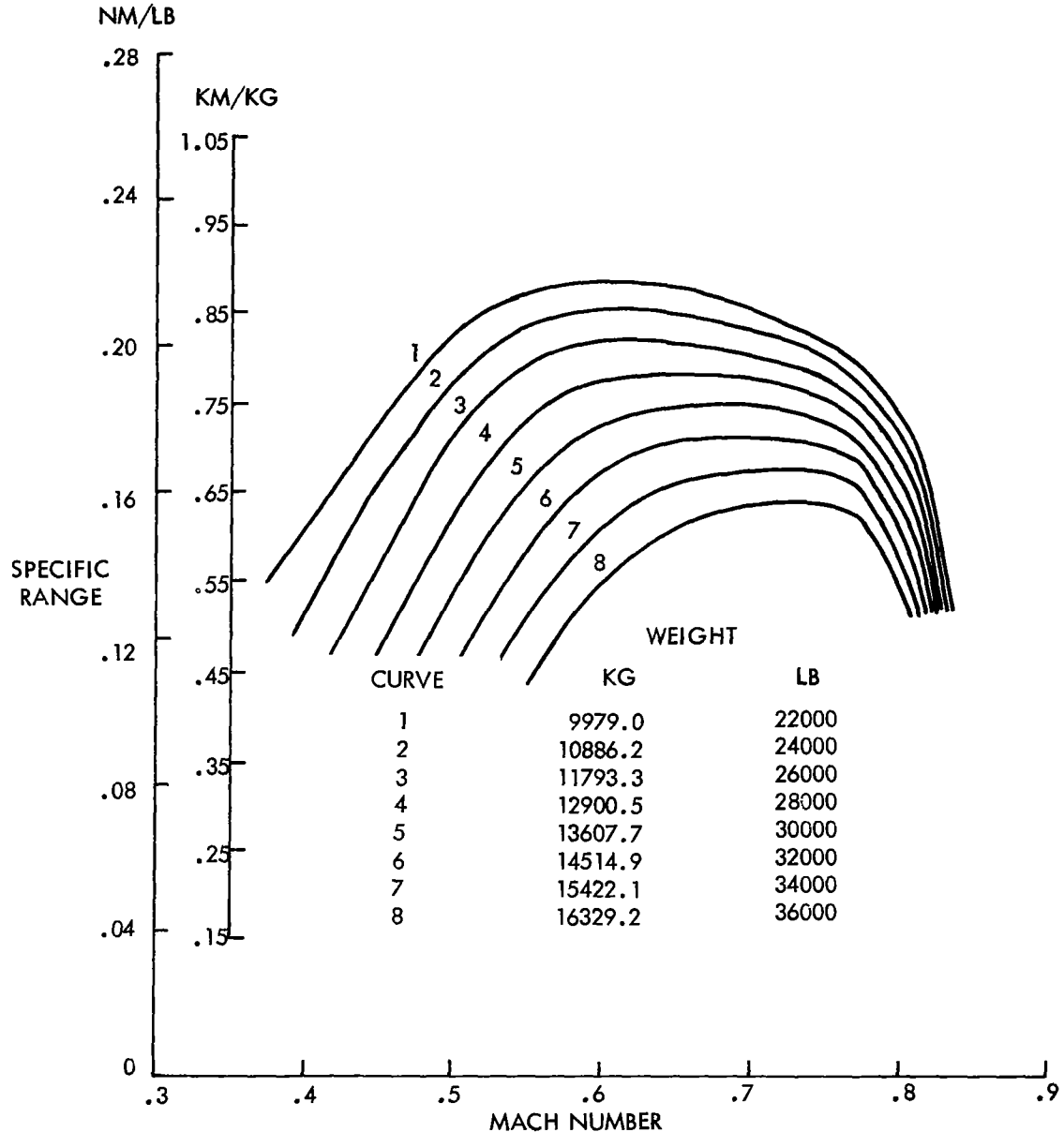

FIGURE 19 ACT CONFIGURATION SPECIFIC RANGE DATA, 11887.2 M (39000 FT)

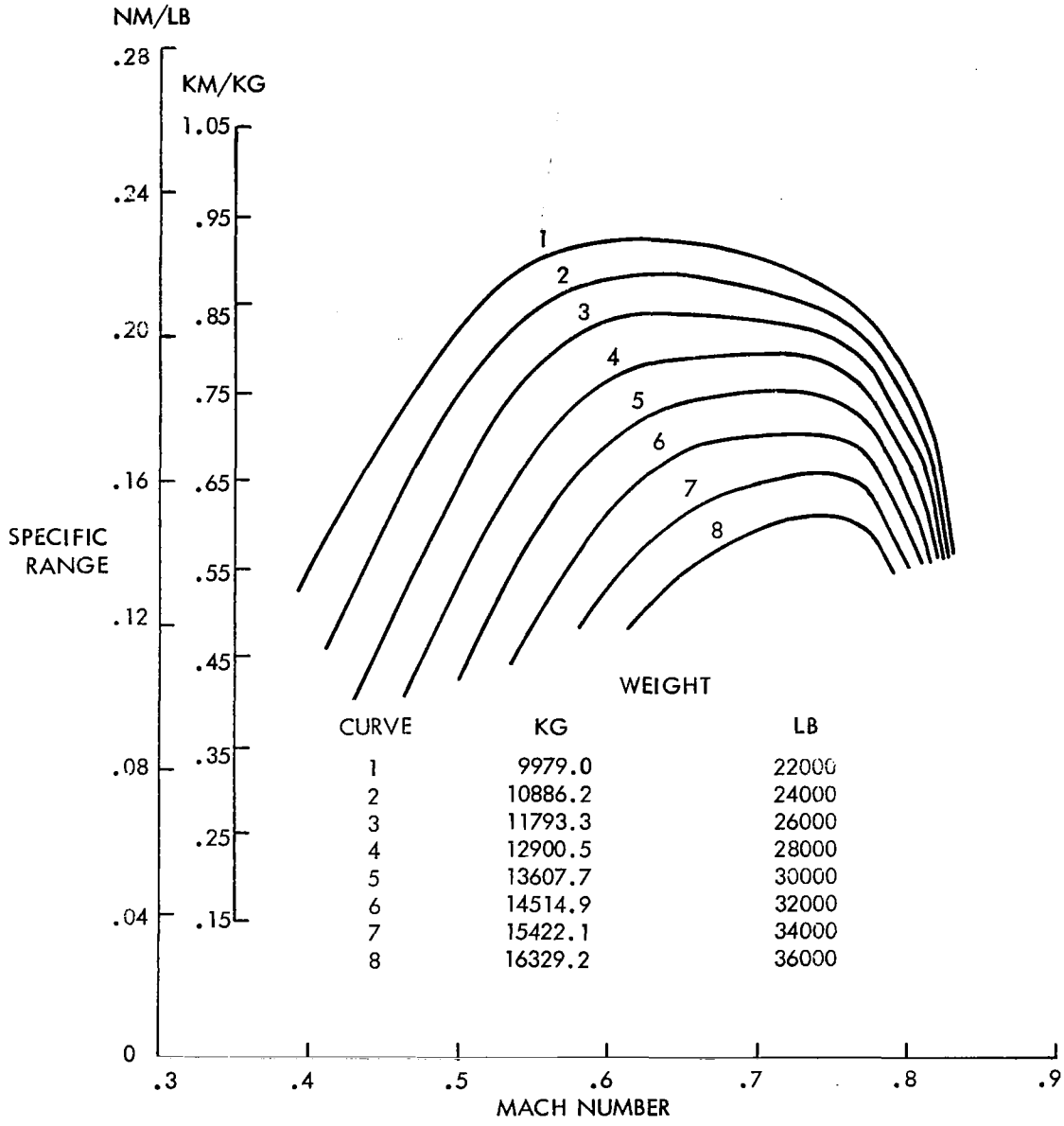

FIGURE 20 ACT CONFIGURATION SPECIFIC RANGE DATA, 12801.6 M (41000 FT)

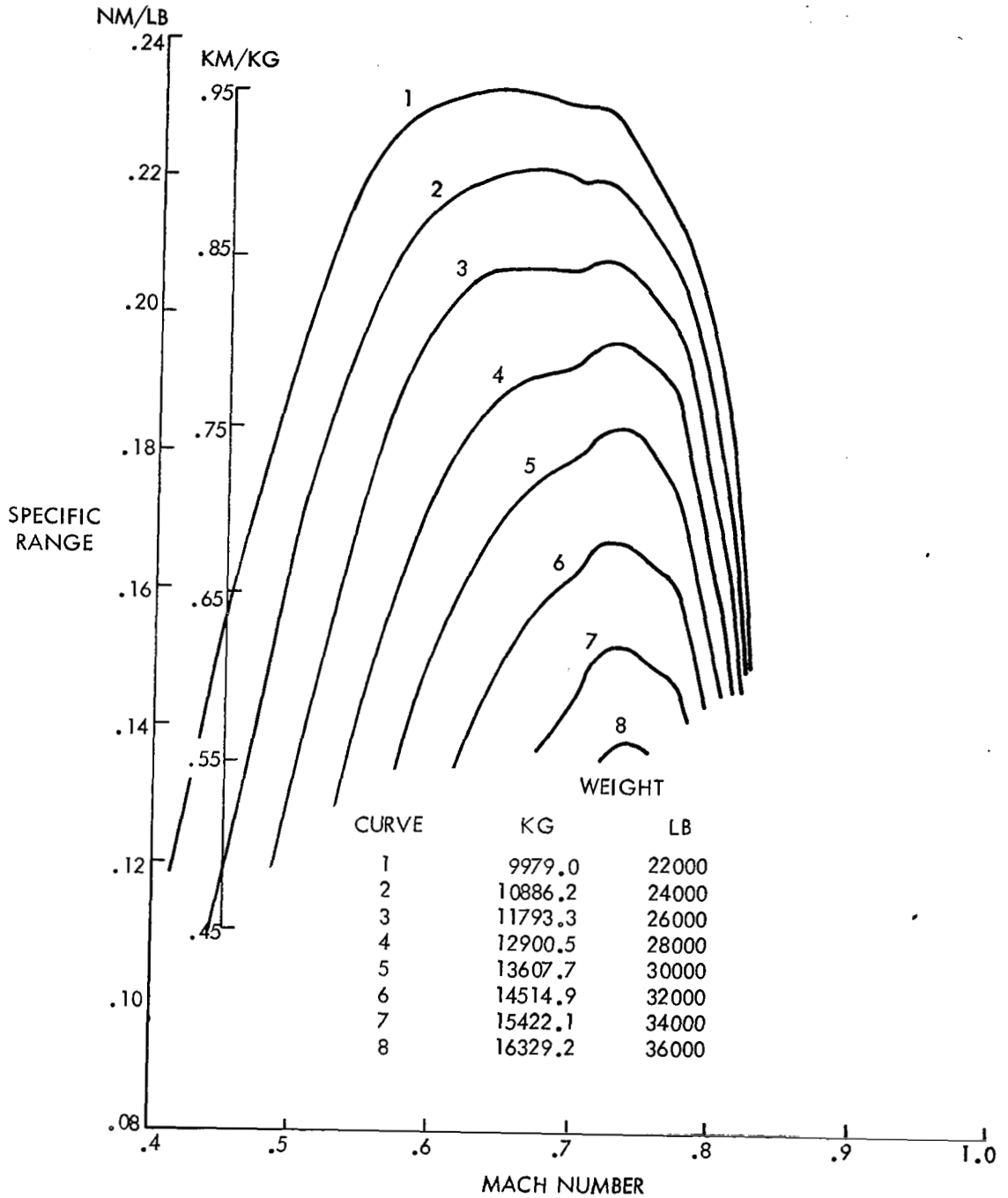

FIGURE 21 ACT CONFIGURATION SPECIFIC RANGE DATA, 13106.4 M (43000 FT)

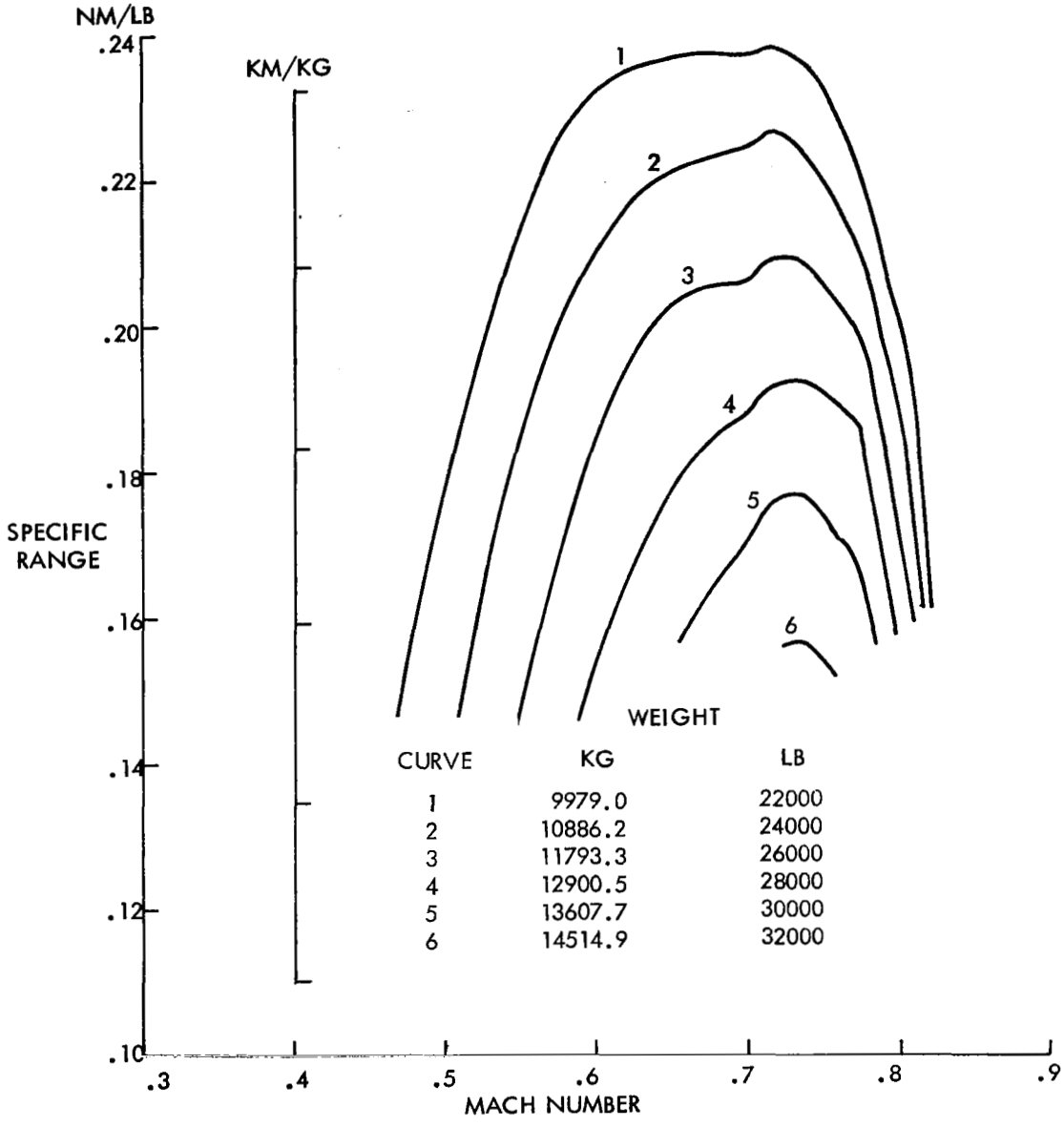

FIGURE 22 ACT CONFIGURATION SPECIFIC RANGE DATA, 13716 M (45000 FT)

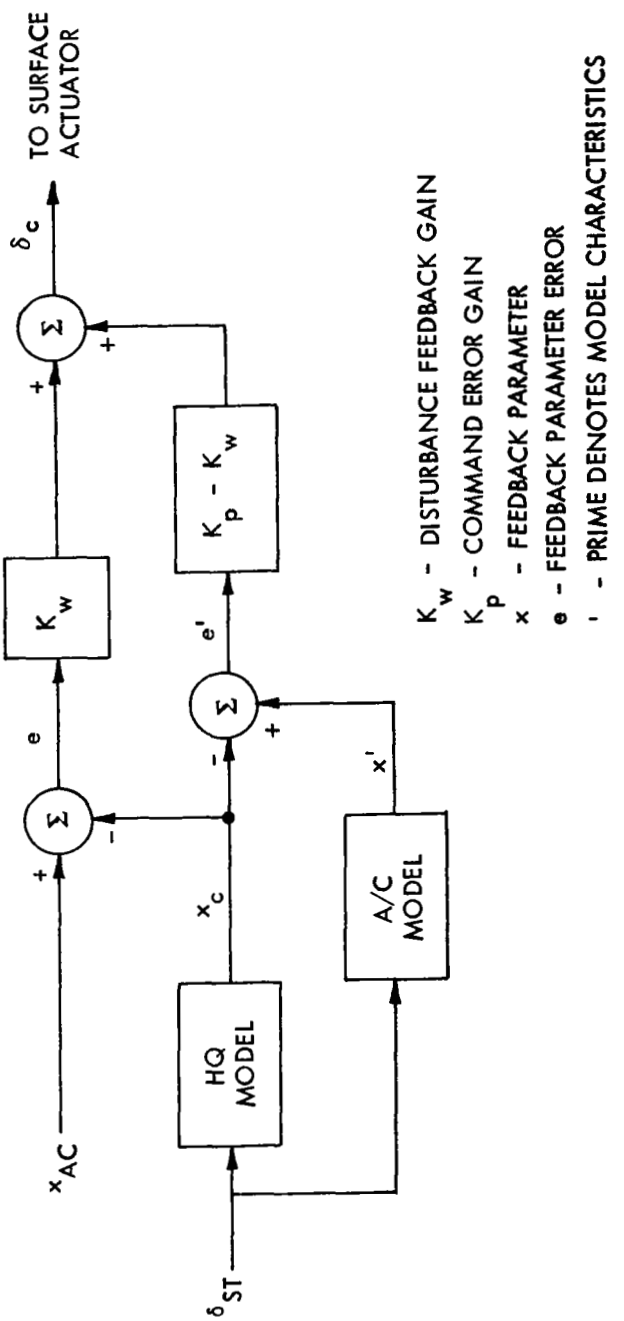

FIGURE 23 COMMAND CONTROL ADDED TO STABILITY AUGMENTATION

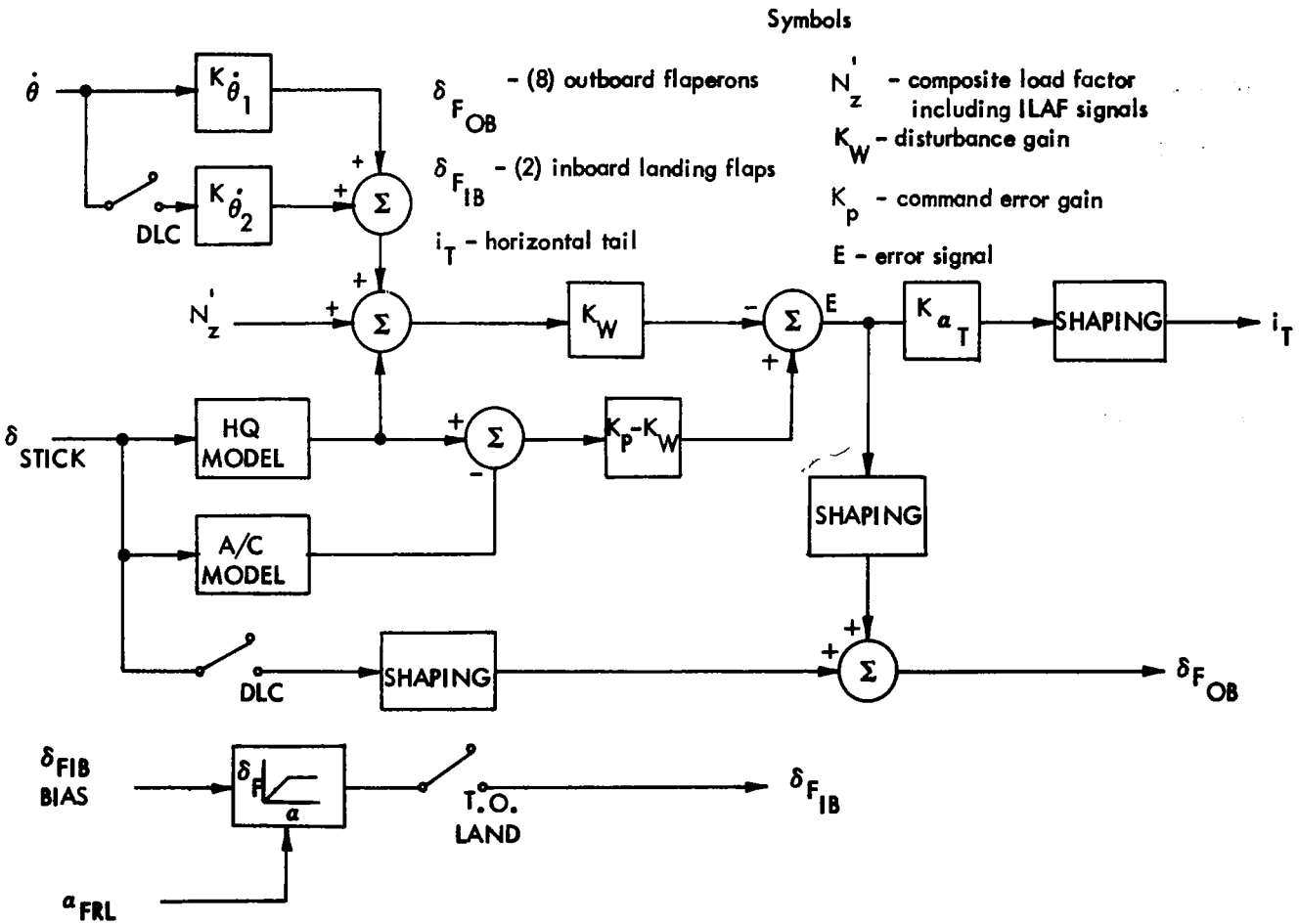

FIGURE 24 FLIGHT CONTROLS PITCH AXIS

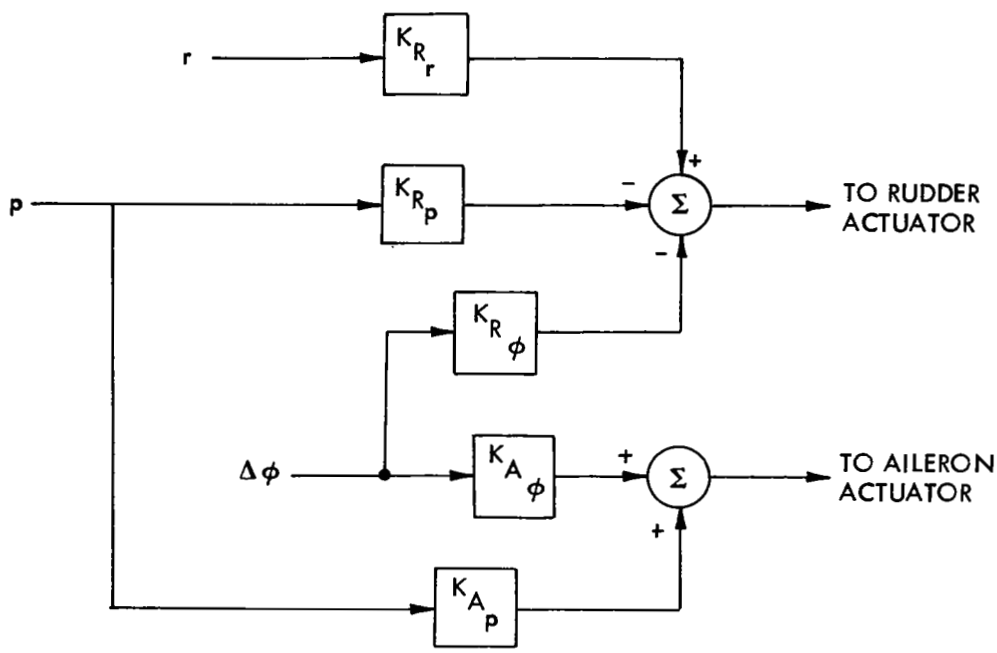

FIGURE 25 LATERAL-DIRECTIONAL AUGMENTATION

M = 0.76 GW = 14514.88KG (32,000 LB)

DERIVATIVE (PER RADIAN)	MODEL 1329-6A JETSTAR	CASE			
		1	2	3	4
C_{Y_β}	-0.750	-0.840	-1.210	-0.790	-0.490
C_{N_β}	0.115	0.103	0.206	0.092	0.0115
C_{ℓ_β}	-0.037	-0.080	-0.119	-0.061	-0.028
C_{Y_r}	-	0.350	0.550	0.322	0.160
C_{N_r}	-0.151	-0.103	-0.158	-0.096	-0.051
C_{ℓ_r}	0.0	0.175	0.198	0.166	0.148
C_{Y_p}	-	0.100	0.100	0.100	0.100
C_{N_p}	0.018	0.052	0.052	0.052	0.052
C_{ℓ_p}	-0.410	-0.700	-0.700	-0.700	-0.700
$C_{Y_{\delta_R}}$	0.180	0.321	0.418	0.344	0.212
$C_{N_{\delta_R}}$	-0.0665	-0.0870	-0.1146	-0.0940	-0.0573
$C_{\ell_{\delta_R}}$	0.0270	0.0356	0.0465	0.0321	0.0155
$C_{\ell_{\delta_A}}$	-0.0573	-0.0573	-0.0573	-0.0573	-0.0573
$C_{N_{\delta_A}}$	0	0	0	0	0

CASE	DESCRIPTION
1	JETSTAR + NEW WING (AR = 9)
2	CASE 1 + TEE TAIL (TAPER RATIO = 0.8)
3	CASE 2 + 65% VERTICAL TAIL AREA
4	CASE 3 + 37.5% VERTICAL TAIL

FIGURE 26 LATERAL-DIRECTIONAL STABILITY DERIVATIVES

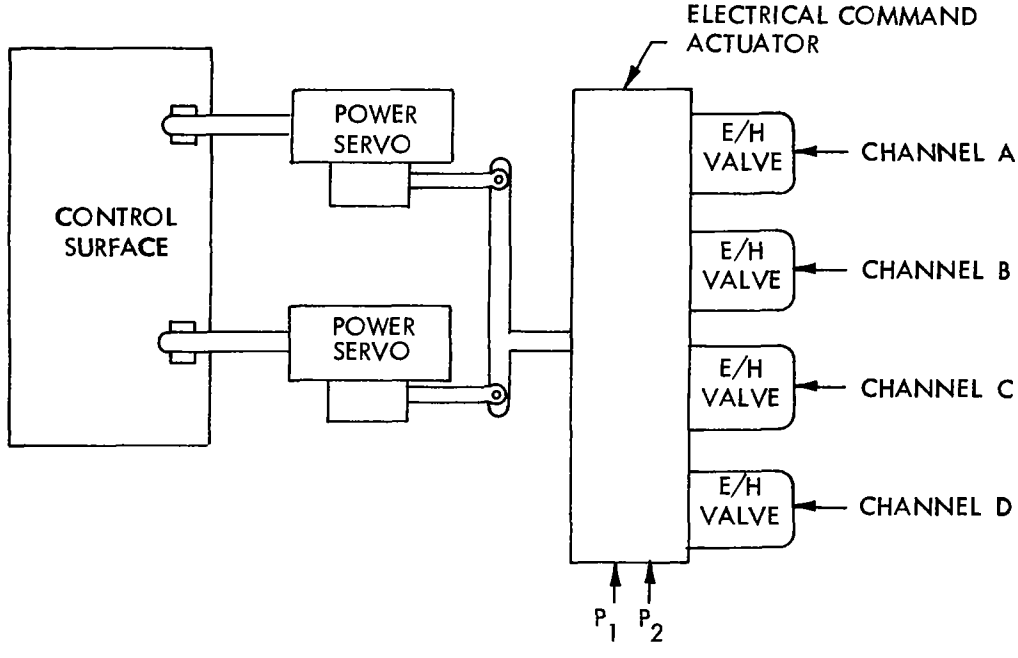

FIGURE 27 POWER SERVO MECHANIZATION

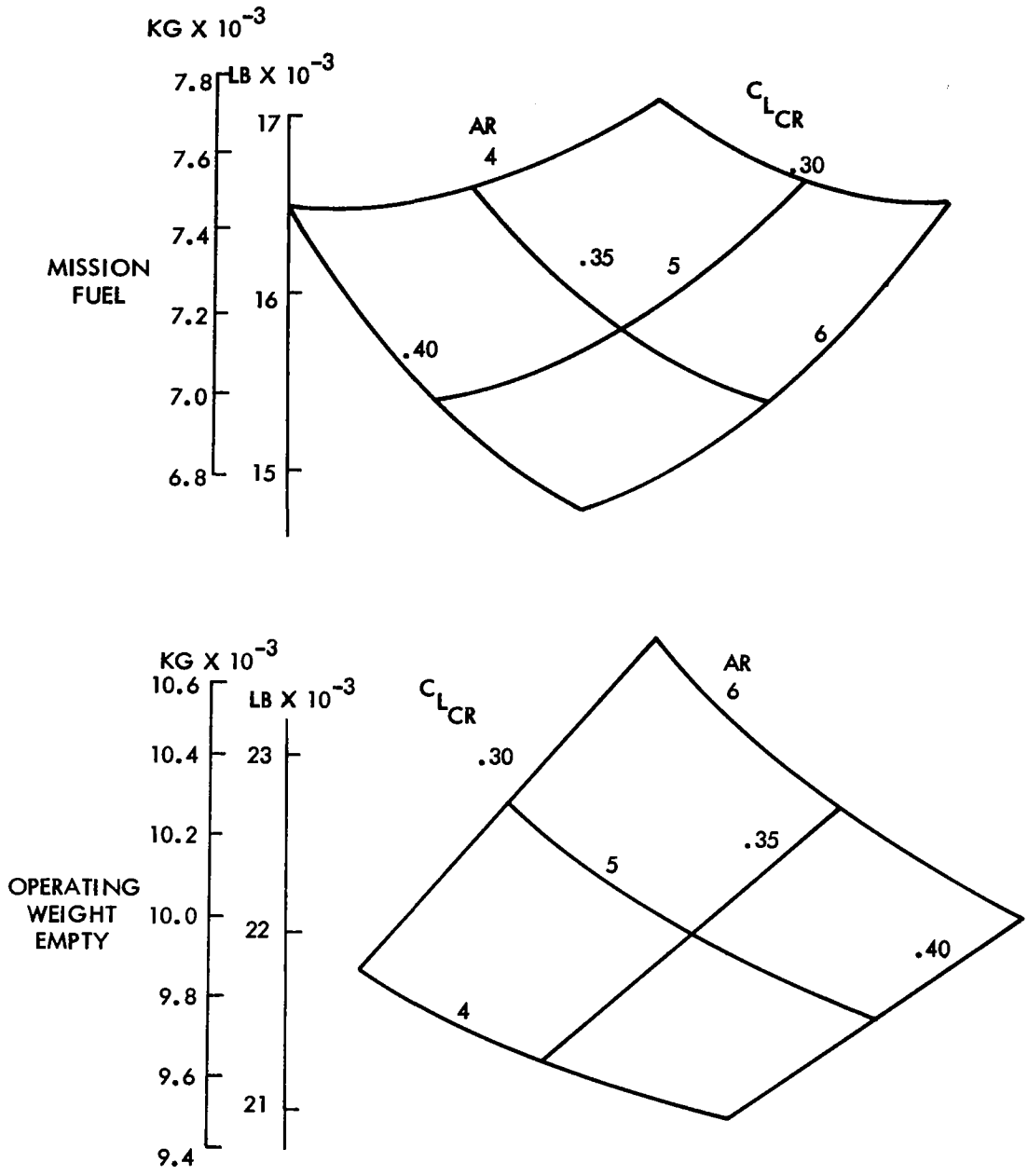

FIGURE 28 MISSION FUEL REQUIREMENT AND OPERATING WEIGHT, INTERMEDIATE CONFIGURATION

Error

An error occurred while processing this page. See the system log for more details.

$\Lambda_{\overline{C/4}}$ = 0.524 RADS (30 DEGS)

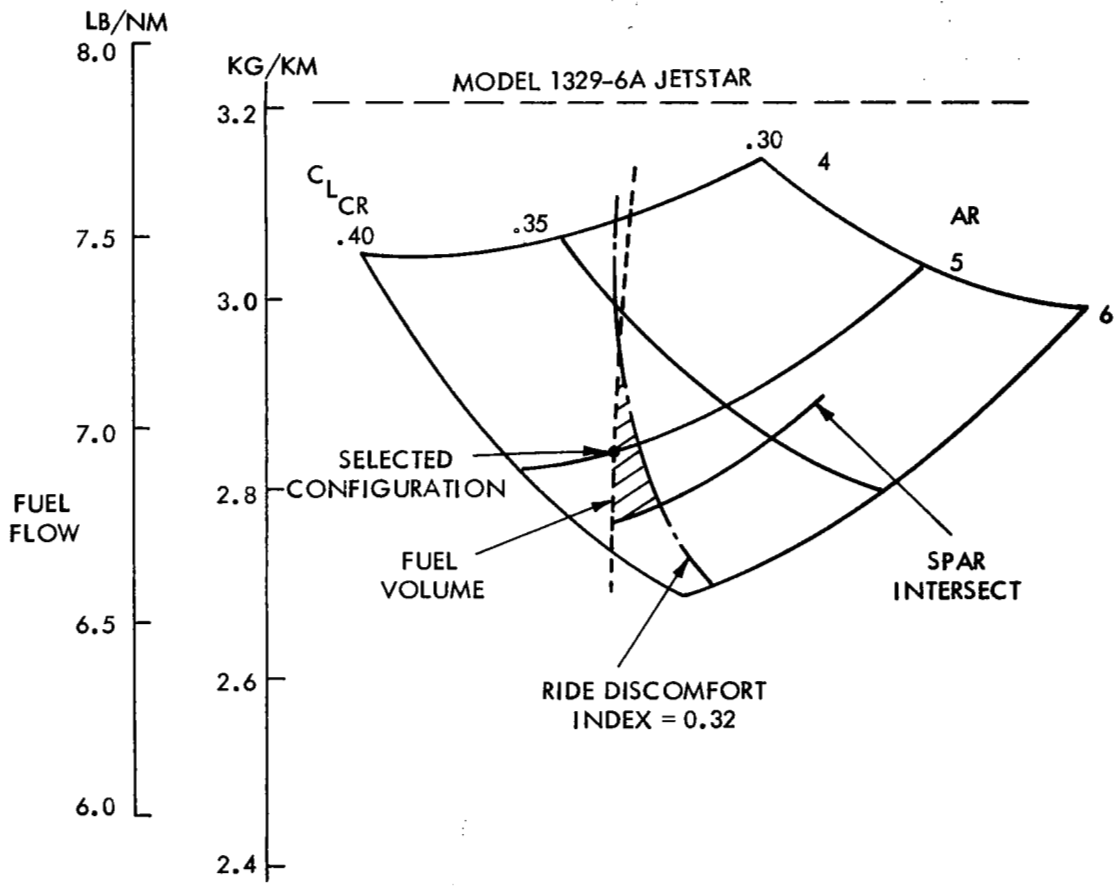

FIGURE 30 INTERMEDIATE CONFIGURATION SELECTION

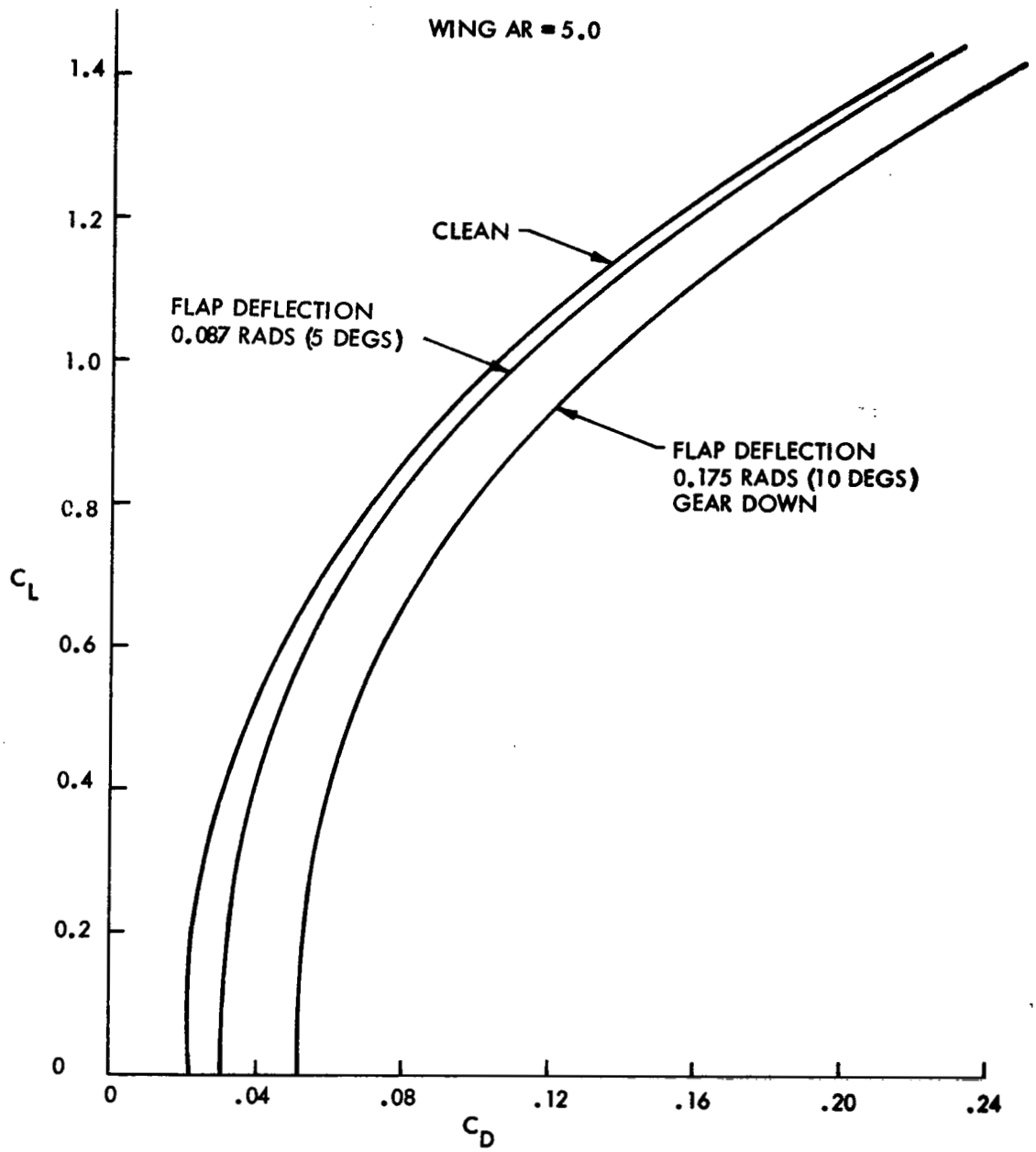

FIGURE 31 INTERMEDIATE CONFIGURATION LOW SPEED DRAG POLARS

SPAN 15.28M (50.13 FT)
LENGTH 18.43M (60.47 FT)
HEIGHT 6.25M (20.5 FT)

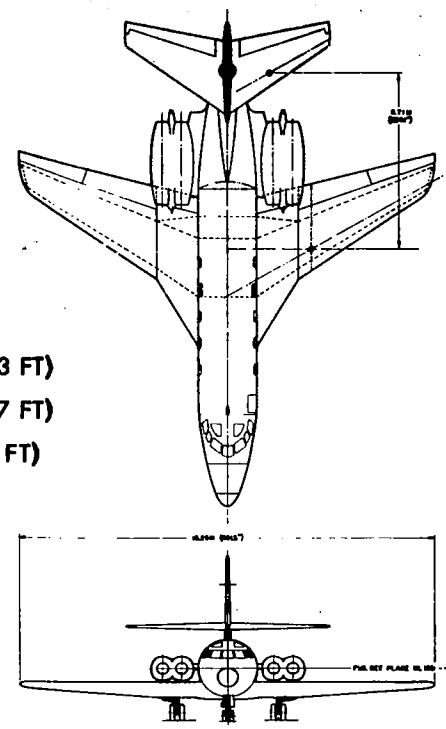

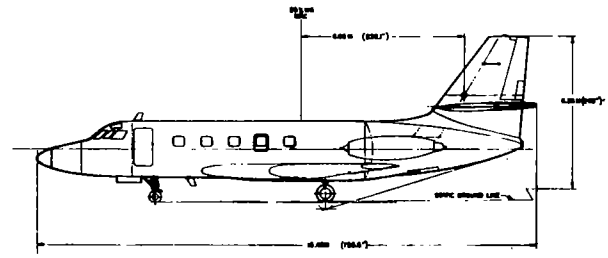

FIGURE 32 INTERMEDIATE CONFIGURATION

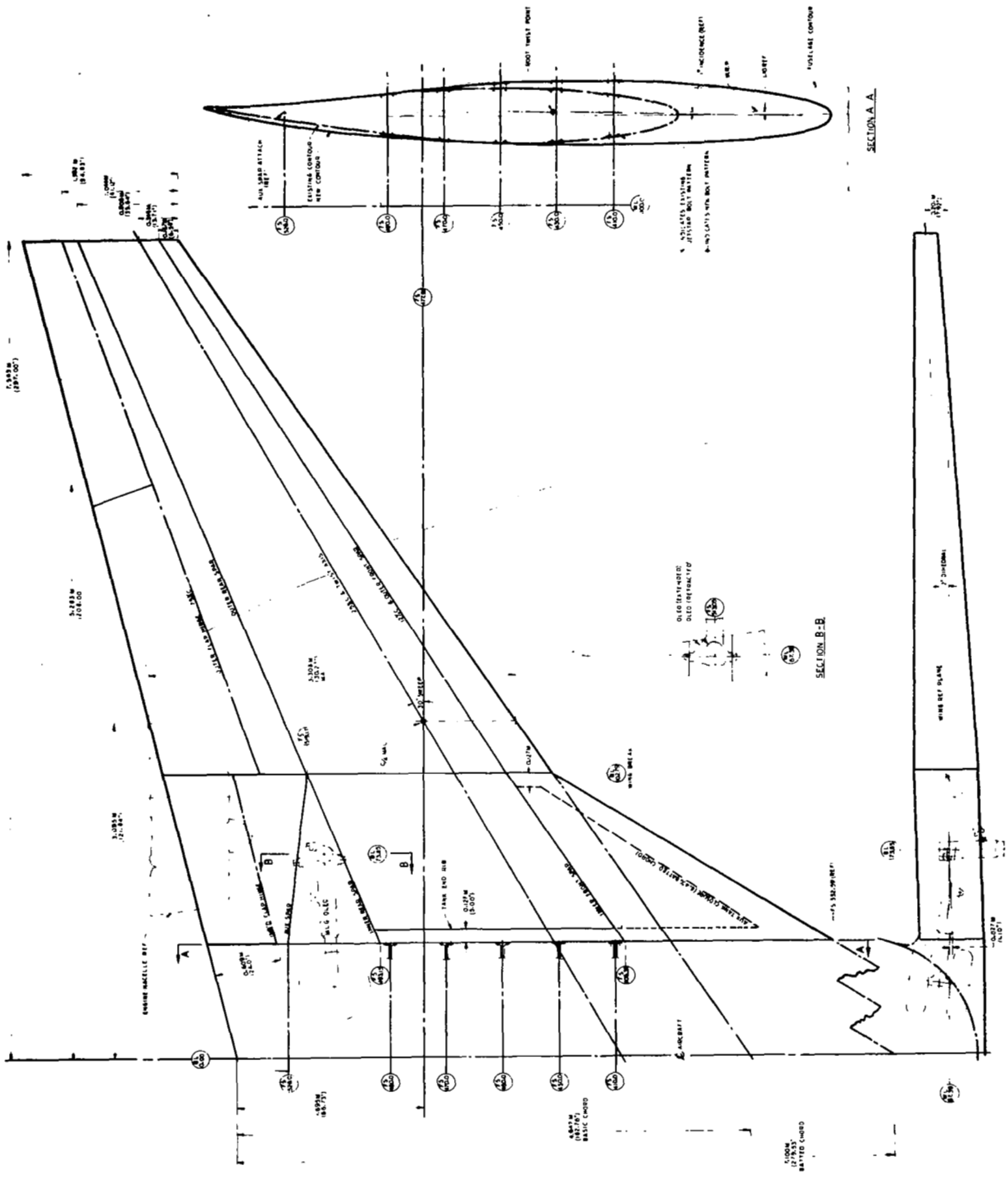

FIGURE 33 INTERMEDIATE AIRPLANE WING LAYOUT

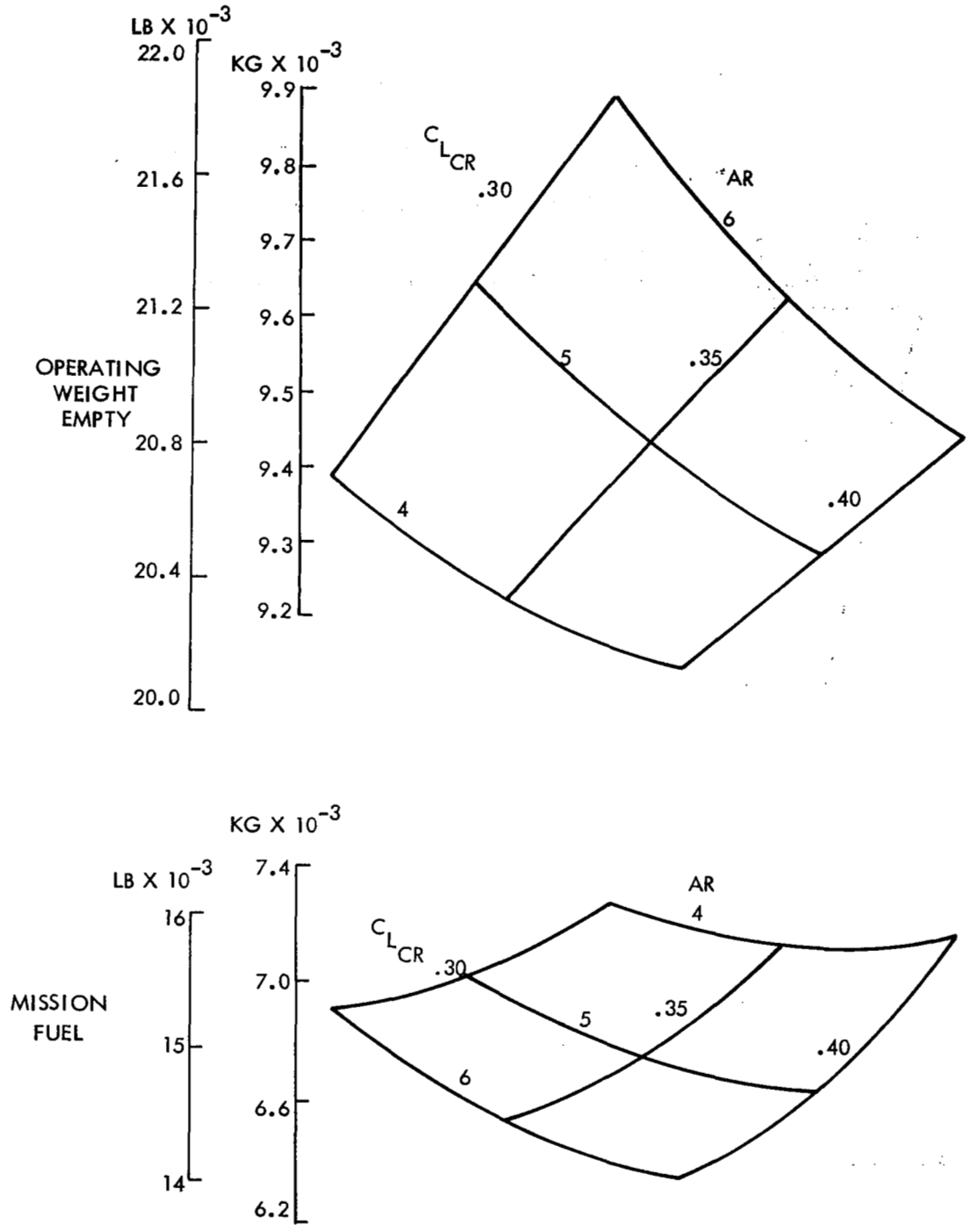

FIGURE 34 ALTERNATE CONFIGURATION MISSION FUEL AND OPERATING WEIGHT

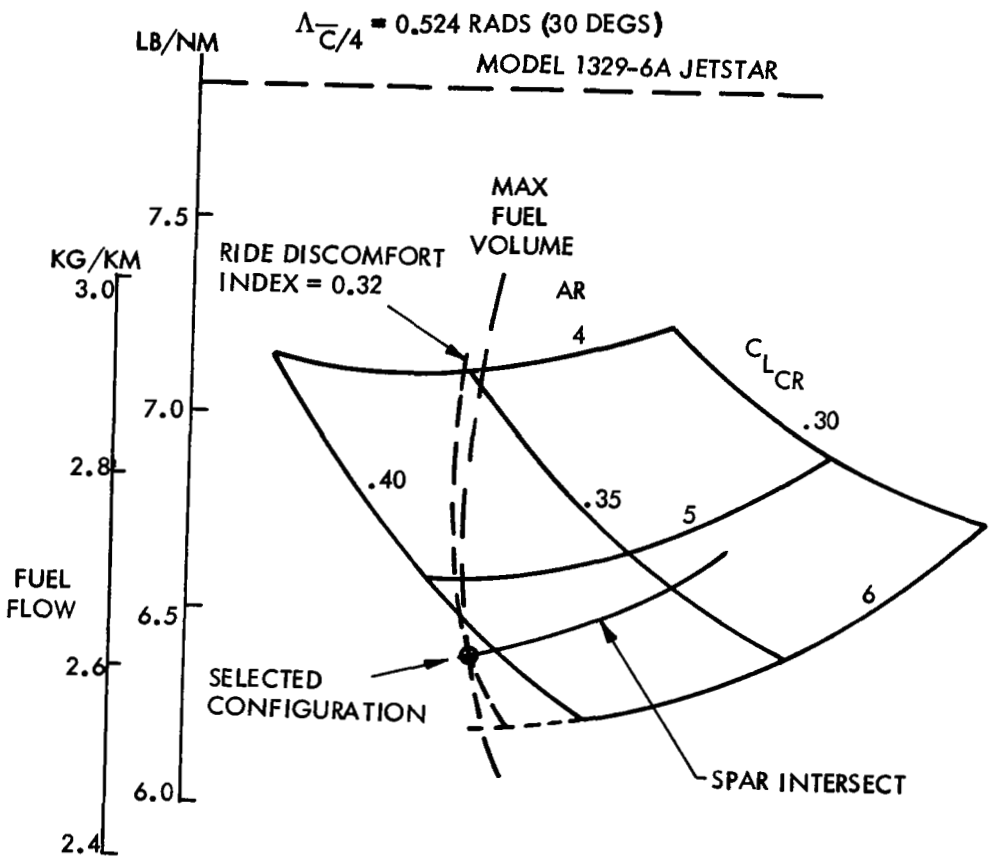

FIGURE 35 ALTERNATE CONFIGURATION SELECTION

SPAN 15.85M (52.0 FT)
LENGTH 18.43M (60.47 FT)
HEIGHT 6.25M (20.5 FT)

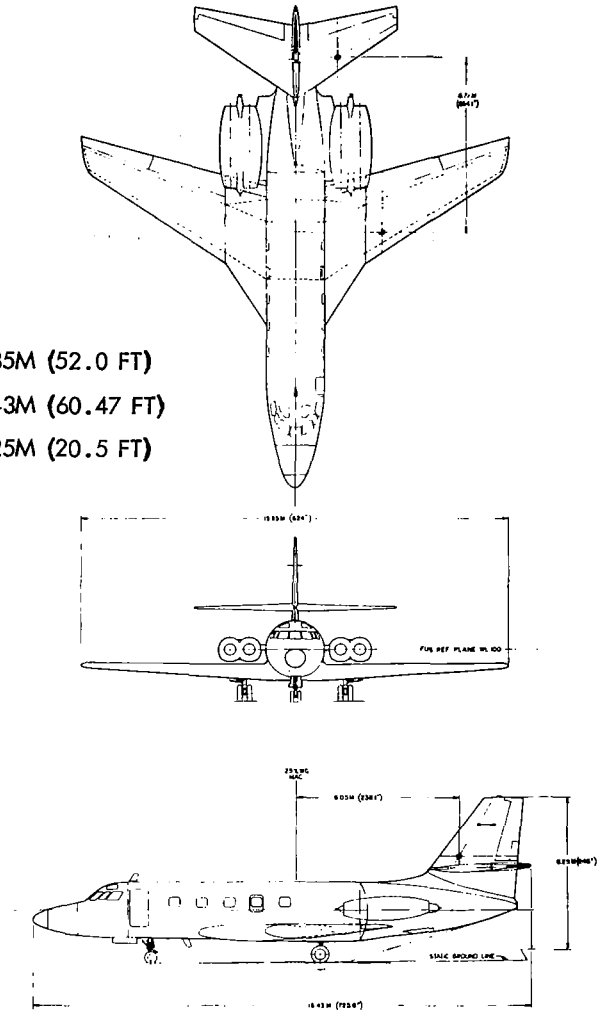

FIGURE 36 ALTERNATE CONFIGURATION

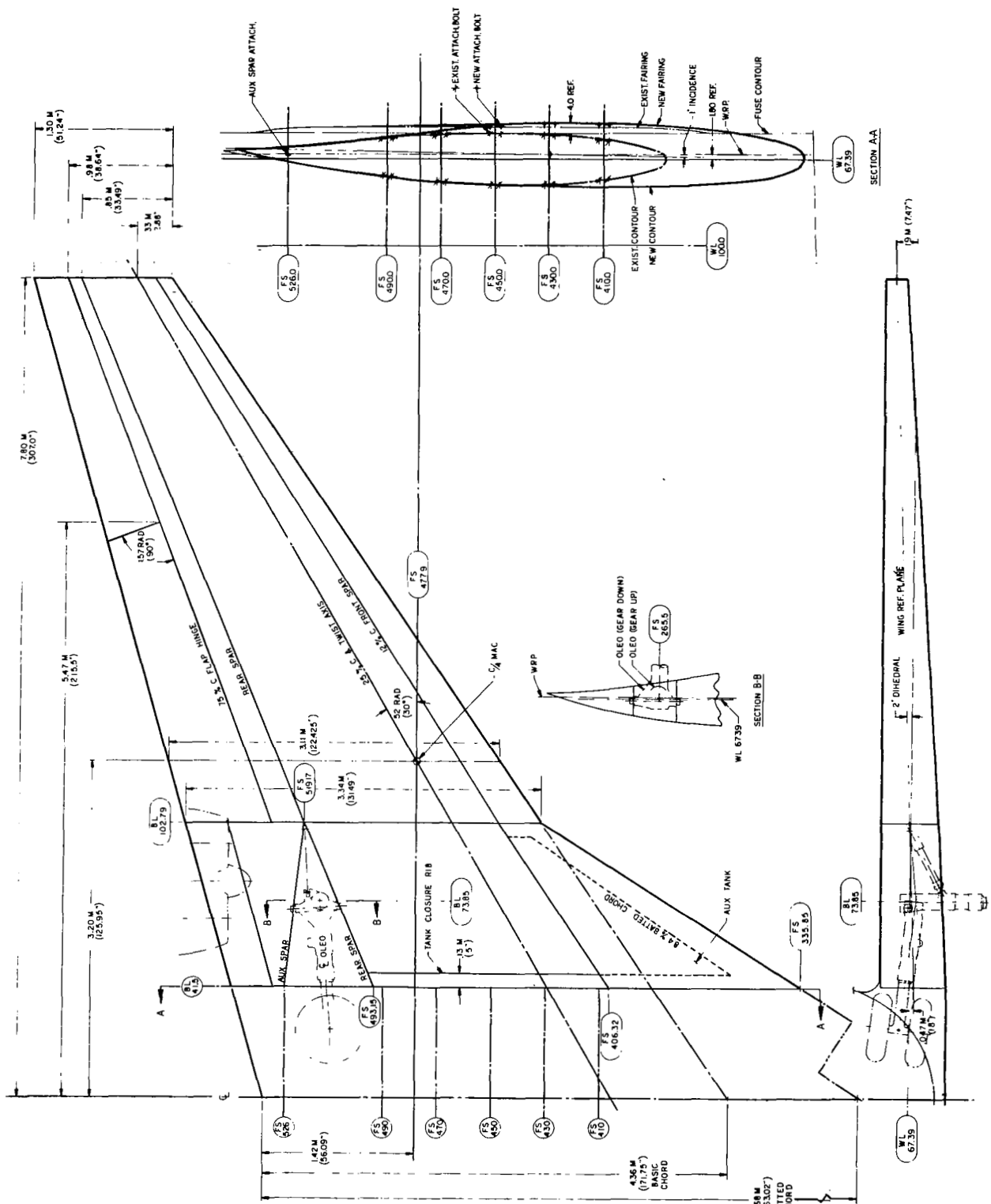

FIGURE 37 ALTERNATE AIRPLANE WING LAYOUT

	$C_{L_{MAX}}$		AR	L/D	
	TAKEOFF	APPROACH		TAKEOFF $1.2\ V_S$	APPROACH $1.3V_S$ + 10 kts GEAR DOWN
MODEL 1329-6A JETSTAR	1.53 δ_f = 0.35 RADS (20 DEGS)	1.70 δ_f = 0.873 RADS (50 DEGS)	5.3	8.95	5.2
ACT CONFIGURATION	1.64 δ_f = 0 RAD (0 DEG)	1.80 δ_f = 0.087 RADS (5 DEGS)	9.0	14.10	11.50
INTERMEDIATE CONFIGURATION	1.50 δ_f = 0.087 RADS (5 DEGS)	1.73 δ_f = 0.175 RADS (10 DEGS)	5.0	8.70	7.88
ALTERNATE CONFIGURATION	1.45 δ_f = 0.087 RADS (5 DEGS)	1.68 δ_f = 0.175 RADS (10 DEGS)	5.5	9.47	8.35

FIGURE 38 HIGH-LIFT PERFORMANCE COMPARISON

	APPROACH EPNdB	ALTITUDE H_1 M (FT)	ALTITUDE H_2 M (FT)	FLYOVER CUTBACK POWER EPNdB
MODEL 1329-6A JETSTAR	107	463 (1520)	496 (1630)	101
ACT JETSTAR	91	866 (2842)	922 (3029)	93
INTERMEDIATE	97	463 (1520)	496 (1630)	101
ALTERNATE CONFIGURATION	96	503 (1650)	533 (1750)	100

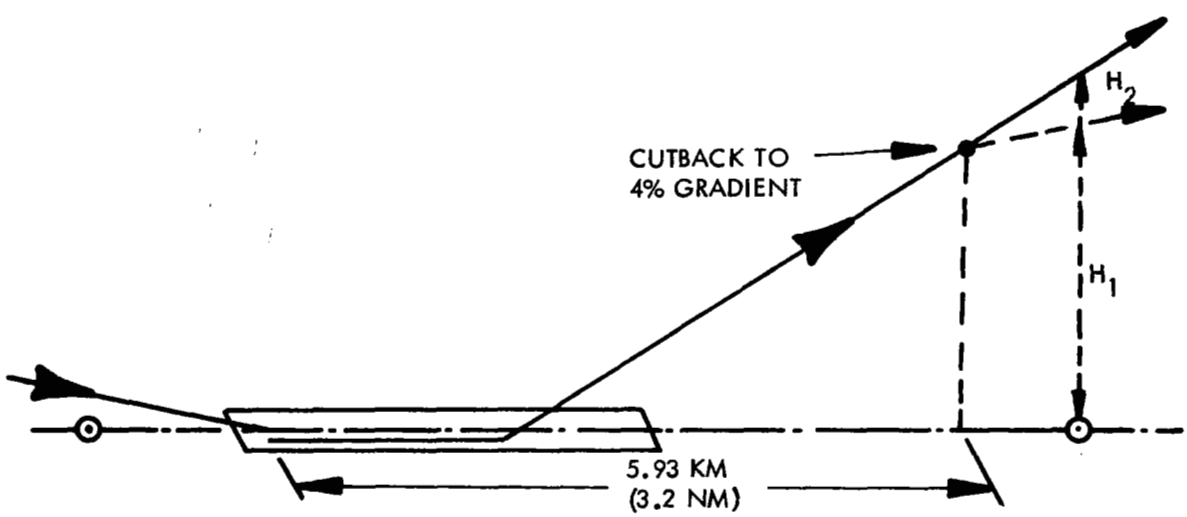

FIGURE 39 NOISE PROFILE COMPARISON
FAR 36 RULES EPNdB

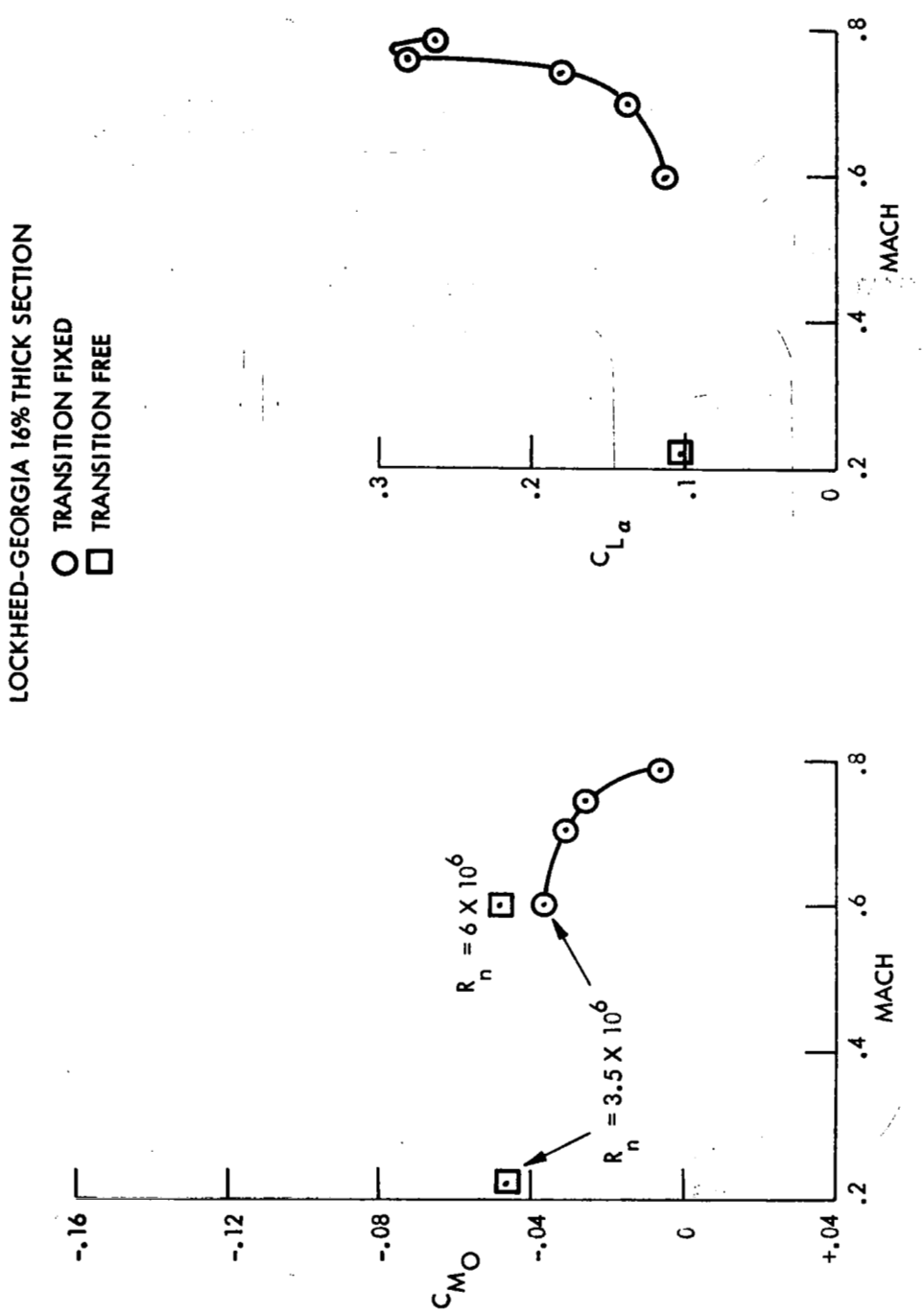

FIGURE A1 EXPERIMENTAL LIFT AND MOMENT DATA

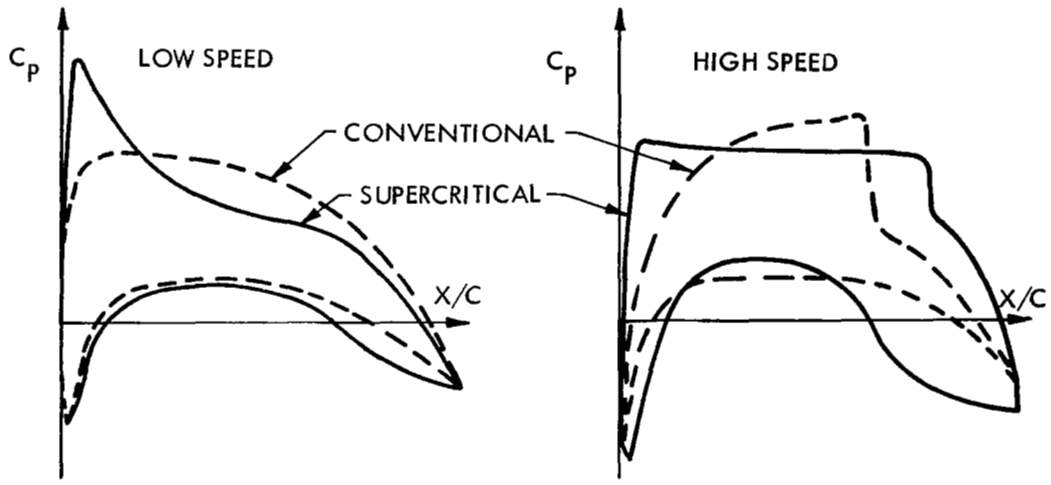

(a) EFFECT OF SUPERCRITICAL DESIGN TECHNOLOGY ON SECTION PRESSURE DISTRIBUTION

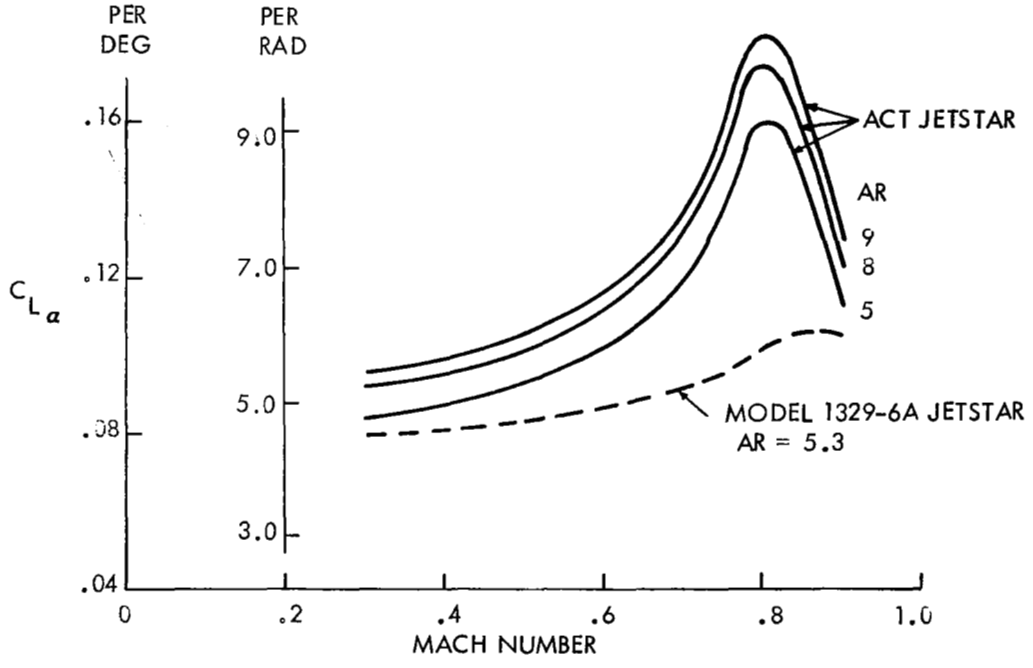

(b) PREDICTED WING LIFT CURVE SLOPES

FIGURE A2 SUPERCRITICAL WING TRANSONIC CHARACTERISTICS

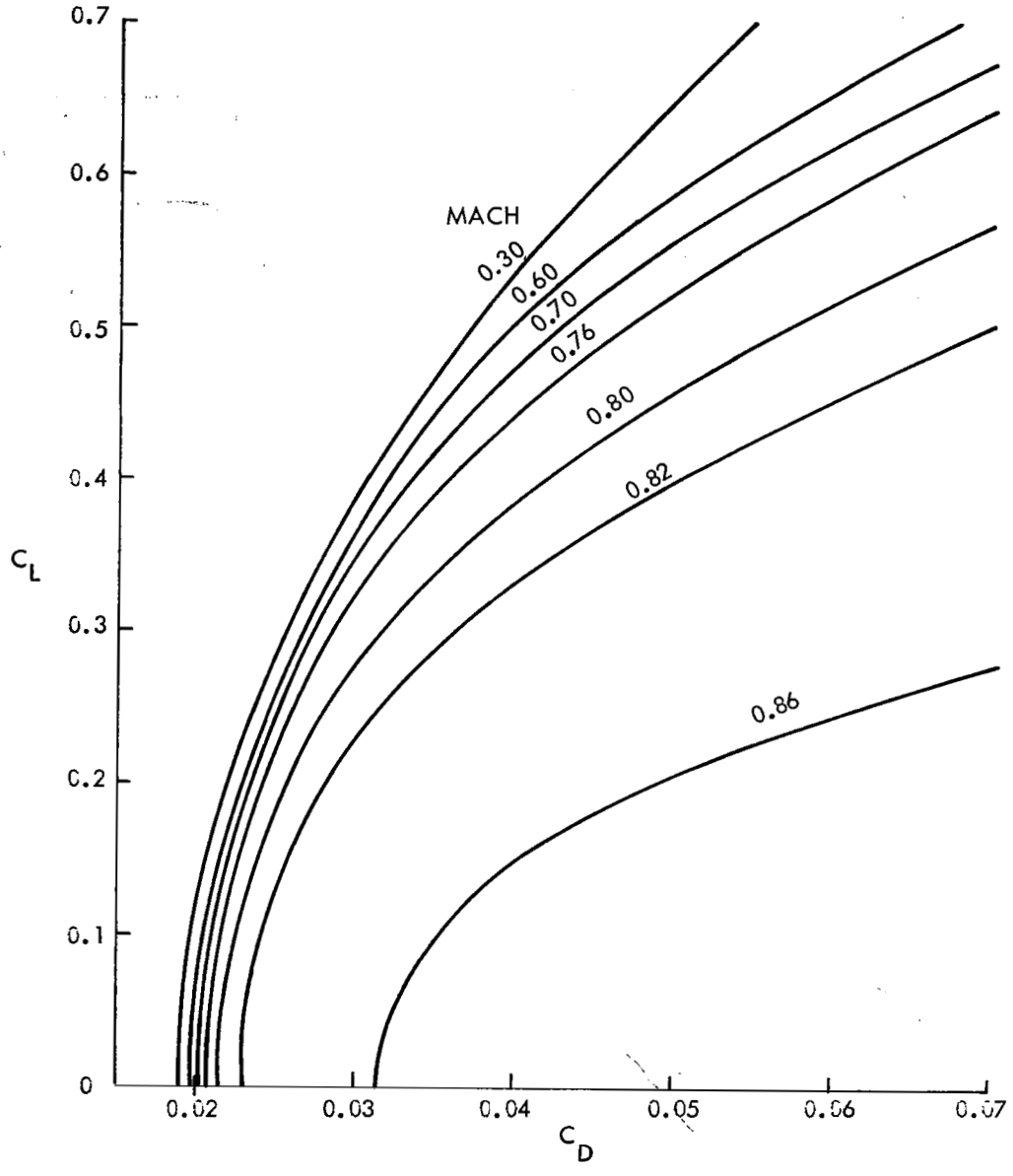

FIGURE A3 JETSTAR MODEL 1329-6A
CLEAN CONFIGURATION DRAG POLARS

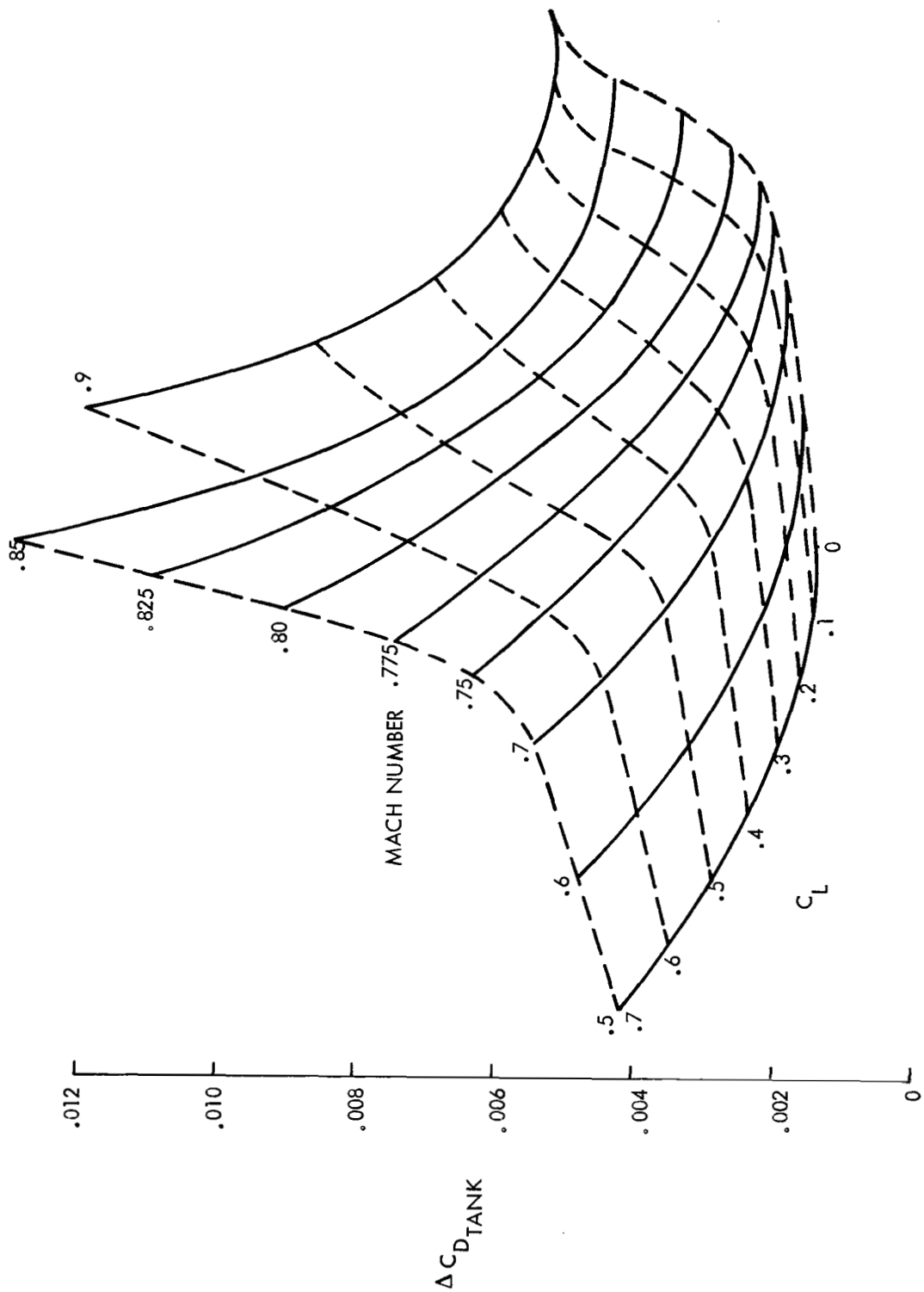

FIGURE A4 JETSTAR MODEL 1329-6A
WING EXTERNAL TANK DRAG

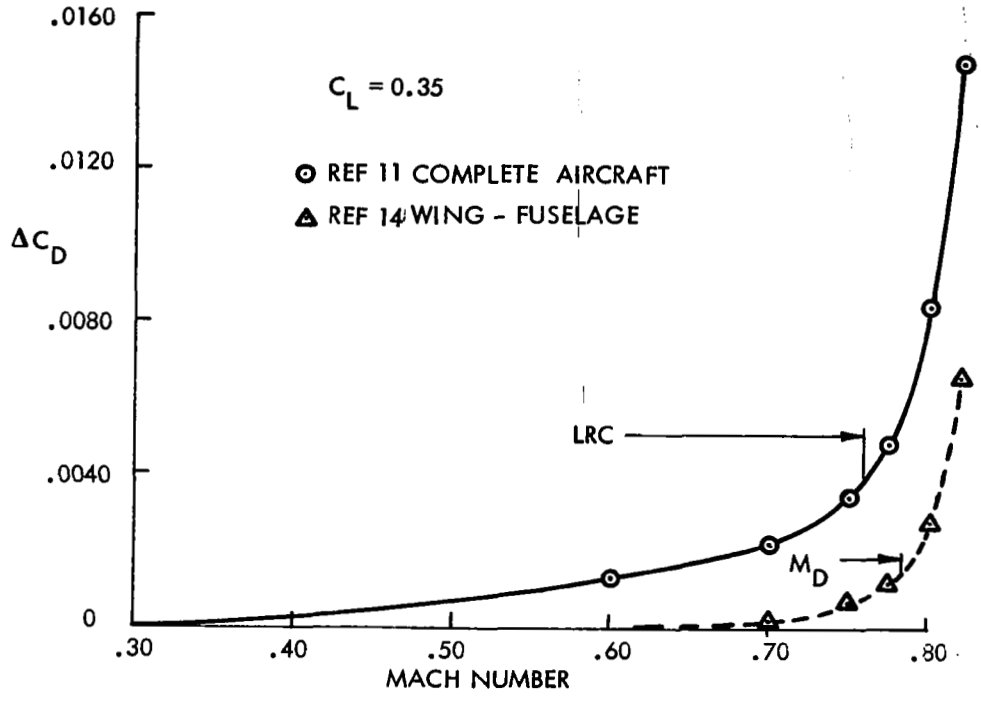

FIGURE A5 JETSTAR MODEL 1329-6A
DRAG-RISE CHARACTERISTICS

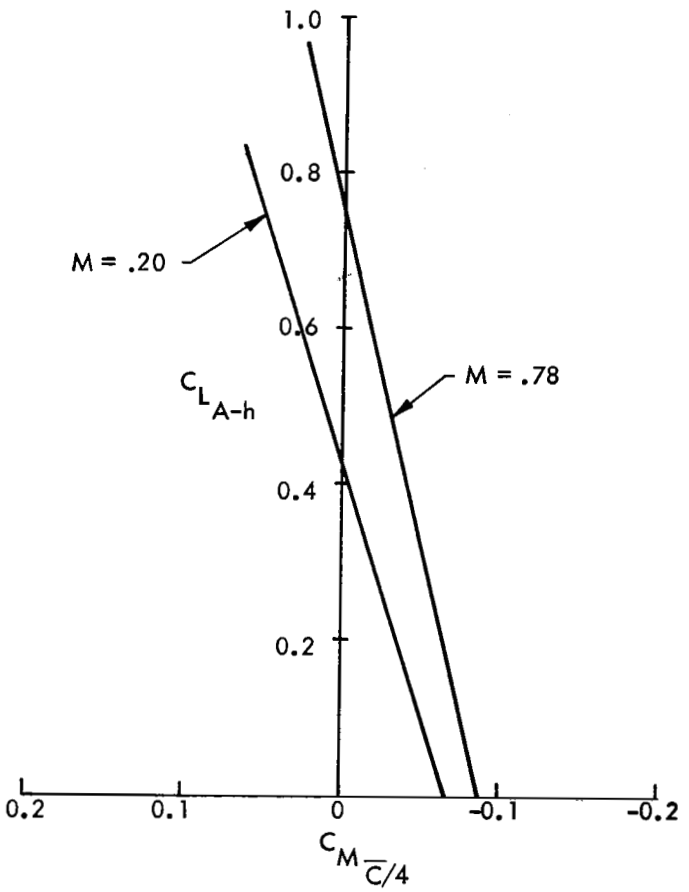

FIGURE A6 TAIL-OFF PITCHING MOMENT CHARACTERISTICS

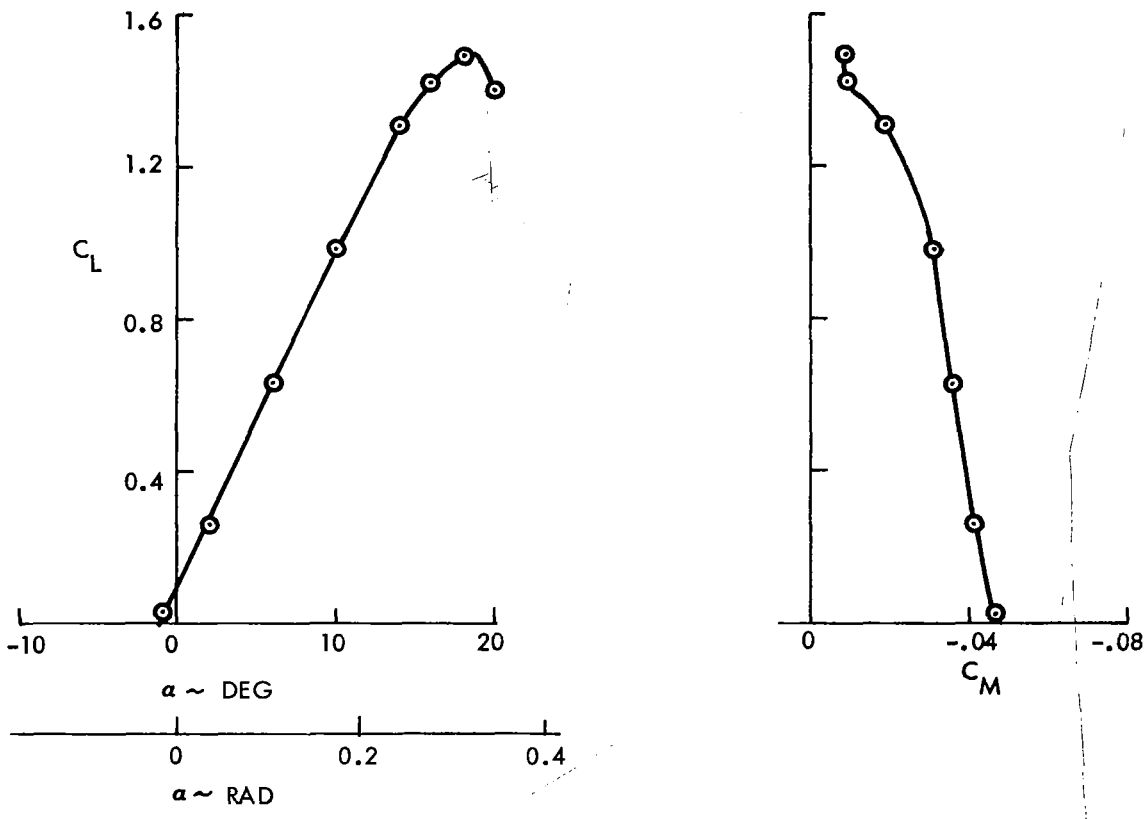

FIGURE A7 AIRFOIL LIFT AND PITCH CHARACTERISTICS

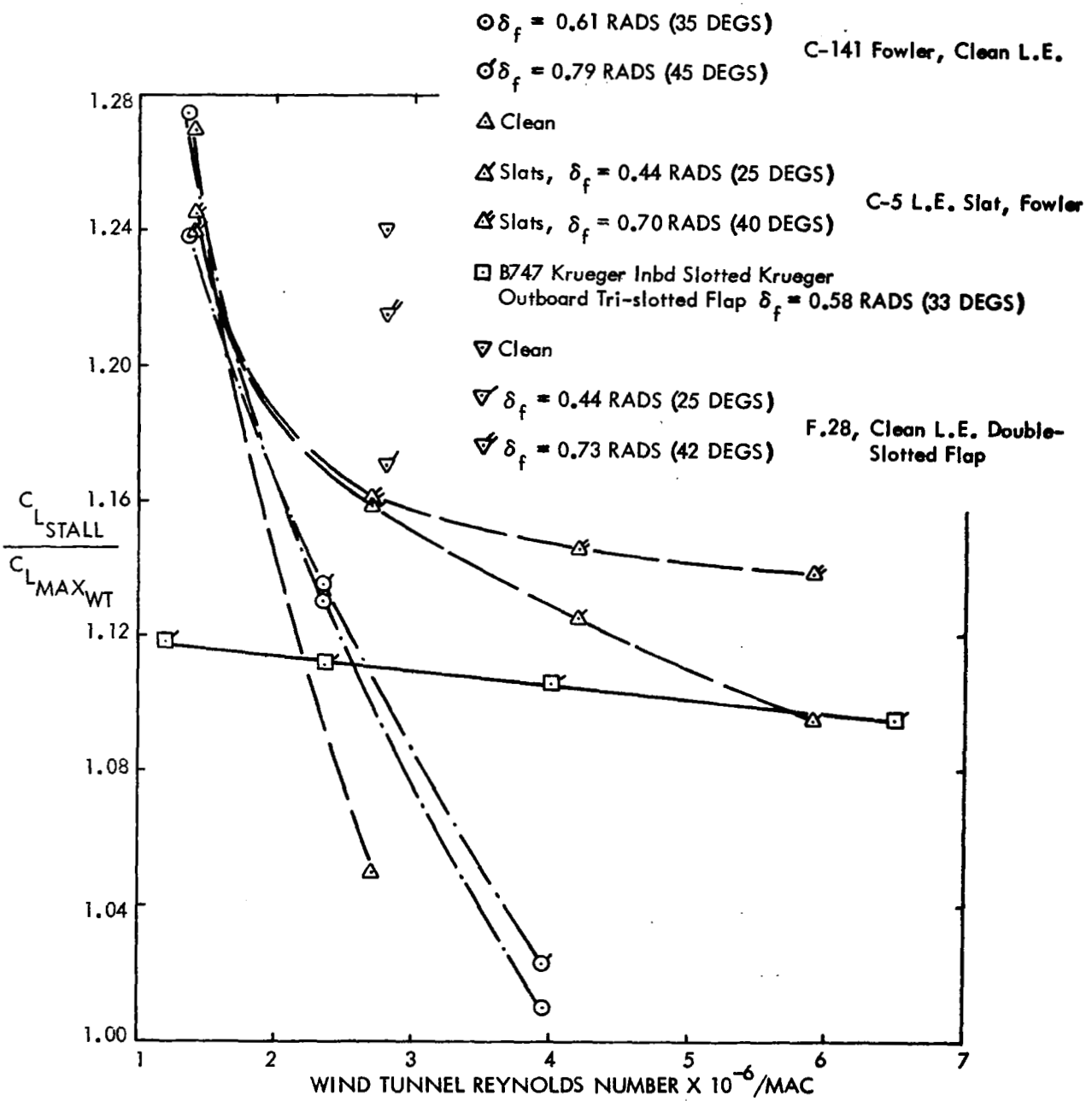

FIGURE A8 FULL SCALE CORRECTIONS TO MAXIMUM LIFT COEFFICIENT

S_{REF} = 53.88 SQ M (580 SQ FT) MAC = 2.85 M (9.34 FT)

WING AR = 8.0

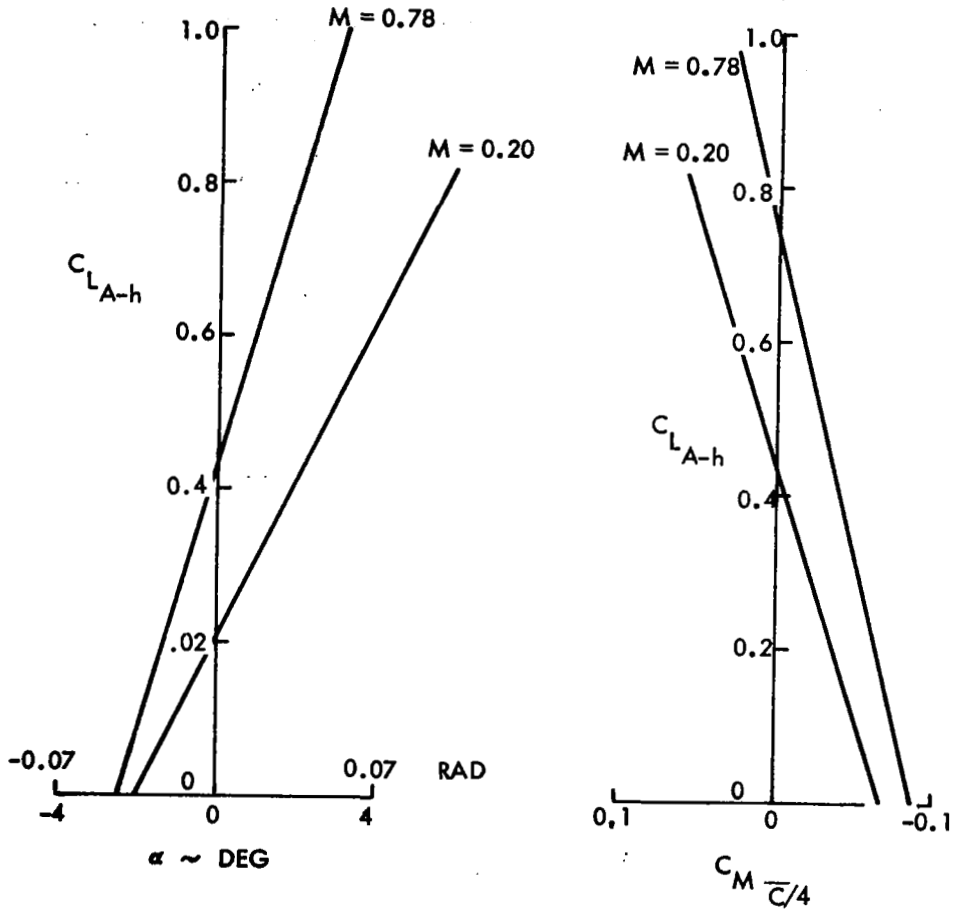

FIGURE A9 TAIL-OFF LIFT AND PITCH CHARACTERISTICS

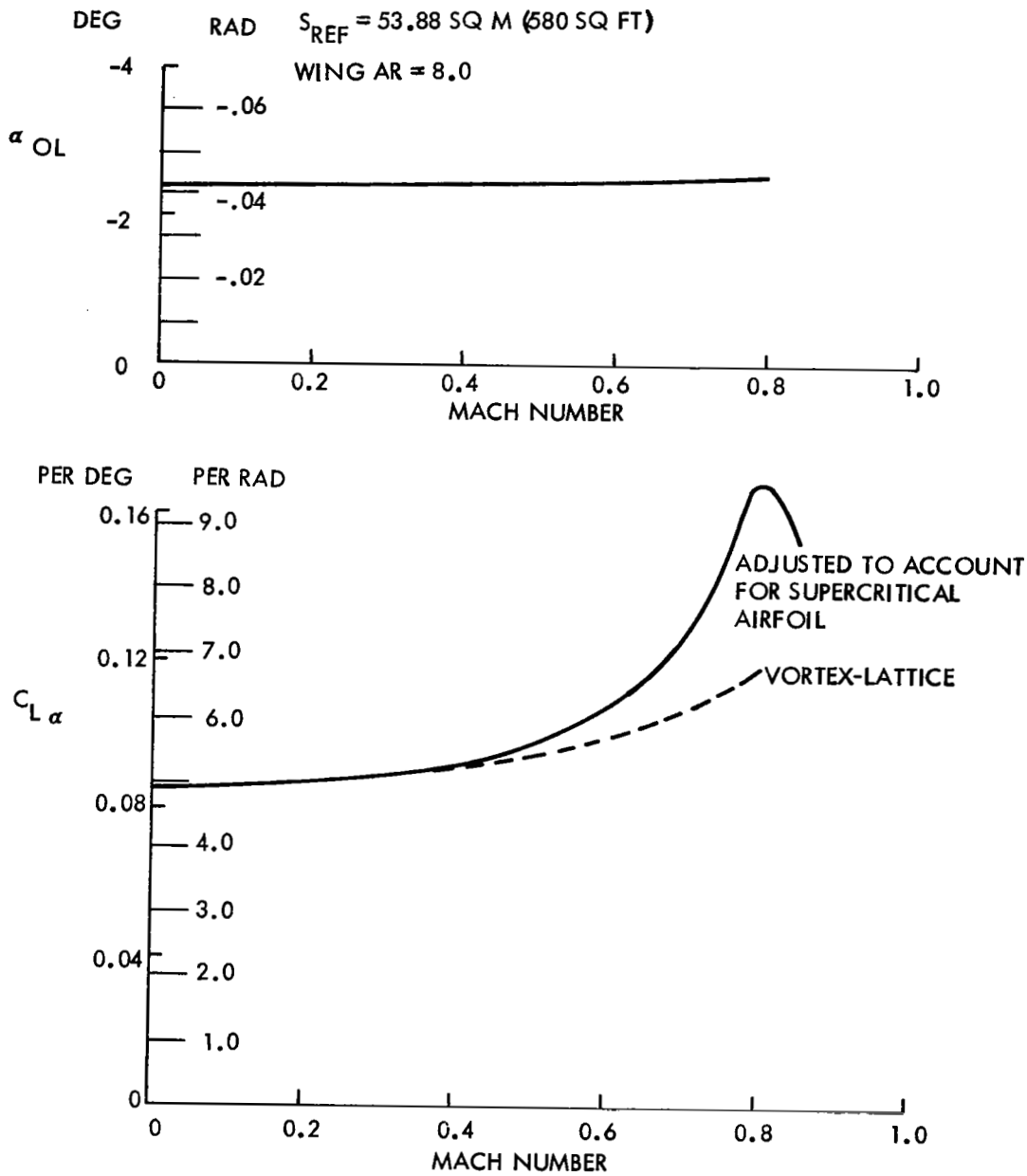

FIGURE A10 WING LIFT CHARACTERISTICS

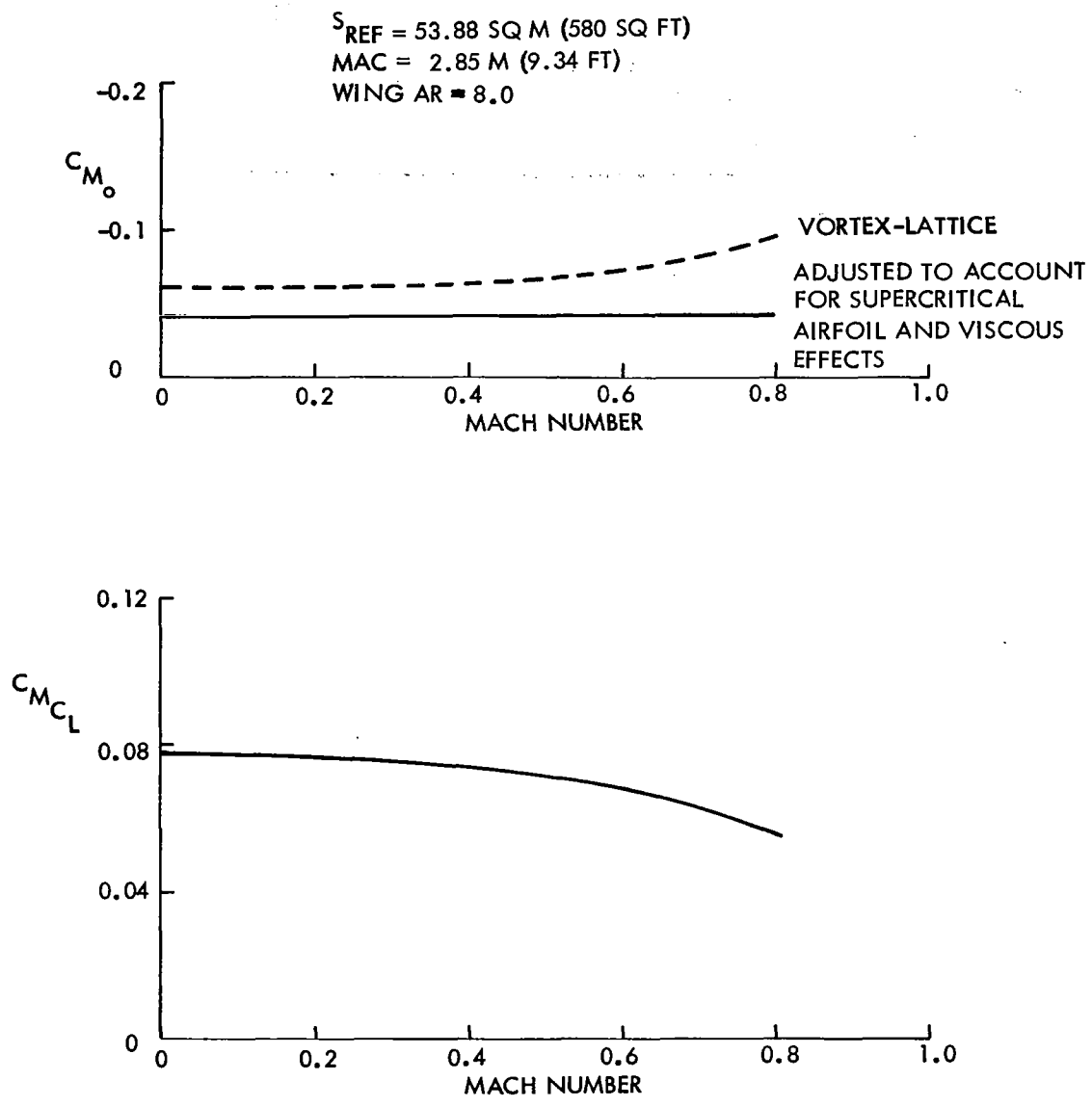

FIGURE A11 WING PITCHING MOMENT CHARACTERISTICS

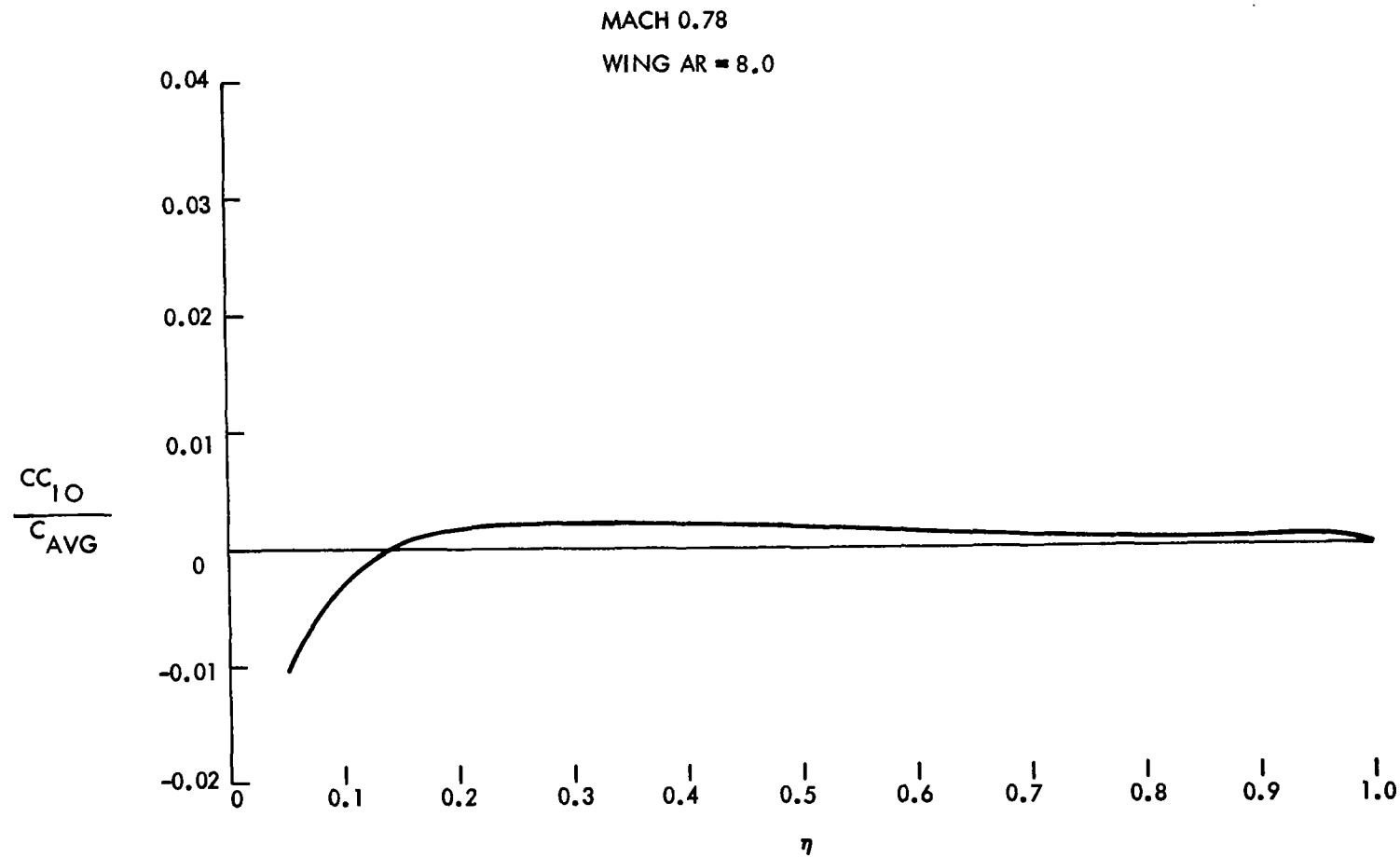

FIGURE A12 WING BASIC LIFT DISTRIBUTION

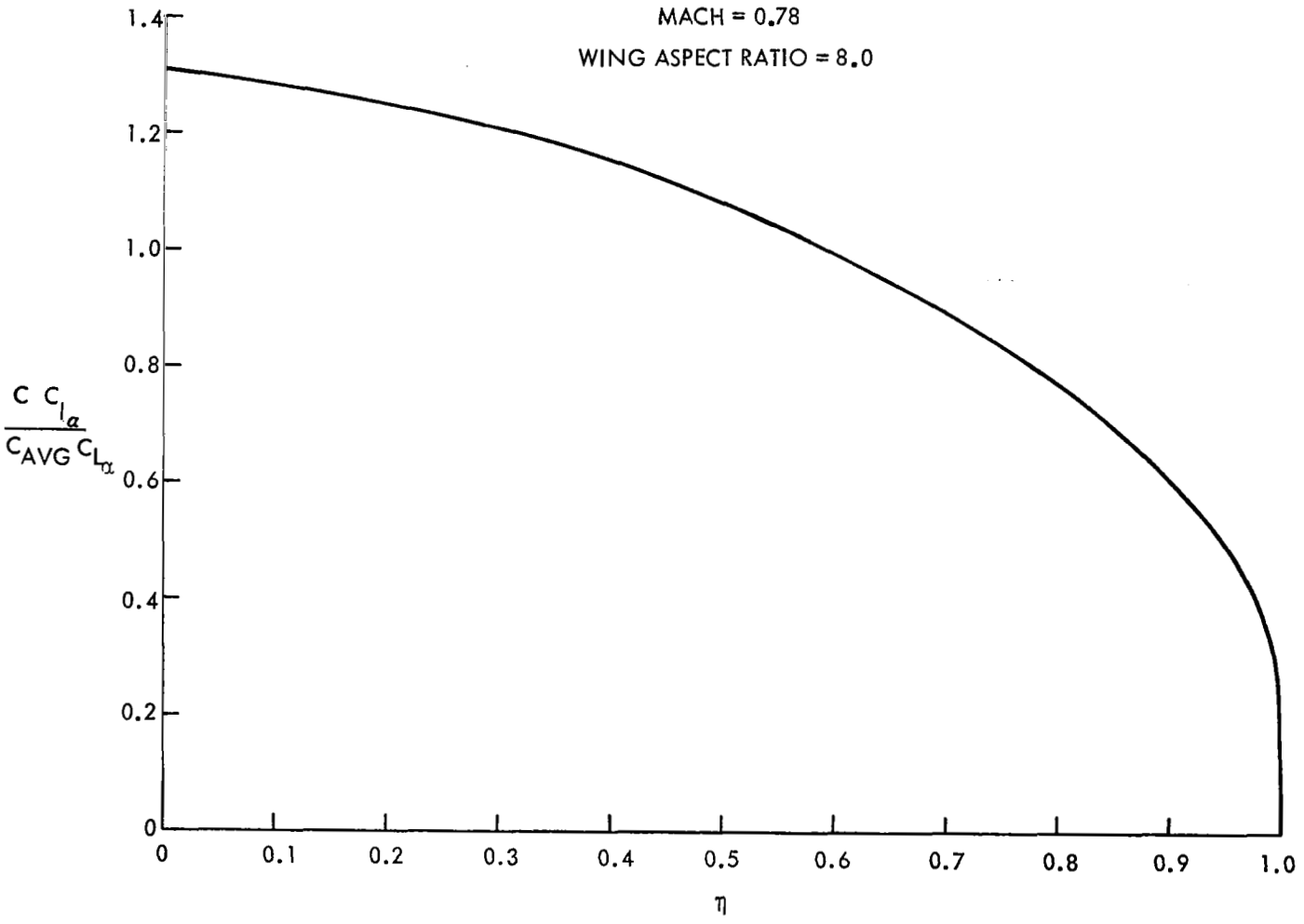

FIGURE A13 WING ADDITIONAL LIFT DISTRIBUTION

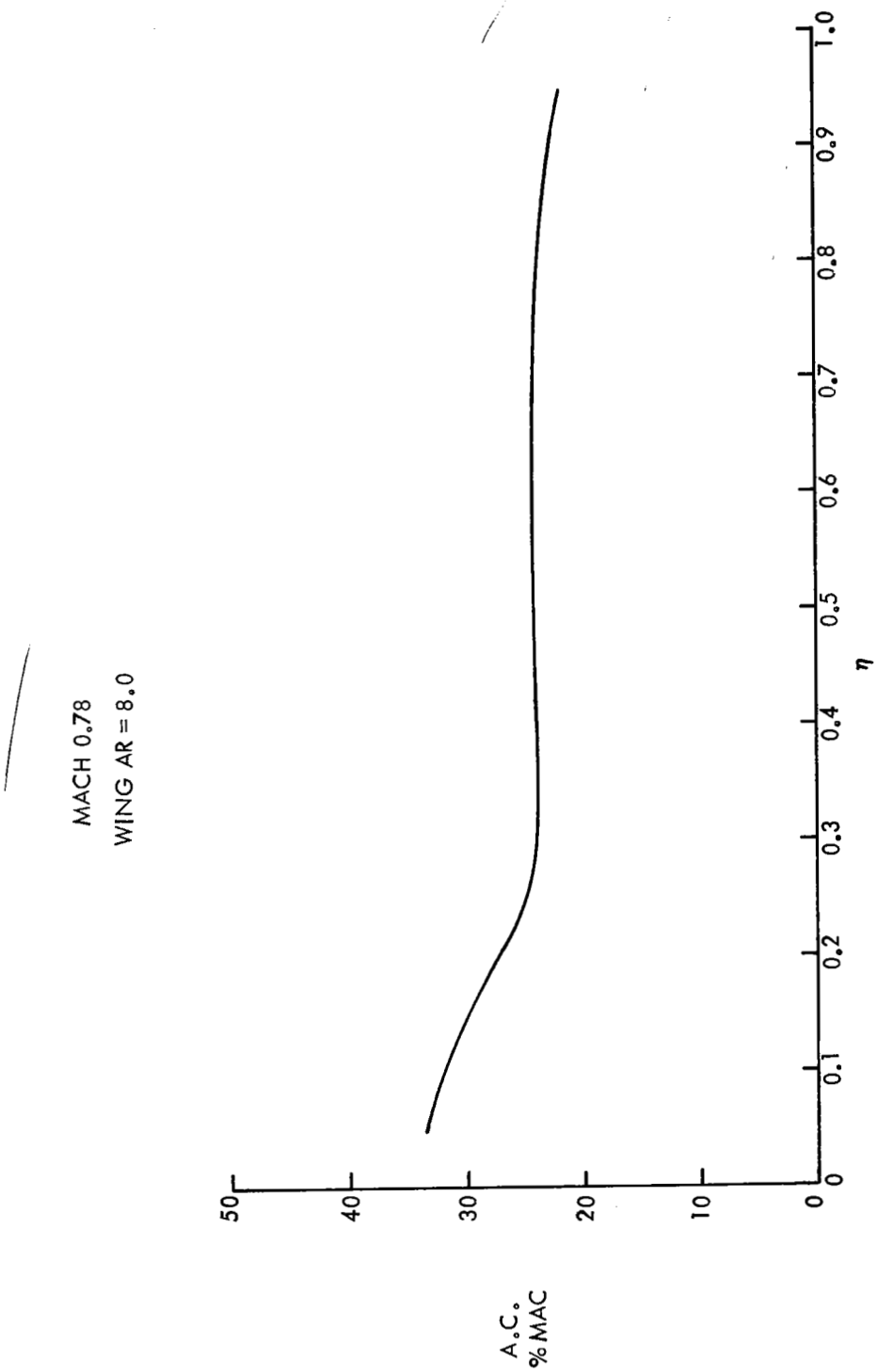

FIGURE A14 WING AERODYNAMIC CENTER DISTRIBUTION

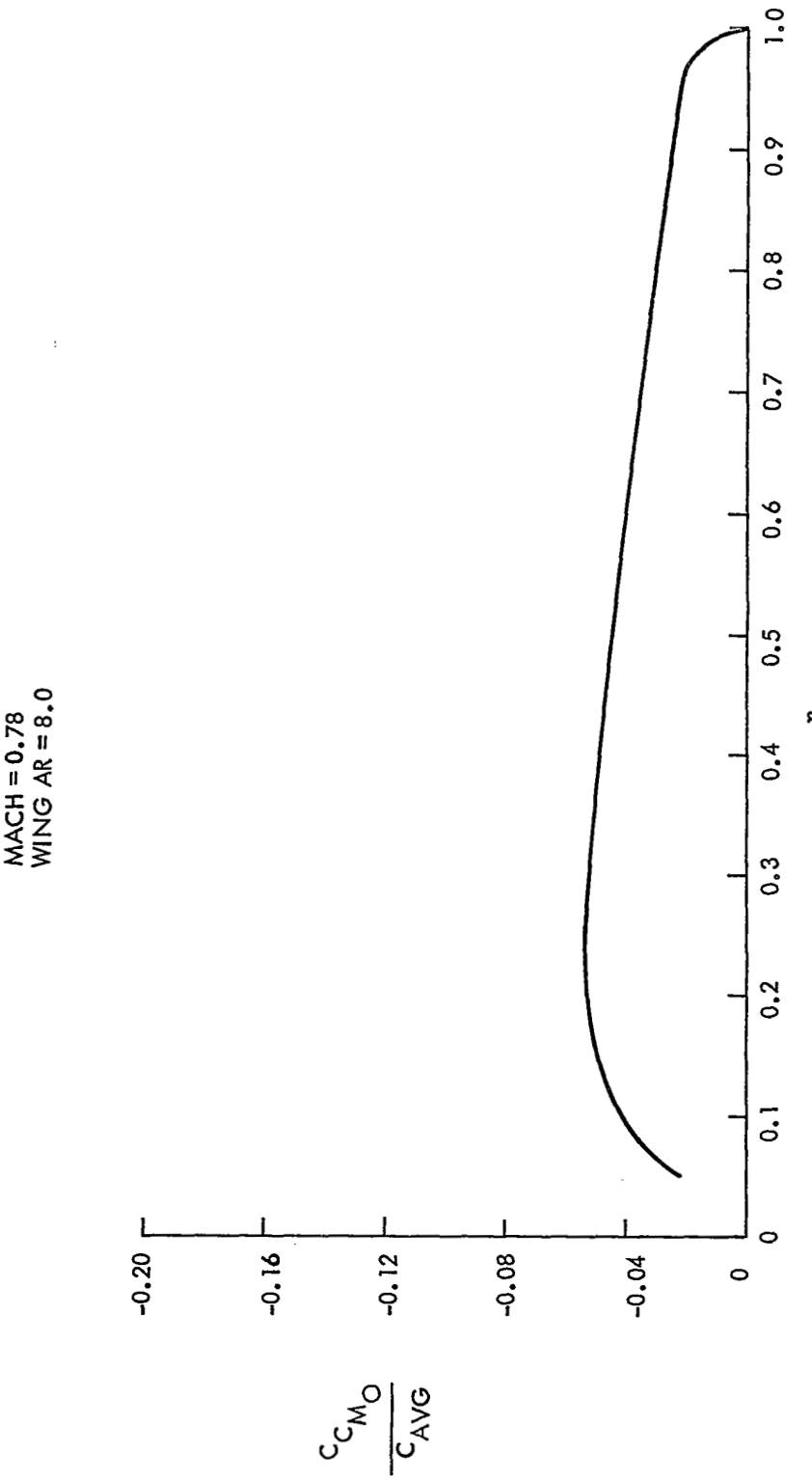

FIGURE A15 WING BASIC PITCHING MOMENT DISTRIBUTION

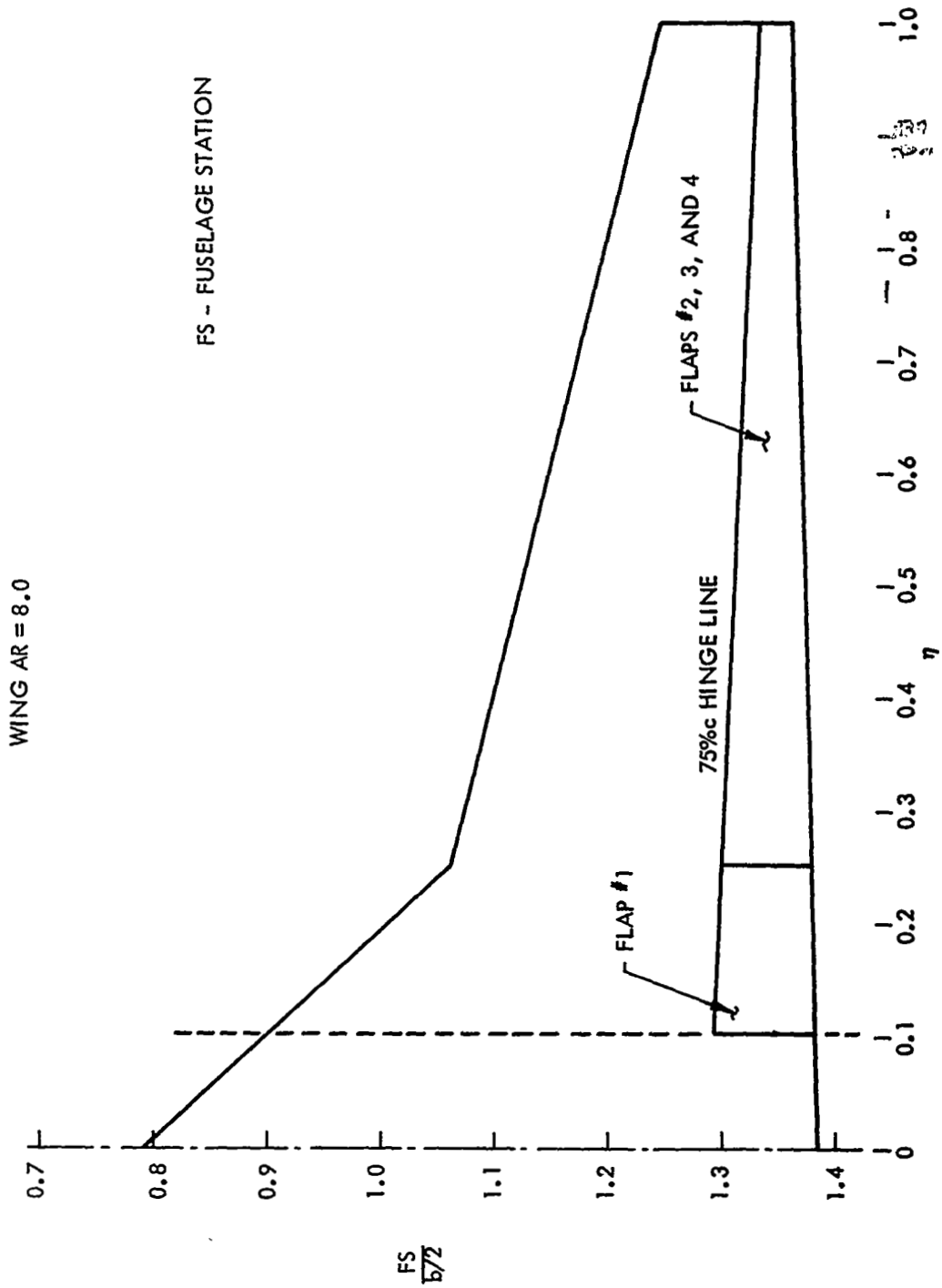

FIGURE A16 WING GEOMETRY FOR LOADS ESTIMATION

S_{REF} = 53.88 M (580 SQ FT) MAC = 2.85 M (9.34 FT) WING AR = 8.0

FLAPS 2, 3, AND 4 DEFLECTED EQUALLY (BOTH SIDES)

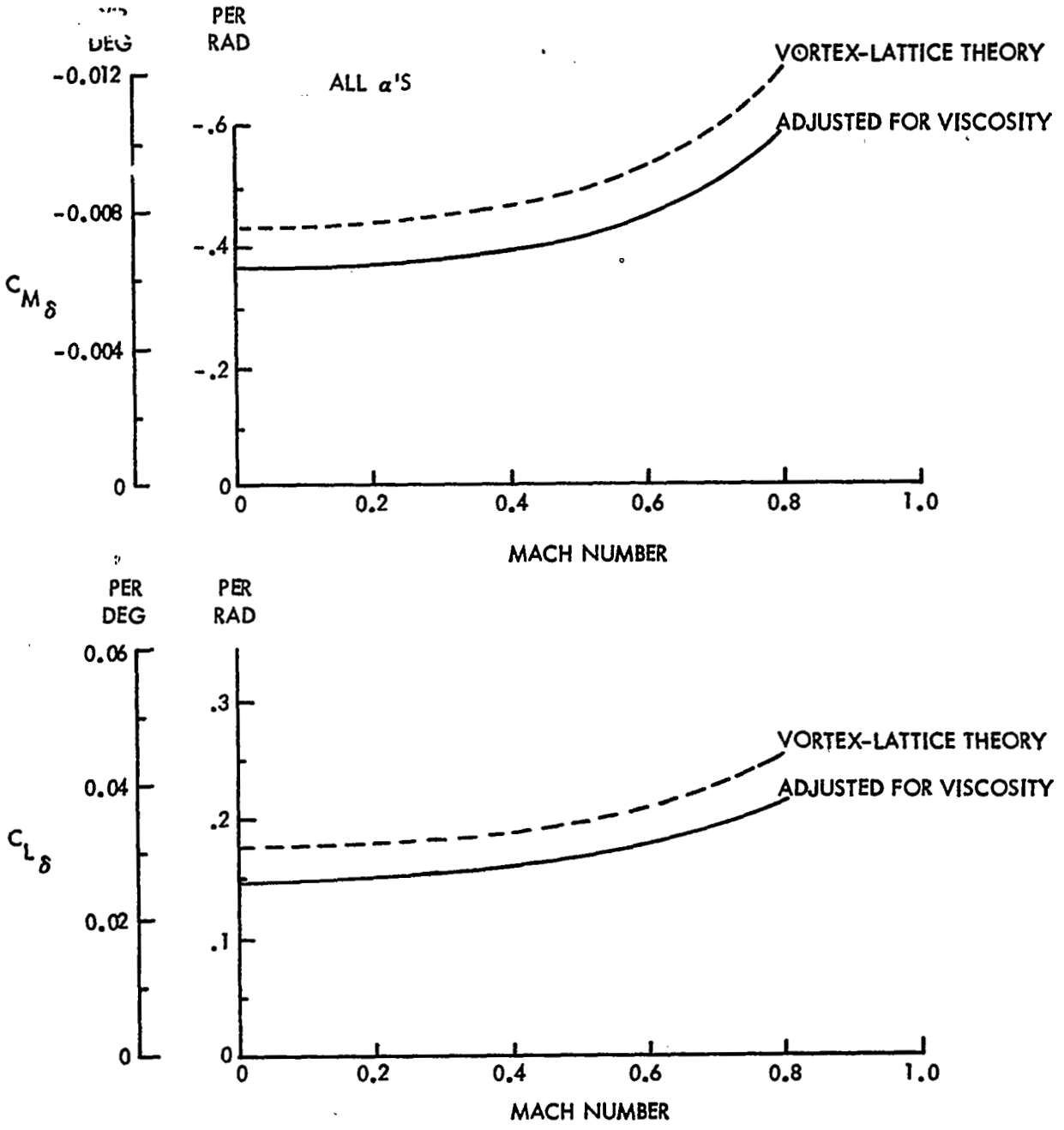

FIGURE A17 FLAP EFFECTIVENESS

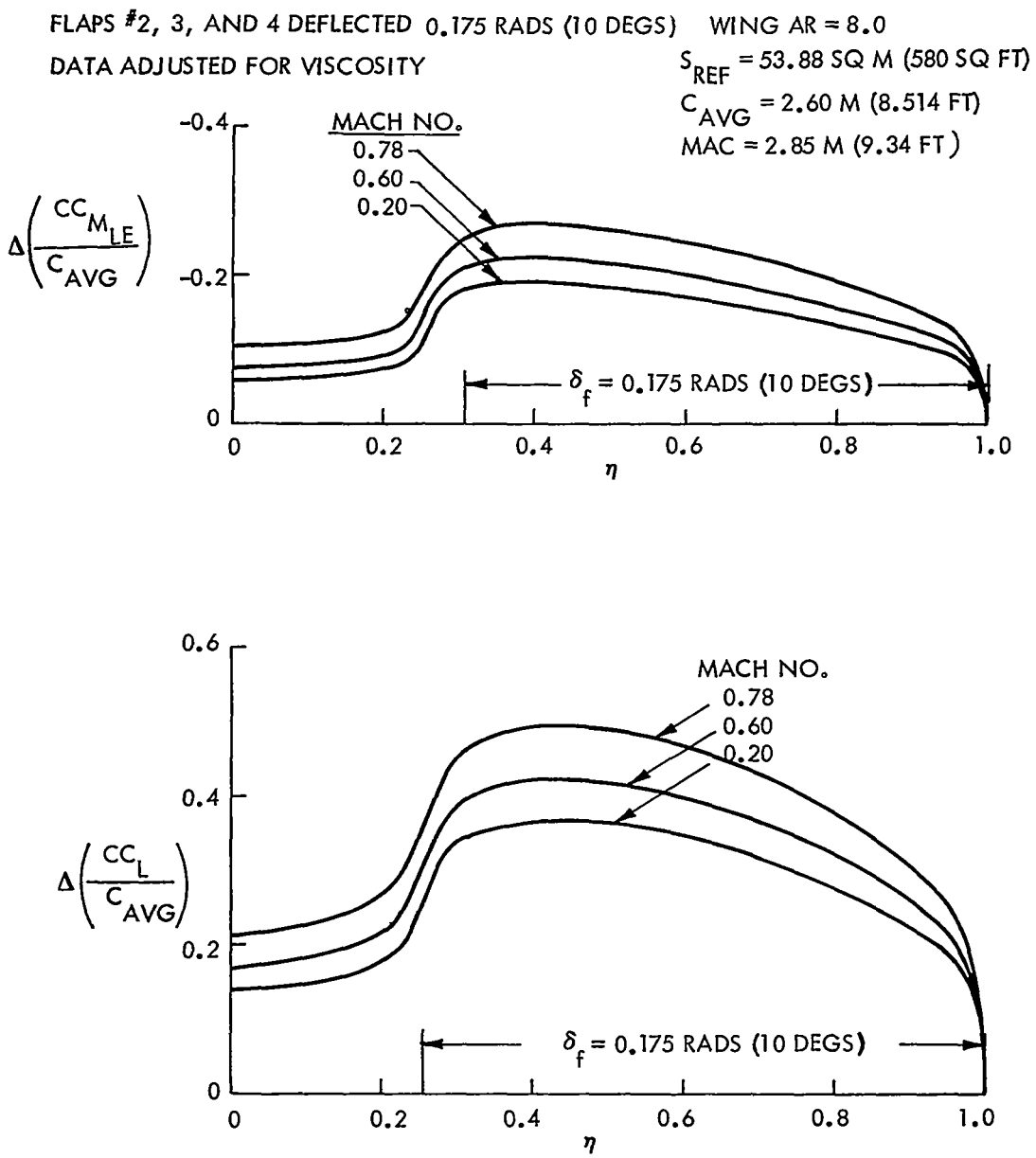

FIGURE A18 FLAP LOAD DISTRIBUTIONS

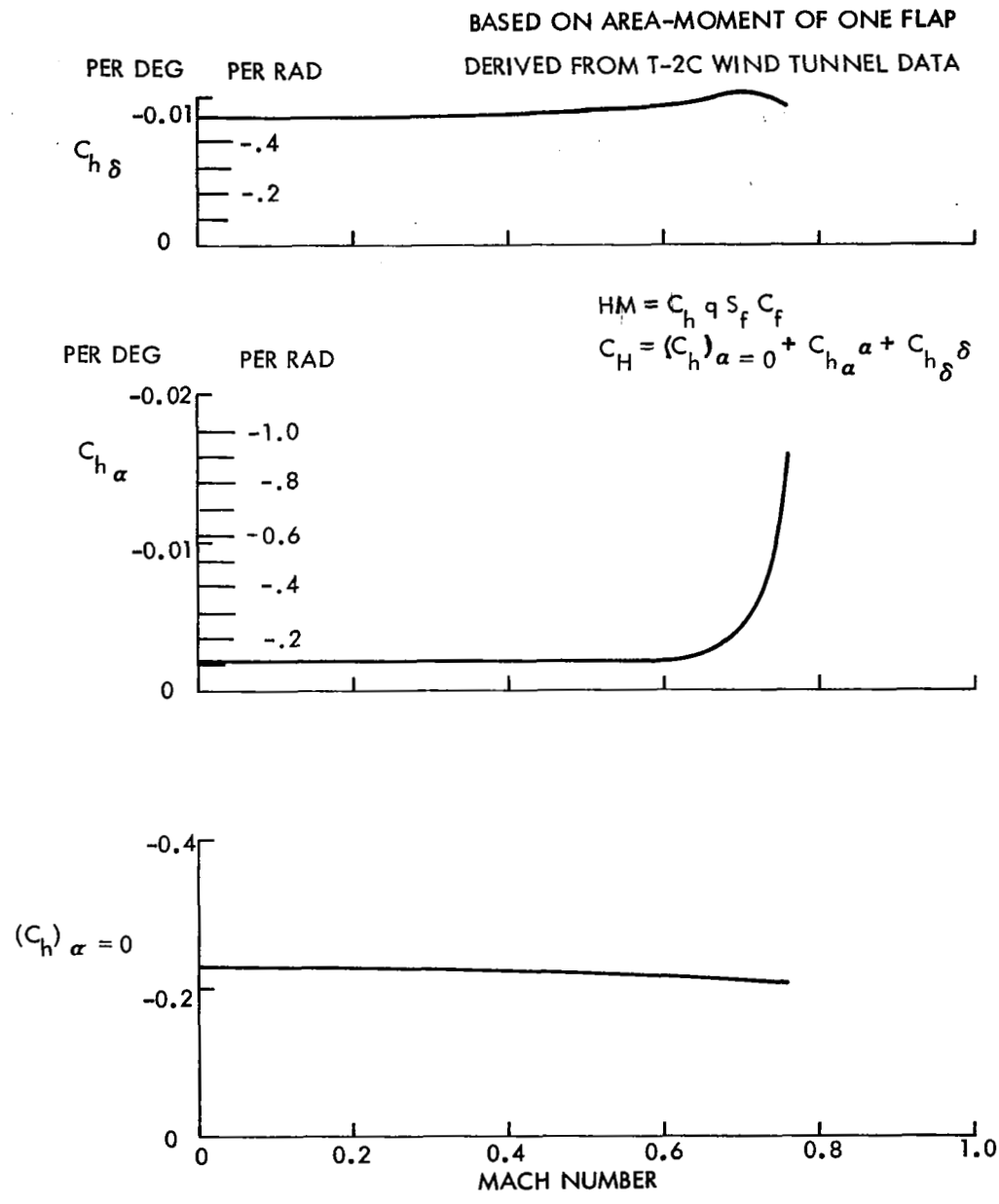

FIGURE A19 FLAP HINGE MOMENT COEFFICIENTS

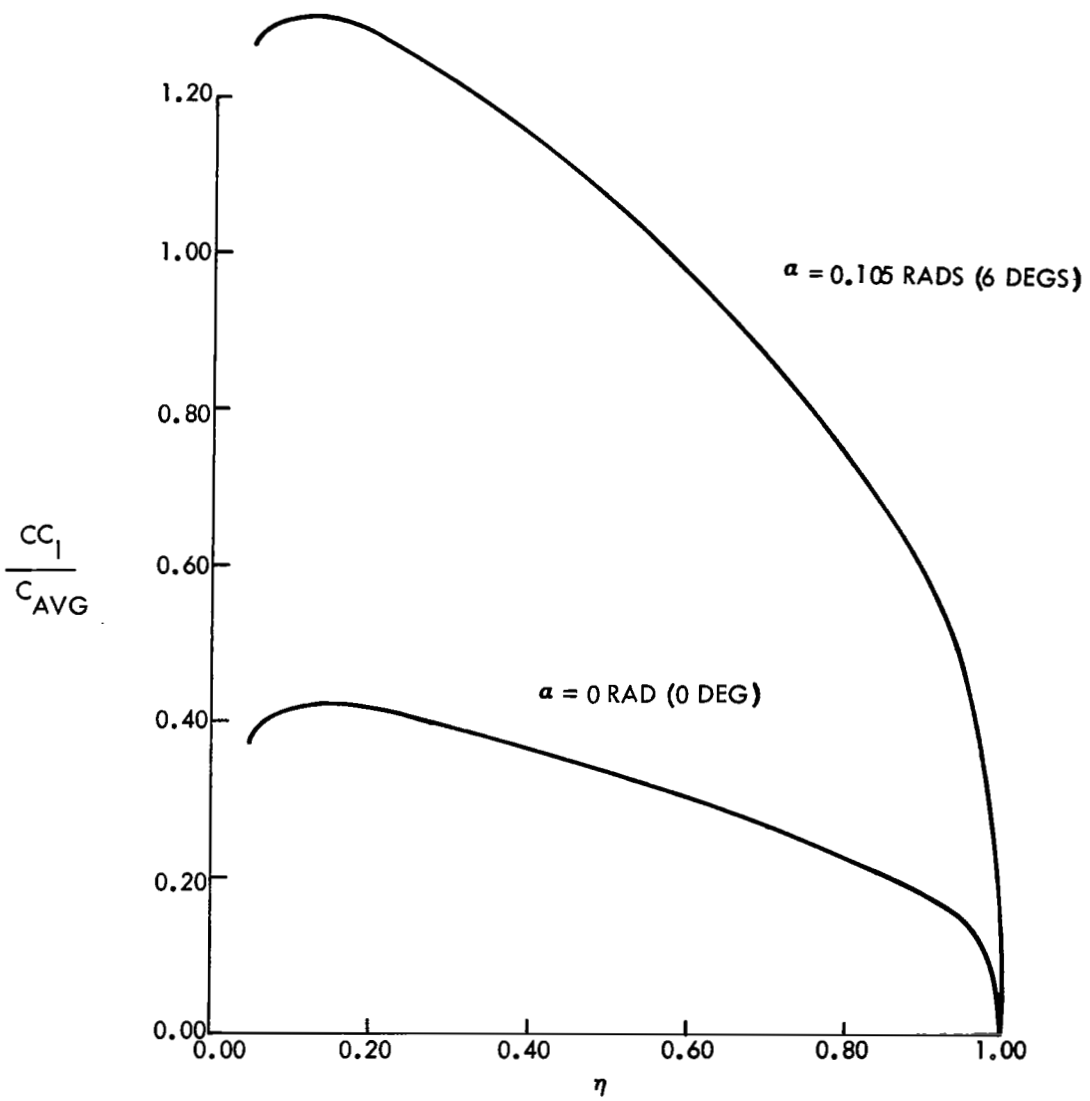

FIGURE A20 WING LIFT DISTRIBUTION - AR = 9
MACH NO. = 0.80

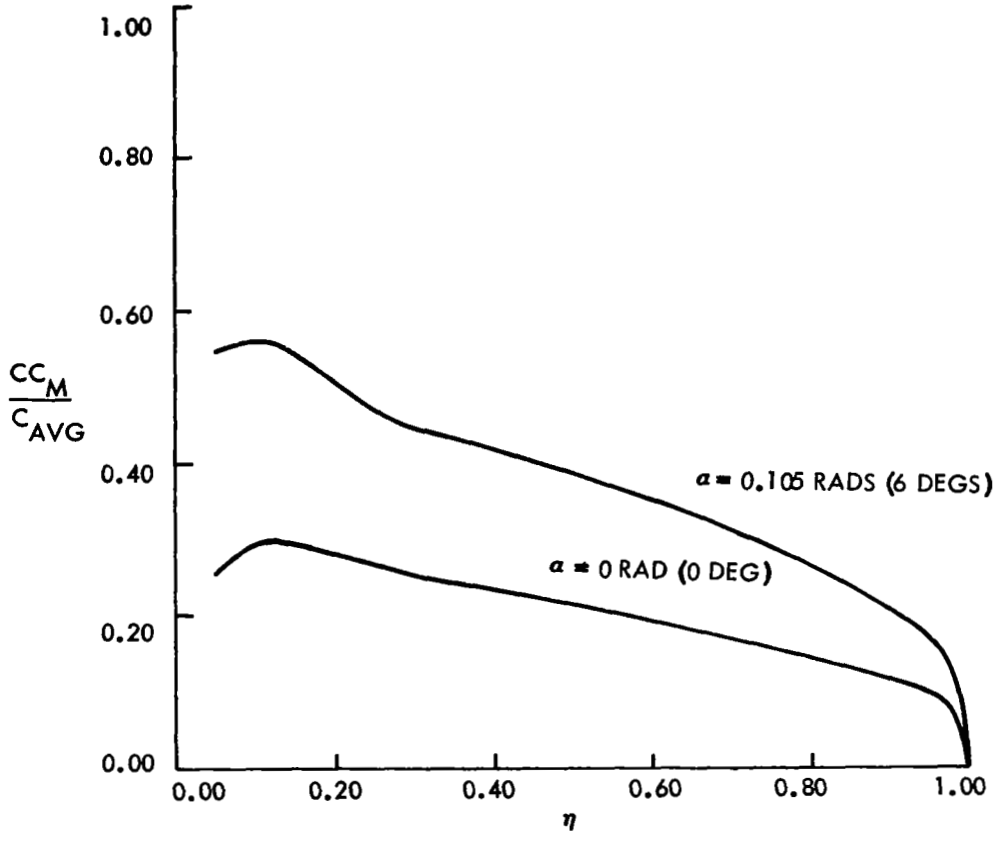

FIGURE A21 WING PITCHING MOMENT DISTRIBUTION
AR = 9 MACH NO. = 0.80

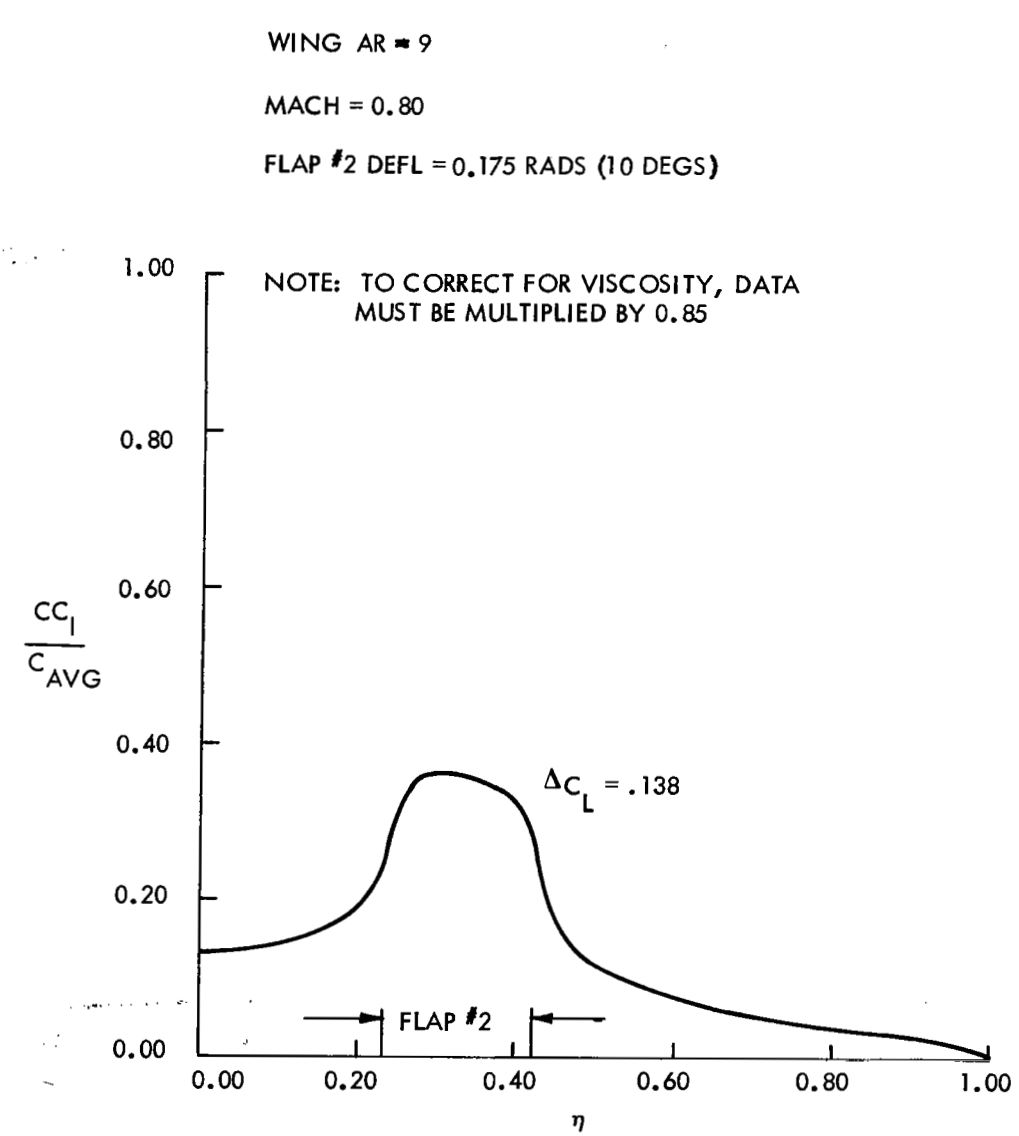

FIGURE A22 INCREMENTAL WING LIFT DISTRIBUTION DUE TO FLAP DEFLECTION

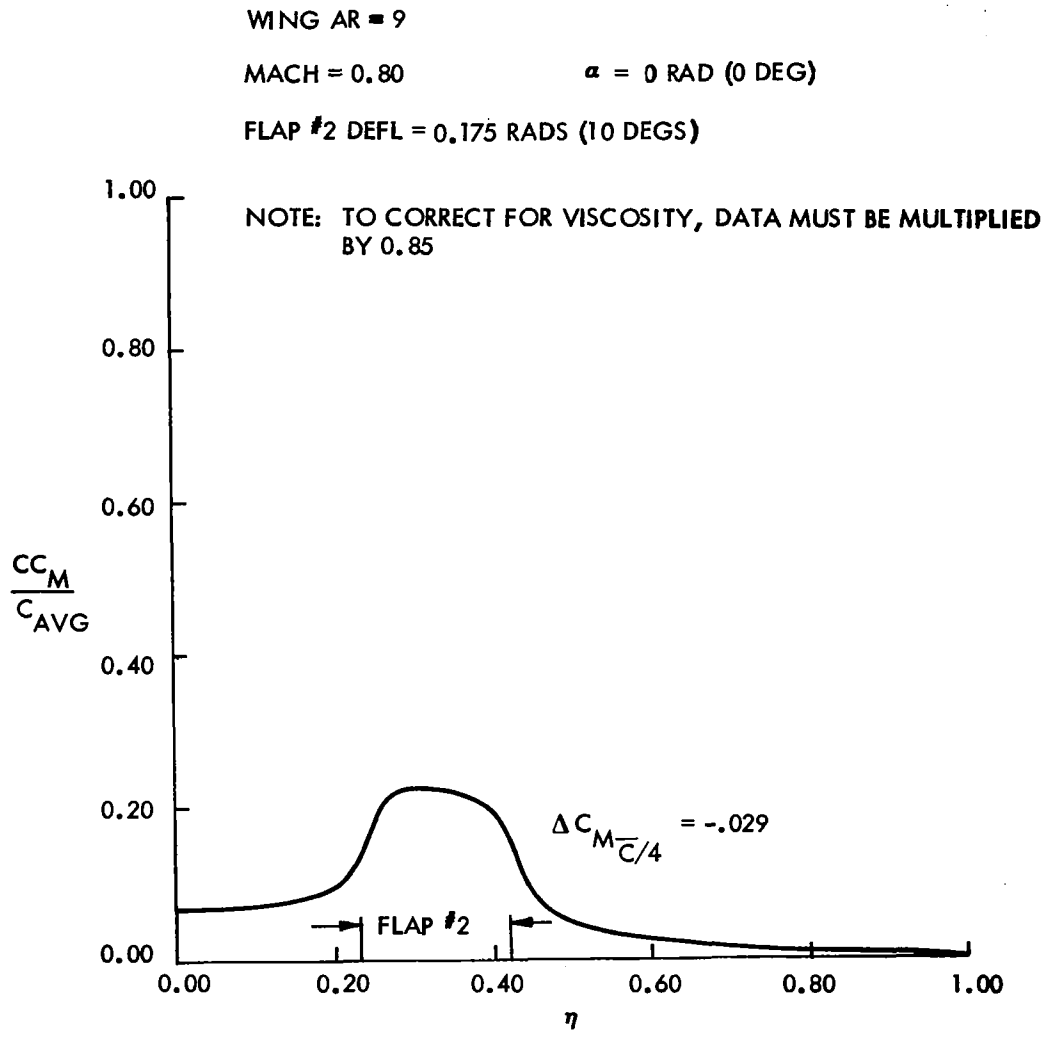

FIGURE A23 INCREMENTAL MOMENT DISTRIBUTION DUE TO FLAP DEFLECTION

WING AR = 9

MACH = 0.80 α = 0 RAD (0 DEG)

FLAP # 3 DEFL = 0.175 RADS (10 DEGS)

NOTE: TO CORRECT FOR VISCOSITY, DATA MUST BE MULTIPLIED BY 0.85

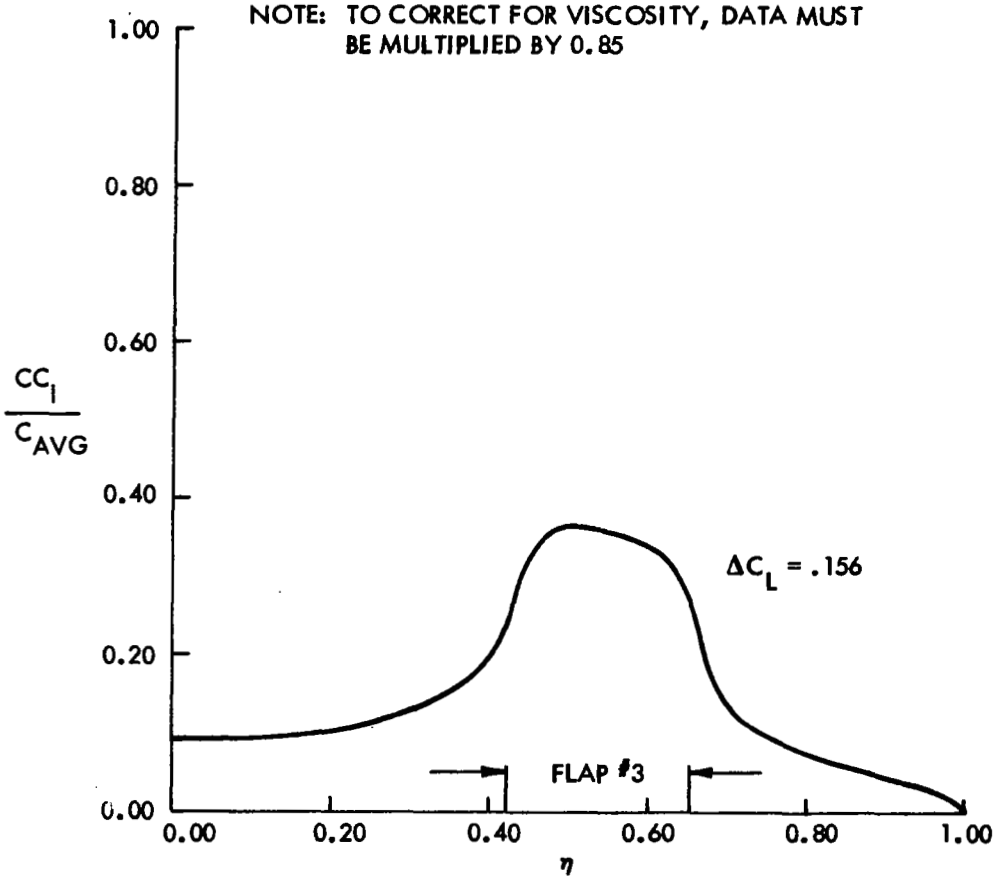

FIGURE A24 INCREMENTAL LIFT DISTRIBUTION DUE TO FLAP DEFLECTION

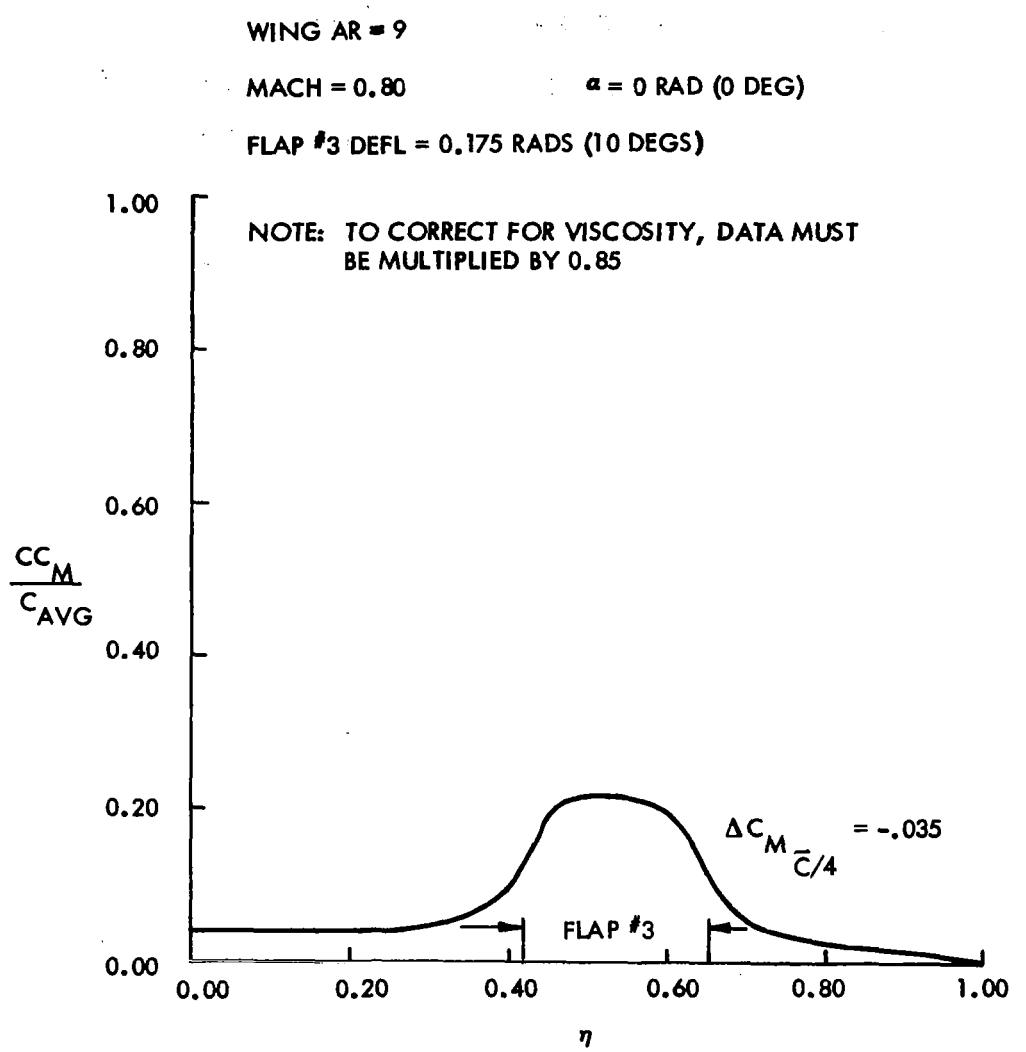

FIGURE A25 INCREMENTAL MOMENT DISTRIBUTION DUE TO FLAP DEFLECTION

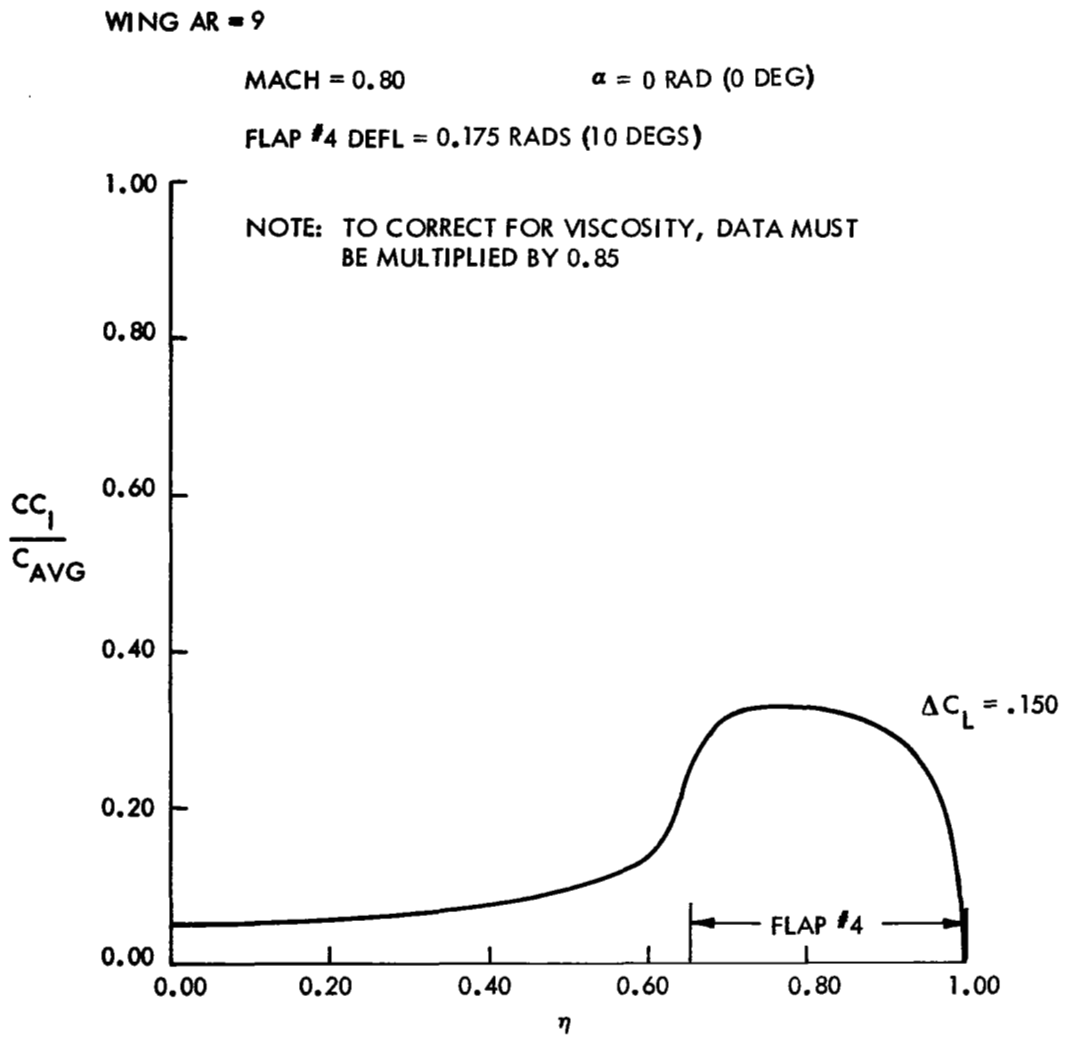

FIGURE A26 INCREMENTAL LIFT DISTRIBUTION DUE TO FLAP DEFLECTION

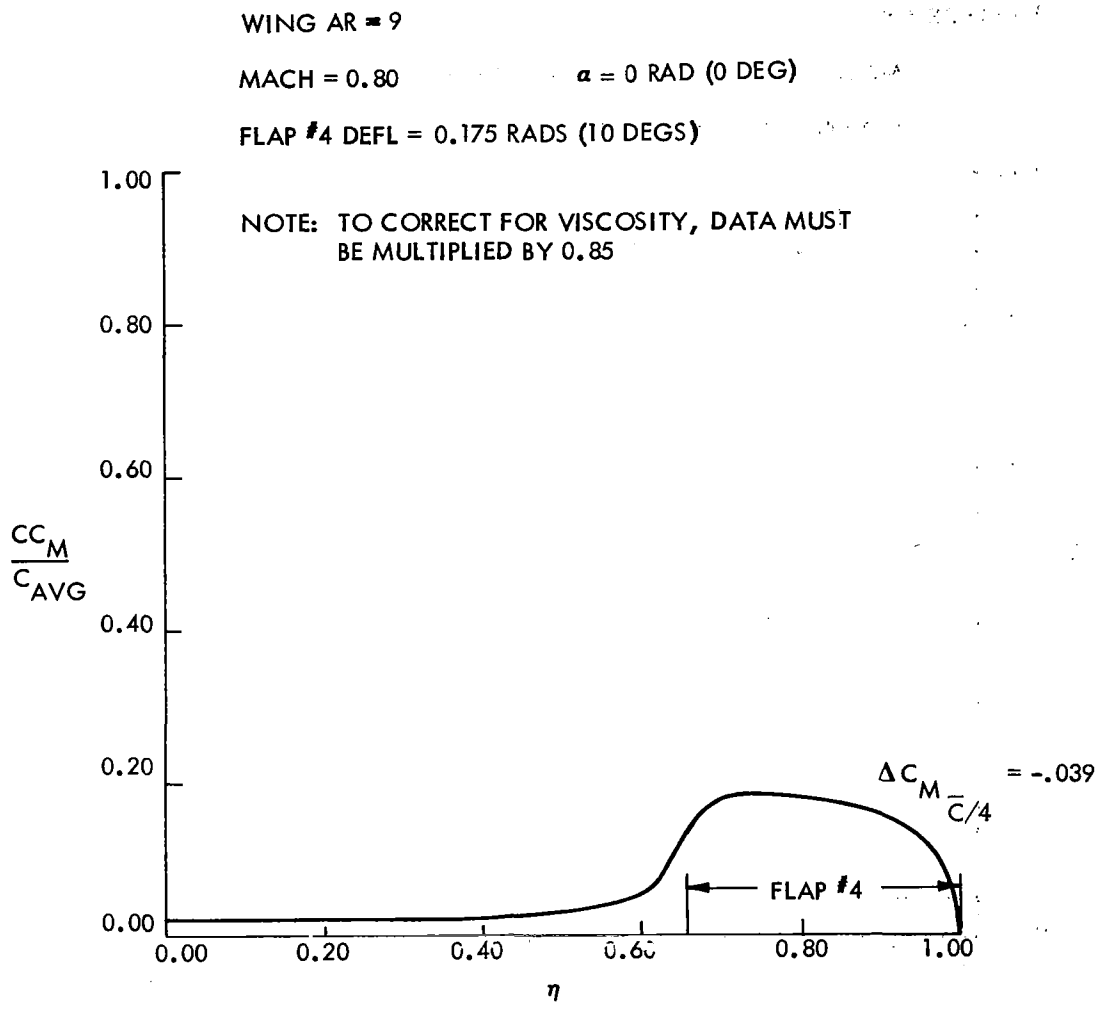

FIGURE A27 INCREMENTAL MOMENT DISTRIBUTION DUE TO FLAP DEFLECTION

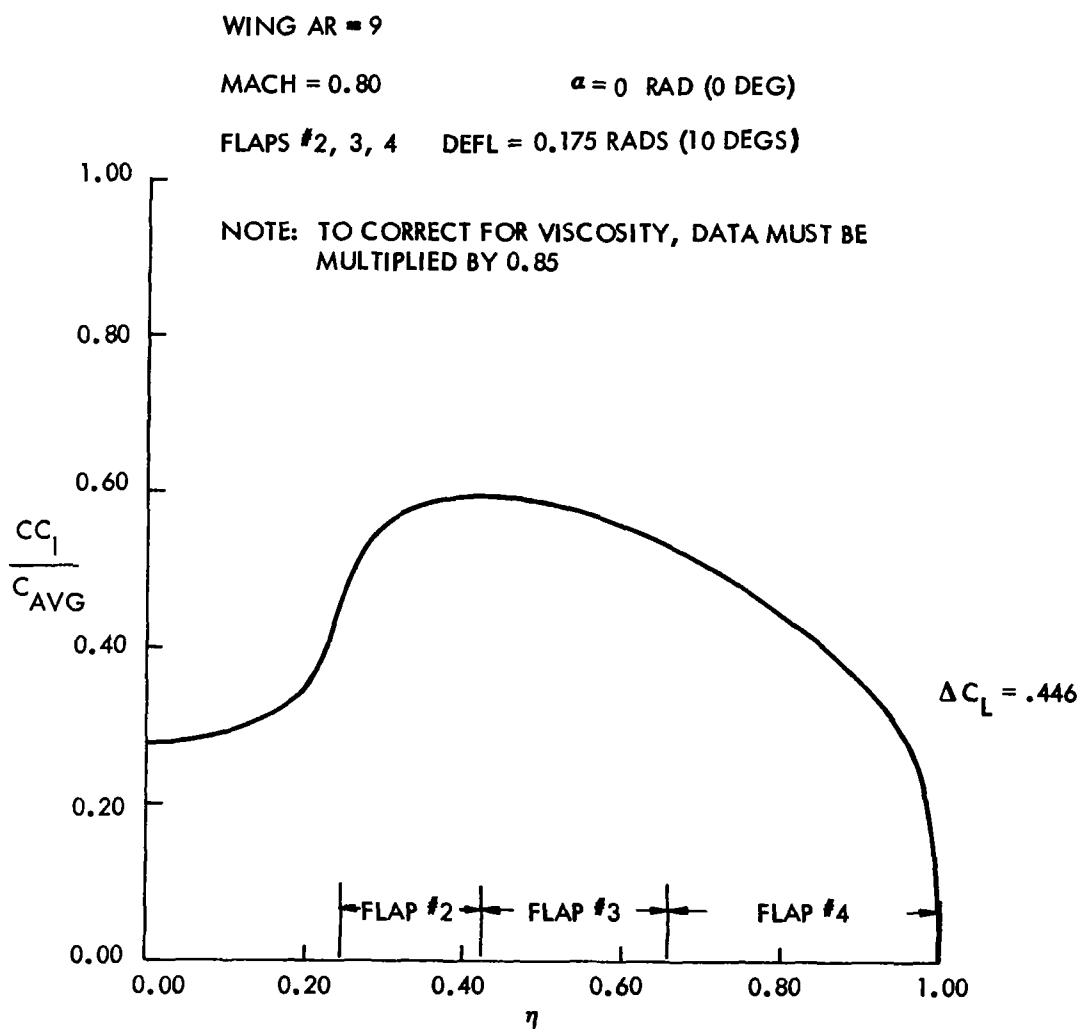

FIGURE A28 INCREMENTAL LIFT DISTIRBUTION DUE TO FLAP DEFLECTION

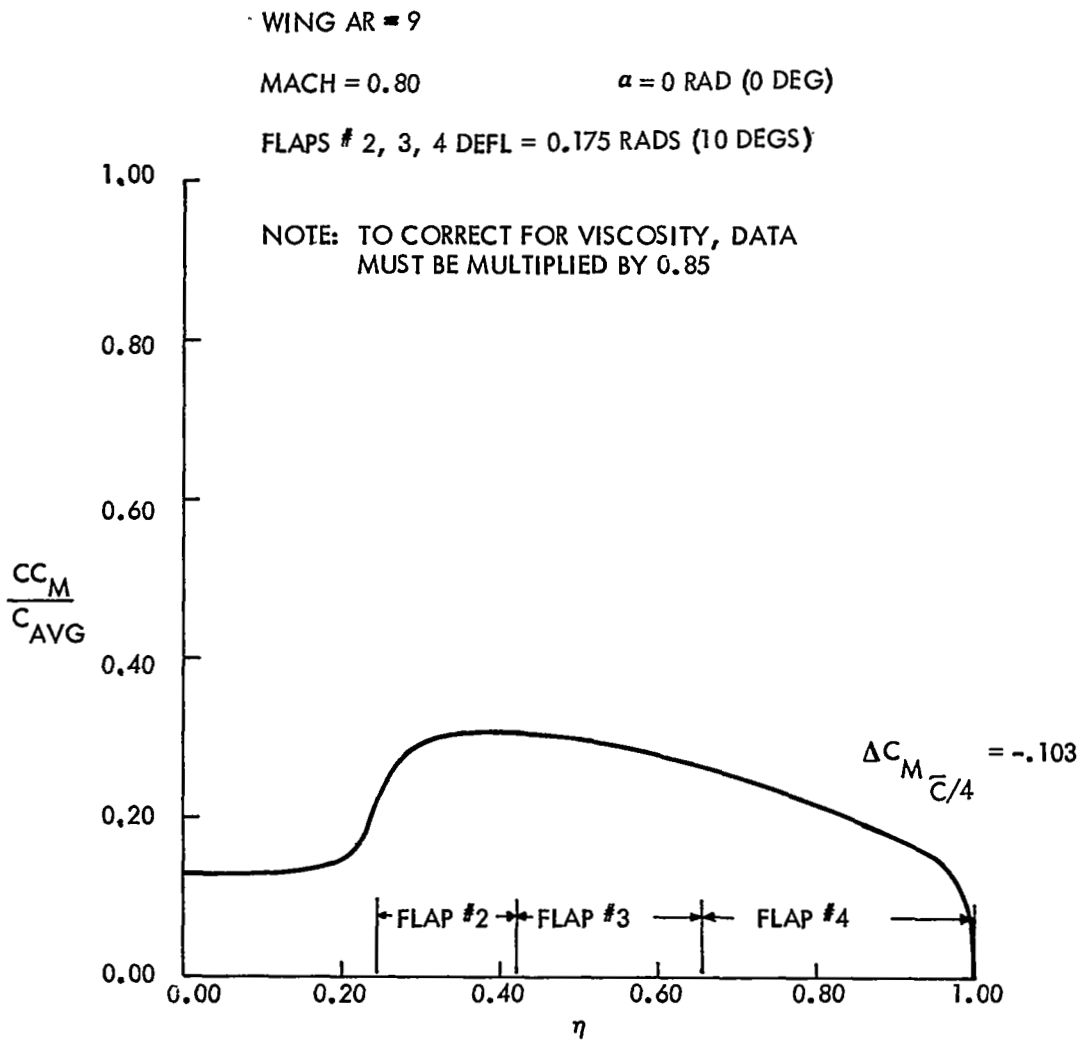

FIGURE A29 INCREMENTAL MOMENT DISTRIBUTION DUE TO FLAP DEFLECTION

S_W = 60.45 SQ M (650.74 SQ FT) $\bar{C}$ = 2.71 M (8.894 FT)

ALL α's

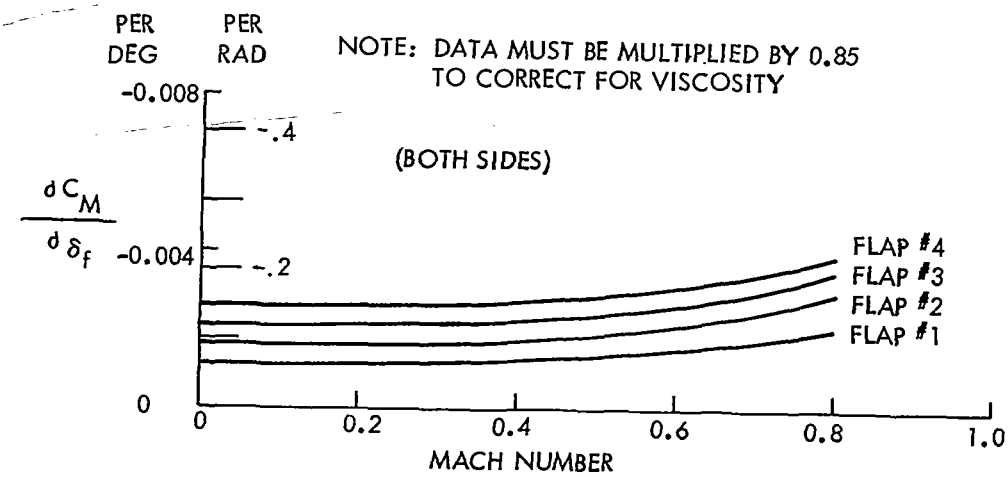

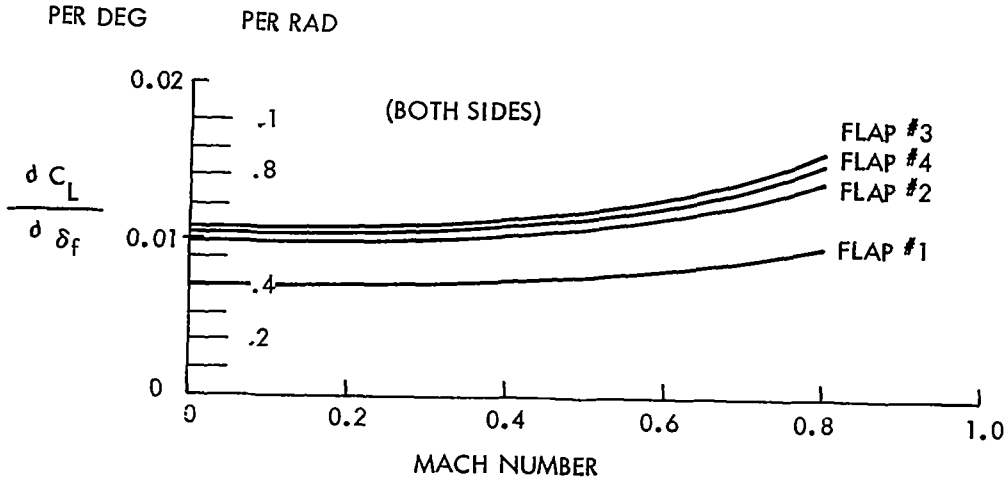

FIGURE A30 FLAP EFFECTIVENESS

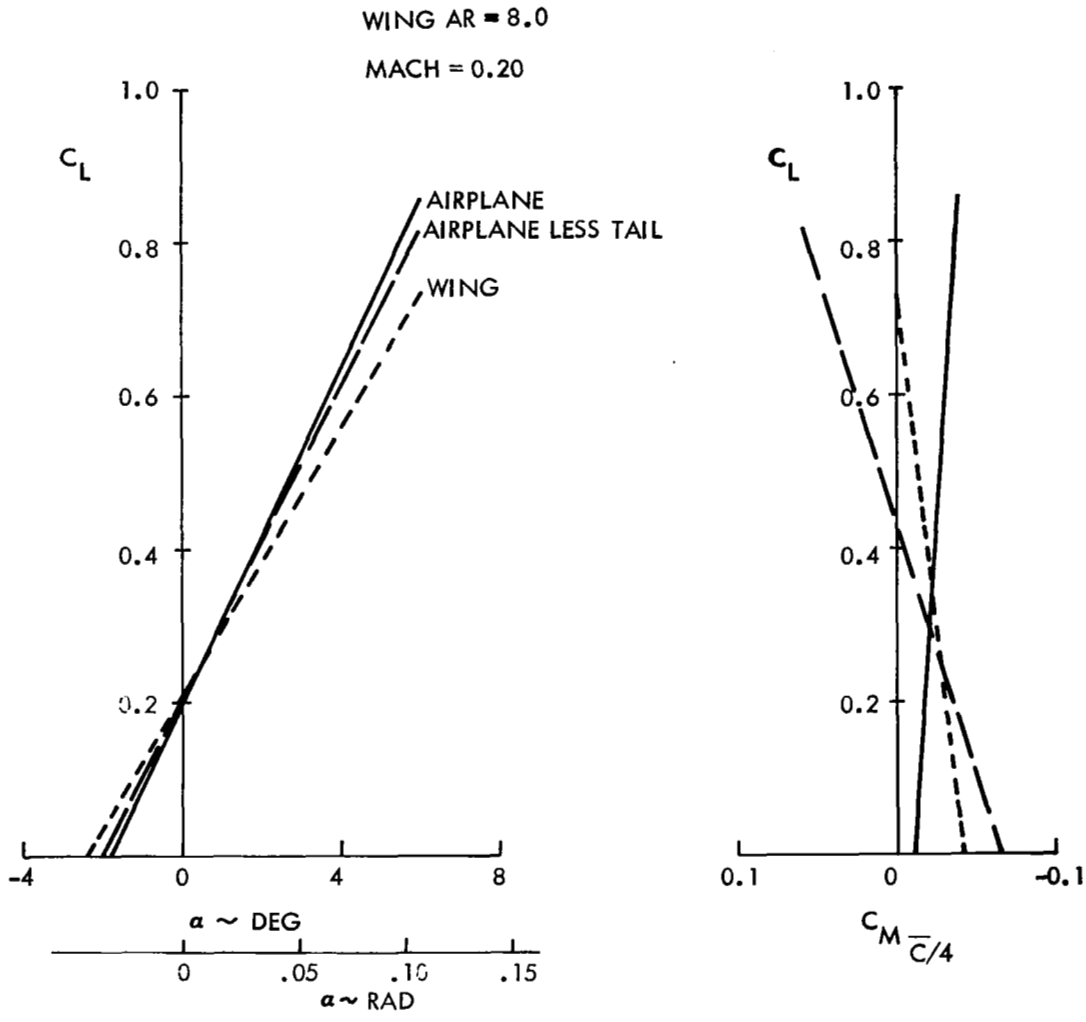

FIGURE A31 AIRPLANE LIFT AND PITCH CHARACTERISTICS

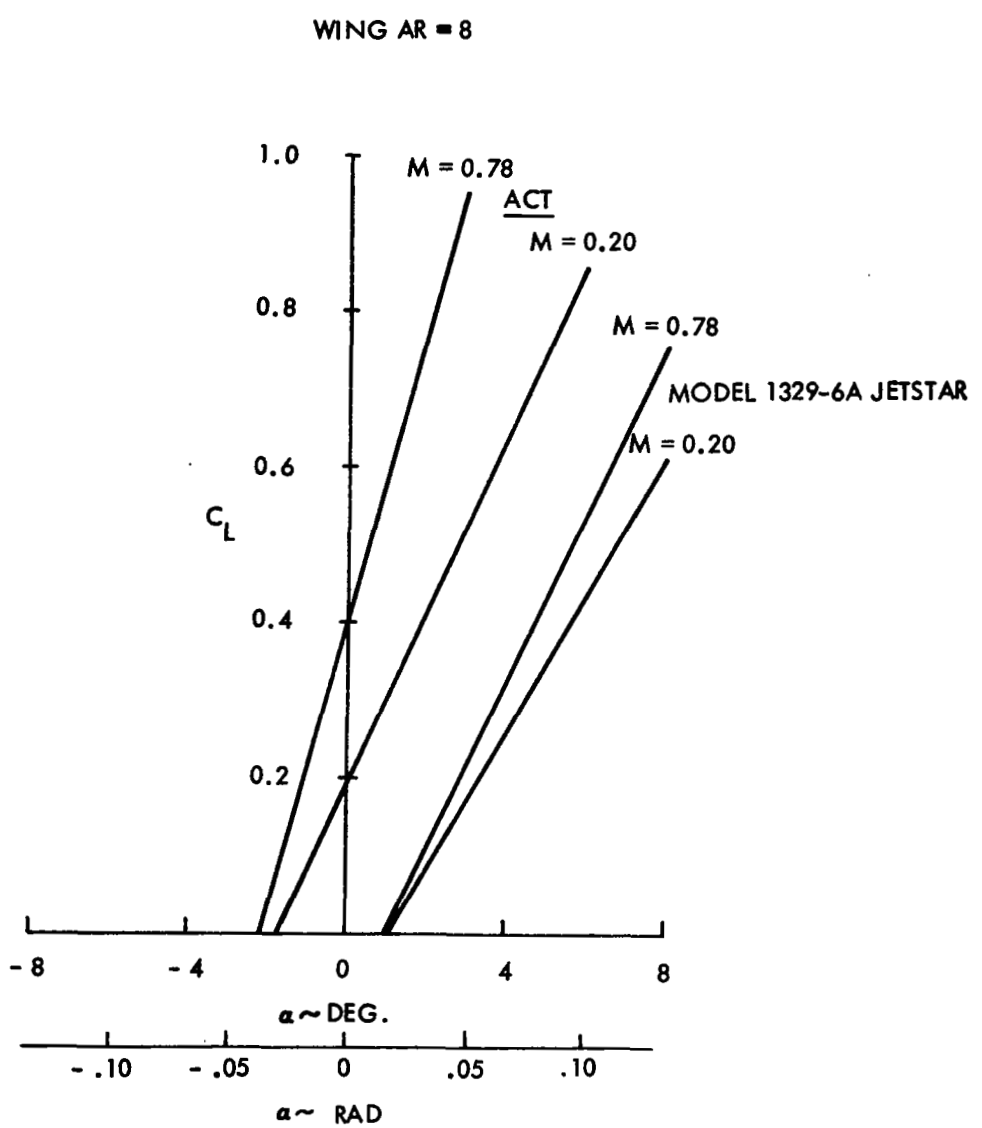

FIGURE A32 COMPARISON OF AIRPLANE LIFT CHARACTERISTICS

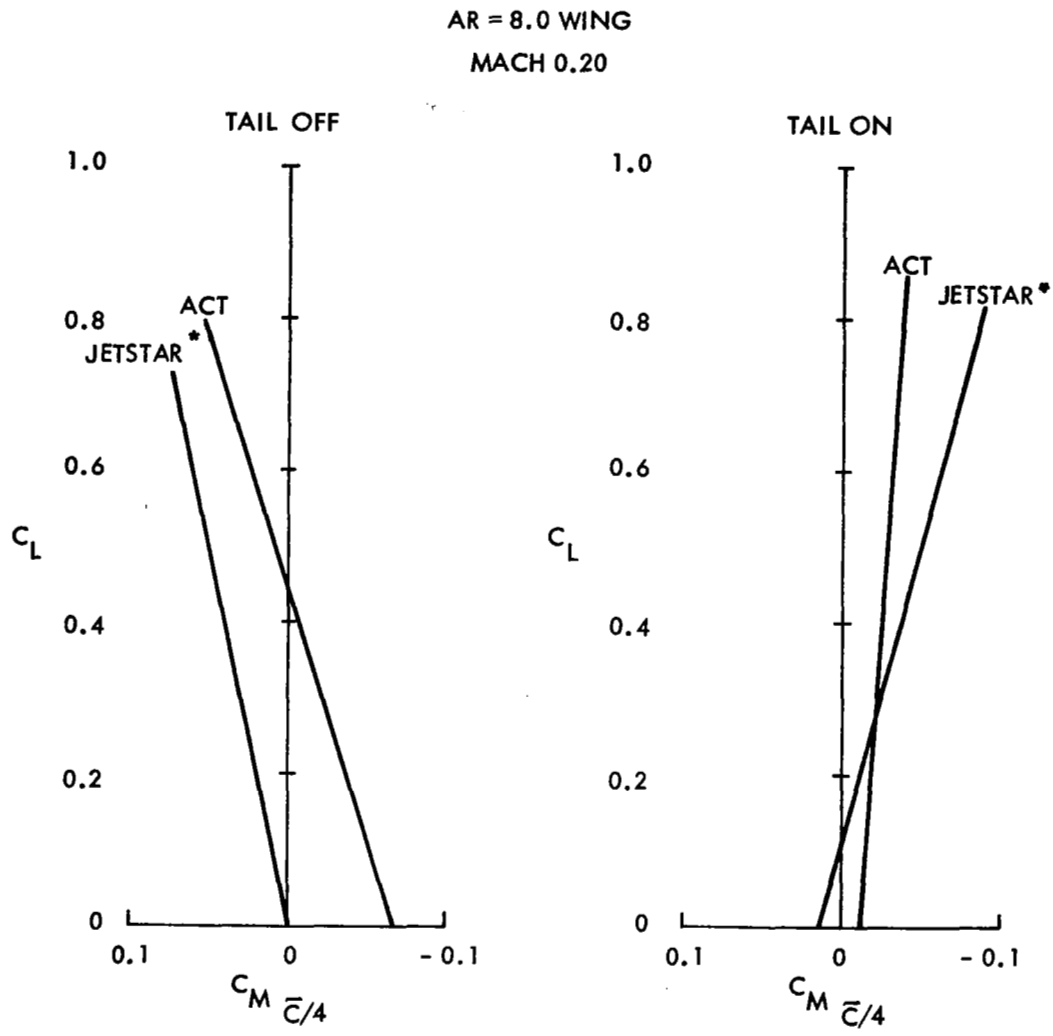

• MODEL 1329-6A JETSTAR

FIGURE A33 COMPARISON OF AIRPLANE PITCHING MOMENT CHARACTERISTICS

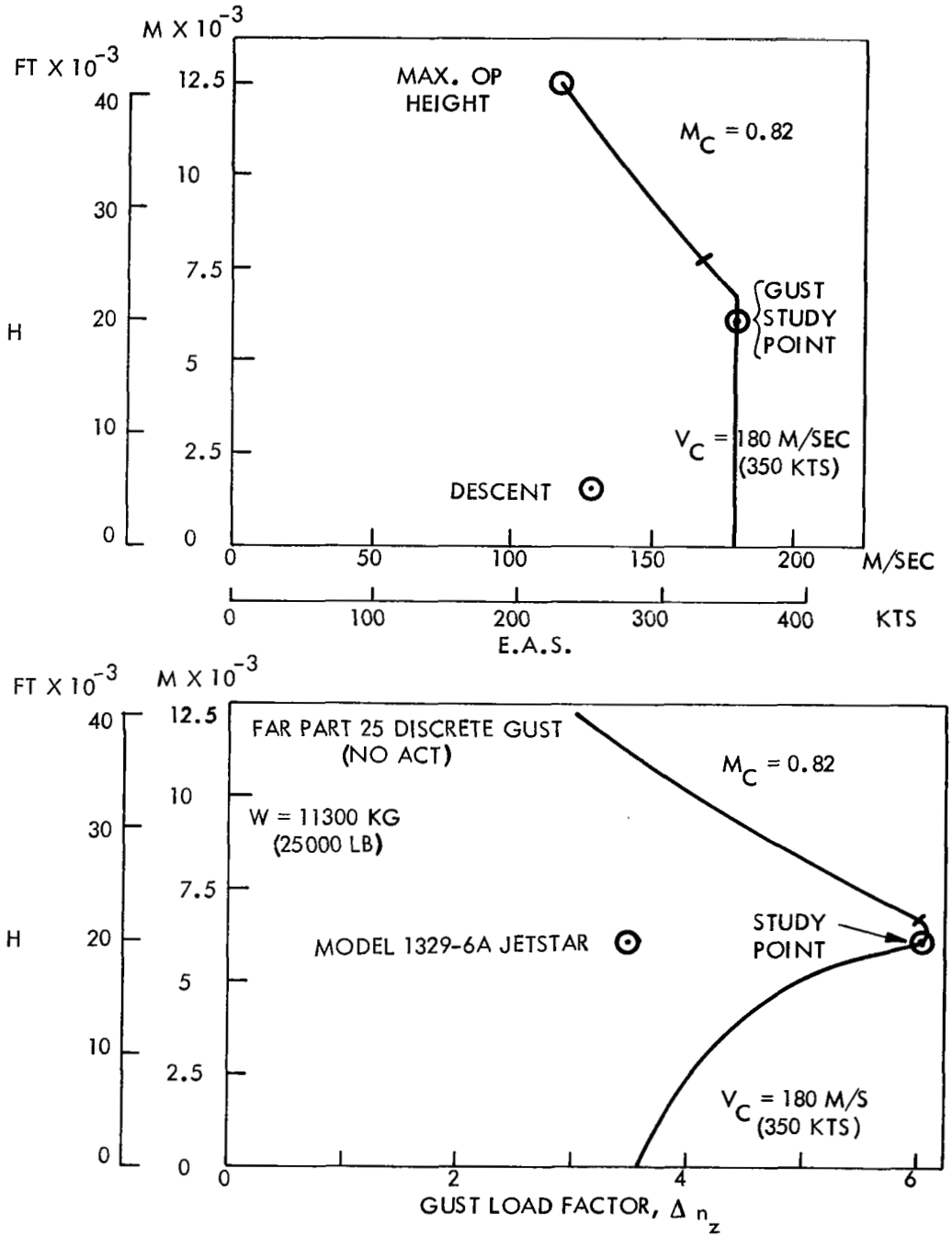

FIGURE B1 SELECTION OF GUST STUDY CONDITION

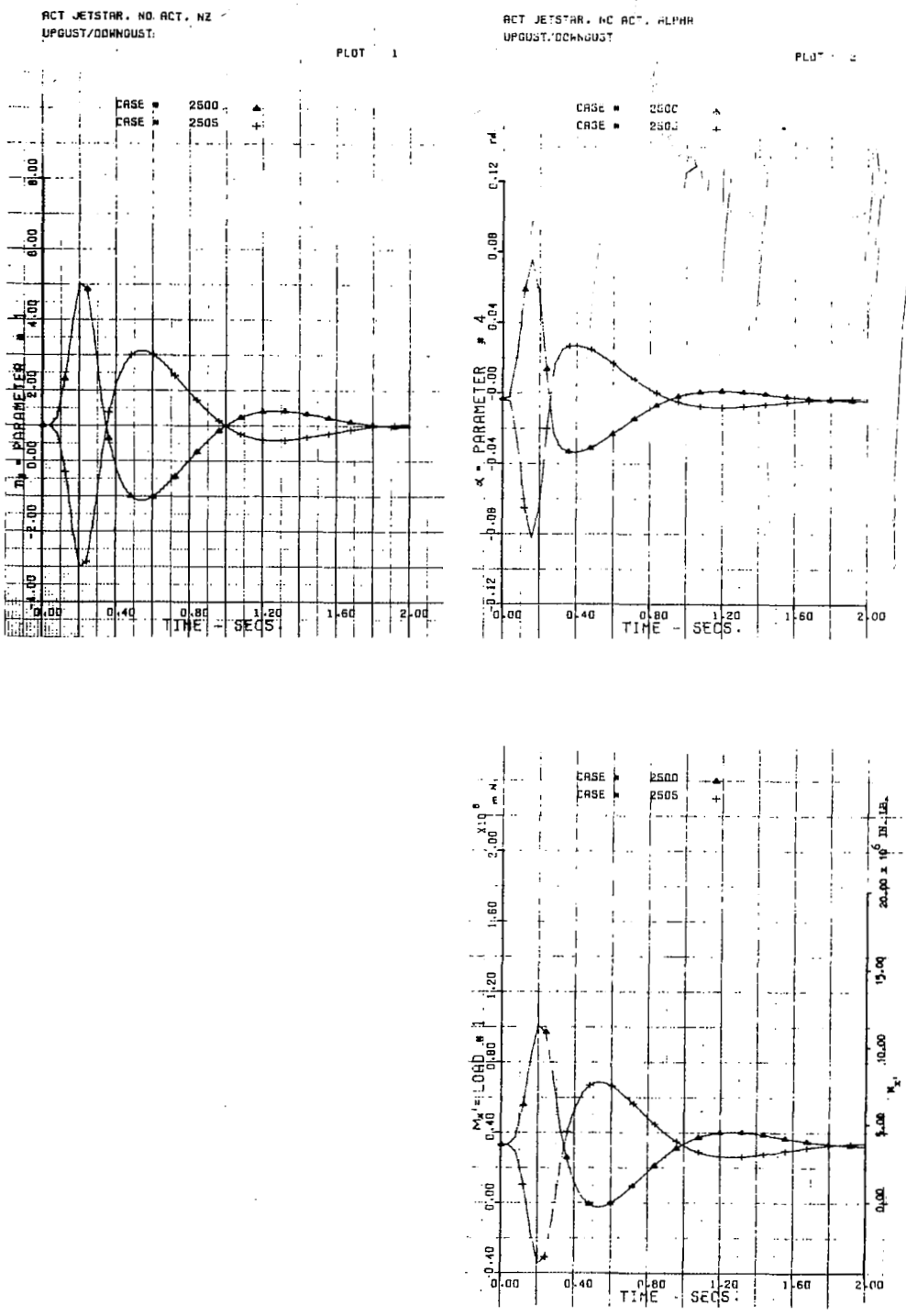

FIGURE B2 RIGID GUST RESPONSE, NO ACTIVE CONTROLS
UP AND DOWN GUSTS

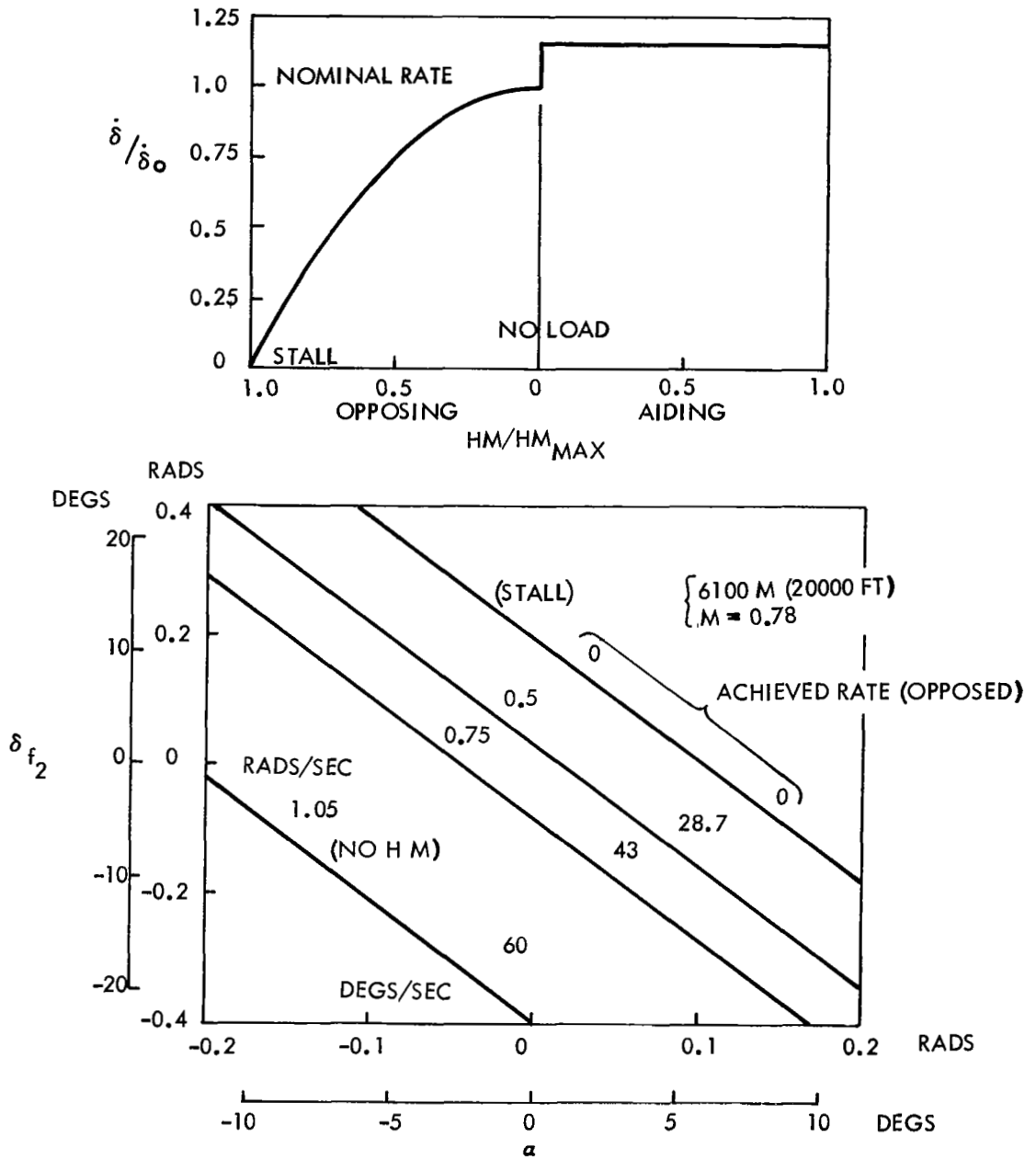

FIGURE B3 ASSUMED FLAP RATE VARIATION WITH HINGE MOMENT

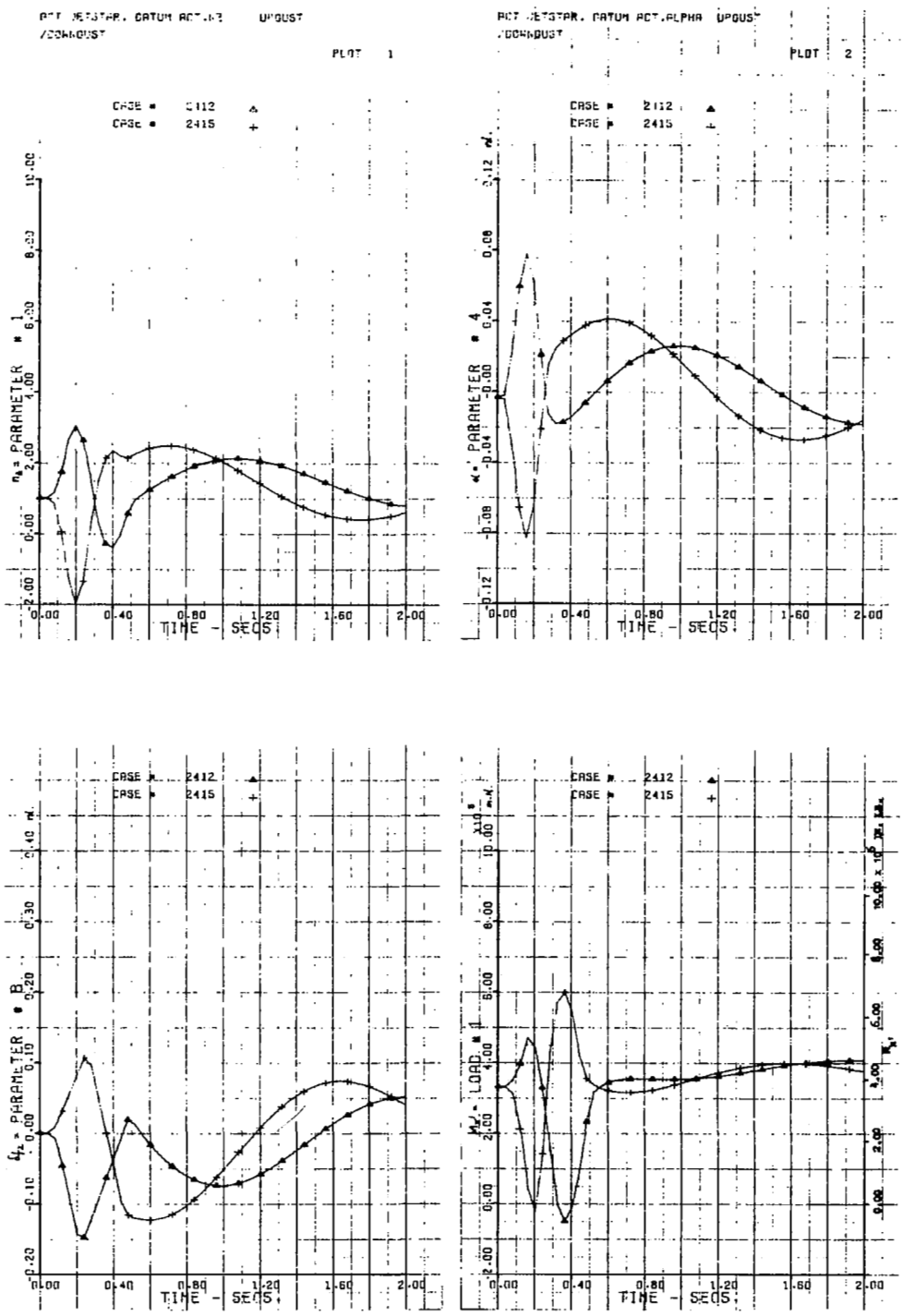

FIGURE B4 RIGID GUST RESPONSE, DATUM CONTROL SYSTEM UP AND DOWN GUSTS

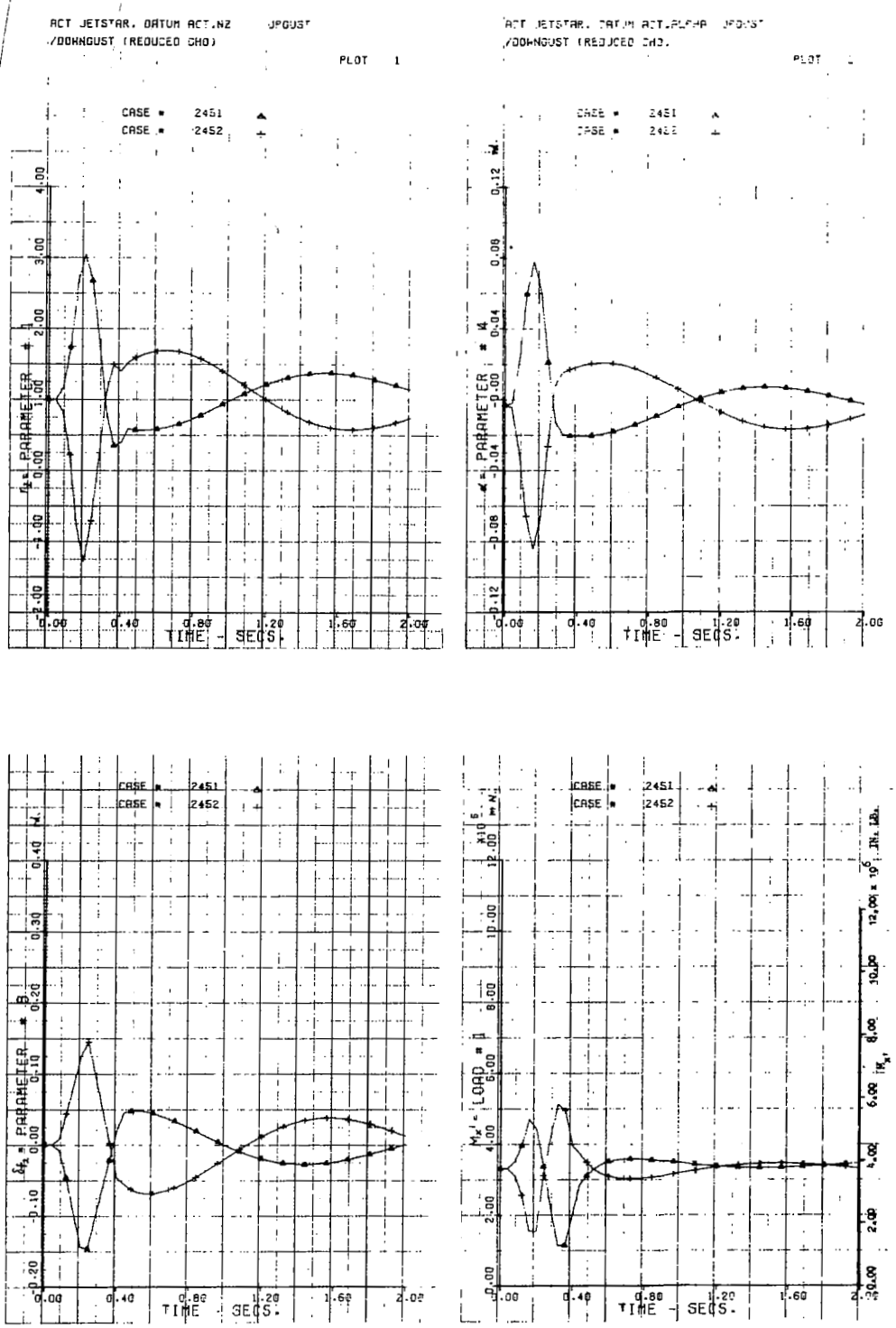

FIGURE B5 RIGID GUST RESPONSE, DATUM CONTROL SYSTEM REDUCED C_{h_o}, UP AND DOWN GUST

RIGID: UPGUST = 15.2 M/S (50 FPS)

—— STRAIGHT GAIN

FLAPS: G_F = -0.087 RADS/g (-5 DEGS/g)

O T = 1 SEC.

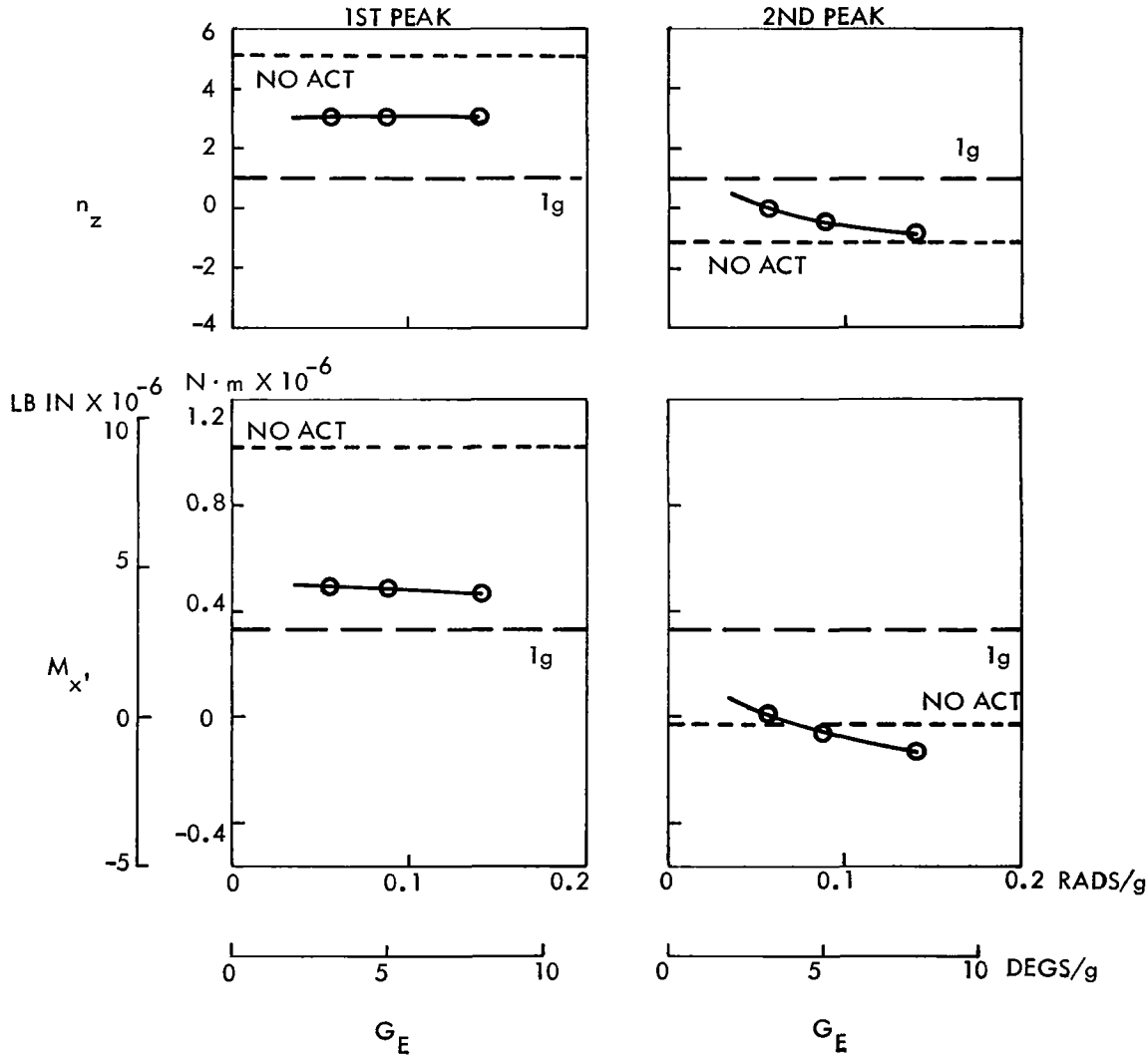

FIGURE B6 EFFECT OF ELEVATOR GAIN, G_E

RIGID UPGUST = 15.2 M/S (50 FPS)

FLAP GAIN, G_F= -0.052 RADS/g (-3.2 DEGS/g) +
-0.087 RADS/g (-5 DEGS/g) —
-0.175 RADS/g (-10 DEGS/g) O

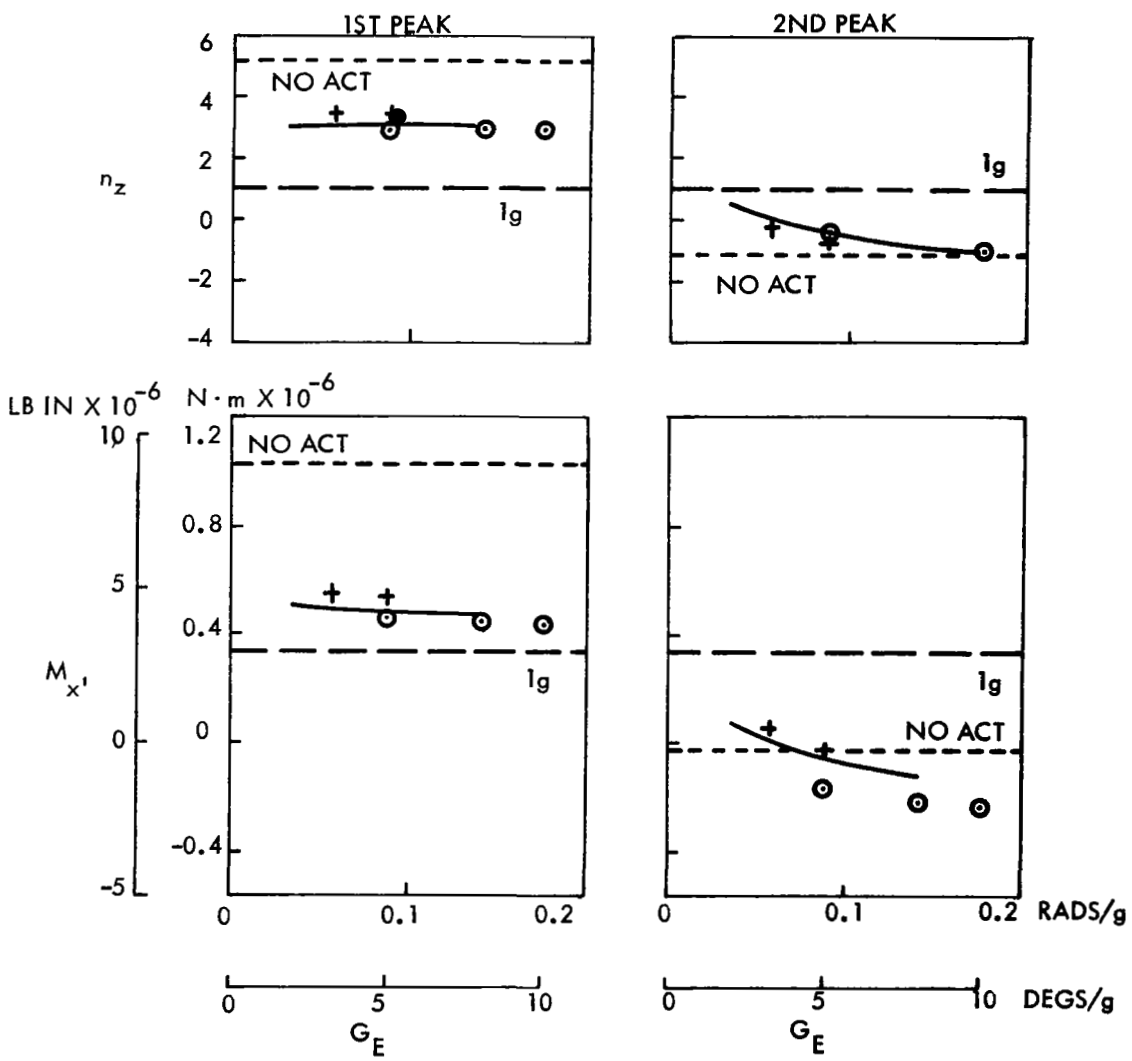

FIGURE B7 EFFECT OF FLAP AND ELEVATOR GAINS

RIGID. UPGUST = 15.2 M/S (50 FPS)

FLAPS: G_F = -0.087 RADS/g (-5 DEGS/g)

ELEV: G_E = 0.087 RADS/g (5 DEGS/g)

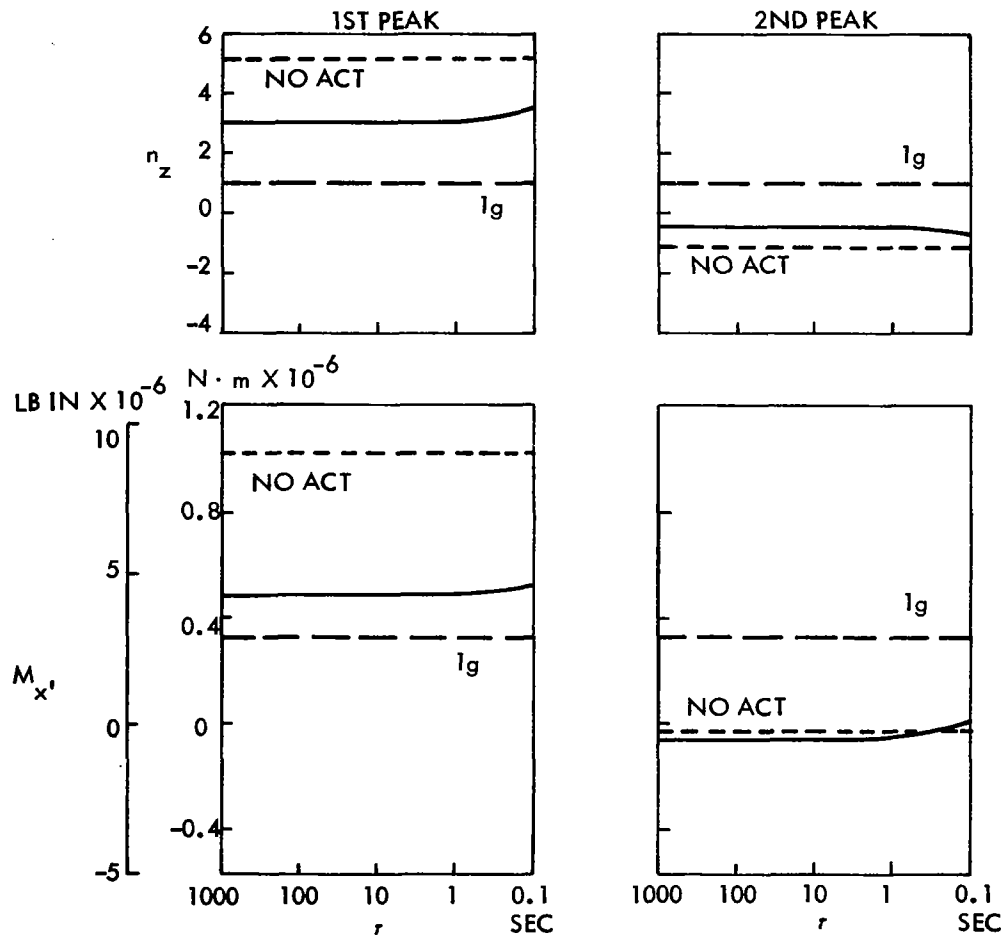

FIGURE B8 EFFECT OF FLAP TIME CONSTANT, τ (WASHOUT)

RIGID. UPGUST = 15.2 M/S (50 FPS)
FLAPS: G_F = -0.052 RADS/g (-3.2 DEGS/g)
ELEV: G_E = 0.087 RADS/g (5 DEGS/g)

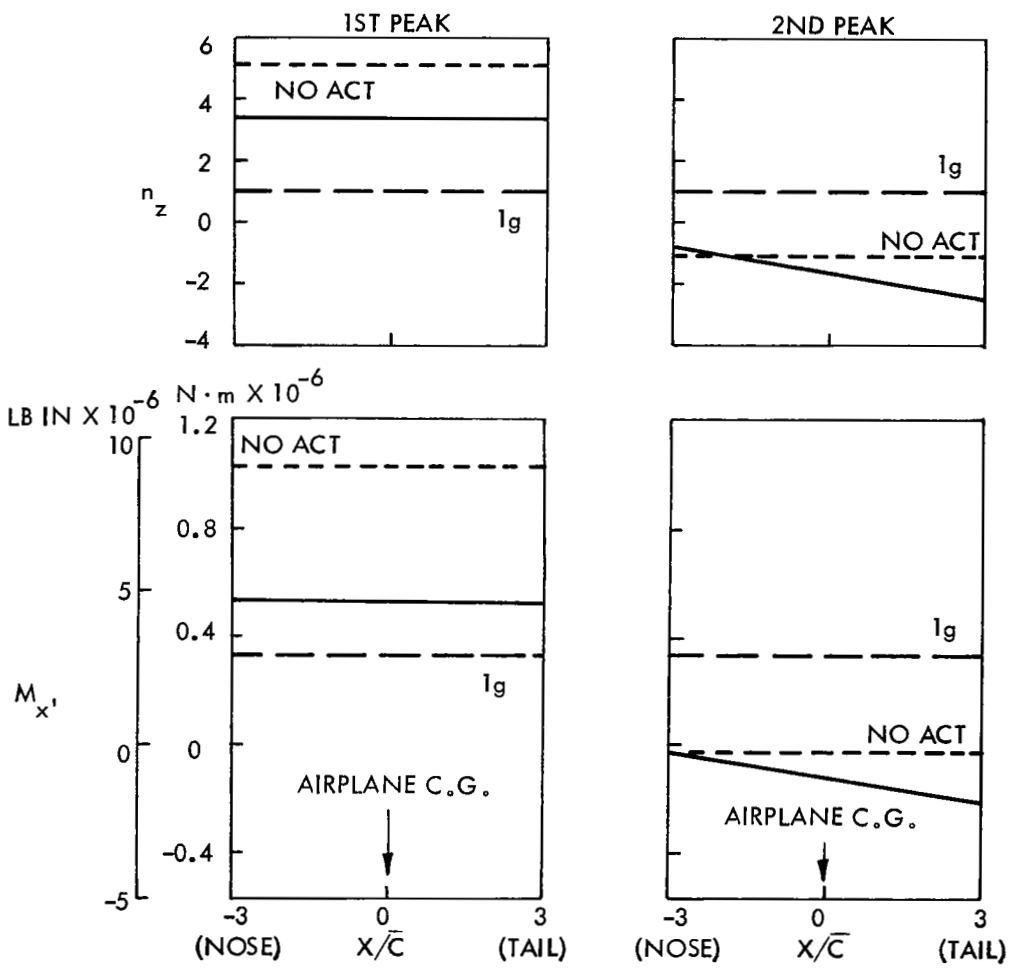

FIGURE B9 EFFECT OF ELEVATOR SENSOR LOCATION

RIGID. UPGUST = 15.2 M/S (50 FPS)

FLAPS: G_F = -0.087 RADS/g (-5 DEGS/g)

ELEV: G_E = 0.087 RADS/g (5 DEGS/g)

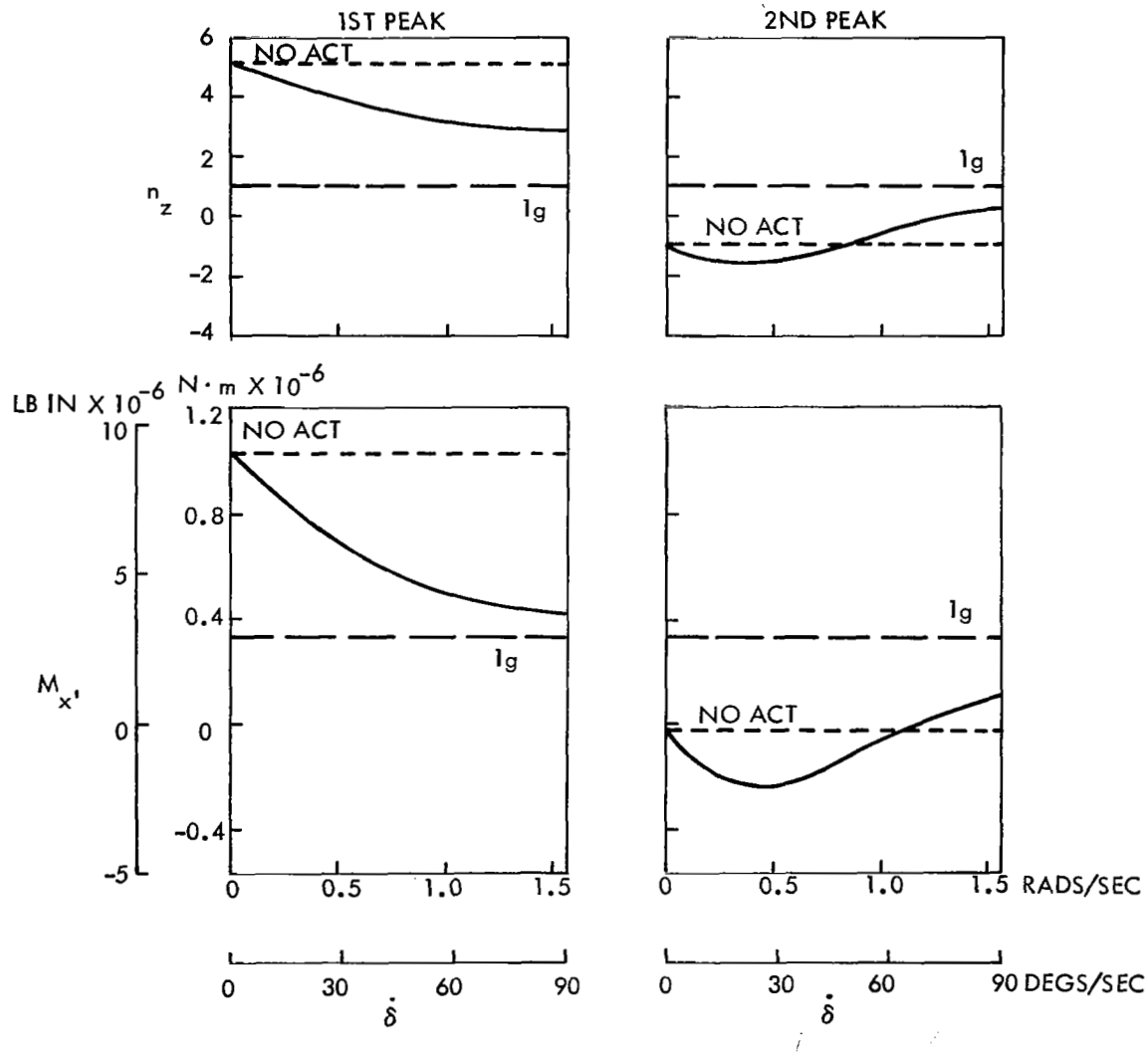

FIGURE B10 EFFECT OF CONTROL SURFACE RATE - $\dot{\delta}$

RIGID. UPGUST = 15.25 M/S (50 FPS)

FLAPS: G_F { -0.087 RADS/g (-5 DEGS/g) ——— ; -0.175 RADS/g (-10 DEGS/g) ⊙

ELEVS: G_E = 0.087 RADS/g (5 DEGS/g)

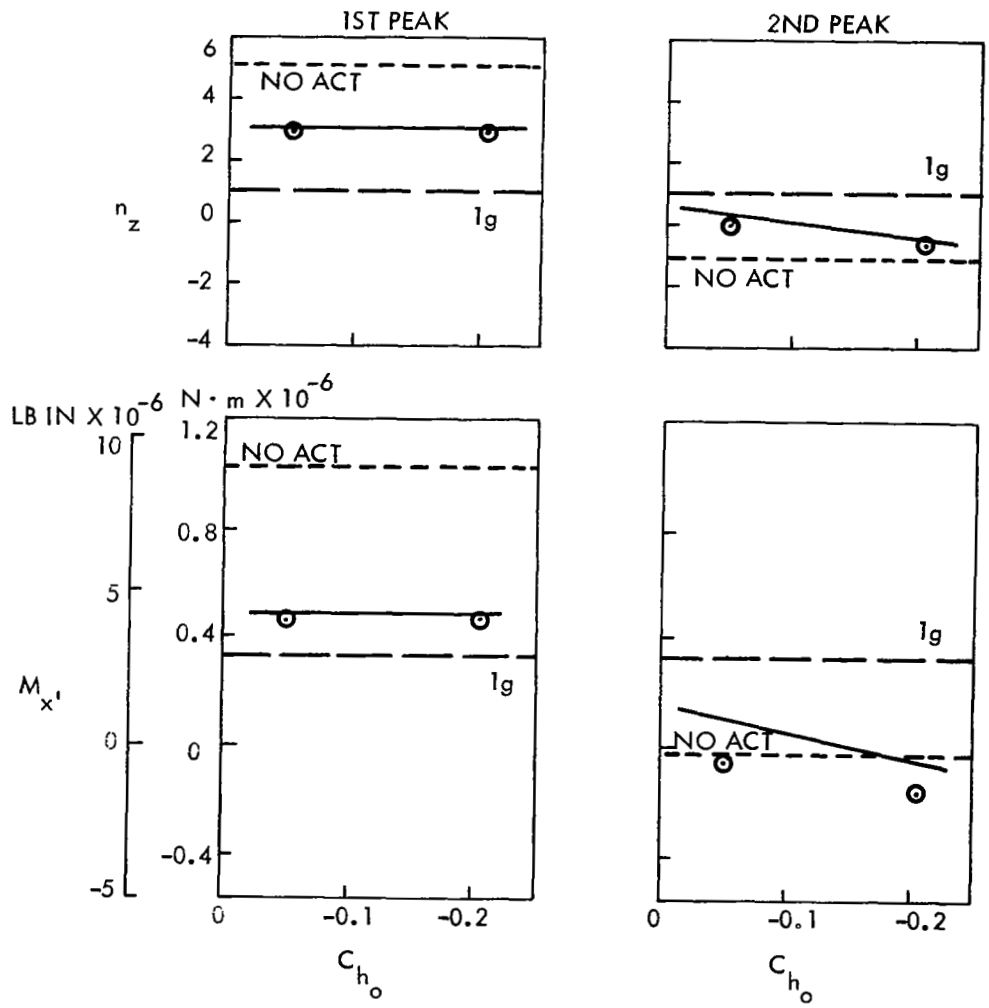

FIGURE B11 EFFECT OF FLAP HINGE MOMENT AT $\alpha = 0$

RIGID. DOWNGUST = -15.2 M/S (-50 FPS)

FLAPS: G_F = -0.087 RADS/g (-5 DEGS/g)

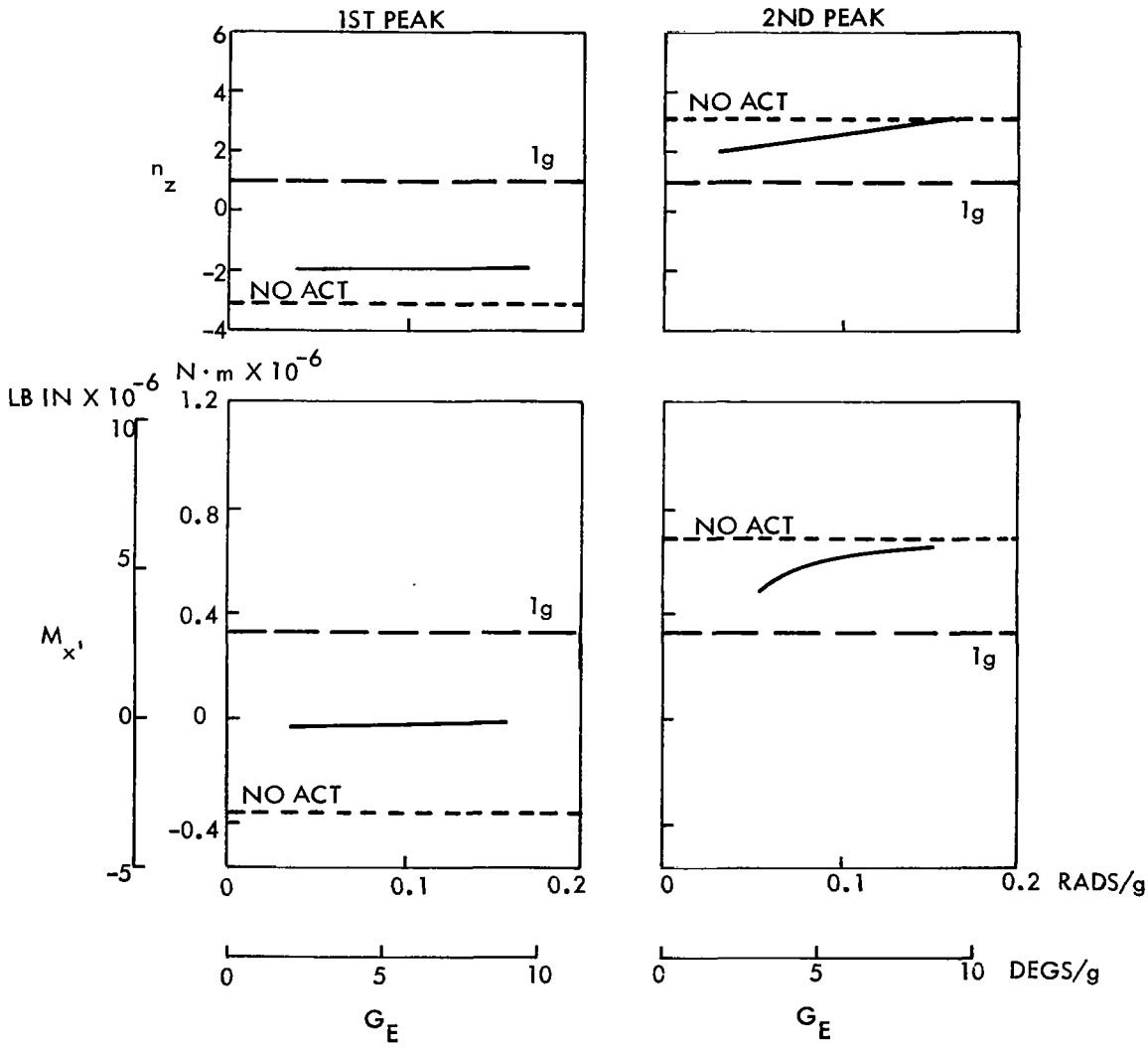

FIGURE B12 EFFECT OF ELEVATOR GAIN, G_E

RIGID. DOWNGUST= -15.25 M/S (-50 FPS)

FLAPS: G_F = -0.087 RADS/g (-5 DEGS/g)

ELEVS: G_E = 0.087 RADS/g (5 DEGS/g)

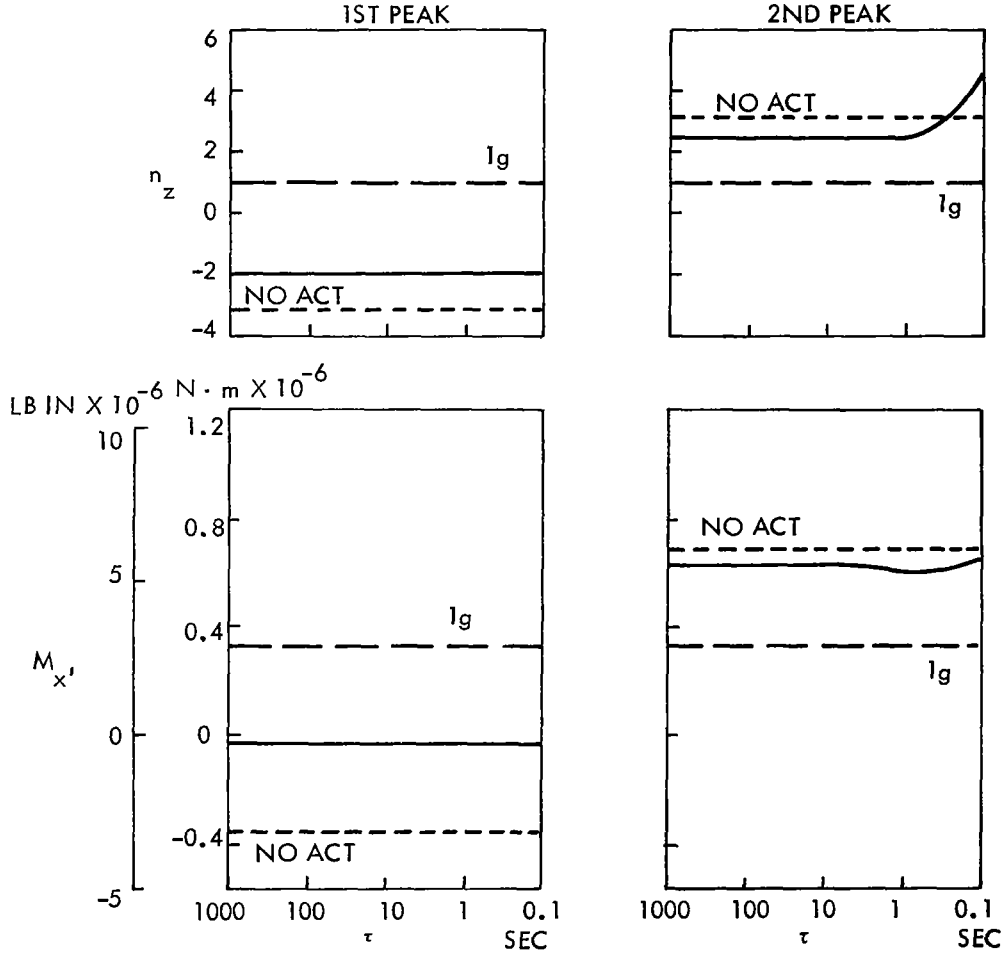

FIGURE B13 EFFECT OF FLAP CONSTANT, τ (WASHOUT)

RIGID. DOWNGUST = -15.2 M/S (-50 FPS)

FLAPS: G_F = -0.087 RADS/g (-5 DEGS/g)

ELEVS: G_E = 0.087 RADS/g (5 DEGS/g)

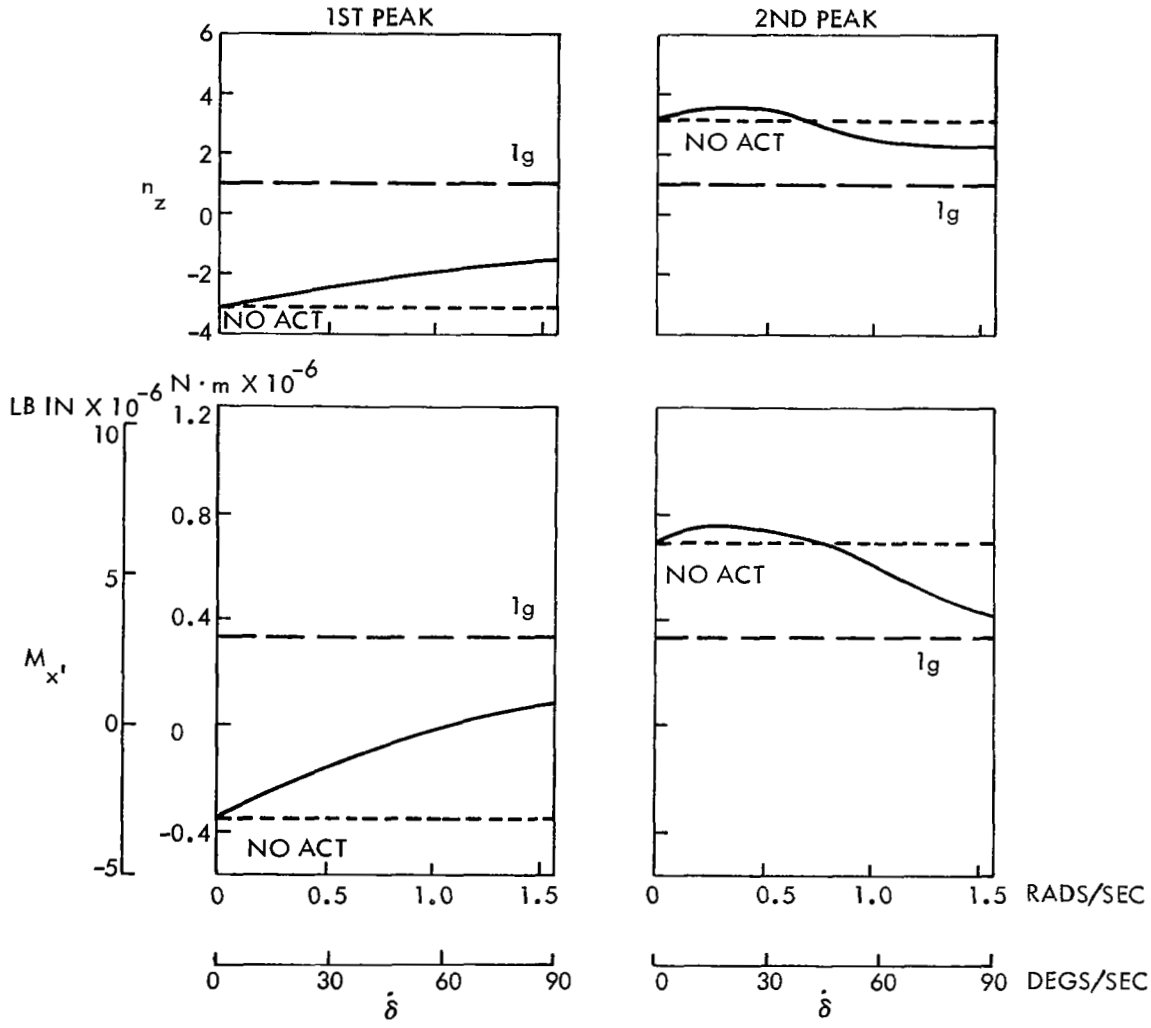

FIGURE B14 EFFECT OF CONTROL SURFACE RATE, $\dot{\delta}$

RIGID. DOWNGUST = -15.2 M/S (-50 FPS)

FLAPS: G_F = -0.087 RADS/g (-5 DEGS/g)

ELEVS: G_E = 0.087 RADS/g (5 DEGS/g)

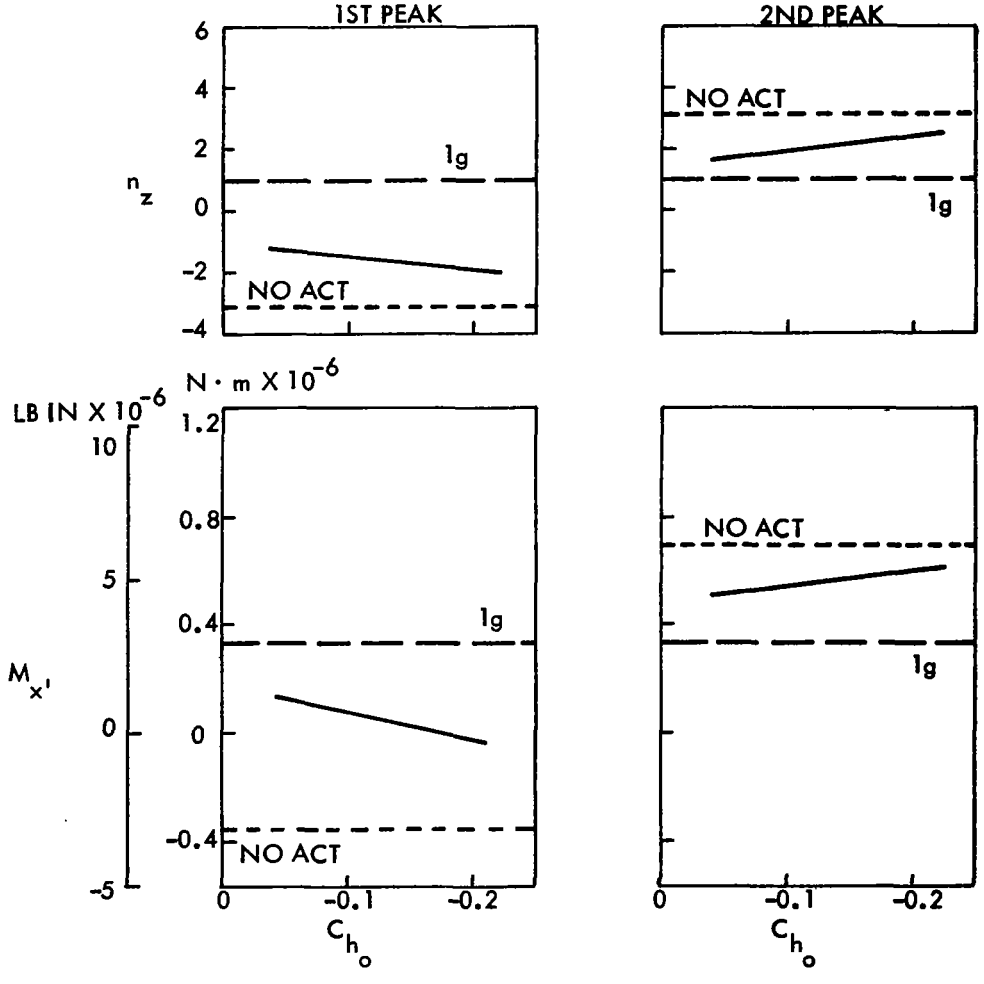

FIGURE B15 EFFECT OF FLAP HINGE MOMENT AT $\alpha = 0$

RIGID.

FLAPS: $G_F = -0.087$ RADS/g (-5 DEGS/g) $C_{h_o} = -0.205$ ——

ELEVS: $G_E = 0.087$ RADS/g (5 DEGS/g) $C_{h_o} = -0.050$ O

w_G = GUST VELOCITY

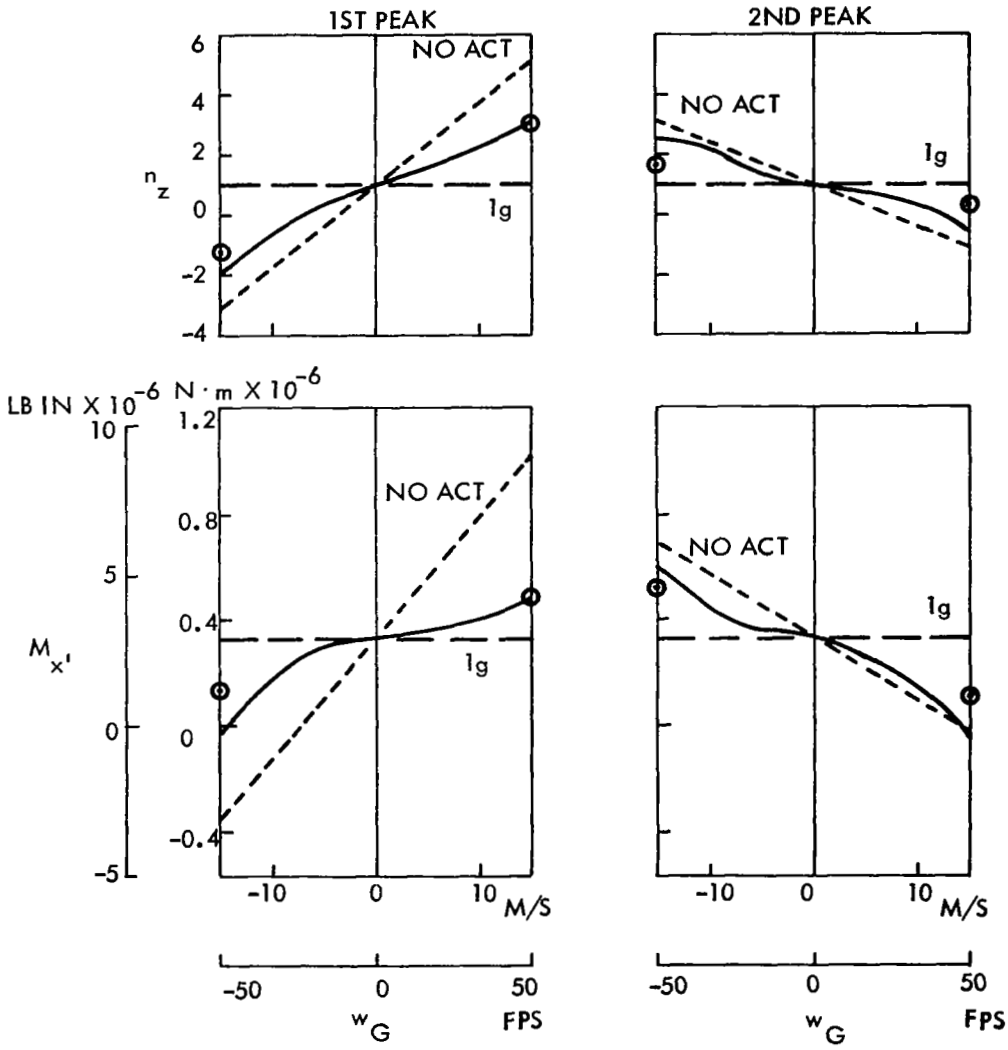

FIGURE B16 EFFECT OF GUST VELOCITY, w_G

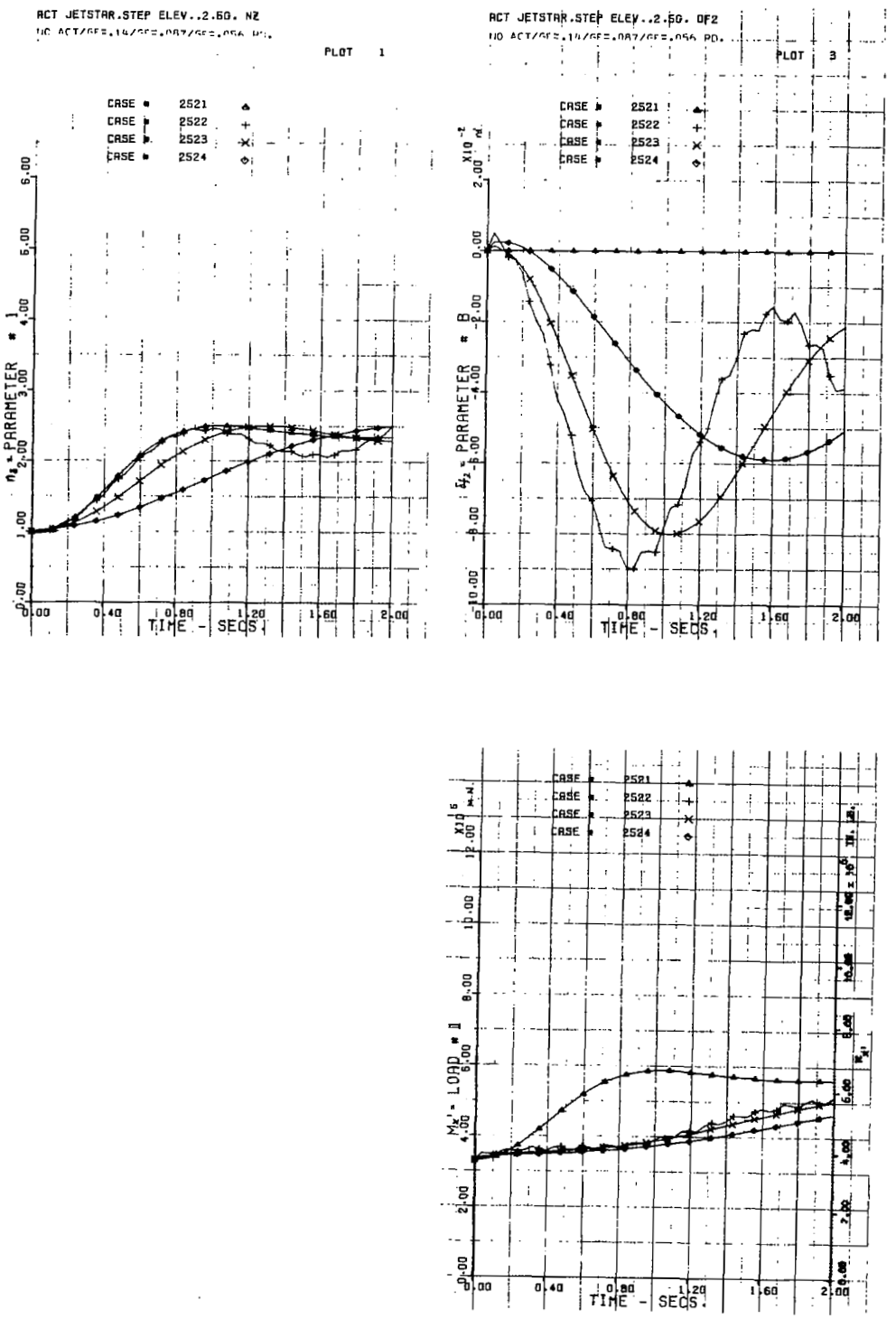

FIGURE B17 RIGID RESPONSE TO STEP ELEVATOR, EFFECT OF ELEVATOR GAIN

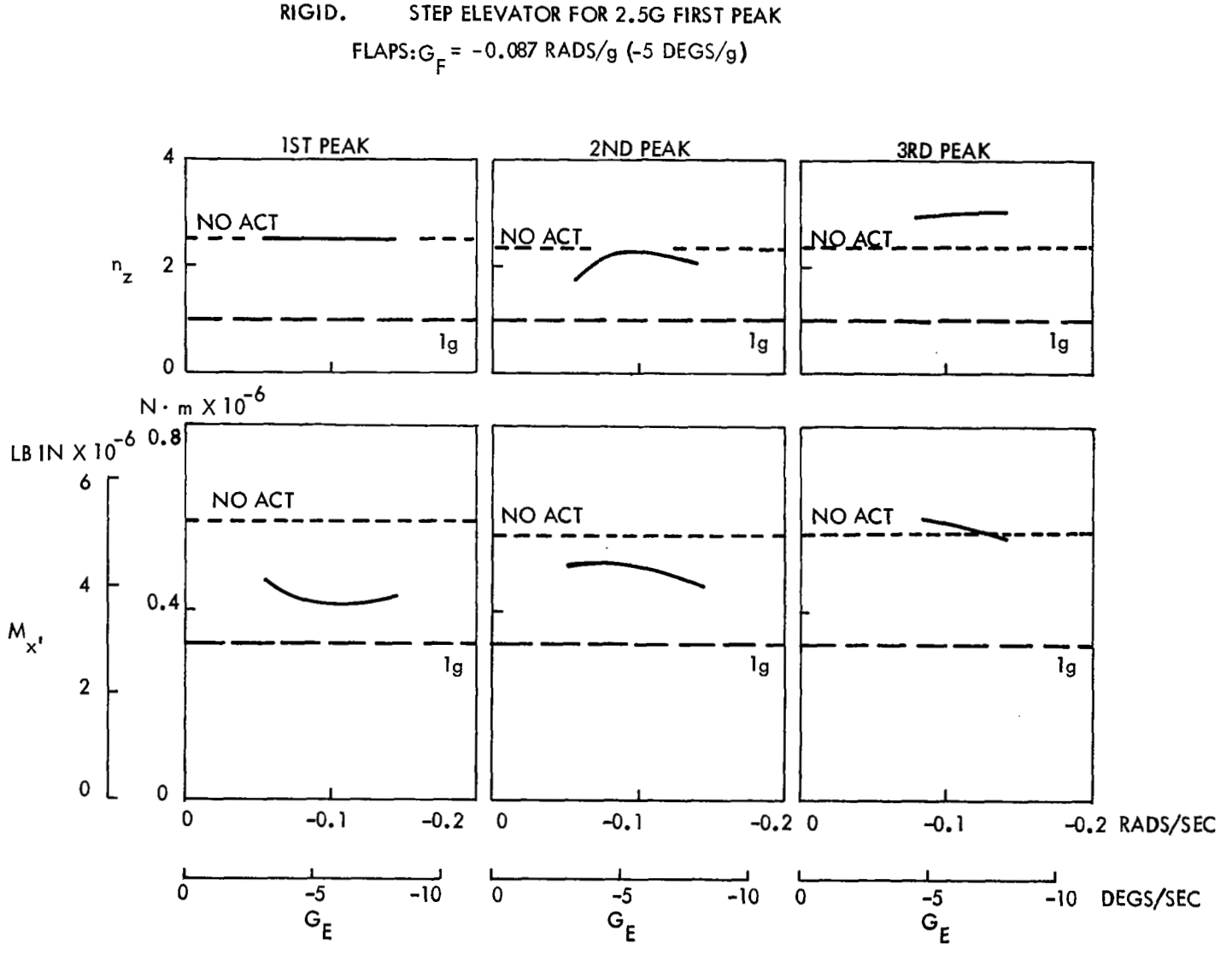

FIGURE B18 MANEUVER LOAD VARIATION WITH ELEVATOR GAIN, G_E

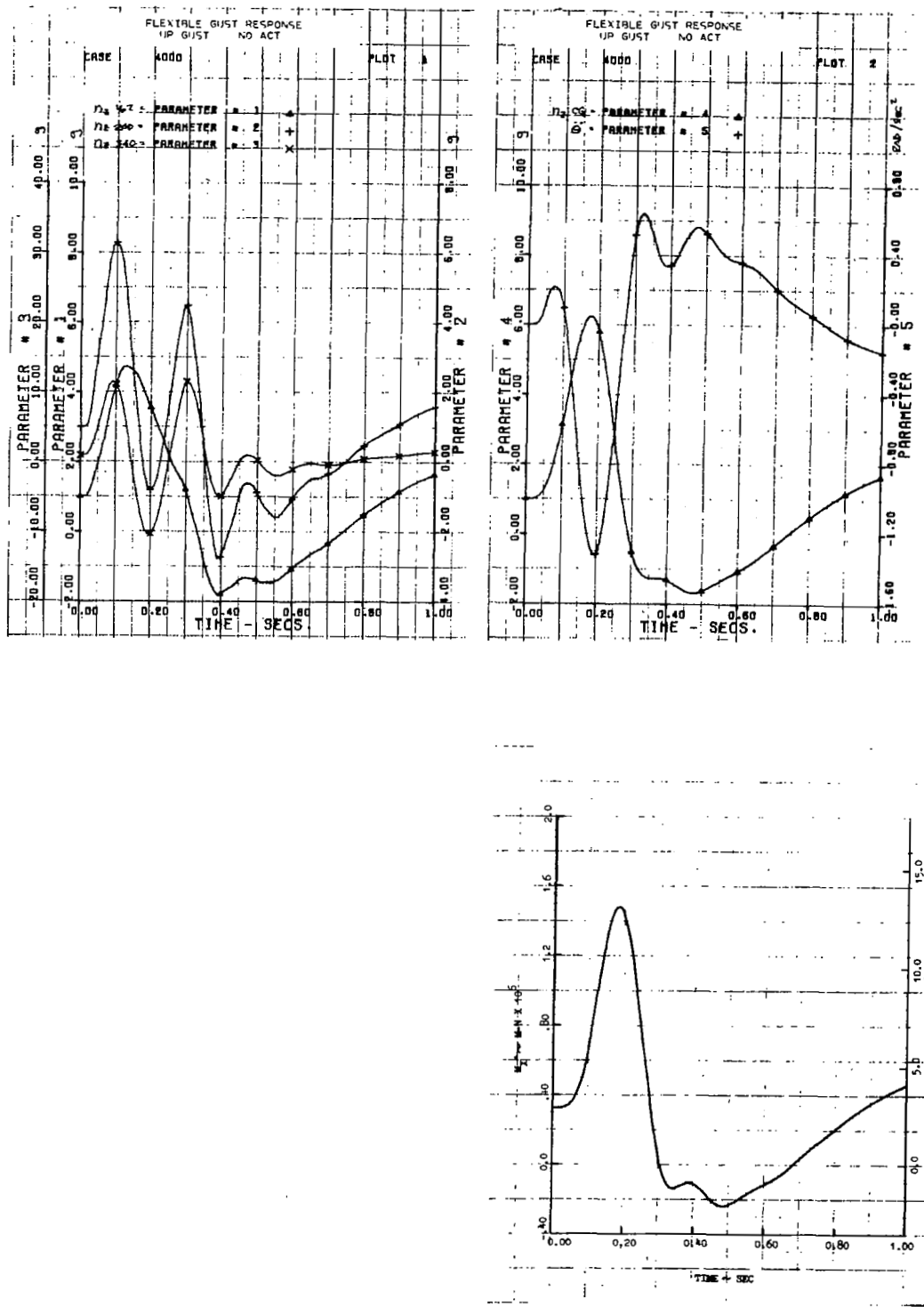

FIGURE B19 FLEXIBLE UPGUST RESPONSE, NO ACTIVE CONTROLS

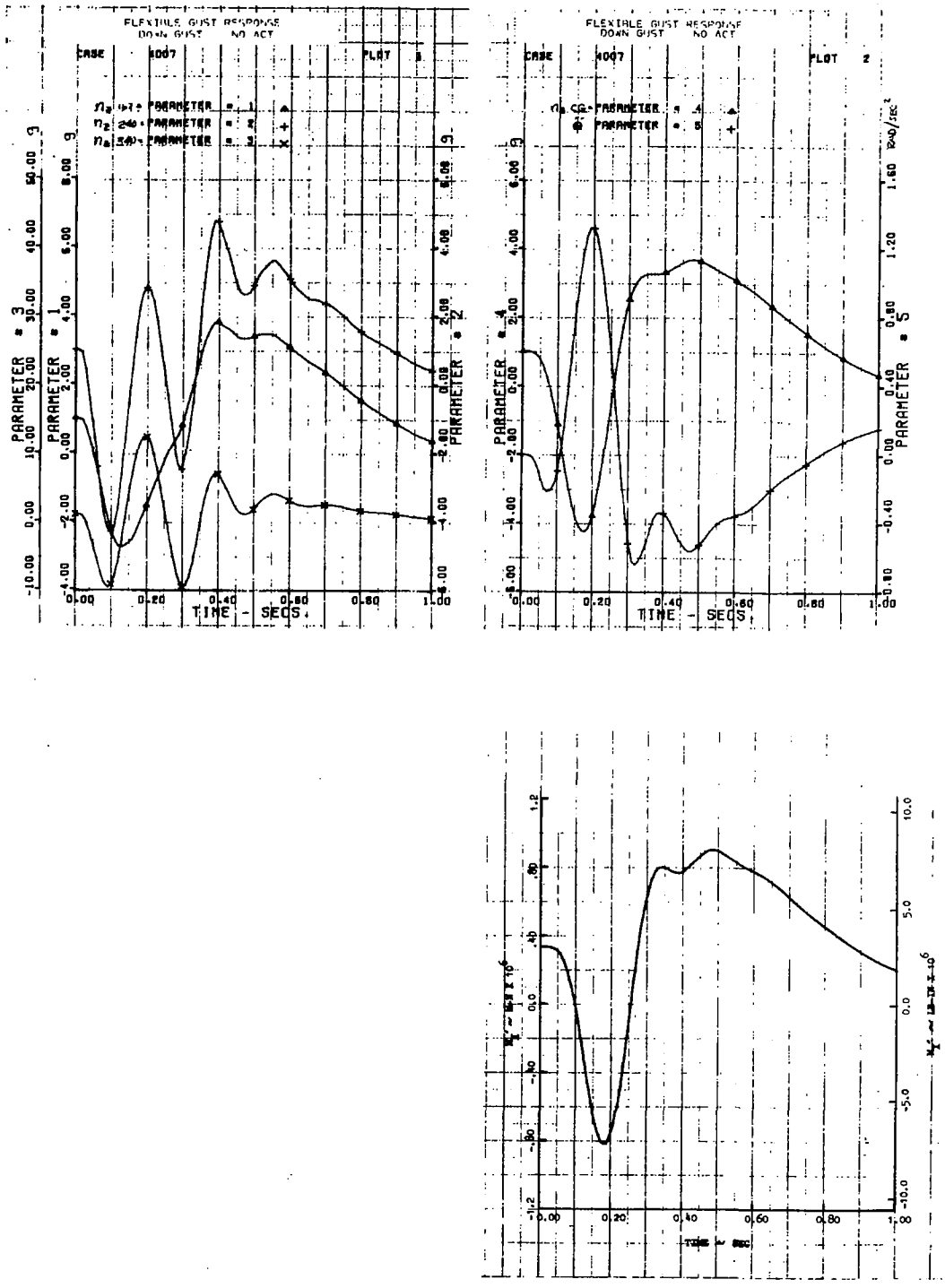

FIGURE B20 FLEXIBLE DOWNGUST RESPONSE, NO ACTIVE CONTROLS

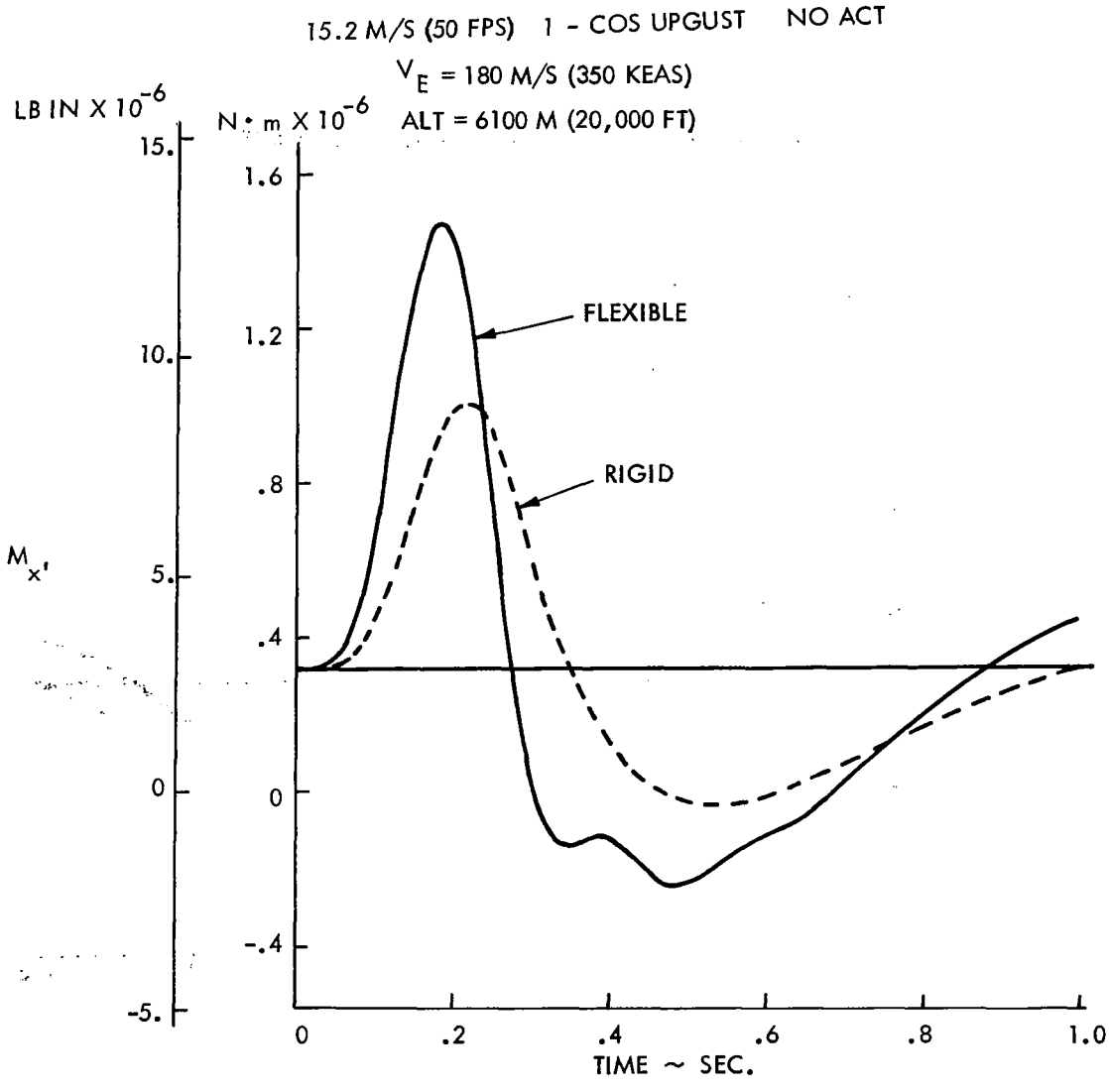

FIGURE B21 WING ROOT BENDING MOMENT

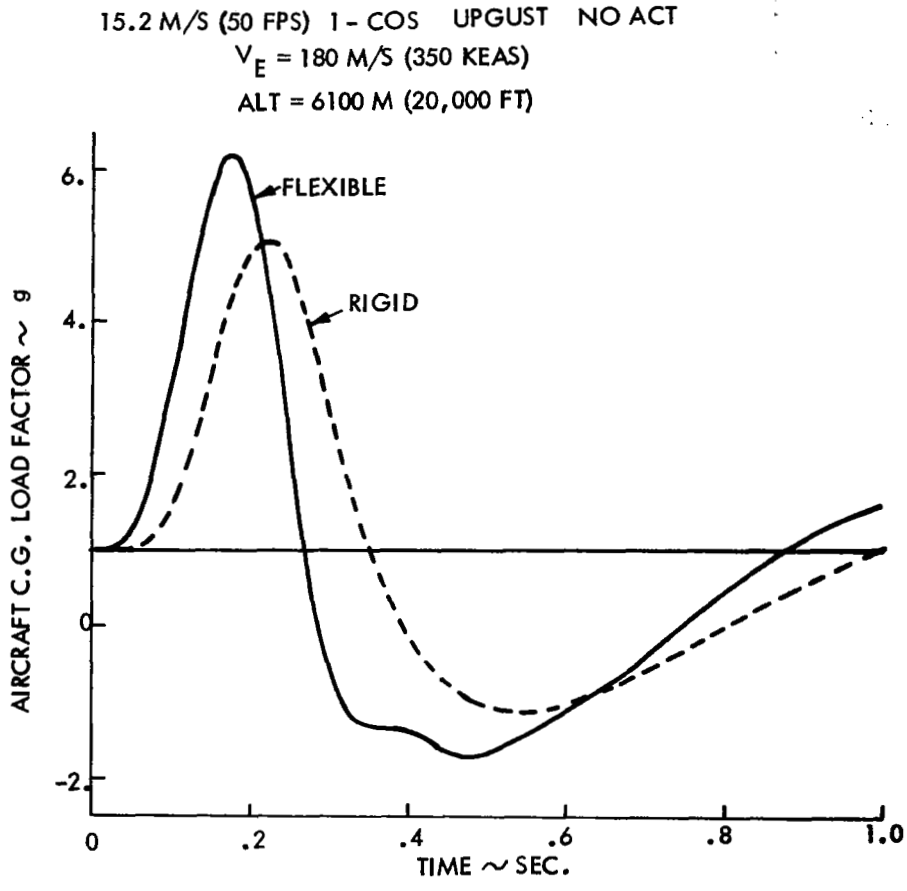

FIGURE B22 C.G. LOAD FACTOR

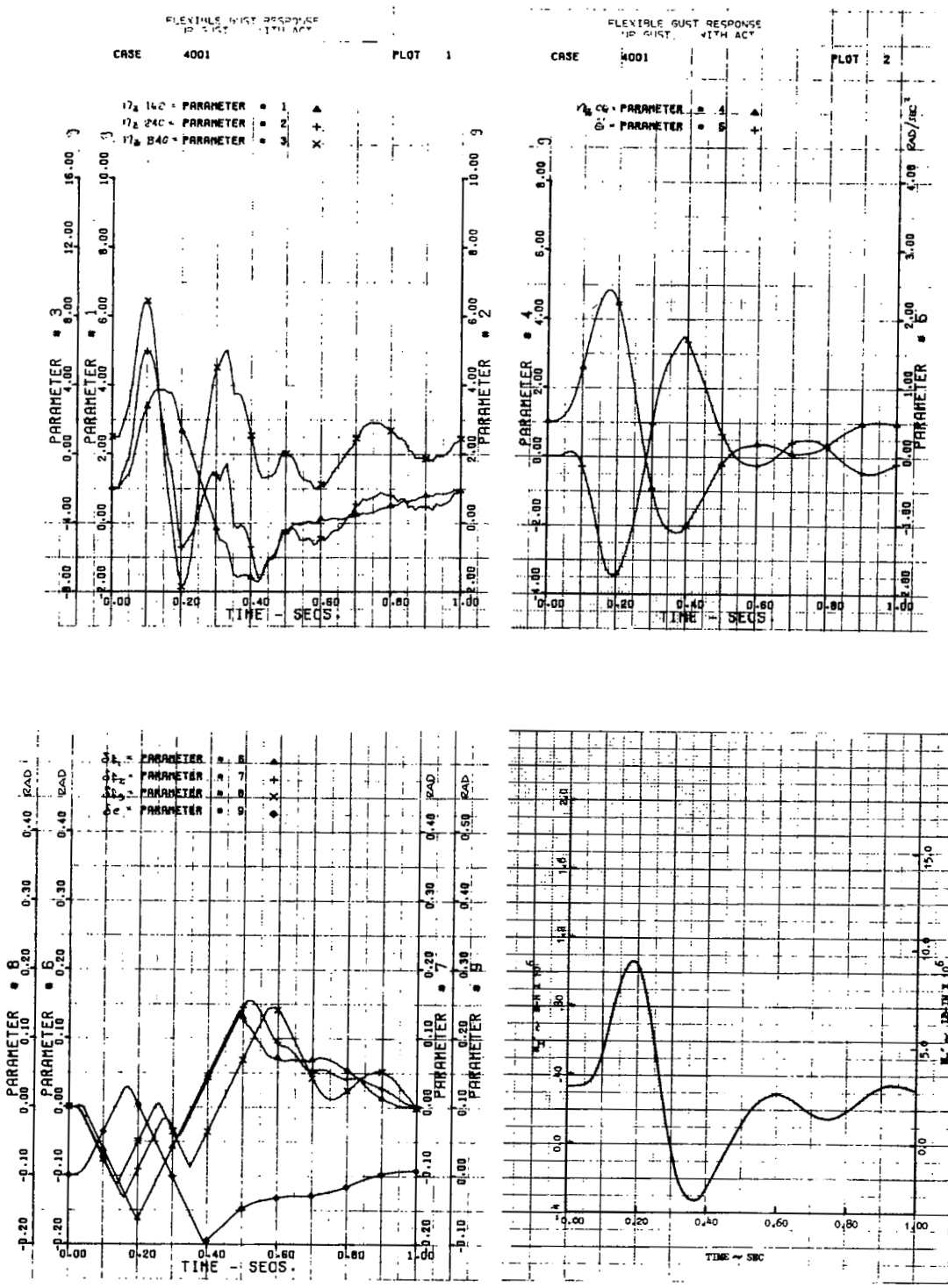

FIGURE B23 FLEXIBLE UPGUST RESPONSE, EFFECT OF LAG PLUS WASHOUT FILTER

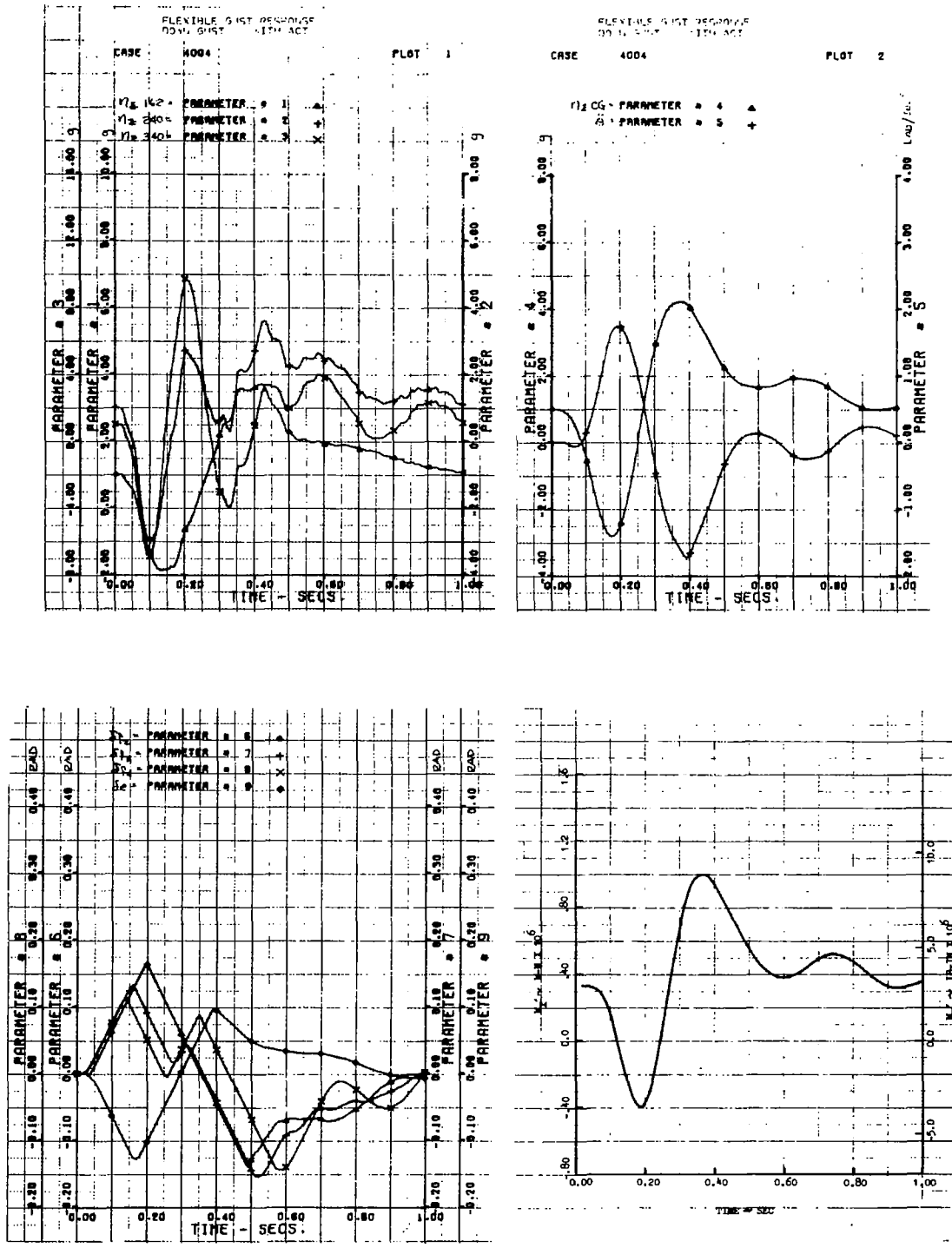

FIGURE B24 FLEXIBLE DOWNGUST RESPONSE, EFFECT OF LAG PLUS WASHOUT FILTER

15.2 M/S (50 FPS) 1 - COS UPGUST

ACT SYSTEM
FLAP GAIN G_F = 0.087 RADS/g (5 DEGS/g)
ELEVATOR GAIN G_E = 0.056 RADS/g (3.21 DEGS/g)
NO-LOAD RATE = 1.05 RADS/SEC (60 DEGS/SEC)

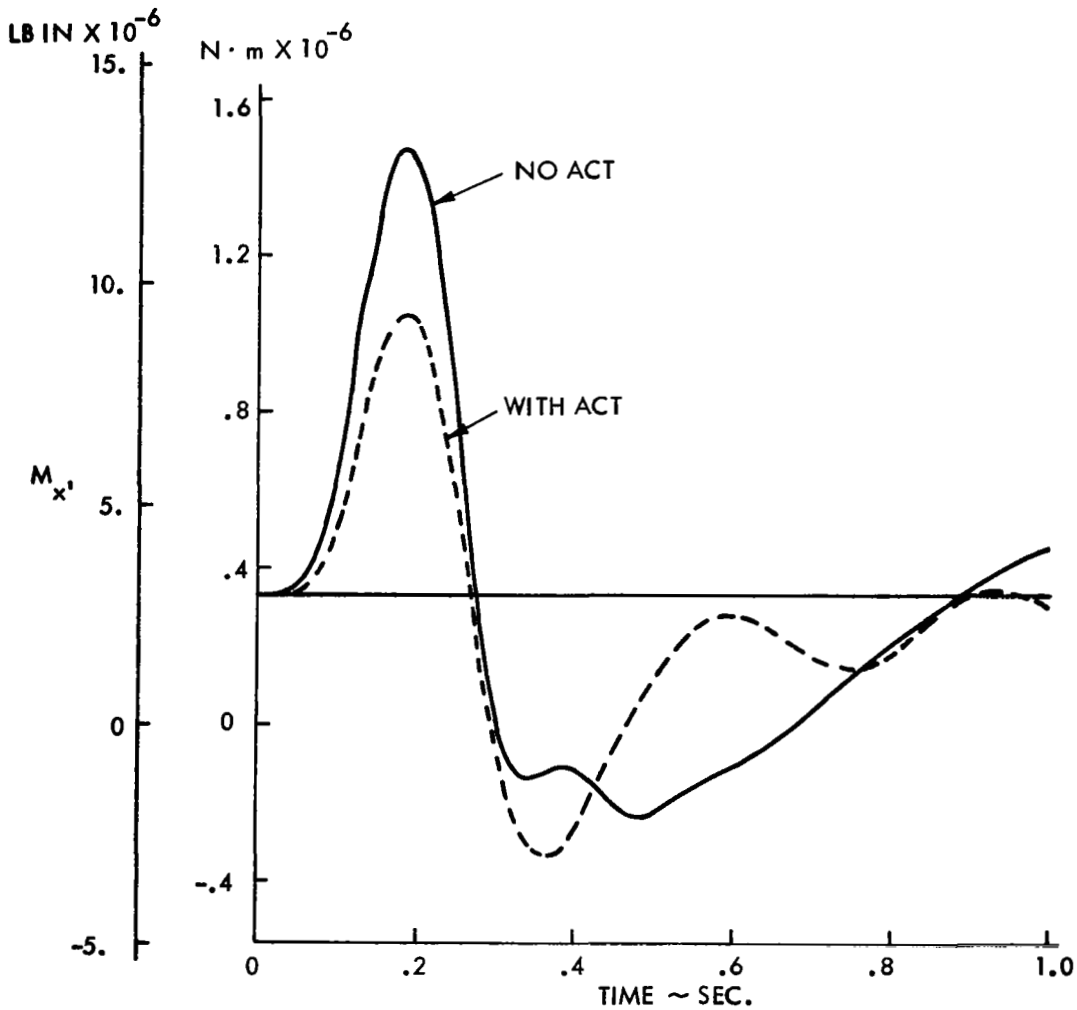

FIGURE B25 FLEXIBLE WING ROOT BENDING MOMENT

FLEXIBLE ACT JETSTAR

15.2 M/S (50 FPS) UPGUST V_E = 180 M/S (350 KEAS) ALT = 6100M (20000 FT)

ELEVATOR GAIN G_E = 0.056 RADS/g (3.21 DEGS/g)
RATES = 1.05 RADS/SEC (60 DEGS/SEC)

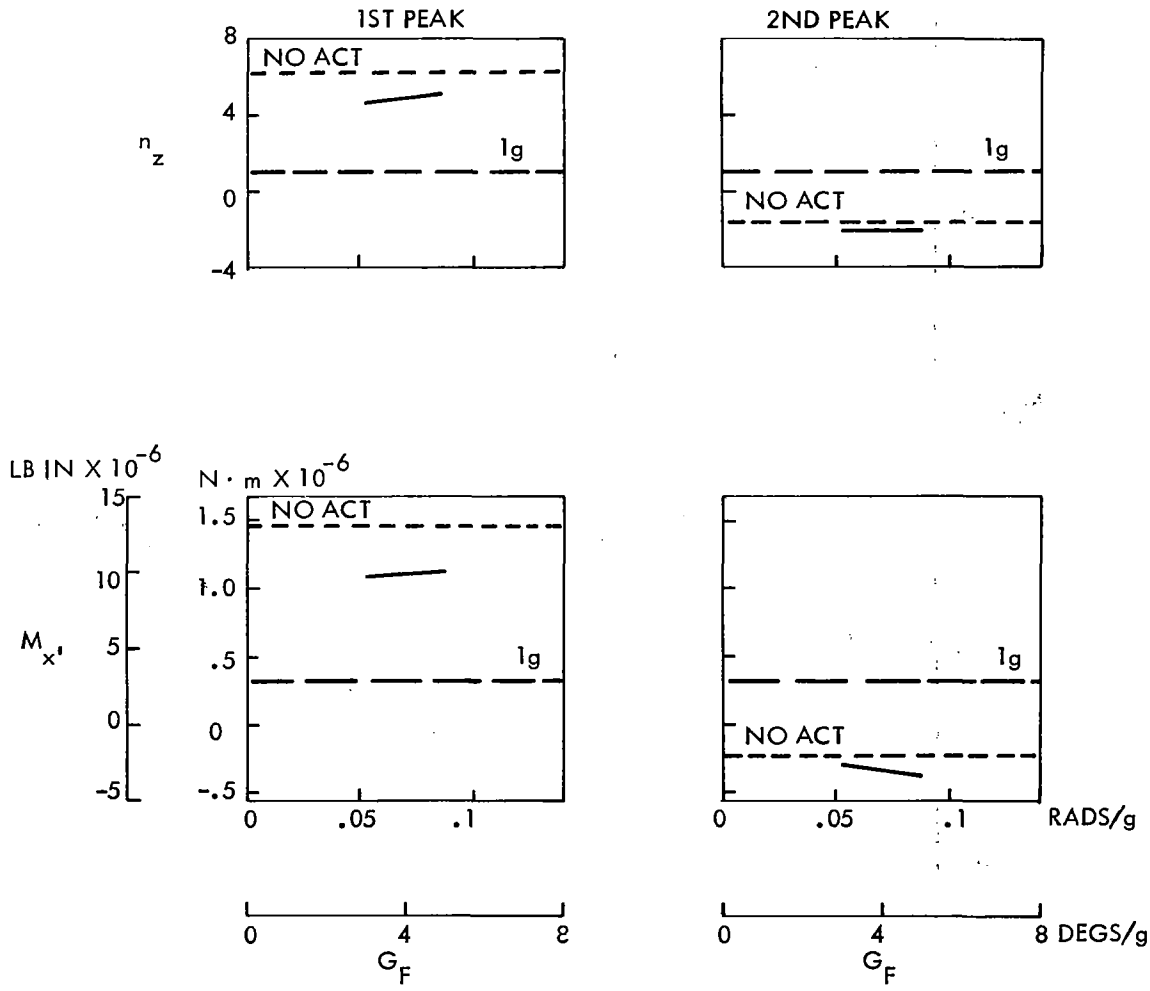

FIGURE B26 EFFECT OF FLAP WASHOUT FILTER GAIN

FLEXIBLE ACT JETSTAR

15.2 M/S (50 FPS) UPGUST V_E = 180 M/S (350 KEAS) ALT = 6100M (20000 FT)

ELEVATOR GAIN G_E = 0.056 RADS/g (3.21 DEGS/g)
RATES = 1.05 RADS/SEC (60 DEGS/SEC)

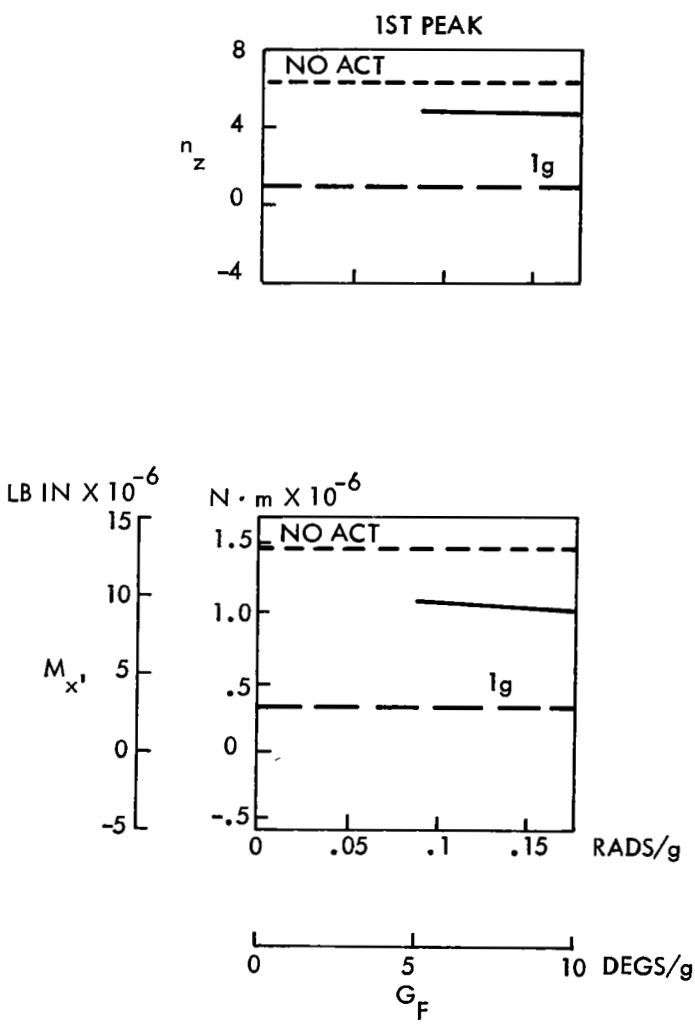

FIGURE B27 EFFECT OF FLAP LAG FILTER GAIN

FLEXIBLE ACT JETSTAR

15.2 M/S (50 FPS) UPGUST V_E = 180 M/S (350 KEAS) ALT = 6100M (20000 FT)

ELEVATOR GAIN G_E = 0.035 RADS/g (2.00 DEGS/g)

RATES = 1.05 RADS/SEC (60 DEGS/SEC)

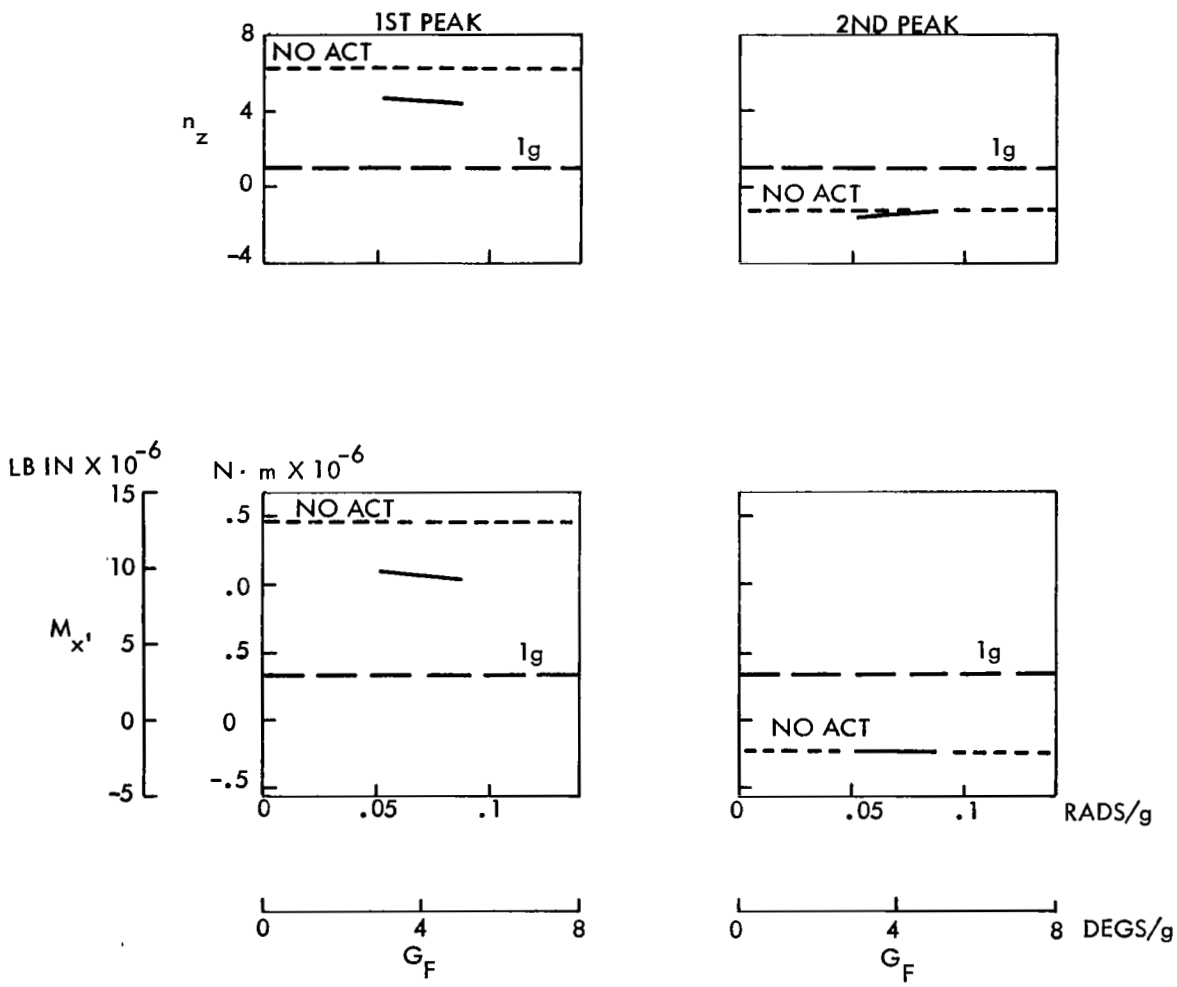

FIGURE B28 EFFECT OF FLAP WASHOUT AND LAG FILTER GAINS

FLEXIBLE ACT JETSTAR

15.2 M/S (50 FPS) UPGUST V_E = 180 M/S (350 KEAS) ALT = 6100M (20000 FT)

FLAP GAIN G_F = 0.087 RADS/g (5 DEGS/g)
ELEVATOR GAIN G_E = 0.056 RADS/g (3.21 DEGS/g)

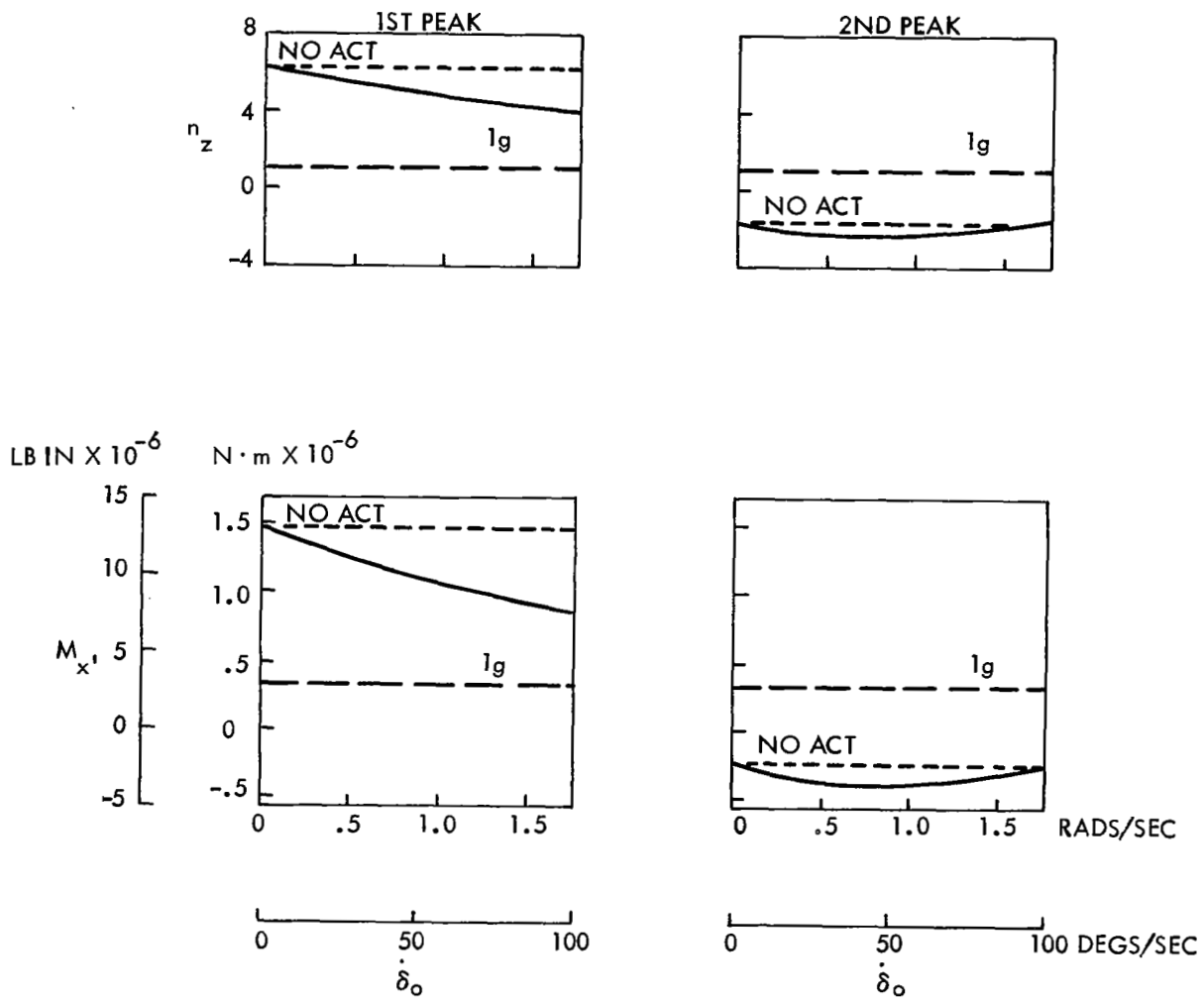

FIGURE B29 EFFECT OF FLAP NO-LOAD RATE $\sim \dot{\delta}_o$

FLEXIBLE ACT JETSTAR

15.2 M/S (50 FPS) UPGUST V_E = 180 M/S (350 KEAS) ALT = 6100M (20000 FT)

FLAP GAIN G_F = 0.087 RADS/g (5 DEGS/g)
ELEVATOR GAIN G_E = 0.056 RADS/g (3.21 DEGS/g)

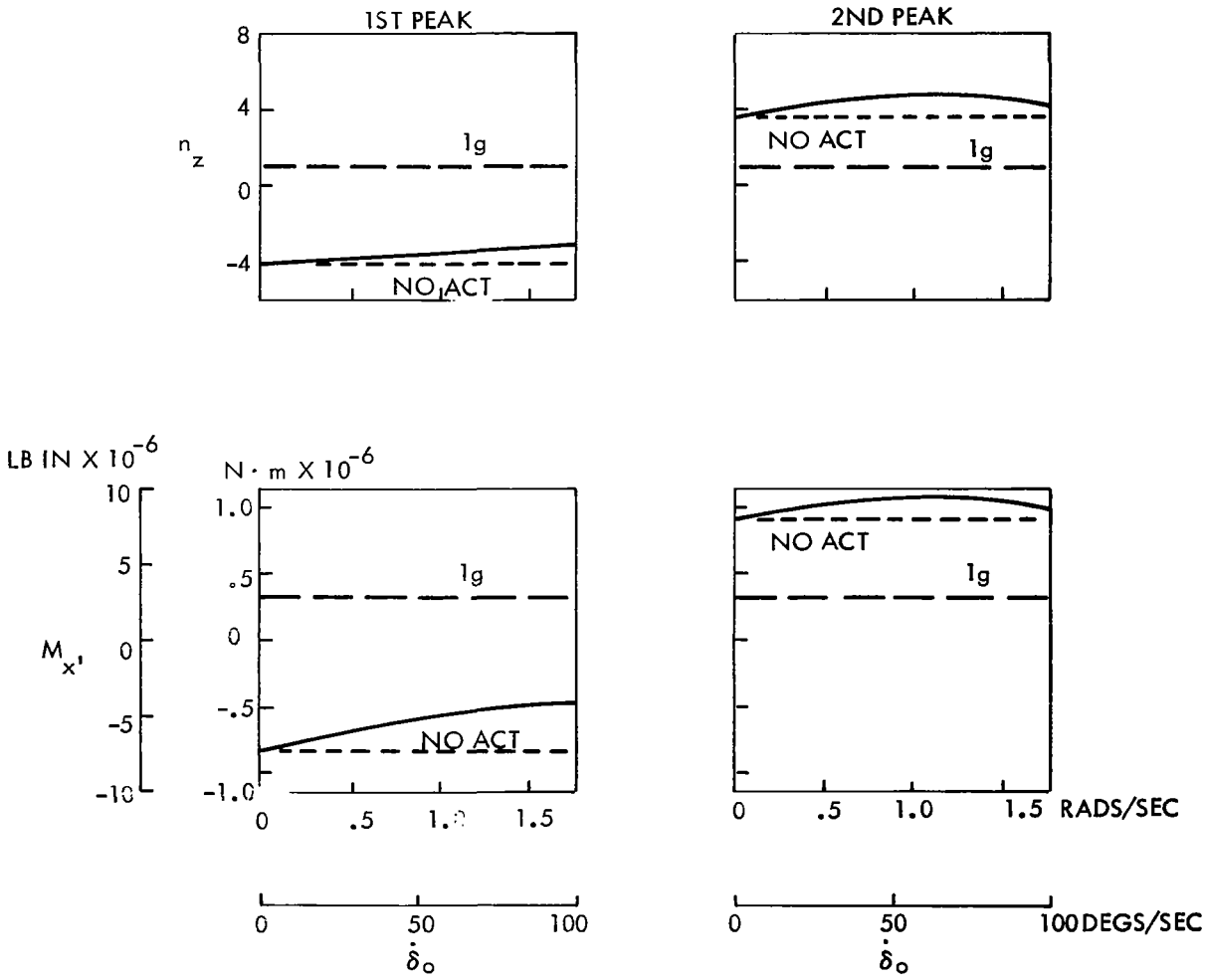

FIGURE B30 EFFECT OF FLAP NO-LOAD RATE ~ $\dot{\delta}_o$

FLEXIBLE ACT JETSTAR

15.2 M/S (50 FPS) UPGUST V_E = 180 M/S (350 KEAS) ALT = 6100M (20000 FT)

FLAP GAIN G_F = 0.087 RADS/g (5 DEGS/g)

RATES = 1.05 RADS/SEC (60 DEGS/SEC)

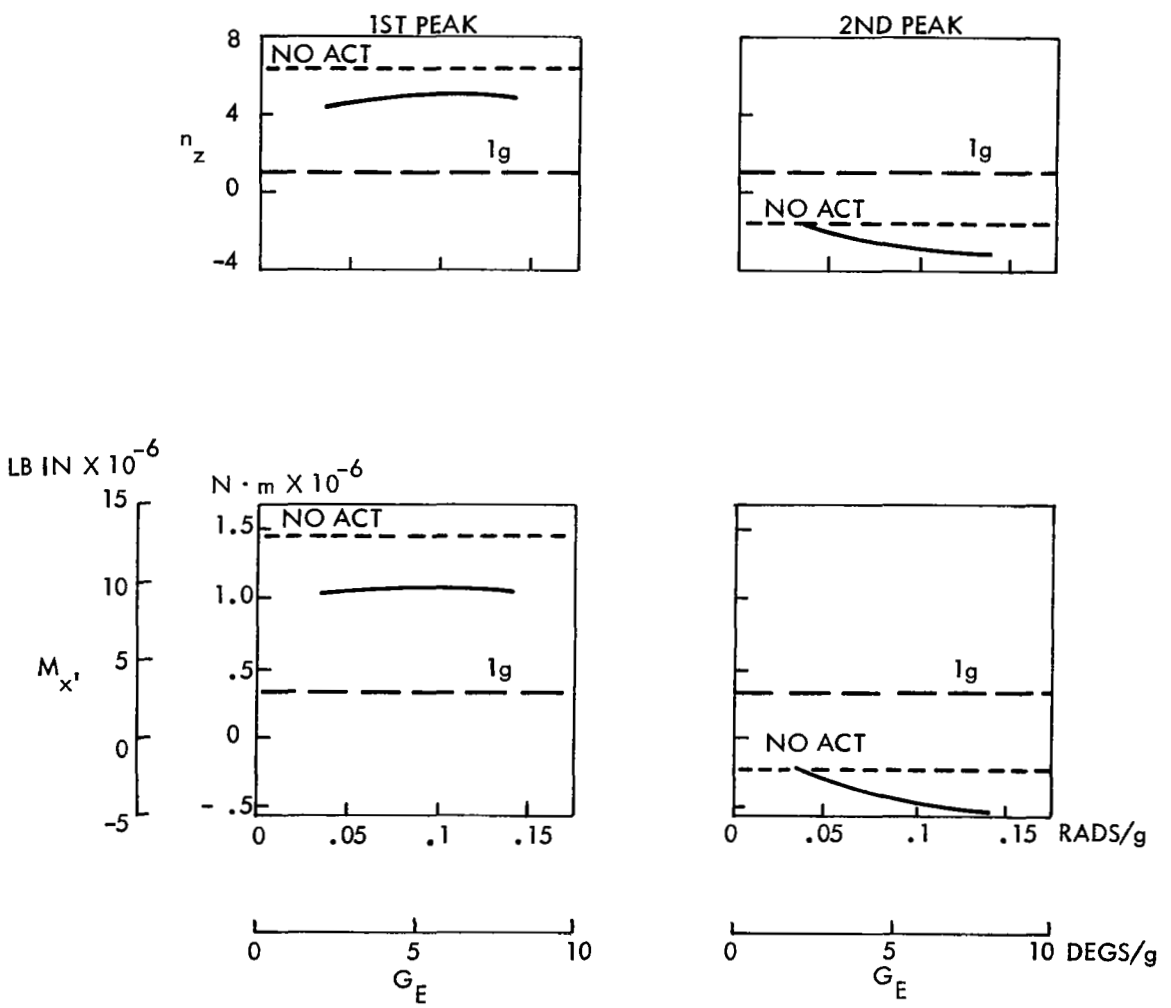

FIGURE B31 EFFECT OF ELEVATOR GAIN

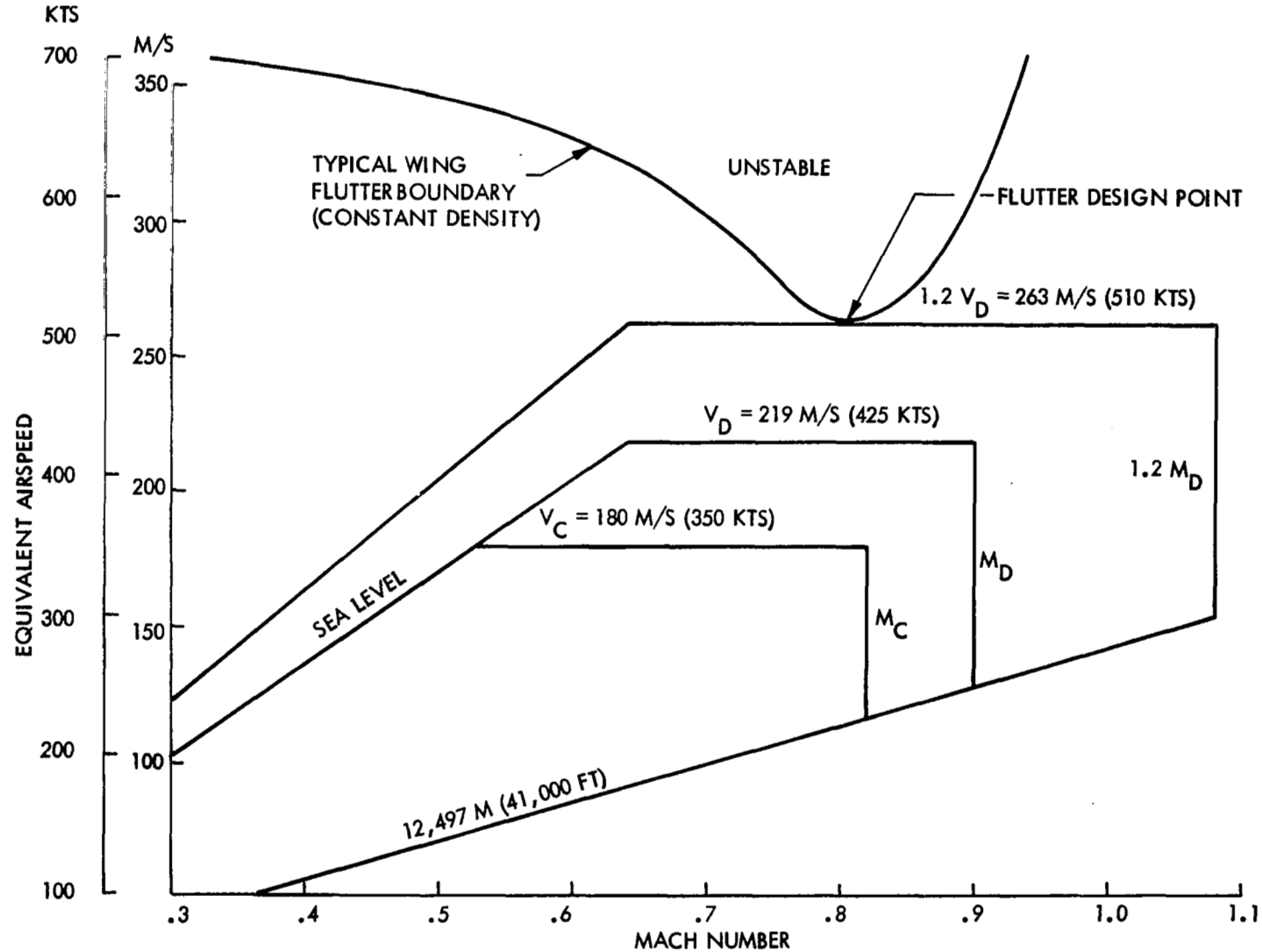

FIGURE B32 STRUCTURAL DESIGN AIRSPEEDS AND FLUTTER DESIGN POINT

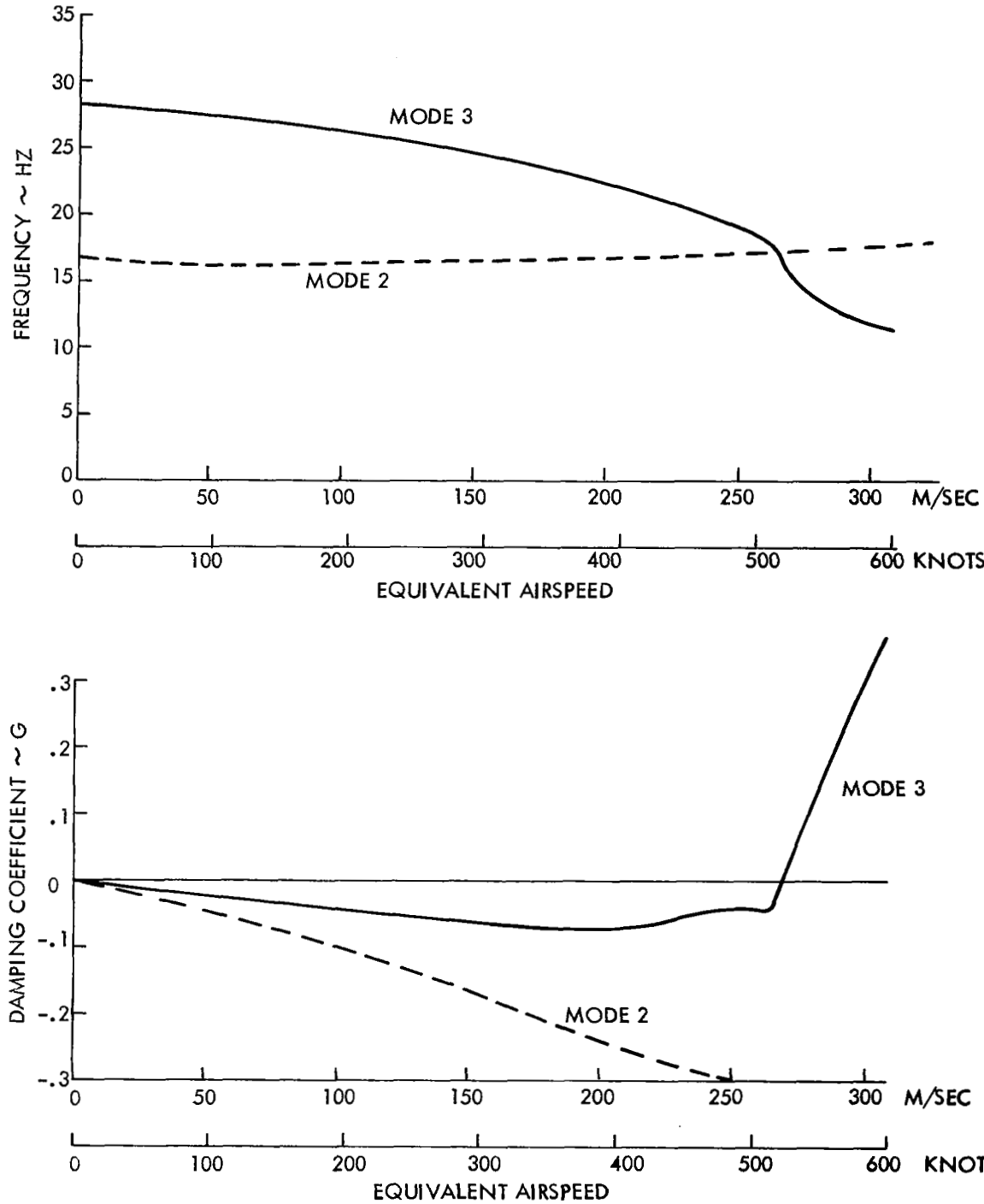

FIGURE B33 TYPICAL FLUTTER ANALYSIS RESULTS
SYMMETRIC CASE - EMPTY FUEL

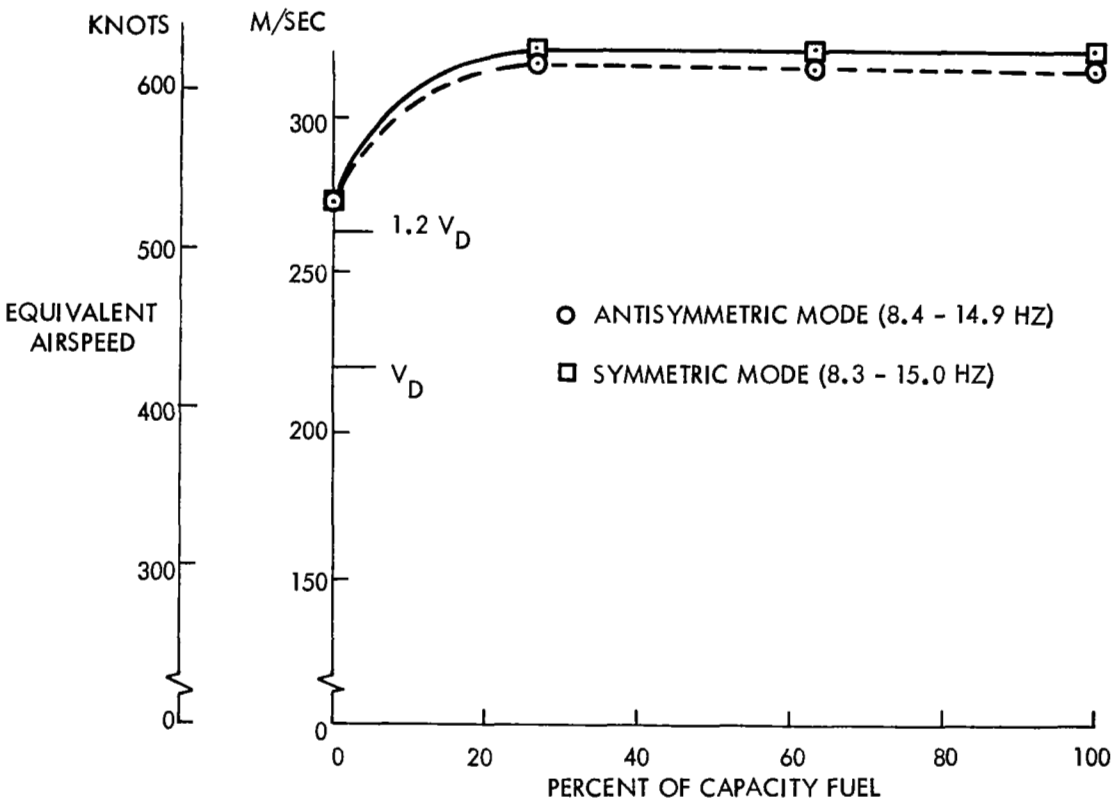

FIGURE B34 EFFECT OF FUEL ON WING FLUTTER SPEED

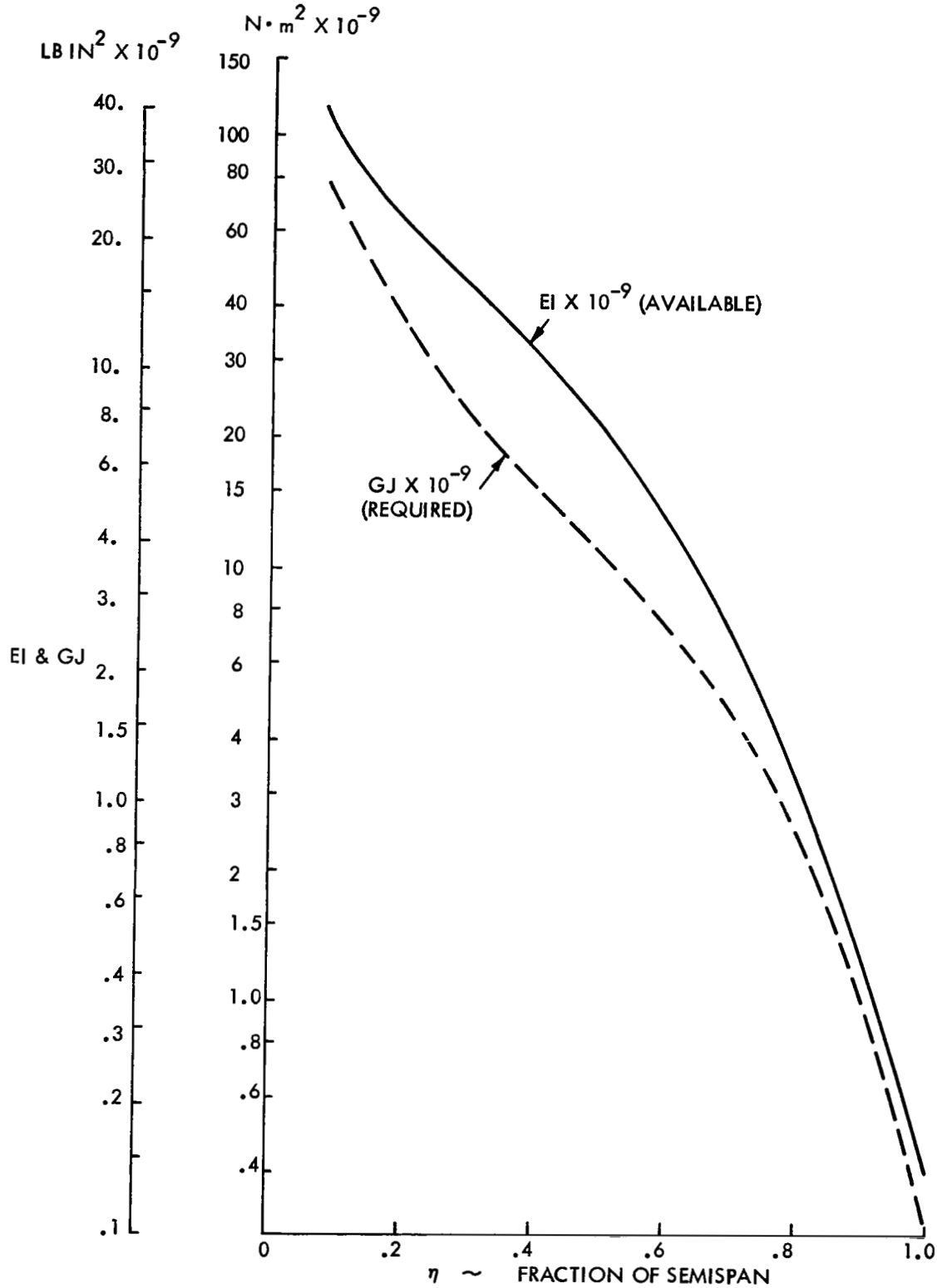

FIGURE B35 WING STIFFNESS

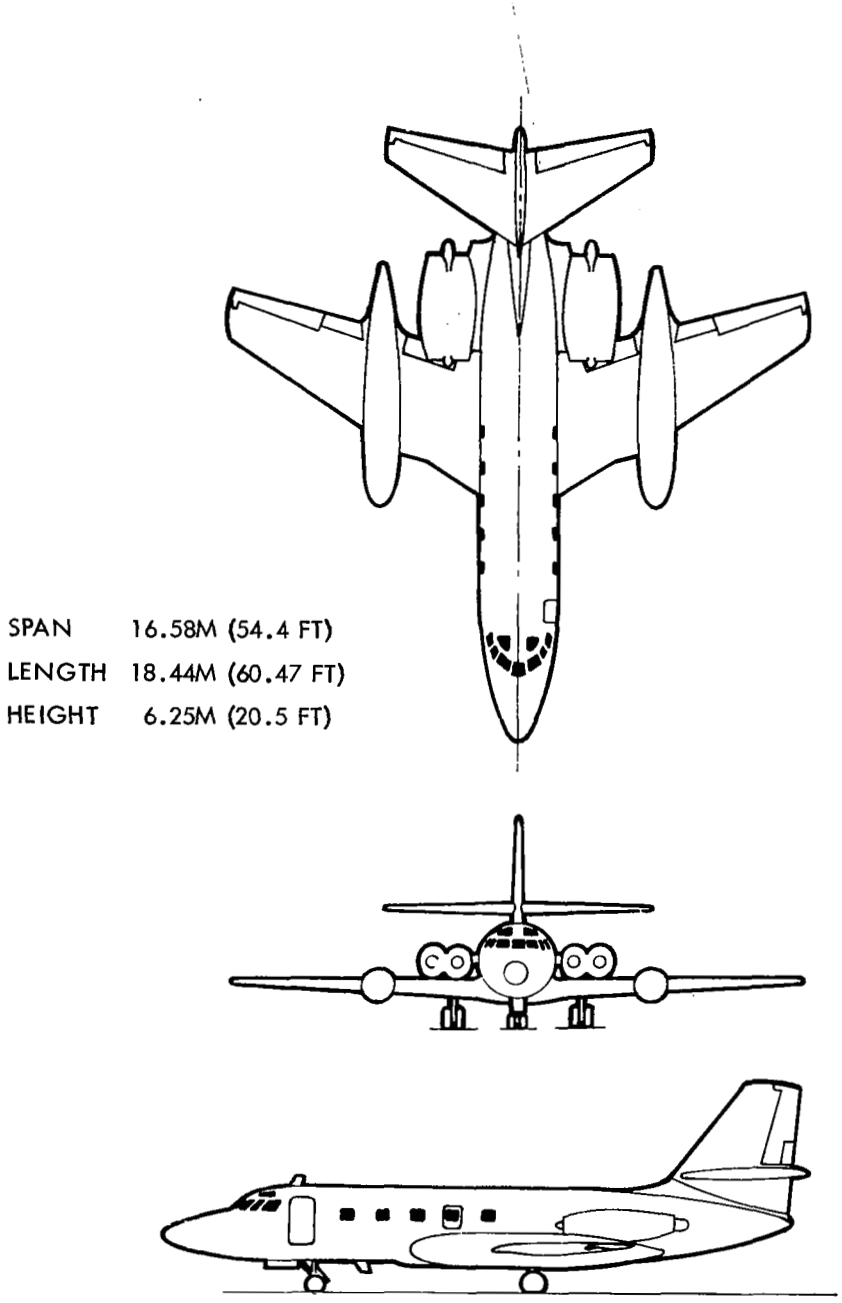

FIGURE C1 JETSTAR MODEL 1329-6A GENERAL ARRANGEMENT

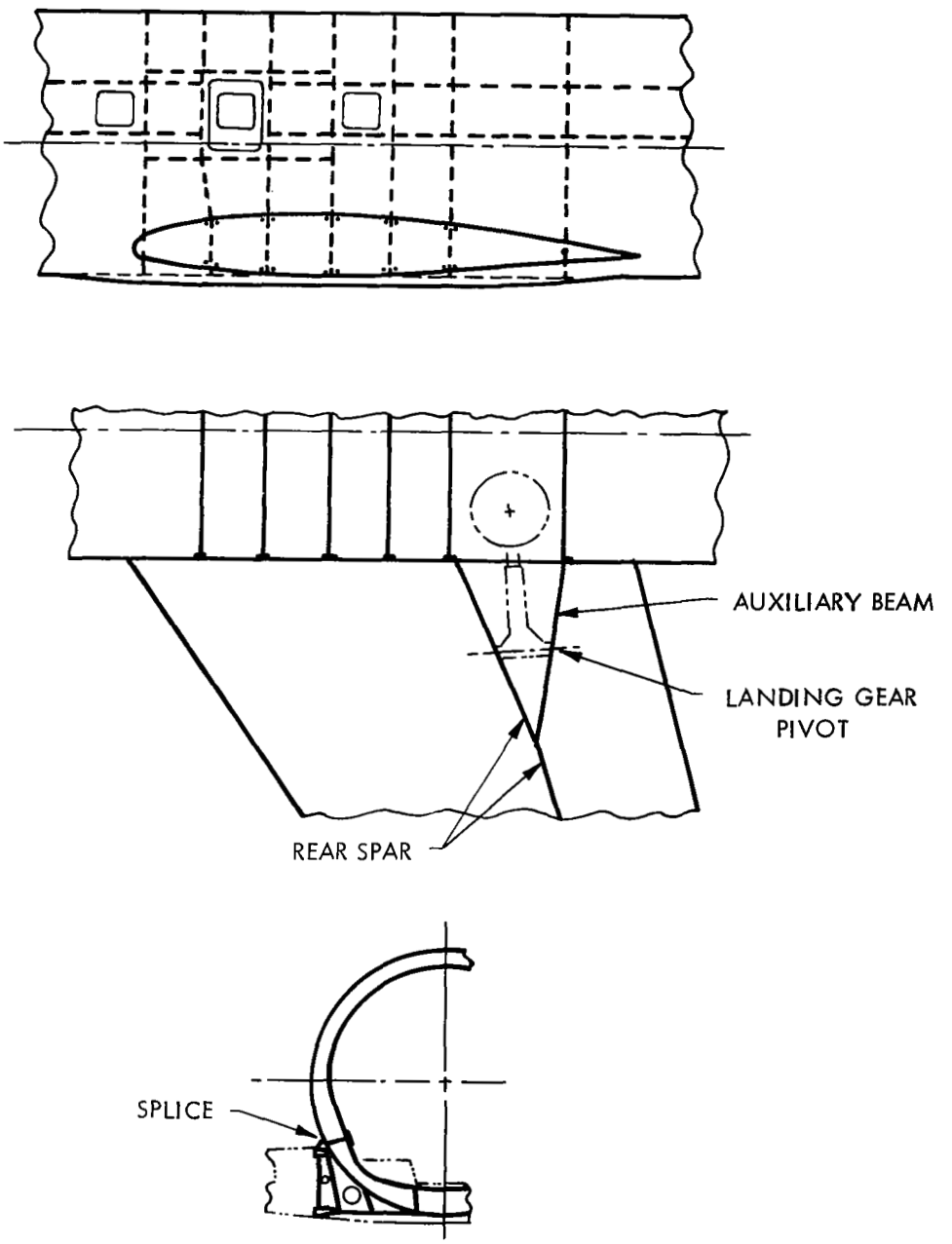

FIGURE C2 JETSTAR EXISTING CENTER SECTION STRUCTURE

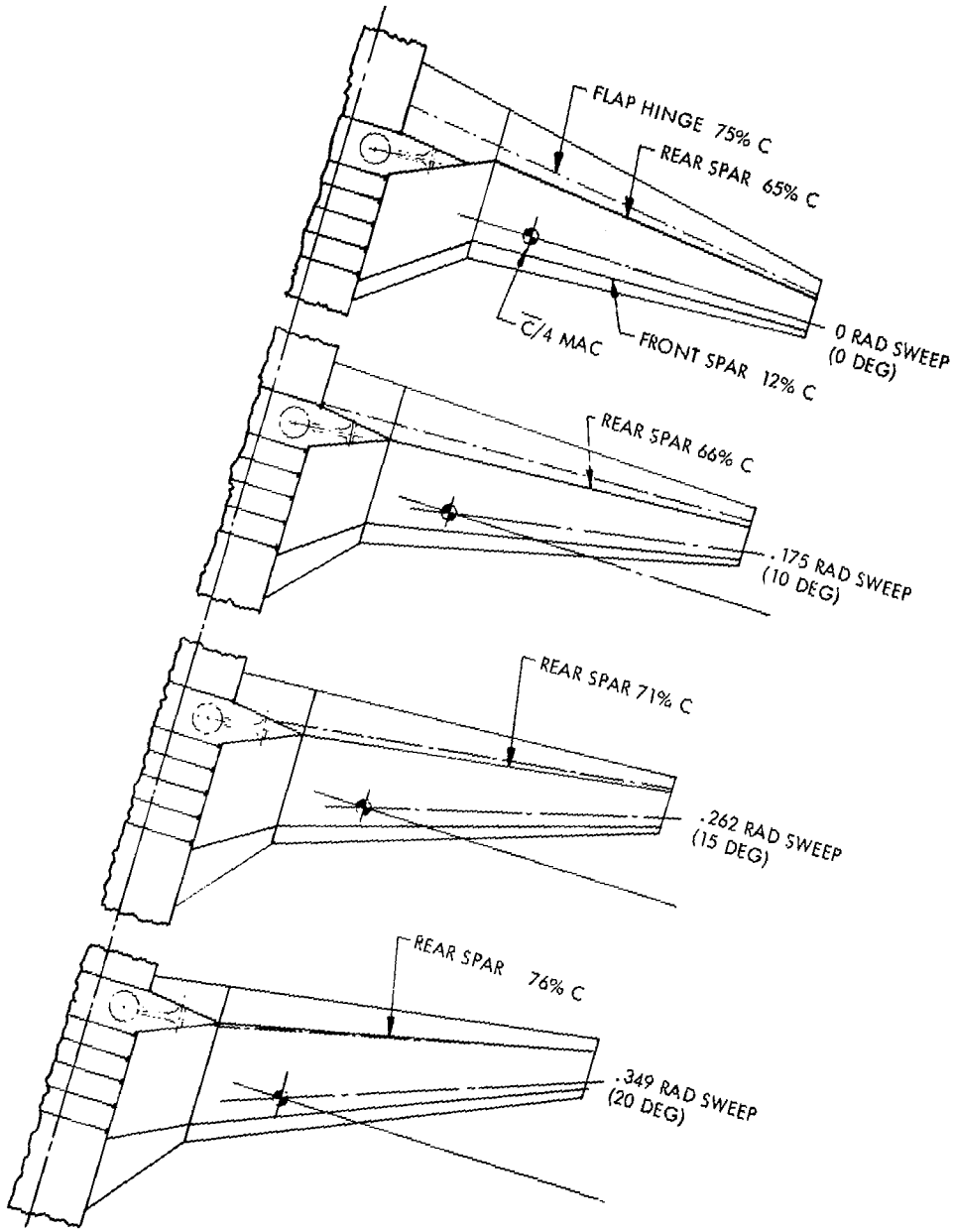

FIGURE C3 GEOMETRIC EFFECTS OF WING SWEEP

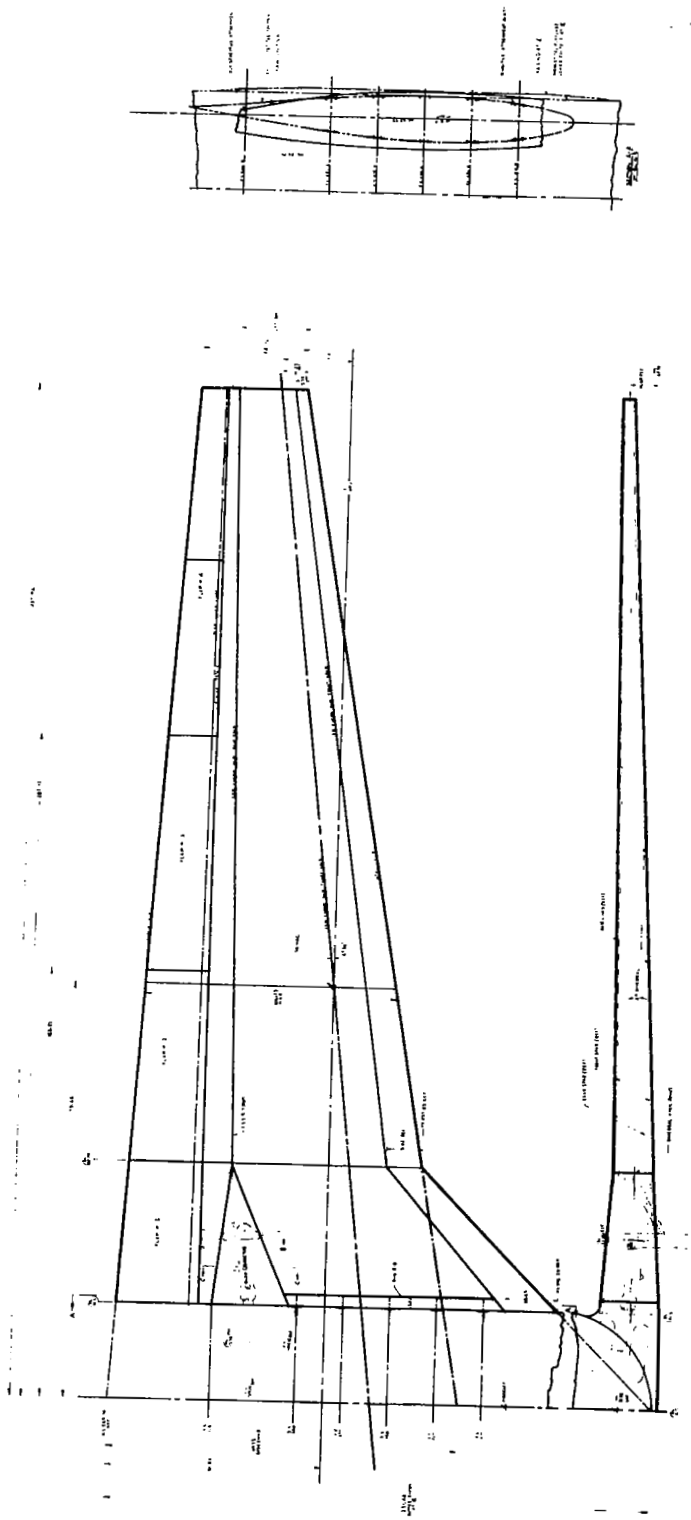

FIGURE C4 BASELINE WING GEOMETRY

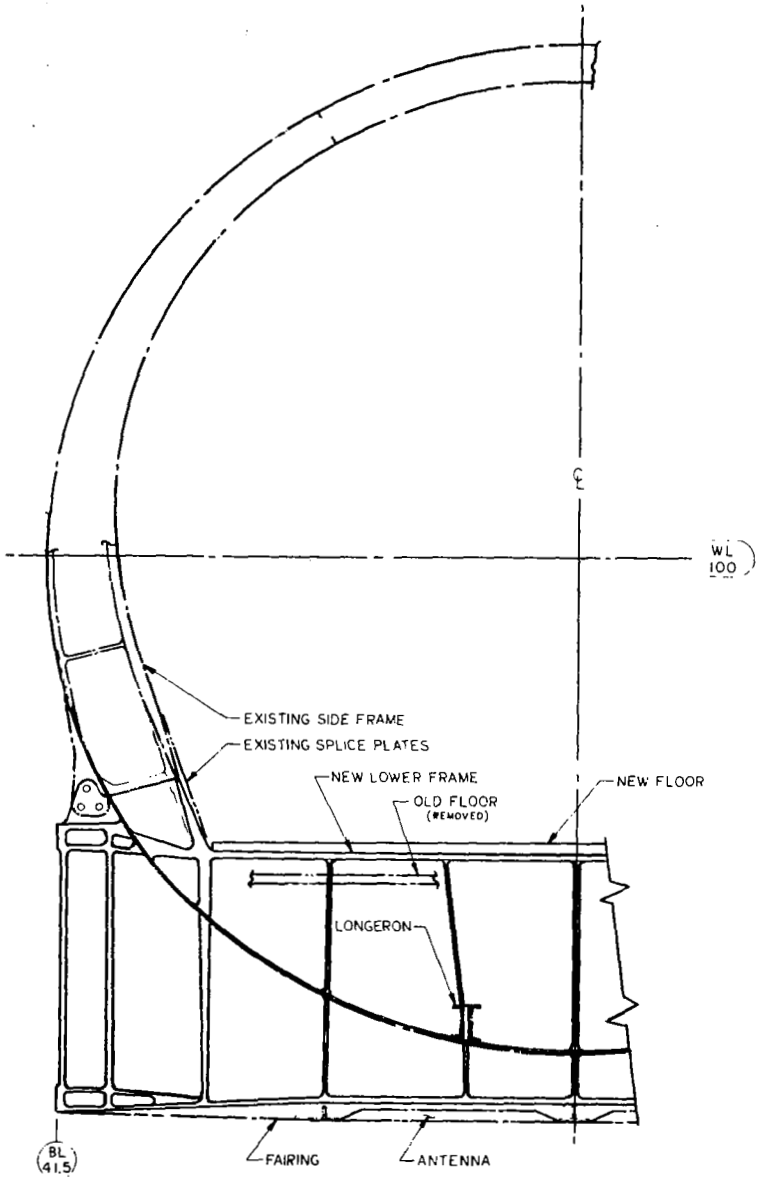

FIGURE C5 ACT AIRPLANE WING ATTACHMENT FRAME MODIFICATION

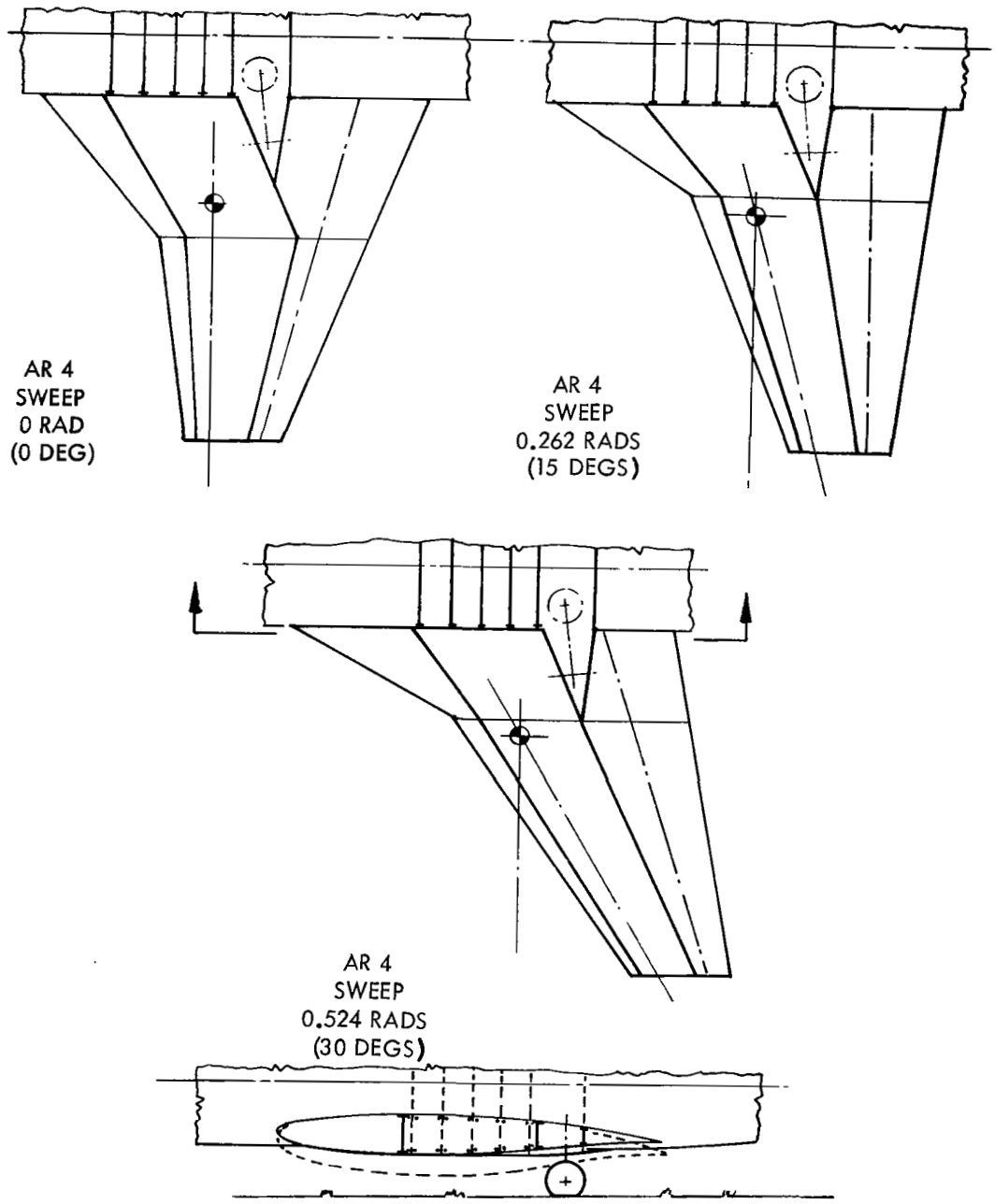

FIGURE C6 INTERMEDIATE AND ALTERNATE CONFIGURATIONS
EFFECT OF SWEEP ON THICKNESS

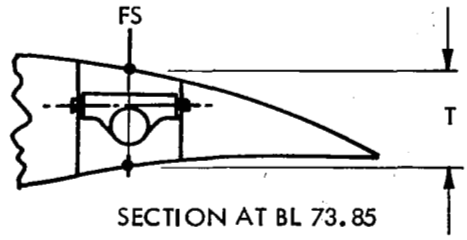

FS - FUSELAGE STATION

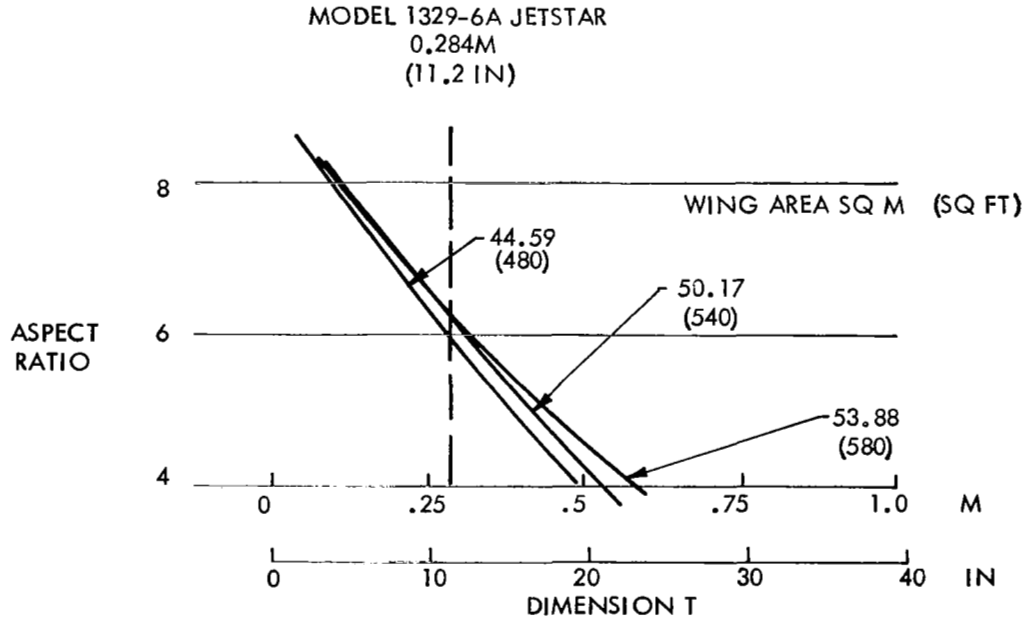

FIGURE C7 WING THICKNESS AT MLG CONSTRAINT
(FOR .524 RAD (30 DEG) SWEEP)

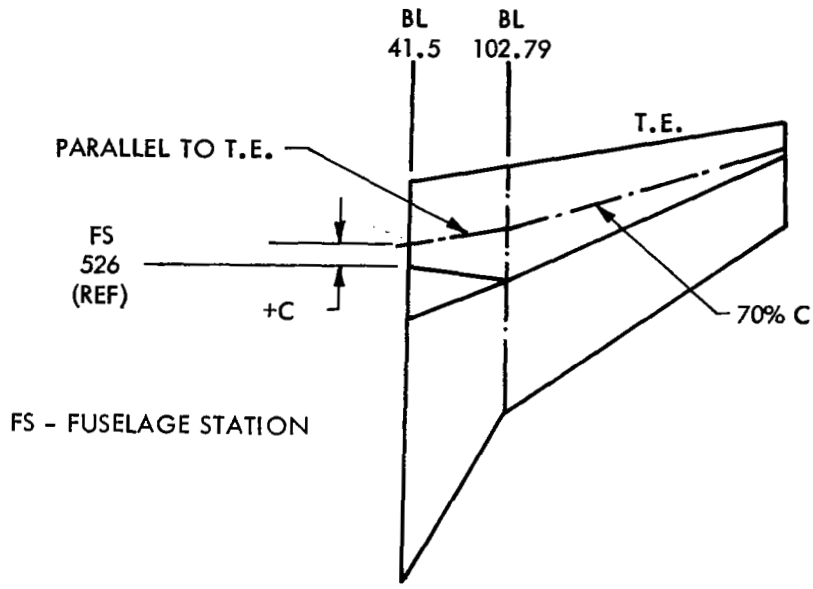

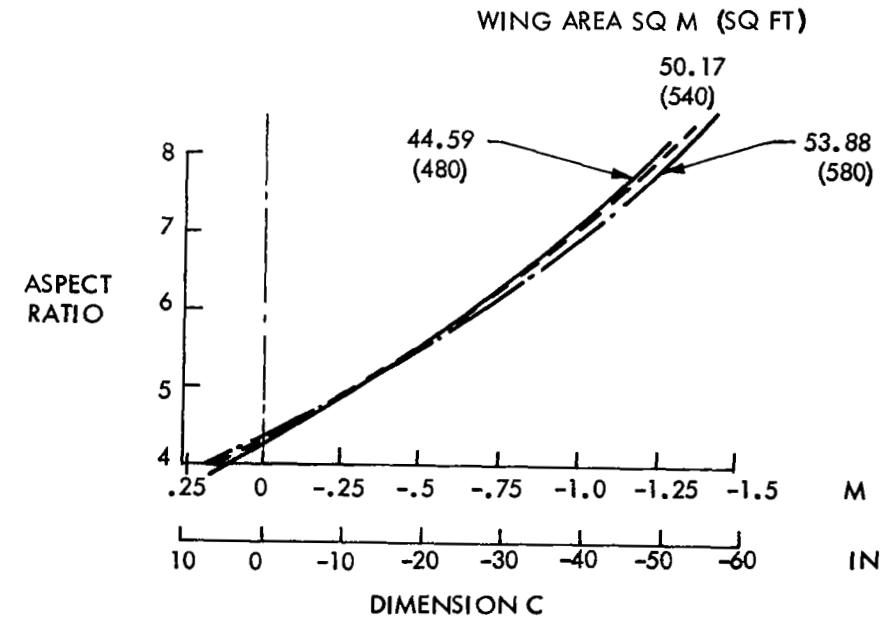

FIGURE C8 INBOARD FLAP CLEARANCE CONSTRAINT
(FOR .524 RAD (30 DEG) SWEEP)

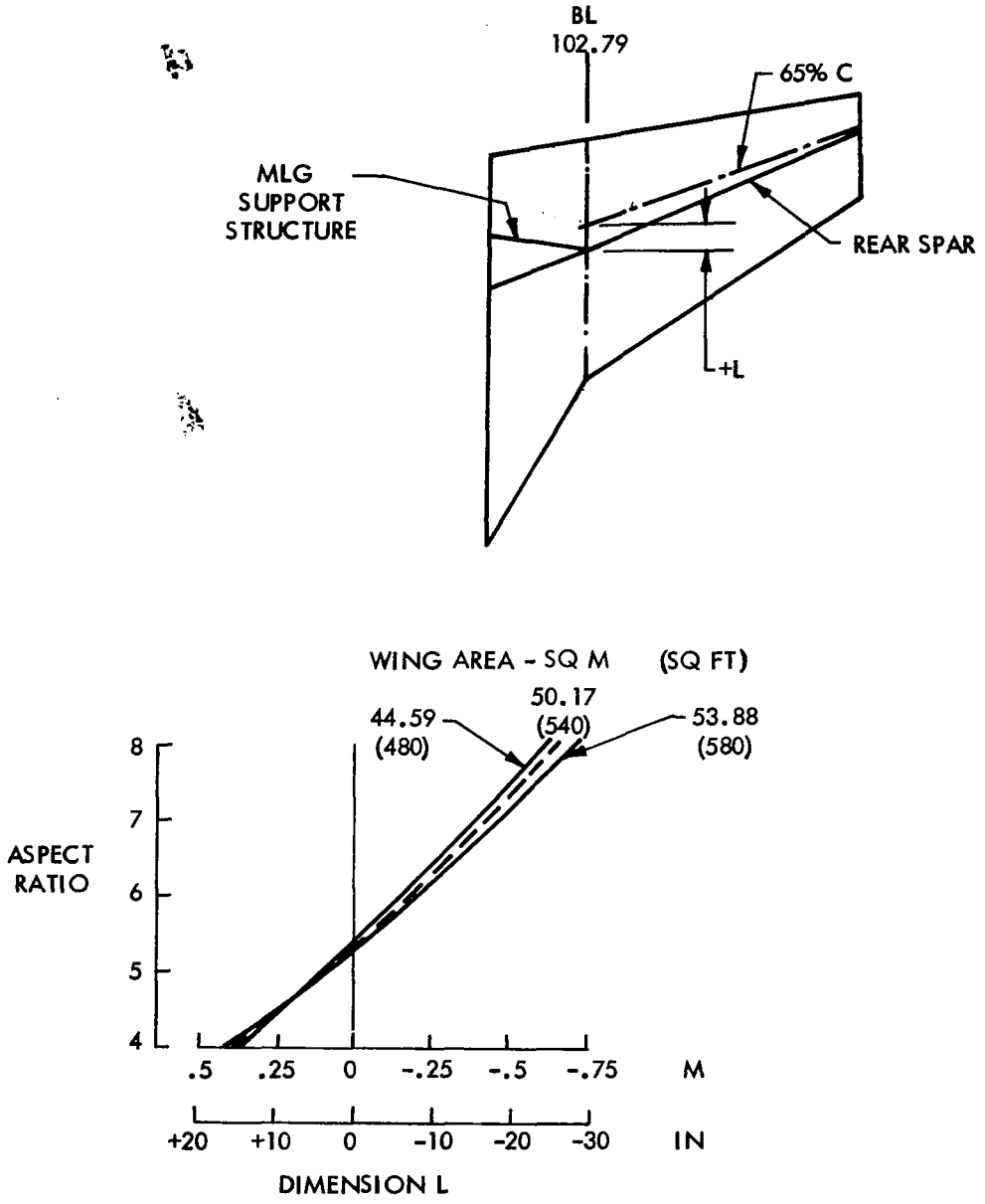

FIGURE C9 REAR SPAR LOCATION CONSTRAINT
(FOR .524 RAD (30 DEG) SWEEP)

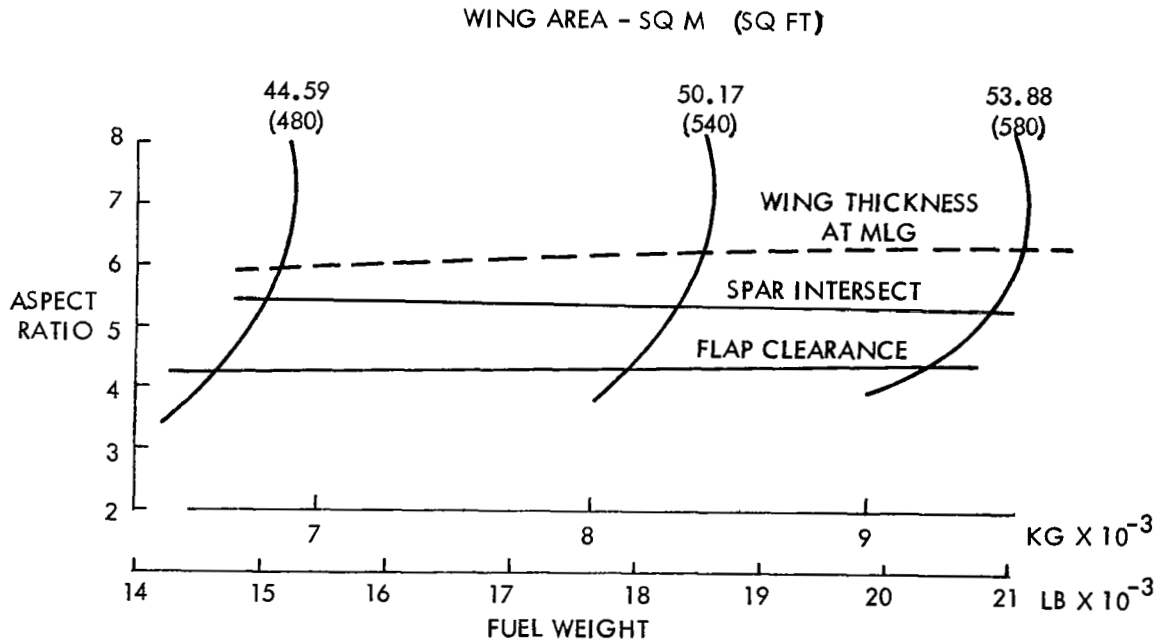

FIGURE C10 EFFECT OF GEOMETRICAL CONSTRAINTS ON ASPECT RATIO AND FUEL WEIGHT

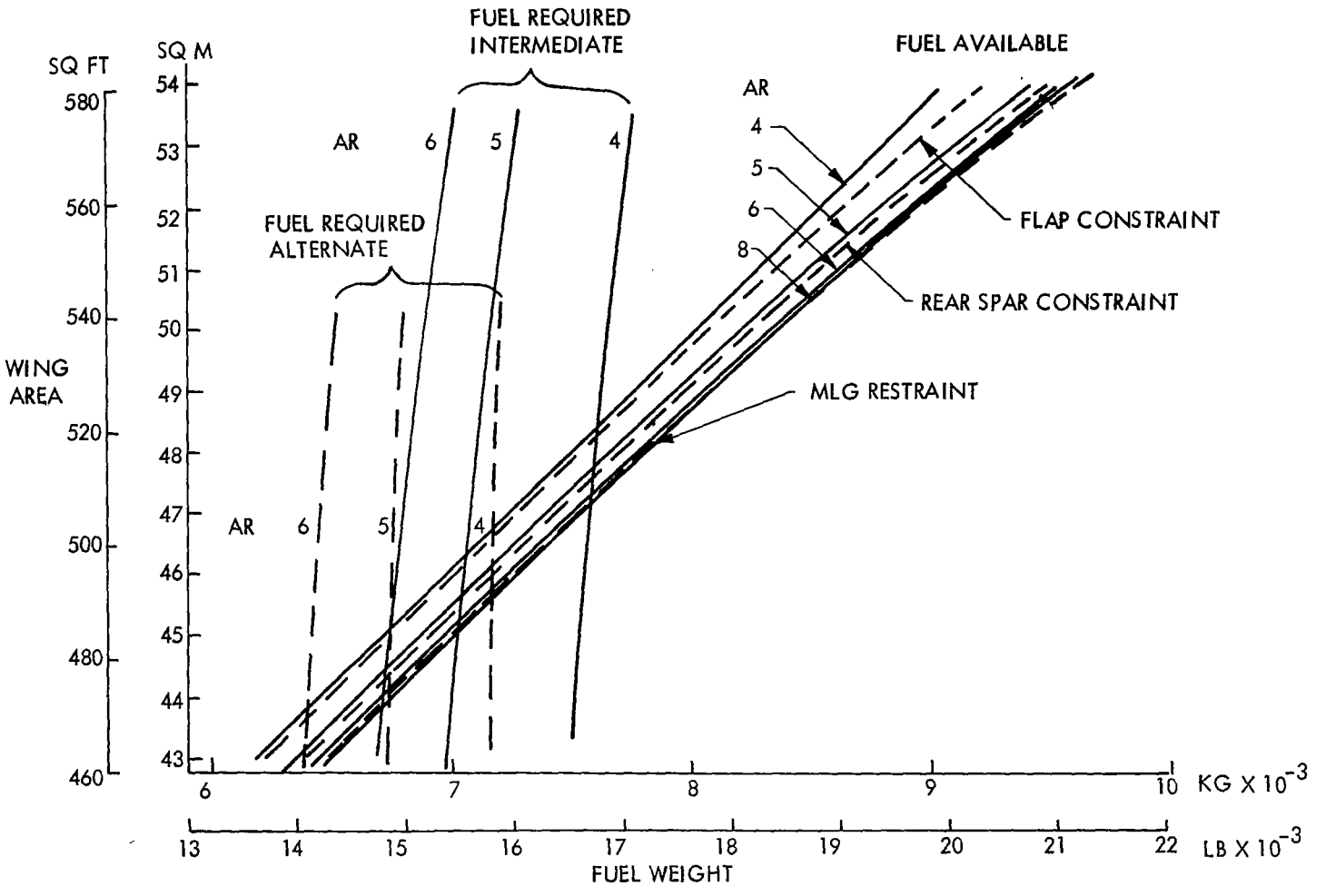

FIGURE C11 FUEL REQUIRED AND AVAILABLE

*U.S. GOVERNMENT PRINTING OFFICE: 1975 - 635-053/93